DOE/NV/10461--T74-Vol.2

Volume II
Appendix B

THE ORIGIN AND HISTORY OF ALTERATION AND CARBONATIZATION OF THE YUCCA MOUNTAIN IGNIMBRITES

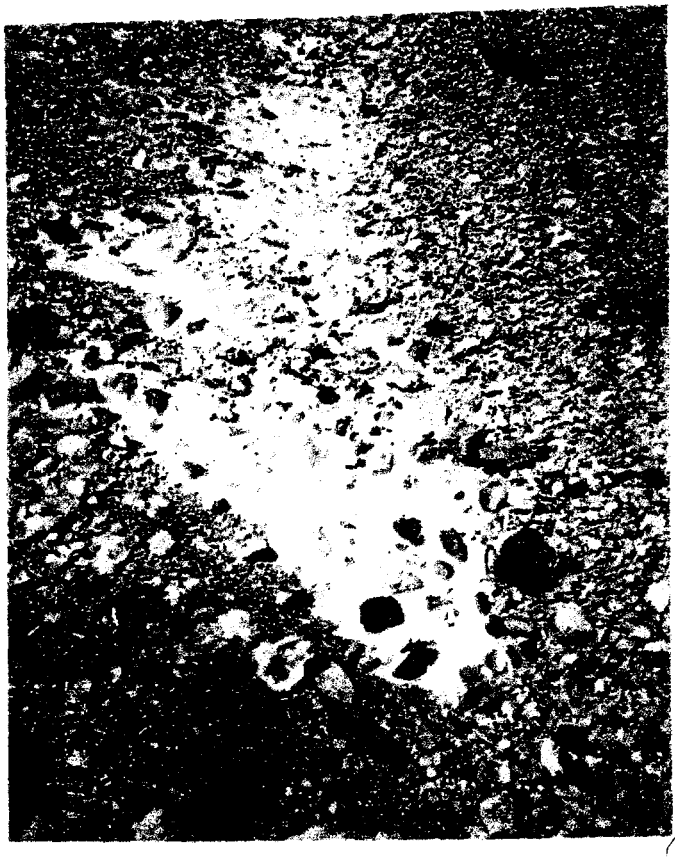

Prepared by:

Jerry S. Szymanski
Physical Scientist
U.S. Department of Energy
DOE Nevada Field Office
Yucca Mountain Site Characterization Project Office

Las Vegas, Nevada
April 1992

LIST OF FIGURES

Section II

Section III

Section IV

Section V

Section VI

Section VII

Section VIII

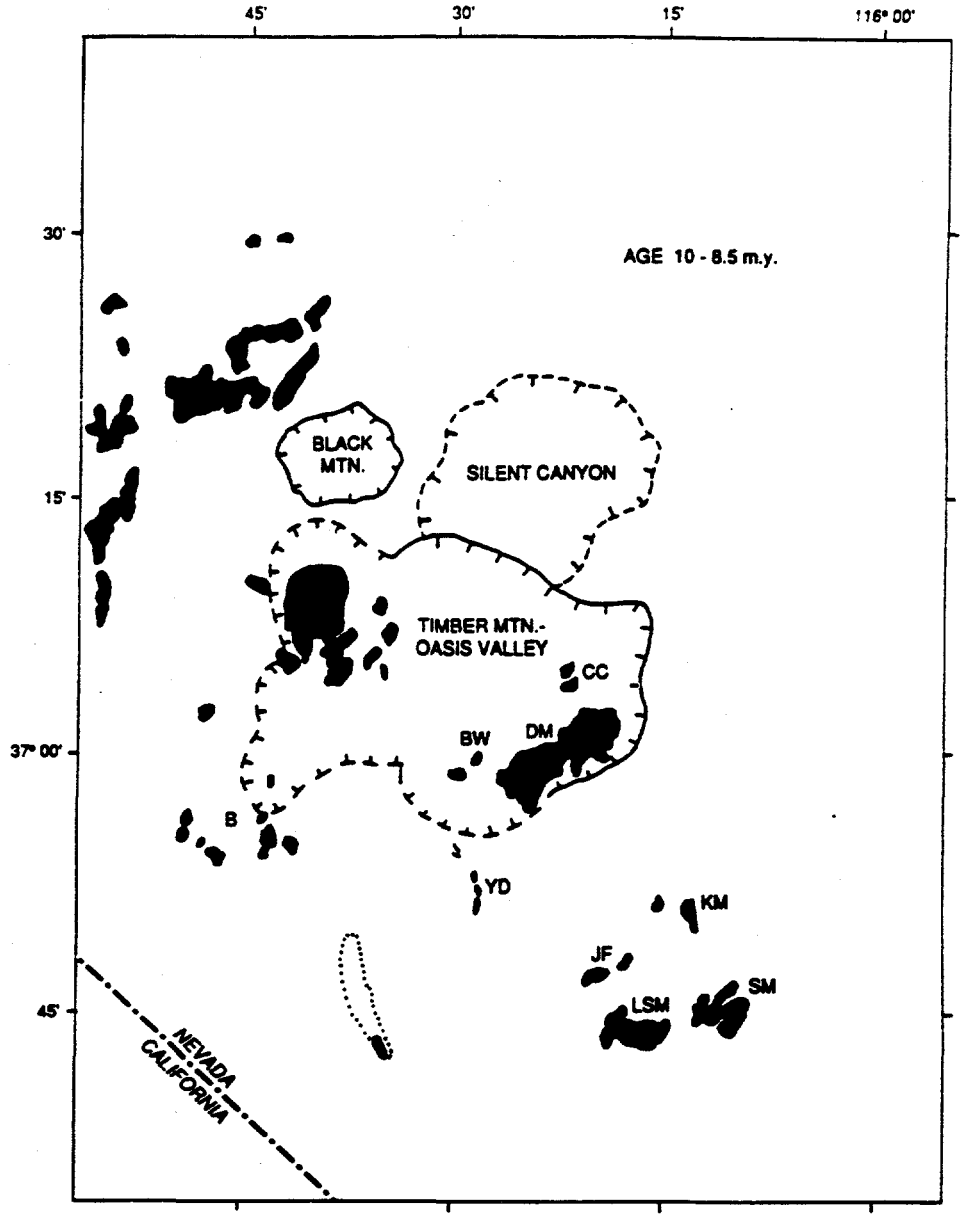

Explanation:

LSM - Little Skull Mountain; SM - Skull Mountain; JF - Jackass Flat; KM - Kiwi Mesa;
YD - dike of Yucca Mountain; DM - Dome Mountain; BW - Beatty Wash; CC - Cat Canyon;
B - Beatty

Location map, older post-Ammonia Tanks Member basalts. Region around Yucca Mountain.
From Crowe (1990)

Figure 2-1a

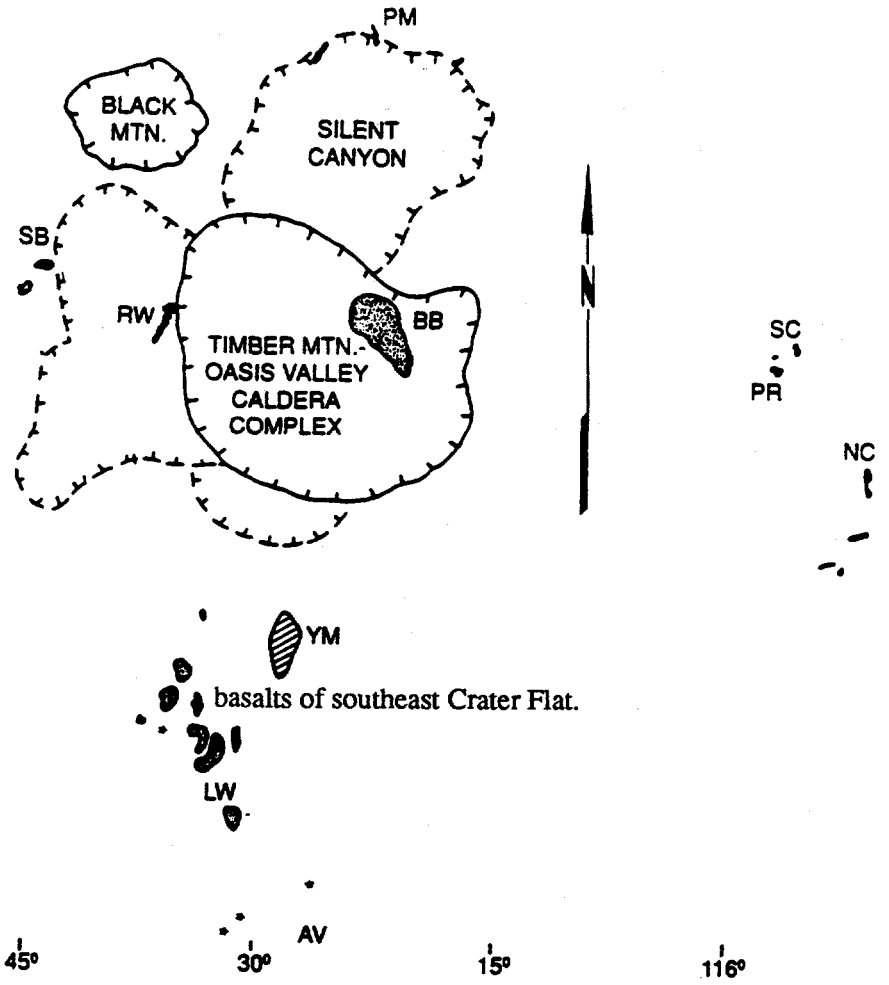

Explanation:

YM - Yucca Mountain; LW - basalt of Lathrop Wells; PM - basalt of Pahute Mesa; RW - basalt of Rocket Wash; SB - basalt of Sleeping Butte; SC - basalt of Scarp Canyon; BB - basalt of Buckboard Mesa; PR - basalt of Paiute Ridge; NC - basalt of Nye Canyon; and stars are approximate locations of aeromagnetic anomalies inferred to represent buried basalt centers or intrusive rocks.

Location map, younger post-Ammonia Tanks Member basalts. Region around Yucca Mountain. From Crowe (1990)

Location	Method	Dated material	Age [x10^6 yrs B.P.]	Stratigraphic position	Source
southern Yucca Mtn.	$^{40}Ar/^{39}Ar$ laser fusion	whole-rock basalt	0.119 ± 0.011	Lathrop Wells cinder cone and lava flows	Turrin and Champion (1990)
do	do	do	0.141 ± 0.010	do	do
central Crater Flat	K/Ar	?	1.16 (mean from 6 samples)	Crater Flat cinder cones and lava flows	Crowe et al. (1982)
30 km north-west of Yucca Mountain	K/Ar	?	0.28 (mean from 3 samples)	basalt of Sleeping Butte	do
20 km north of Yucca Mountain	K/Ar	?	2.81 (mean from 2 samples)	basalt and basaltic andesite of Buckboard Mesa	Crowe (1990)
western Yucca Mountain	K/Ar	?	3.7 (mean from 2 samples)	basalt flows of southeast Crater Flat	Crowe (1990)
northeast Frenchman Flat	K/Ar	?	6.3 - 7.2	basalt of Nye Canyon	Crowe (1990)
~15km north of Yucca Mountain	K/Ar	?	8.0	basalt of Rocket Wash	Crowe (1990)
eastern Nevada Test Site	K/Ar	?	8.0 - 8.5	basalt of Paiute Ridge	Crowe (1990)
northern Nevada Test Site	K/Ar	?	8.5 - 9.0	basalt of Pahute Mesa	Crowe (1990)
west side of Yucca Mountain	K/Ar	?	10.0 ± 0.4	basaltic dike	Carr and Parrish (1985)
southern edge of Crater Flat	K/Ar	?	10.5 ± 0.1	basalt flow overlying the Ammonia Tanks Member of the Timber Mtn. Tuff	do

Radiometric ages from samples of basaltic intrusive and extrusive rocks, region around Yucca Mountain.

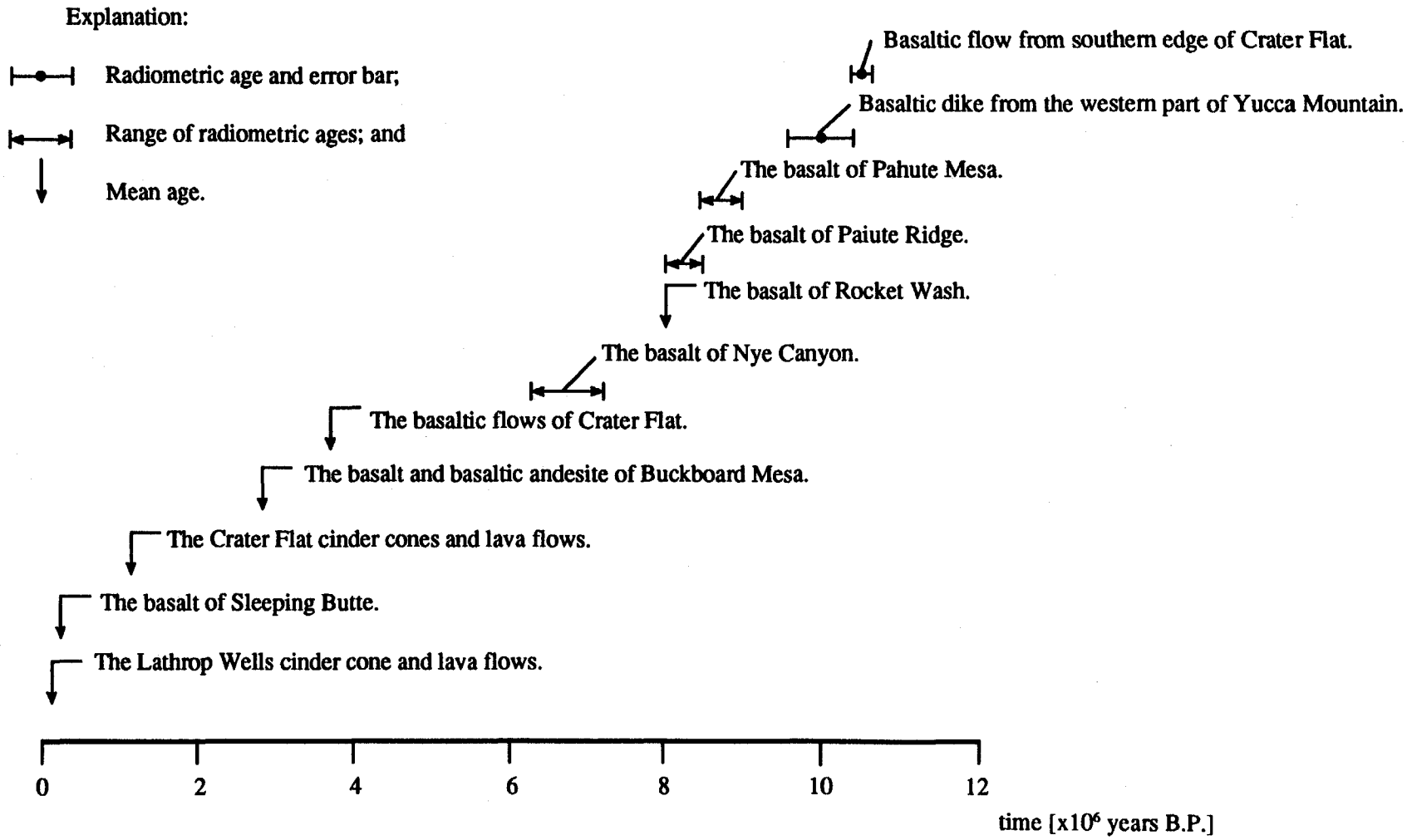

History of post-Ammonia Tanks Member basaltic volcanism, based on radiometric data. Region around Yucca Mountain.

Figure 2-2b

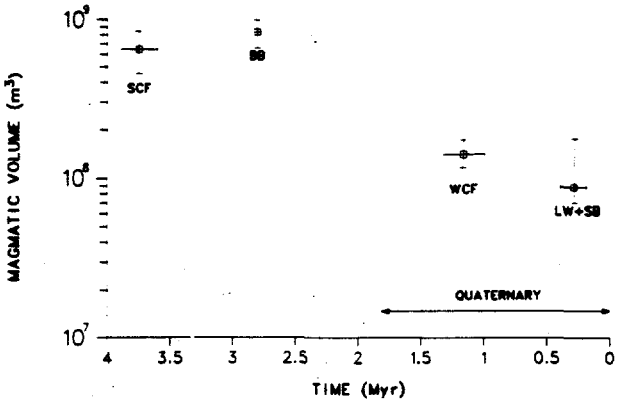

a) Magmatic volume vs. time relationship for the Nevada Test Site region. From Crowe et al. (1982).

Explanation:

SCF - southern Crater Flat basalts; BB - Buckboard Mesa basalts and dacites; WCF - western Crater Flat basalts; and LW + SB - combined Lathrop Wells and Sleeping Butte basalts.

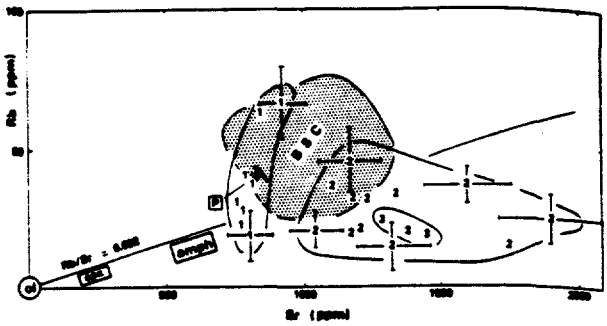

b) The Rb and Sr contents for various Nevada Test Site basalts. From Vaniman et al. (1982).

Explanation:

BSC - basalts older than 6 x 10^6 years B.P.; 1 - 3.7 x 10^6 years B.P. old basalts; 2 - 1.2 x 10^6 years B.P. old basalts; and 3 - 0.3 x 10^6 years B.P. old basalts.

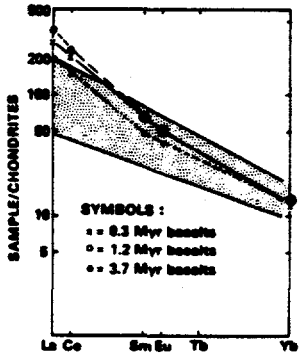

c) The chondrite-normalized REE abundance pattern. From Vaniman et al. (1982).

Note:

The fine-stippled field represents the typical REE abundance pattern for hawaiite and related basalt types.

Temporal changes in eruptive volume and trace elements concentrations, basalts from Yucca Mountain region.

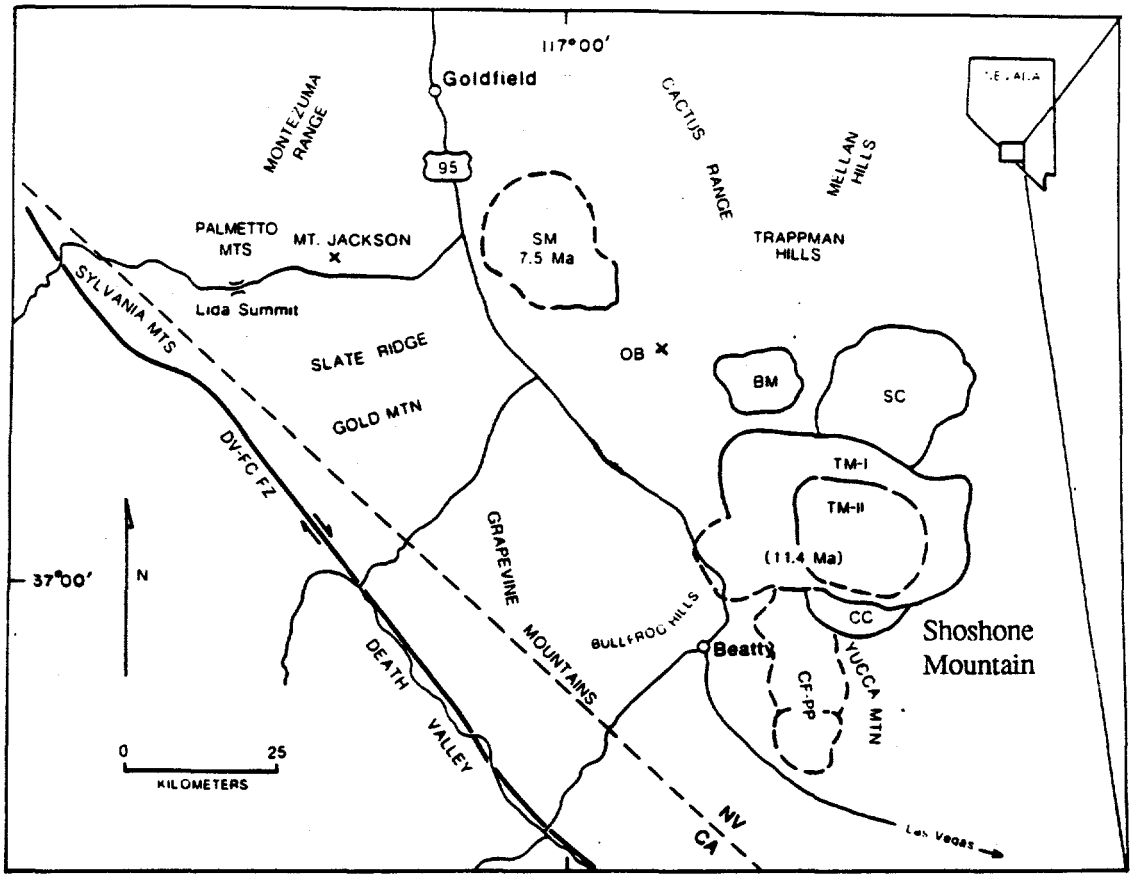

Explanation:

SM - Stonewall Mountain volcanic center; Mt. Jackson - Mount Jackson rhyolitic lavas and dacites; OB - rhyolitic lavas of the Obsidian Butte; BM - Black Mountain volcanic center; SC - Silent Canyon caldera; TM-1 - Timber Mountain caldera I (the Rainier Mesa Member); TM-II - Timber Mountain caldera II (the Ammonia Tanks Member).

Location map, volcanic centers for youngest silicic activity, region around Yucca Mountain. From Noble et al. (1991)

Location	Method	Dated material	Age [x10^6 yrs B.P.]	Stratigraphic position	Source
southwest of Goldfield - Mount Jackson	$^{40}Ar/^{39}Ar$ laser fusion	sanidine phenocryst	2.93 ± 0.16	high-silica rhyolitic lavas of the Mount Jackson domes	McKee et al. (1989)
10-20 miles west of Mount Jackson	?	?	4.50	silicic tuff possibly correlative with the rhyolitic lavas of Montezuma Range	do
east-central Crater Flat	fission track on zircon	zircon from silicic pumice	6.3 ± 0.8	below basaltic flow, in a sandy poorly indurated alluvium	Carr (1982)
Stonewall Mtn. volcanic center	$^{40}Ar/^{39}Ar$ laser fusion	?	7.4	Civet Cat Canyon Member of the Stonewall Flat Tuff	Noble et al. (1991)
Stonewall Mtn. volcanic center	$^{40}Ar/^{39}Ar$ laser fusion	?	7.6	Spearhead Member of the Stonewall Flat Tuff	do
Obsidian Butte	K/Ar	non-hydrated glass	8.8 ± 0.3	rhyolitic lavas of the Obsidian Butte area	do
Black Mtn. volcanic center	?	?	8.5 - 9.0	Thirsty Canyon Tuff.	do
north-end of Burton Mtn.	K/Ar	biotite from rhyolitic tuff	10.1 ± 0.3	tuffs and lavas of the Bullfrog Hills (Rainbow Mountains)	do
western flank of the Transvaal Hills	K/Ar	sanidine from rhyolitic tuff	10.4 ± 0.3	distal tuffs and lavas of the Bullfrog Hills	do
central Shoshone Mtn.	K/Ar	glass from rhyolitic lava	10.3 ± 0.3	rhyolitic lavas of Shoshone Mtns.	do
Shoshone Mountain	?	?	9.3	rhyolitic lavas of Shoshone Mtns.	Frizzel and Shulters (1990)

Radiometric ages from samples of rhyolitic intrusive and extrusive rocks, region around Yucca Mountain.

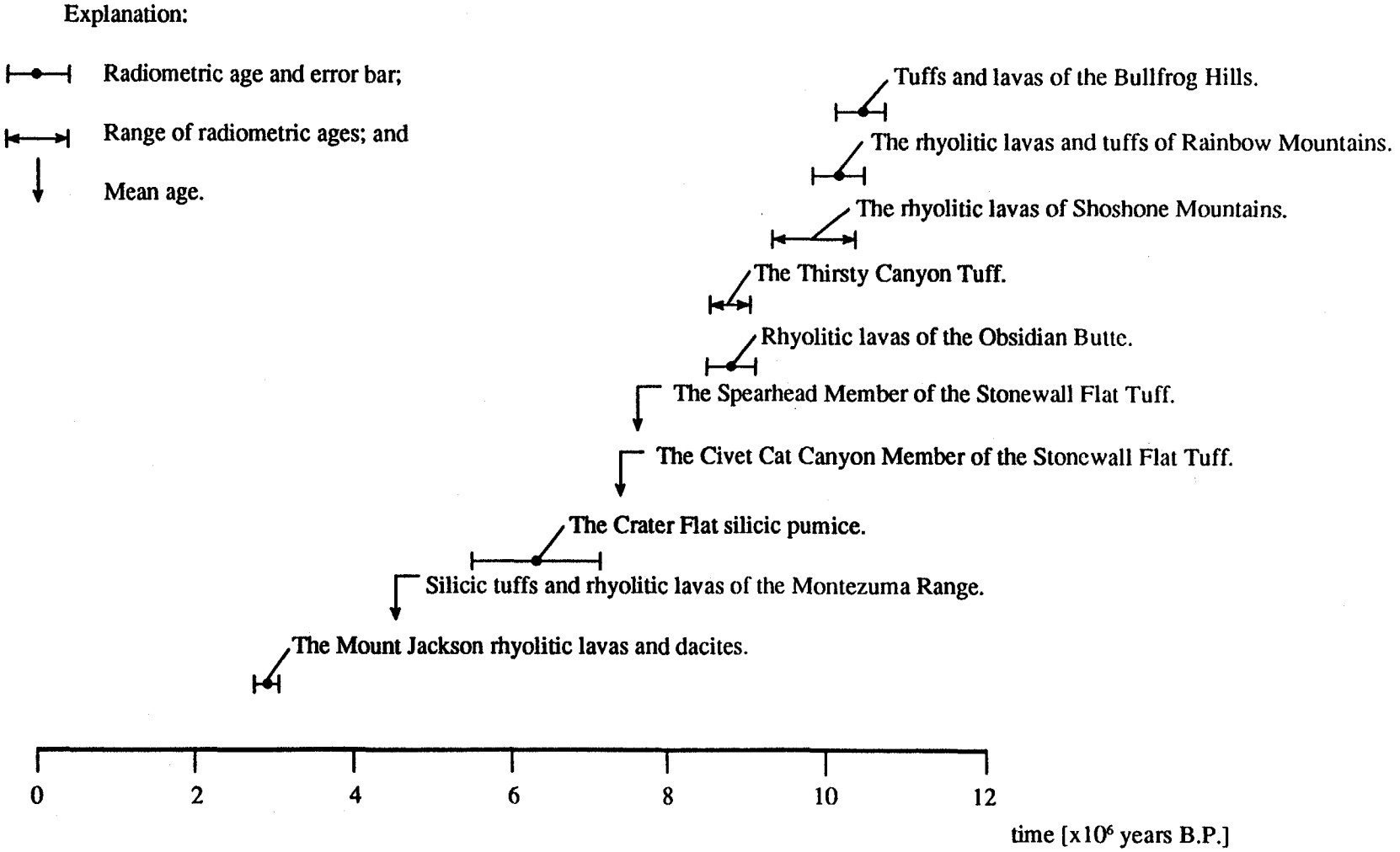

History of post-Ammonia Tanks Member silicic volcanism, based on radiometric data. Region around Yucca Mountain.

Figure 2-5b

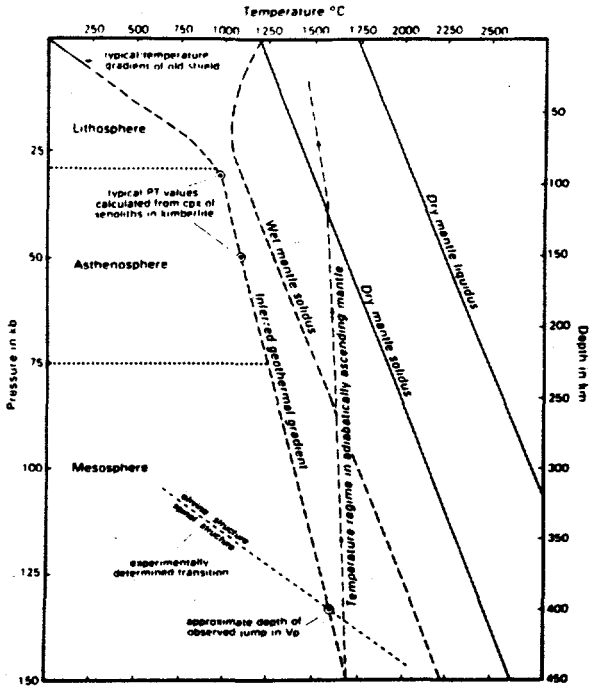

a) Mantle solidus temperatures as a function of pressure, for dry and wet melting. From Hughes (1982).

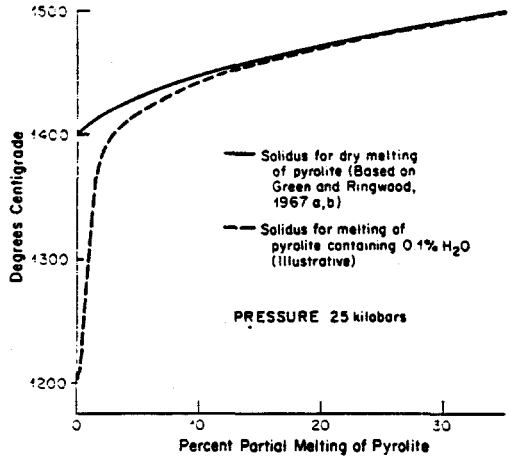

b) Diagrammatic representation of degree of melting vs. temperature in pyrolite under anhydrous conditions and in the presence of 0.1 percent H_2O. From Ringwood (1969).

Note:

a) pyrolite is a hypothetical mantle material, composed of one part basalt to three parts of dunite and consisting mainly of olivine and pyroxene.

Melting behavior of upper mantle.

Figure 2-6

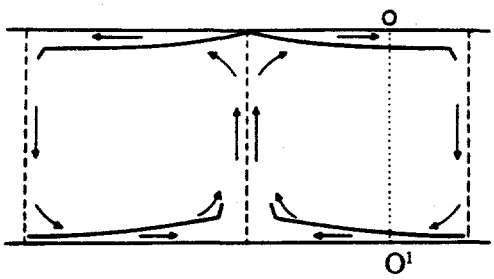

a) Flow pattern in a convecting system.

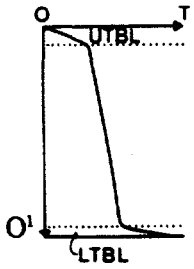

b) temperature profile in a center of a convection cell.

Note:

a) Upper and lower thermal boundary layers (UTBL and LTBL, respectively) are delimited by solid lines in A and dotted lines in B;

b) In a convecting system, the temperature gradient must be close to the adiabatic gradient except in thermal boundary layers;

c) The adiabatic gradient is the rate of increase of temperature with depth resulting from increase in pressure - $(dT/dz)_s \sim 0.25 - 0.30^{\circ}$ Celsius per 1km of depth;

d) On time scales of 10-20 $x10^6$ years, plumes of the asthenospheric material (with a pressure-dependent viscosity) intrude and erode the lithosphere; and

e) The net effect of the lithosphere erosion is thinning of the upper thermal boundary layer and upward migration of the adiabatic temperature gradient.

Depthward distribution of temperature, for a convecting upper mantle. From Ranalli (1987).

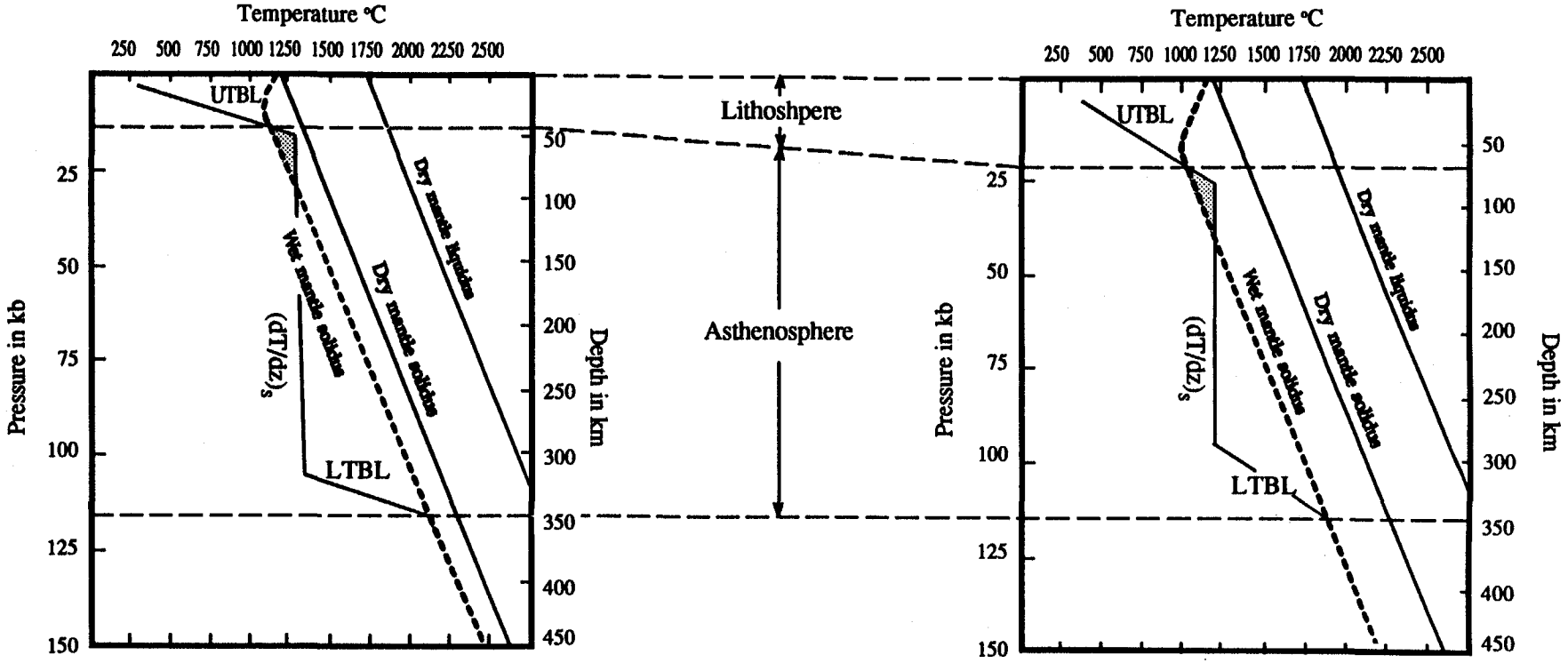

a) Present time - amphibole is present in the refractory residuum, the availability of water is low and, consequently, the wet solidus temperature is relatively high and the degree of partial melting is relatively low.

b) Late-Miocene time - amphibole is not present in the refractory residuum, the availability of water is high and, consequently, the wet solidus temperature is relatively low and the degree of partial melting is relatively high.

Explanation:

a) UTBL - the upper thermal boundary layer;
b) LTBL - the lower thermal boundary layer; and
c) $(dT/dz)_s$ - the adiabatic temperature gradient.

Interpretation of the observed rates of volcanic activity vs. time trends, the Yucca Mountain region.

Figure 2-8

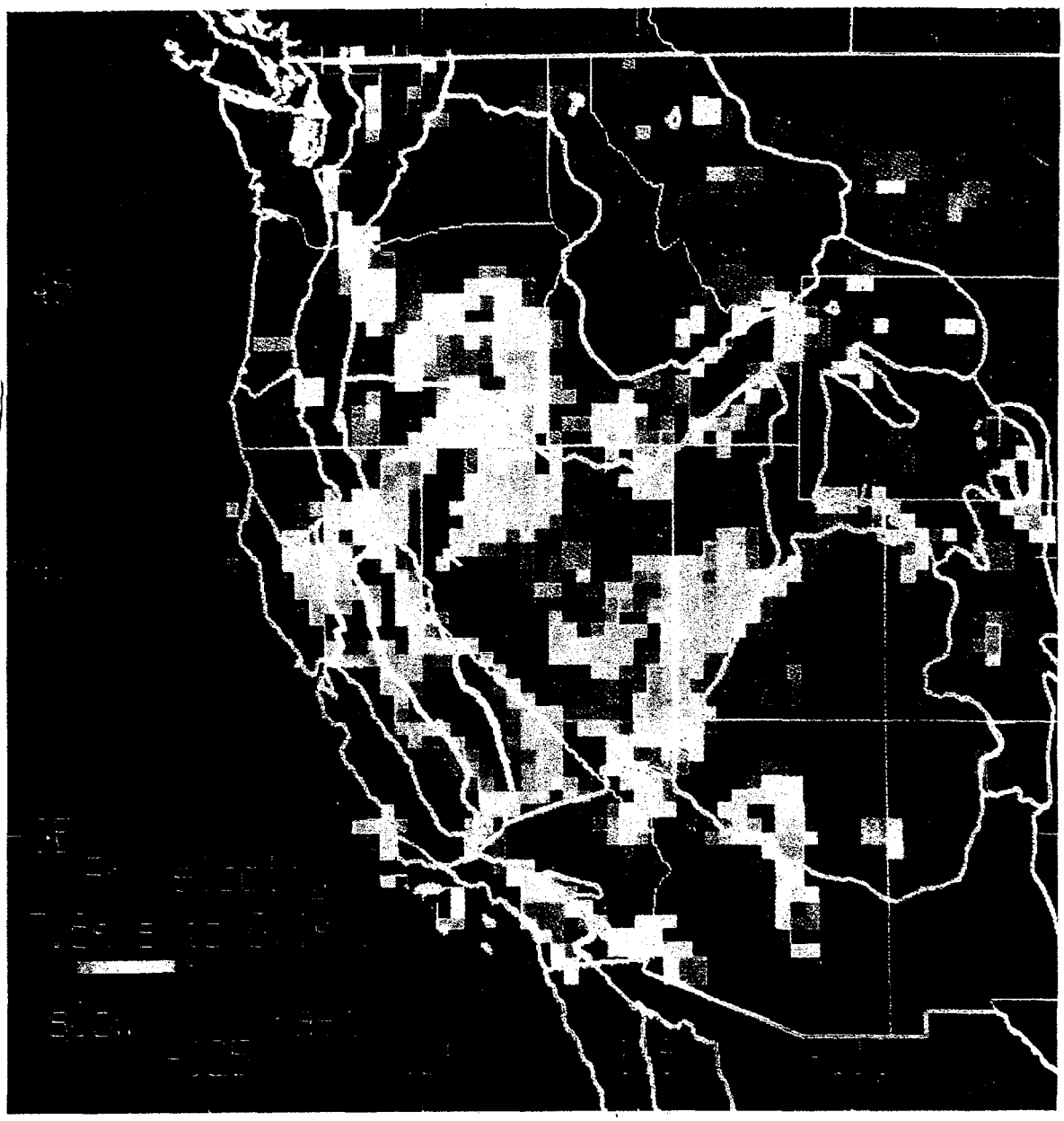

Seismic tomography map. The uppermost mantle in the western United States. From EOS (1990).

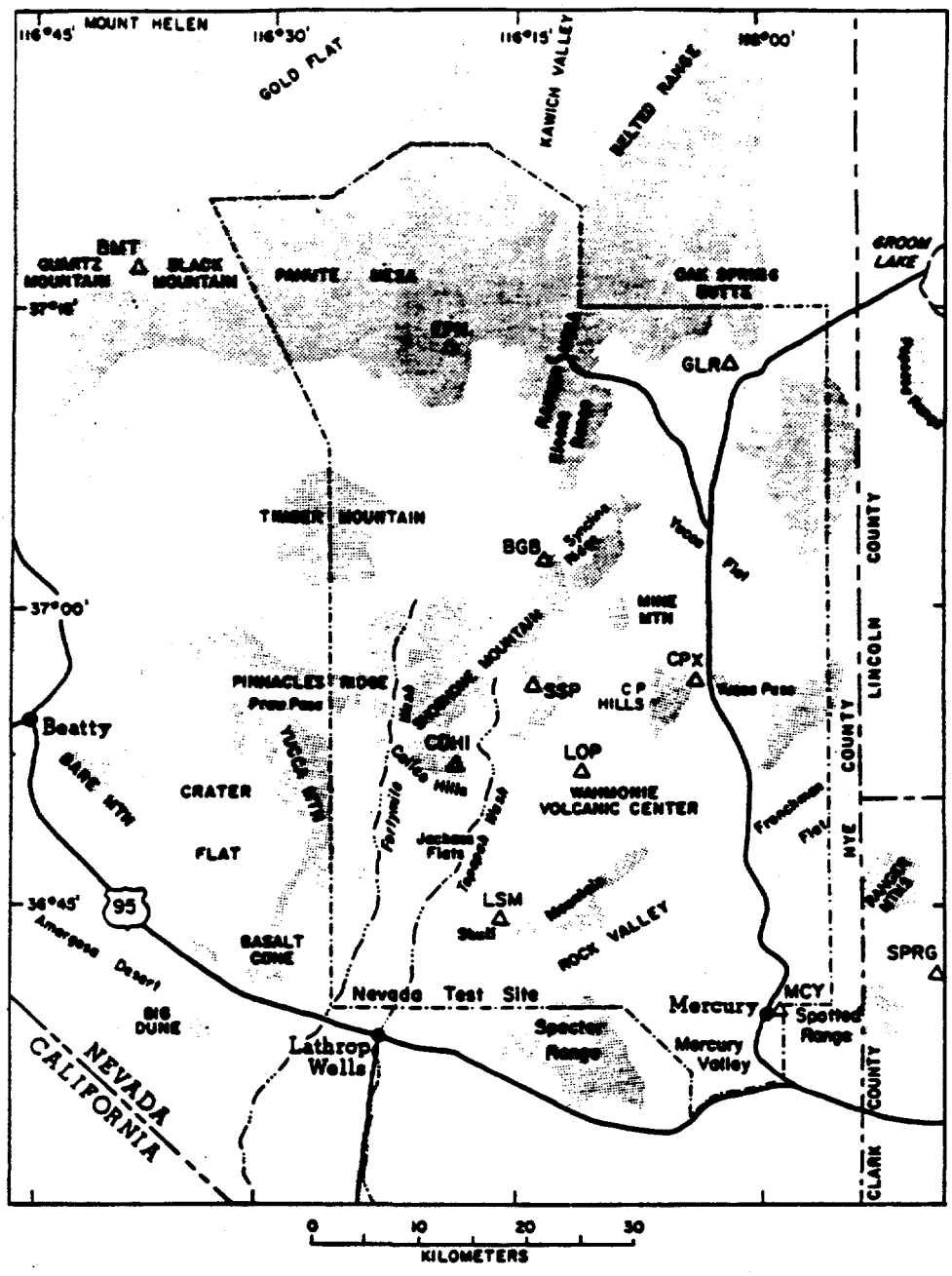

Location map. Seismic monitoring stations used for detailed analyses of the P-wave residuals. The Nevada Test Site area. From Monfort and Evans (1982).

Figure 2-10a

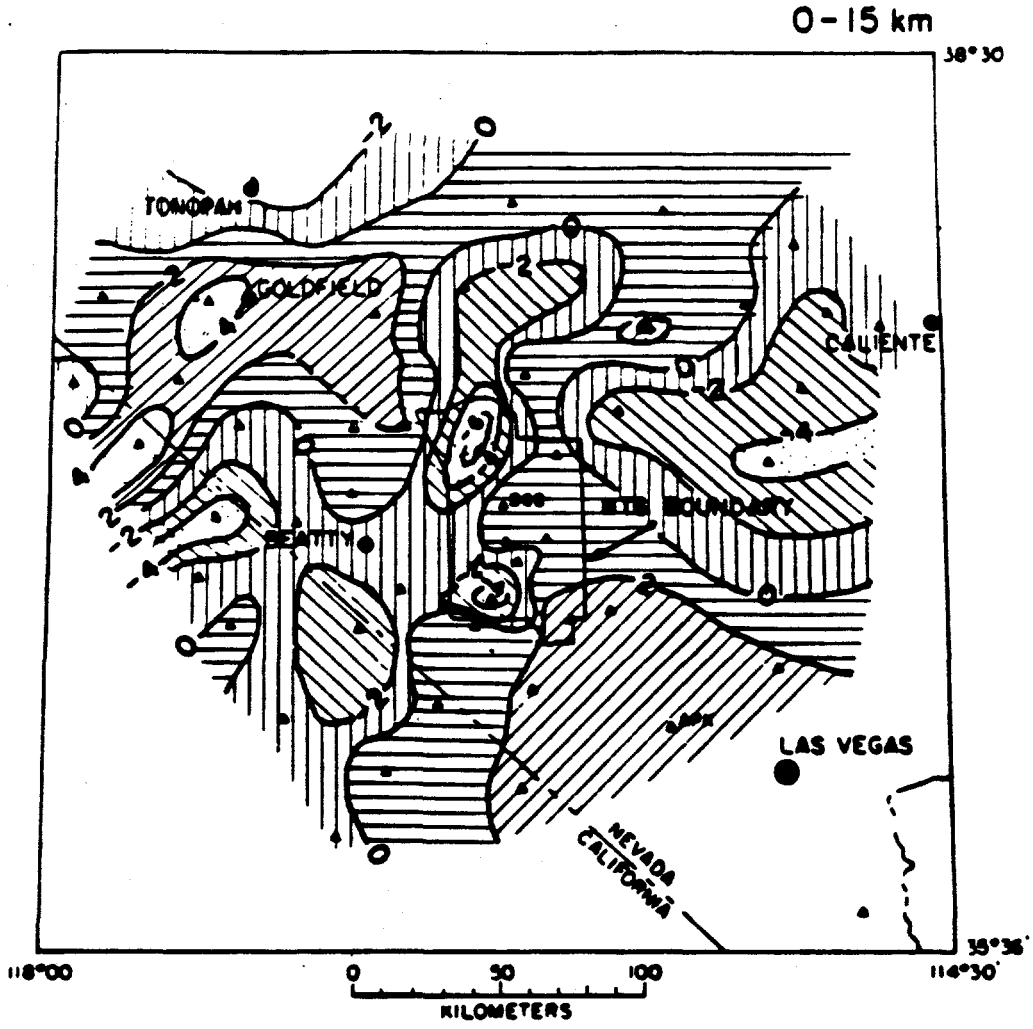

EXPLANATION:

- **ZERO VELOCITY PERTURBATION IS THE MEAN LAYER VELOCITY**
- **VELOCITY PERTURBATIONS ARE IN PERCENTS**
- **POSITIVE VELOCITY PERTURBATIONS ARE RELATIVE HIGH VELOCITIES**

Seismic velocity structure, based on teleseismic P-wave residuals. Upper crust at and near the Nevada Test Site. From Monfort and Evans (1982).

Figure 2-10b

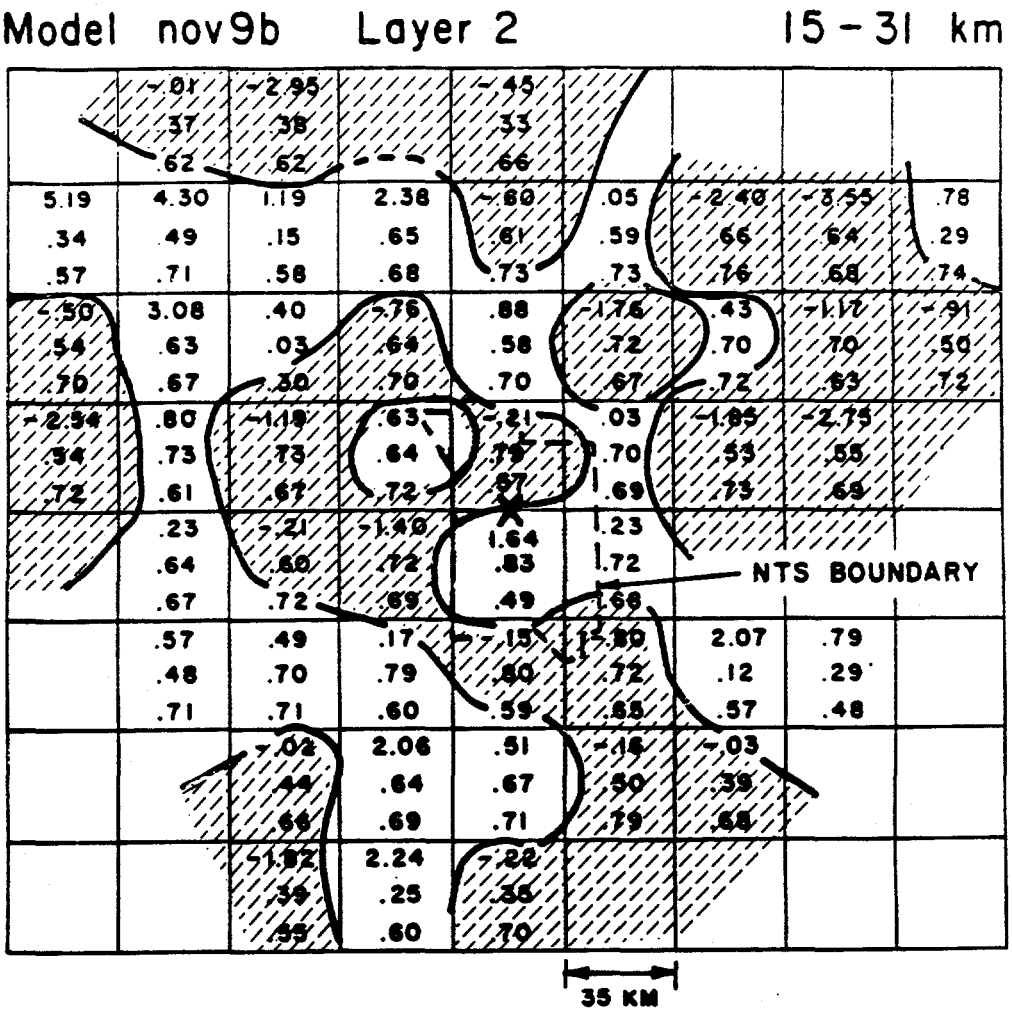

Explanation:

- Contours shown are zero velocity perturbations; and
- In each block, the upper number is velocity perturbation (%), the middle number is the diagonal element of the resolution matrix, and the bottom number is the standard error for the block.

Seismic velocity structure, based on teleseismic P-wave residuals. Lower crust at and near the Nevada Test Site. From Monfort and Evans (1982).

Figure 2-10c

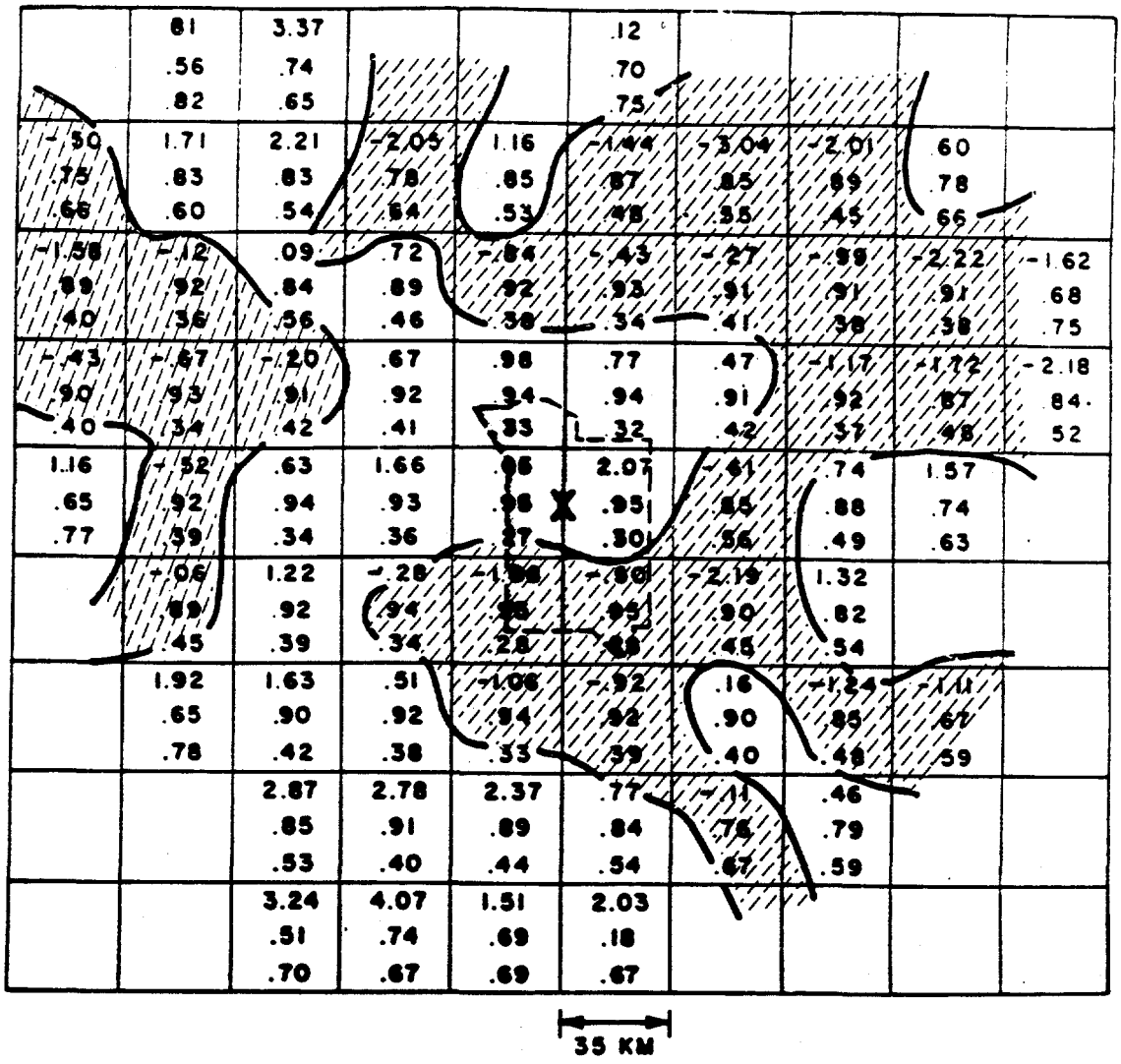

Explanation:

- Contours shown are zero velocity perturbations; and
- In each block, the upper number is velocity perturbation (%), the middle number is the diagonal element of the resolution matrix, and the bottom number is the standard error for the block.

Seismic velocity structure, based on teleseismic P-wave residuals. Upper mantle (depth 31-81 km) at and near the Nevada Test Site. From Monfort and Evans (1982).

Figure 2-10d

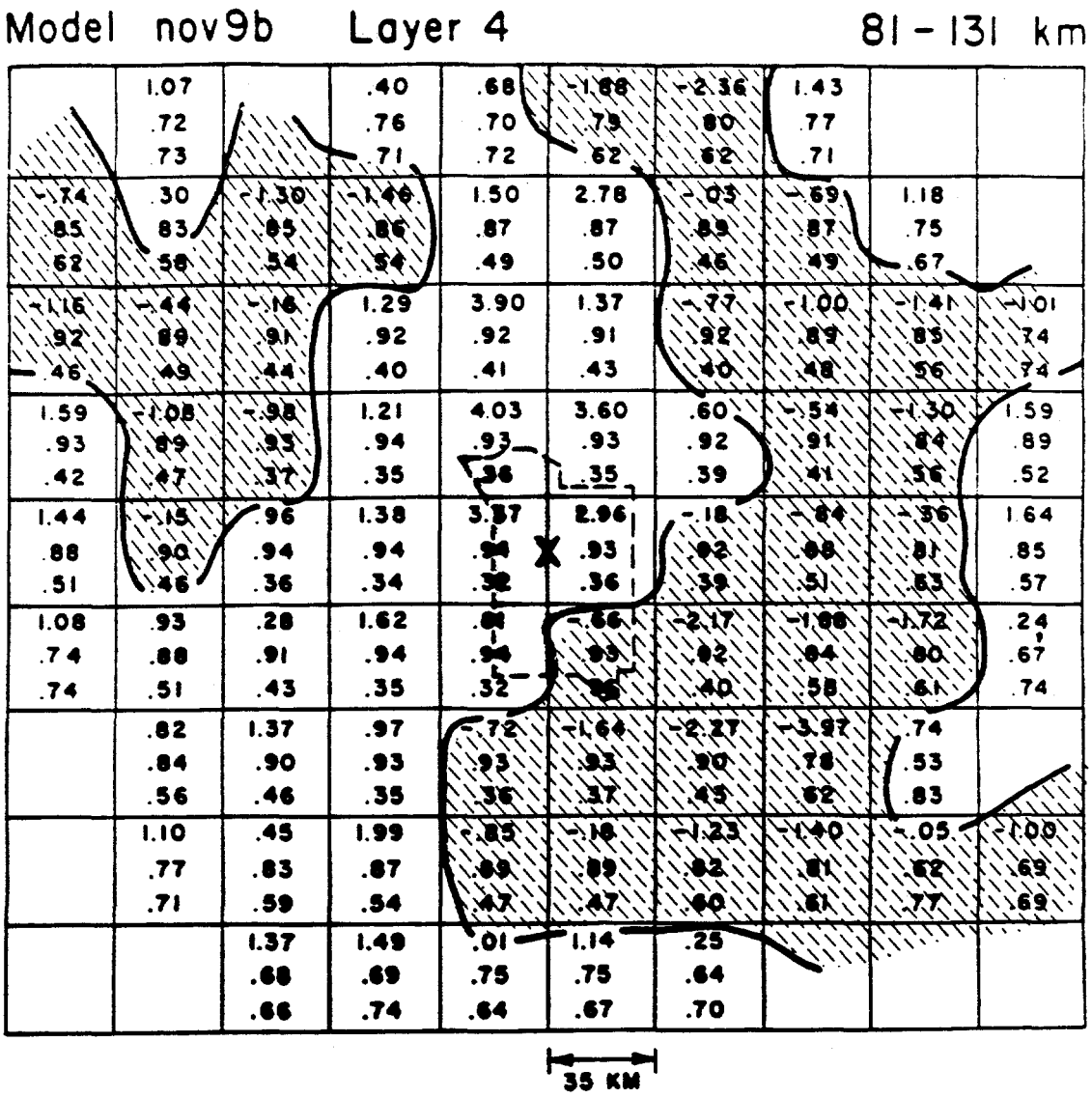

Explanation:

- Contours shown are zero velocity perturbations; and
- In each block, the upper number is velocity perturbation (%), the middle number is the diagonal element of the resolution matrix, and the bottom number is the standard error for the block.

Seismic velocity structure, based on teleseismic P-wave residuals. Upper mantle (depth 81 - 131 km) at and near the Nevada Test Site. From Monfort and Evans (1982).

Figure 2-10e

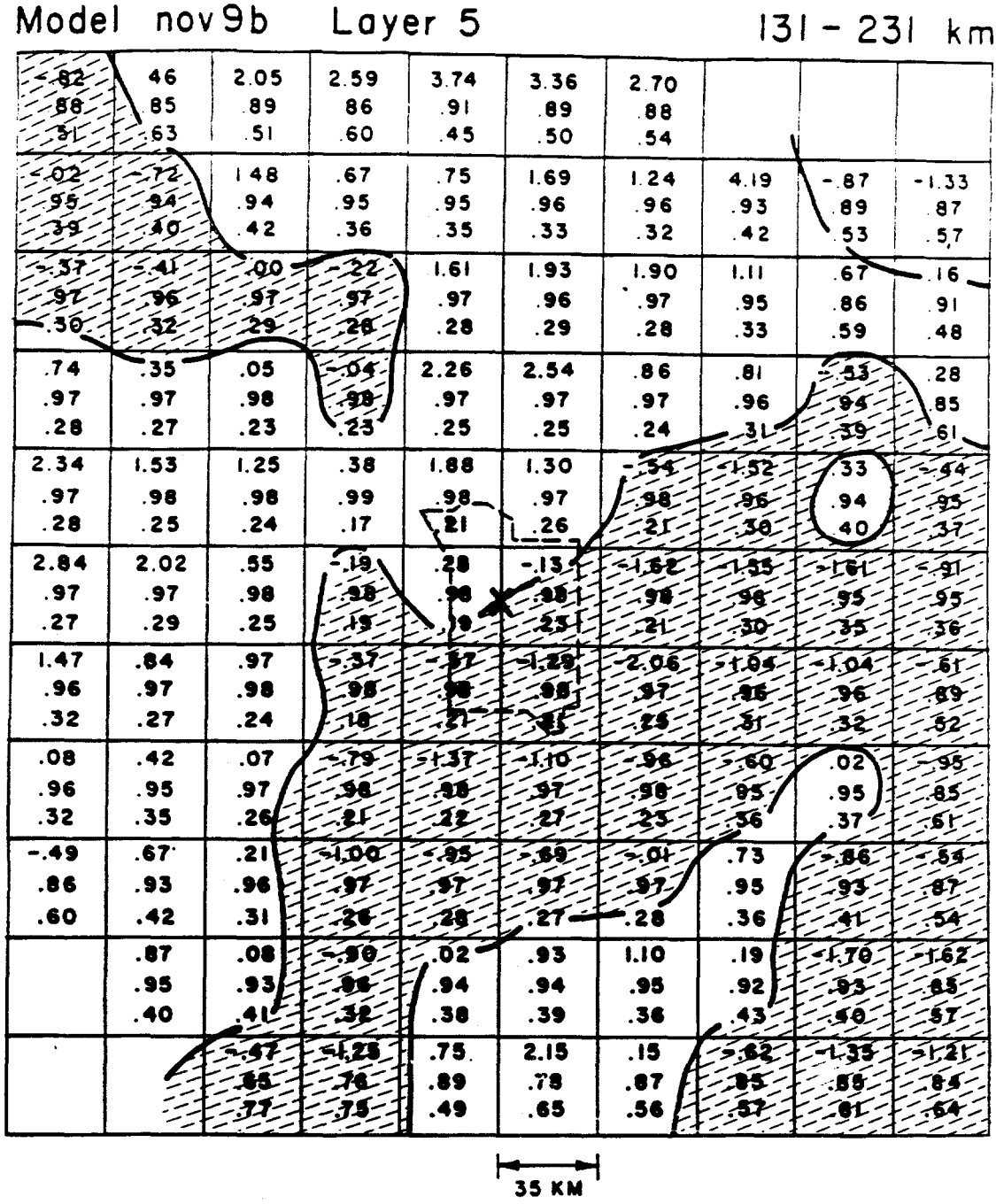

Explanation:

- Contours shown are zero velocity perturbations; and
- In each block, the upper number is velocity perturbation (%), the middle number is the diagonal element of the resolution matrix, and the bottom number is the standard error for the block.

Seismic velocity structure, based on teleseismic P-wave residuals. Upper mantle (depth 131-231 km) at and near the Nevada Test Site. From Monfort and Evans (1982).

Figure 2-10f

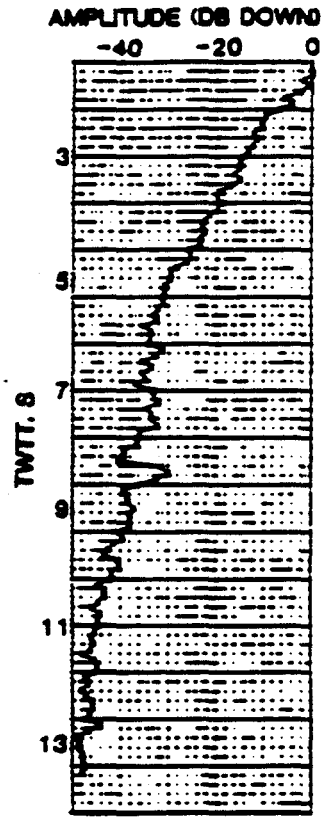

Average amplitude vs. travel time decay curve. 40 traces from the explosion record for the shot at station 1549. From Brocker et al. (1989).

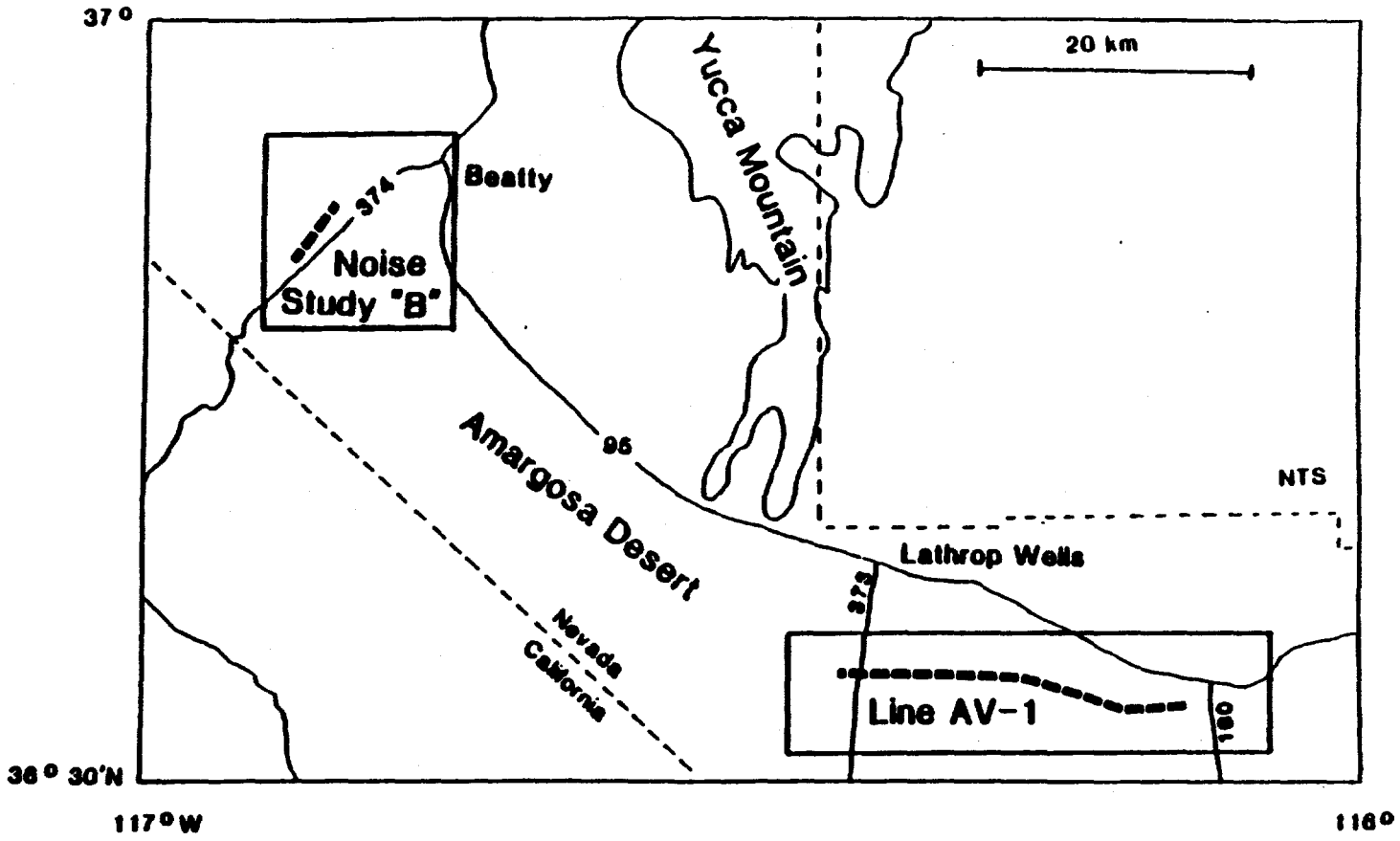

Location map. The Amargosa Desert seismic line AV-1. From Brocker et al. (1989).

Figure 2-11b

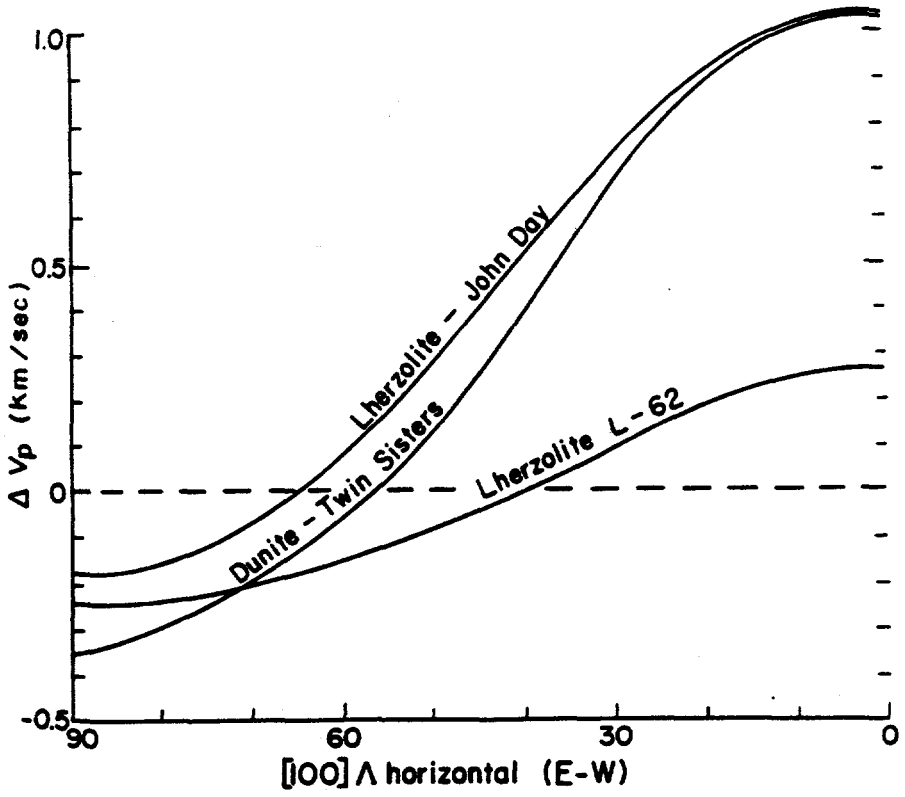

P-wave velocity anisotropy as a function of [100] concentrations to the horizontal, natural specimens of lherzolites and dunites. From Carter et al. (1972).

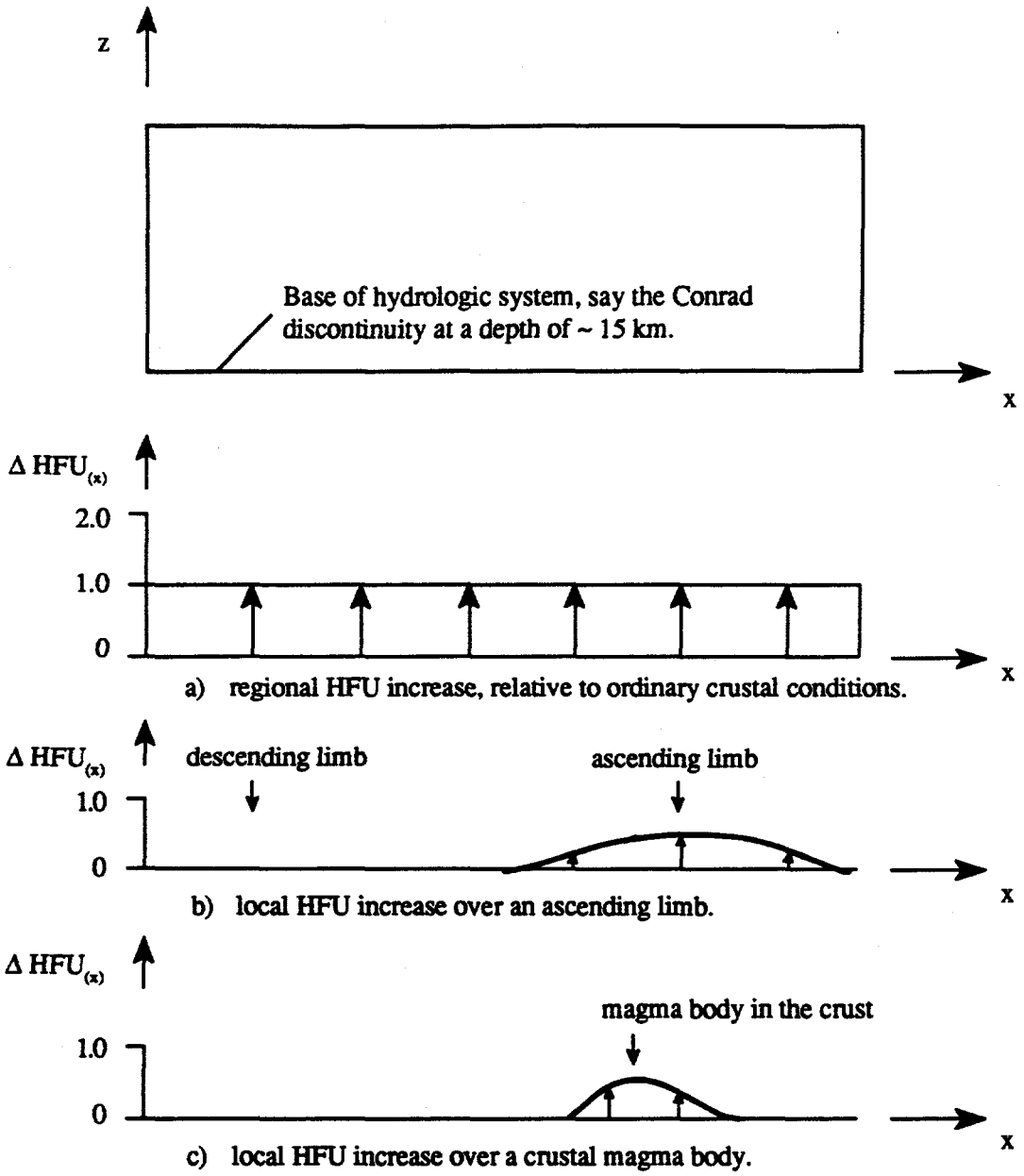

Note:

a) in the Yucca Mountain region, the heat flux from the upwelling mantle ranges from 2.0 to about 2.5 HFU; and

b) over crustal magma bodies, the heat flow may be as high as 2.5-3.0 HFU.

Estimate of heat flow, the Yucca Mountain region.

Figure 2-13

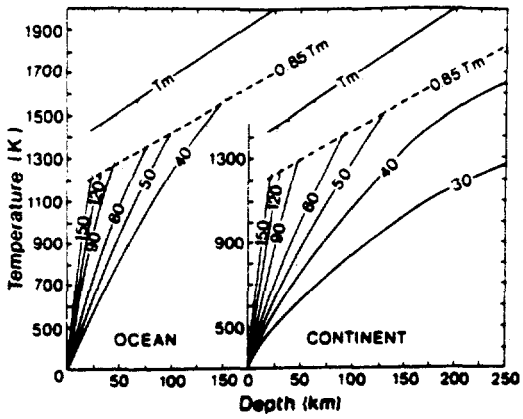

a) Lithospheric thickness as a function of heat flow [mW/m^2]. From Ranalli, 1987.

Note: for Great Basin, the representative thickness of the lithosphere is ~ 30km, Scholtz et al. 1971.

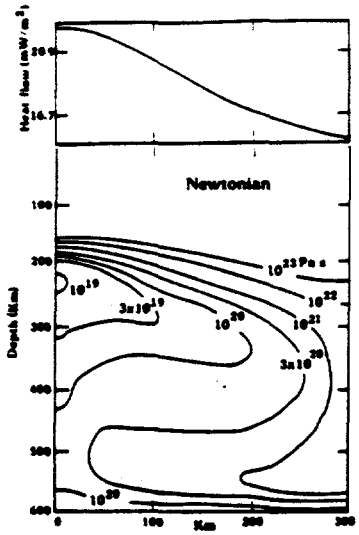

b) Heat flow over a convective instability in the upper mantle. From Fleitout and Yuen, 1984.

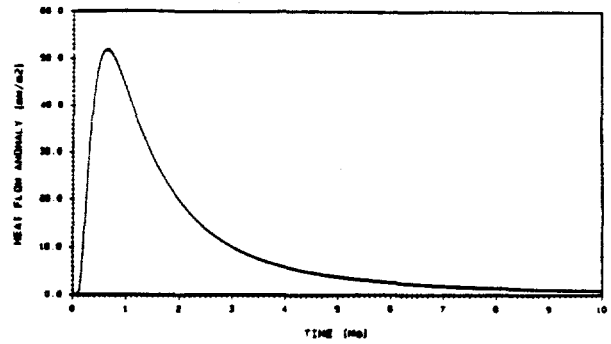

c) Heat flow over an intrusive body in the crust. From Griesser and Rybach (1987).

Heat flow for various geodynamic configurations.

Figure 2-14

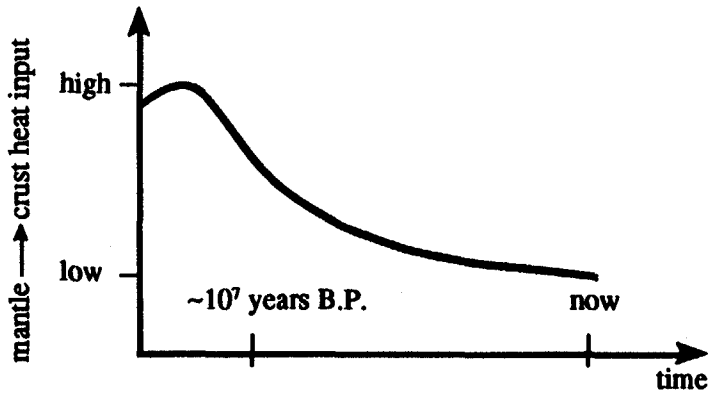

a) advective.

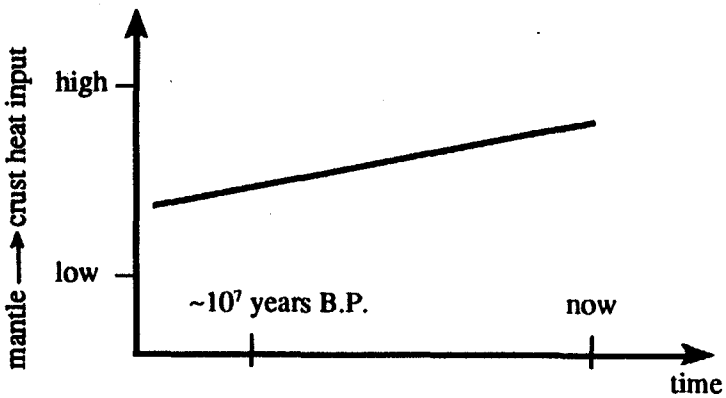

b) conductive.

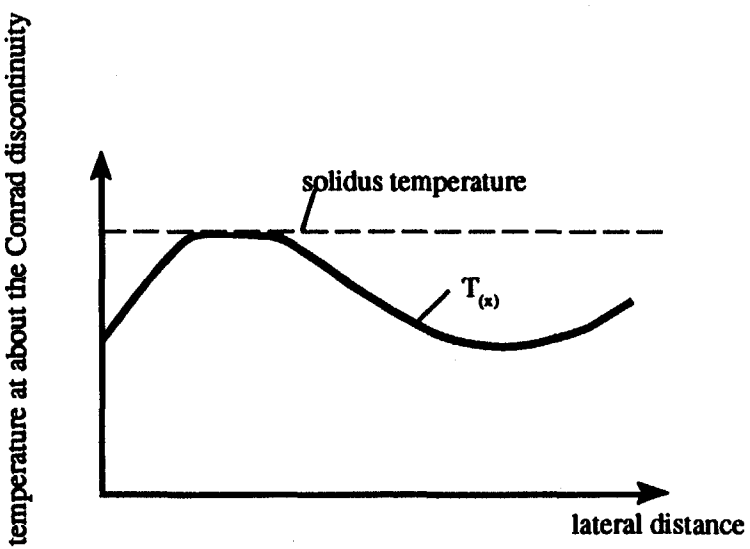

c) ~10⁷ years B.P.

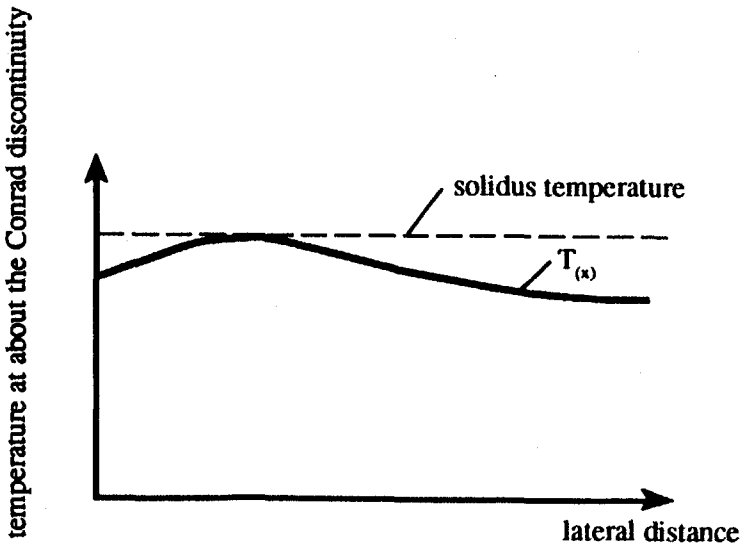

d) present time.

Schematic representation of the thermal states of the crust as a function of time. The Yucca Mountain region.

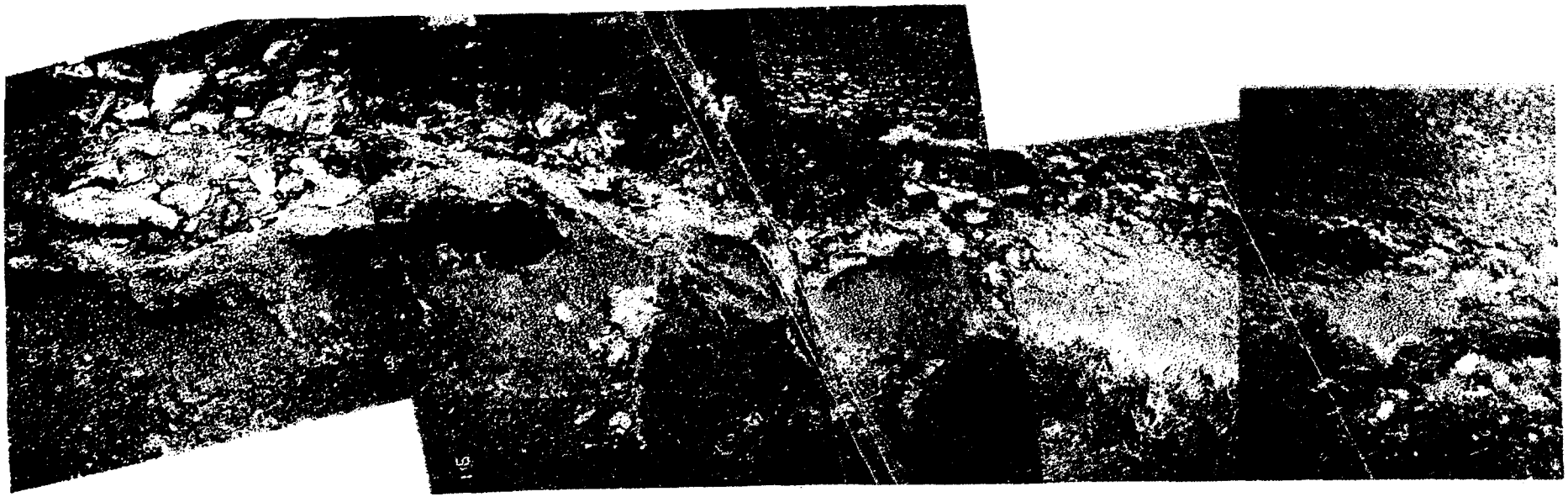

Note:

a) host rock is the Pah Canyon - Yucca Mountain Member of the Paintbrush Tuff.

Example - fault-based oxidation of unwelded ignimbrites (1 km north of Stage Coach Road).

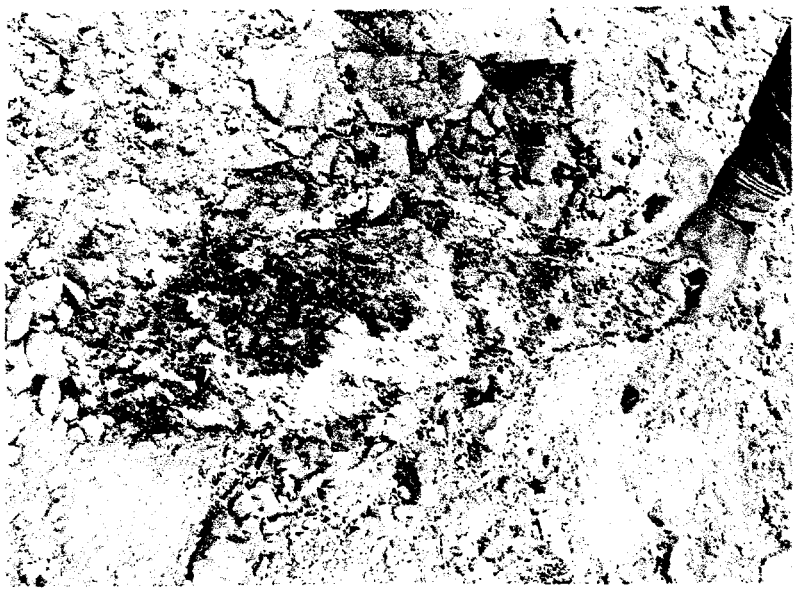

a) Hydro-clastic injection (?) dike, the host rock is the "columnar zone" of the Tiva Canyon Member.

b) hydraulic fracture (?) calcite residuum, the host rock is the bedded tuff from the Upper Topopah Spring Member.

Example - possible epigenetic hydrothermal features, Harper Valley.

a) Hydro-clastic injection (?) dike, the host rock is the "columnar zone" of the Tiva Canyon Member.

b) close-up.

Example - possible epigenetic hydrothermal features, Harper Valley.

Figure 3-3

a) the lower Harper Valley boiling (?) zone.

b) the upper Harper Valley boiling (?) zone.

Example - possible epigenetic hydrothermal features in unwelded tuff.

Figure 3-4

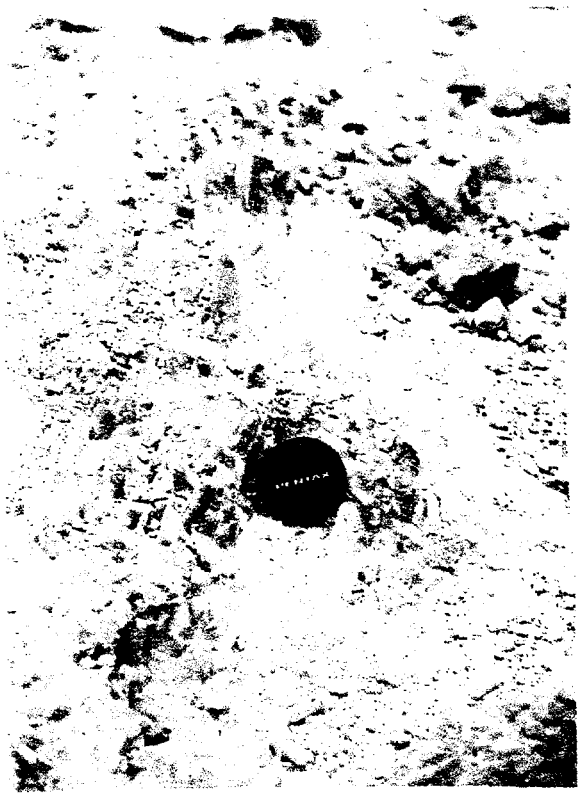

a) the lower Harper Valley boiling (?) zone.

b) the upper Harper Valley boiling (?) zone.

Example - possible epigenetic hydrothermal features in poorly cemented eolian sand.

Figure 3-5

a) splay of the Solitario Canyon fault.

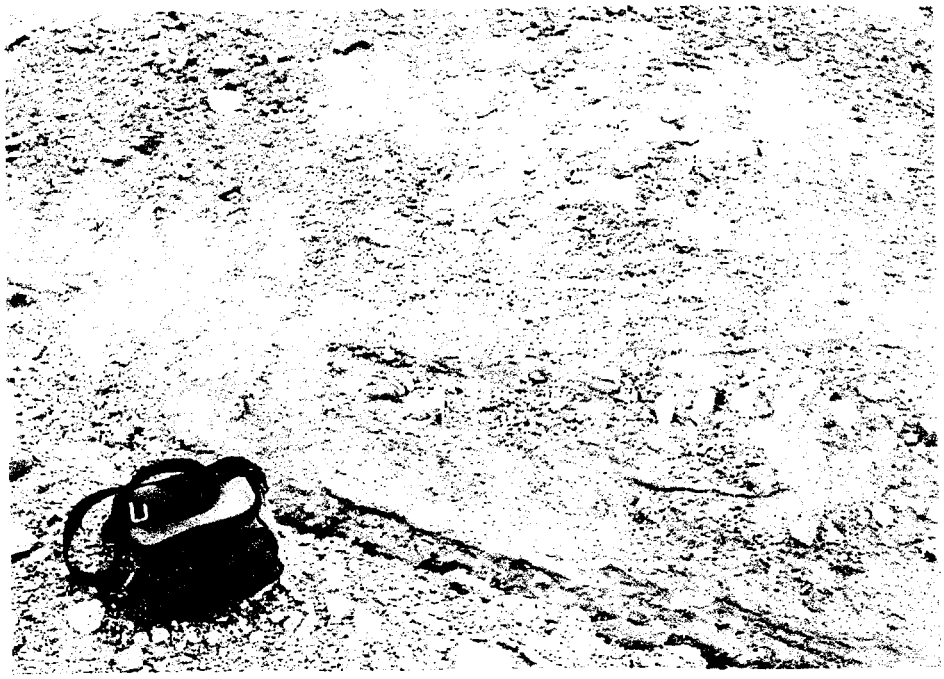

b) Windy Wash fault.

Example - GS-textured calcretes.

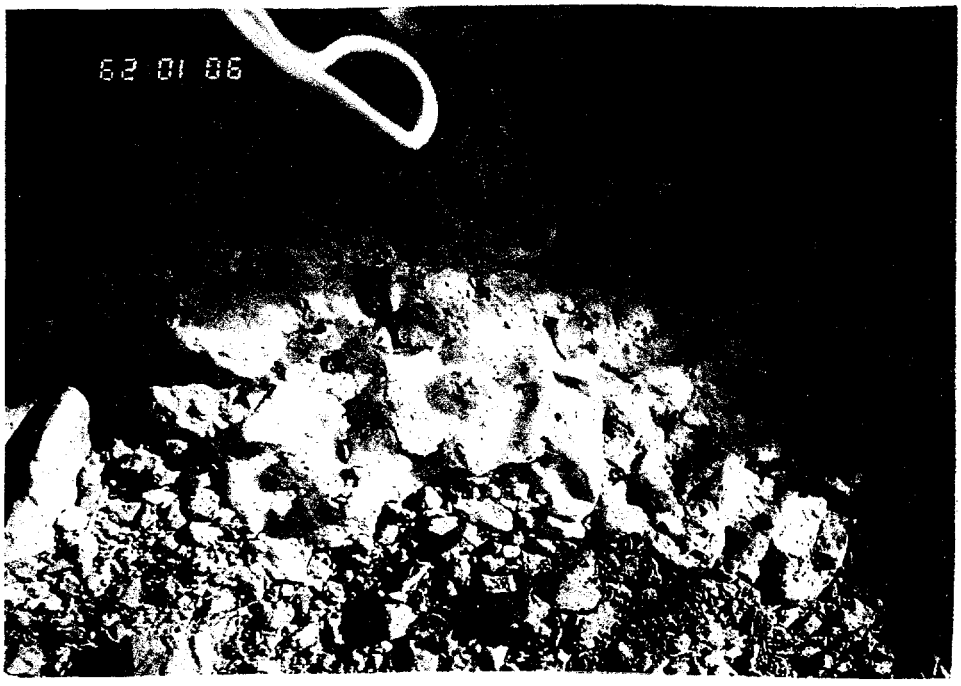

Example - F-textured calcrete (south-central Yucca Mountain).

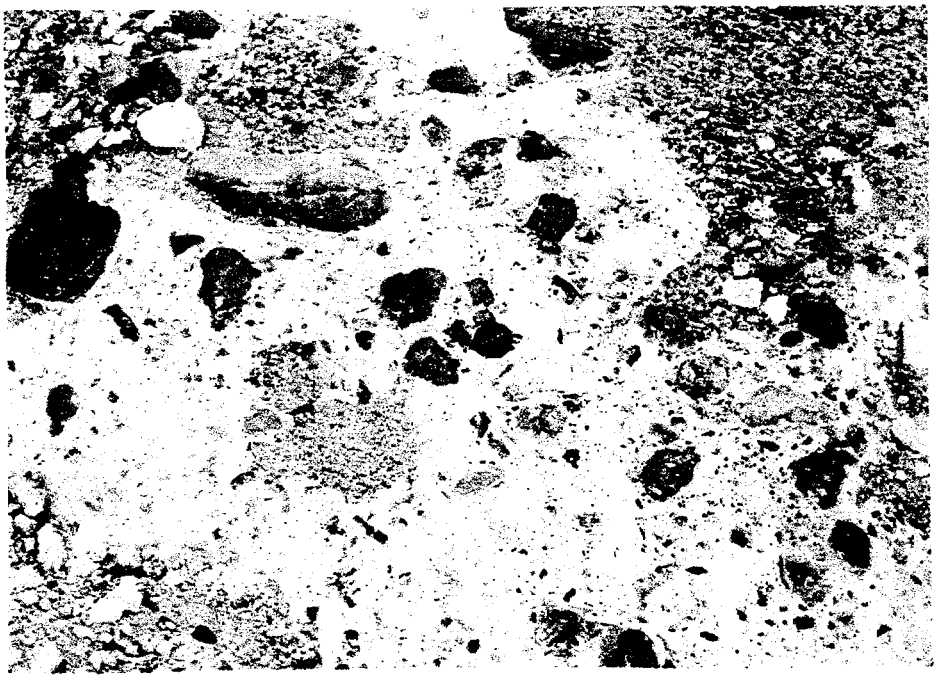

Example - F-textured calcretes

Figure 3-8

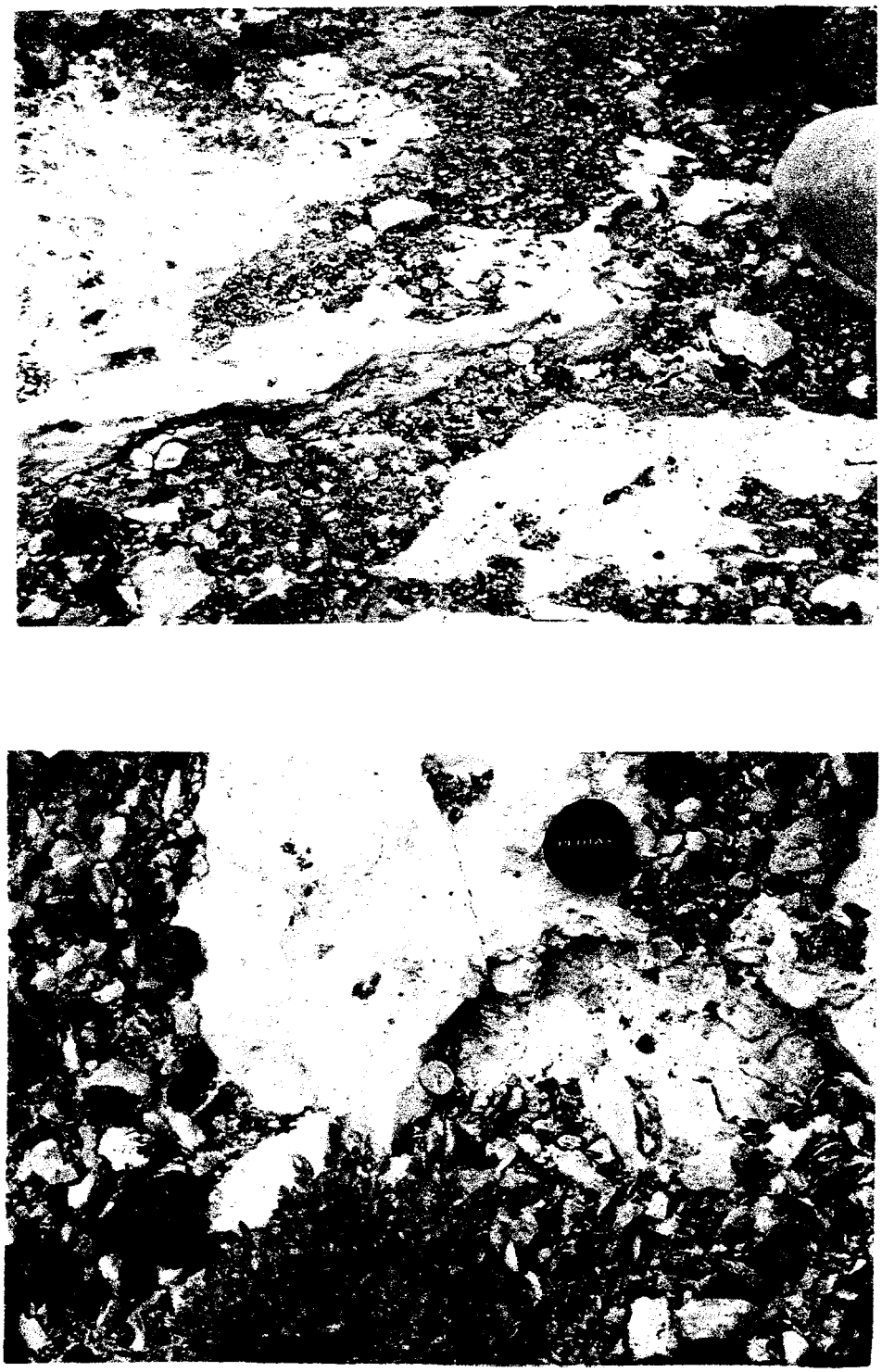

Example - M-textured calcretes or sinters (Solitario Canyon fault).

Example - M-textured calcretes or opal-carbonate laminated sinters (well pad WT#7).

Figure 3-10

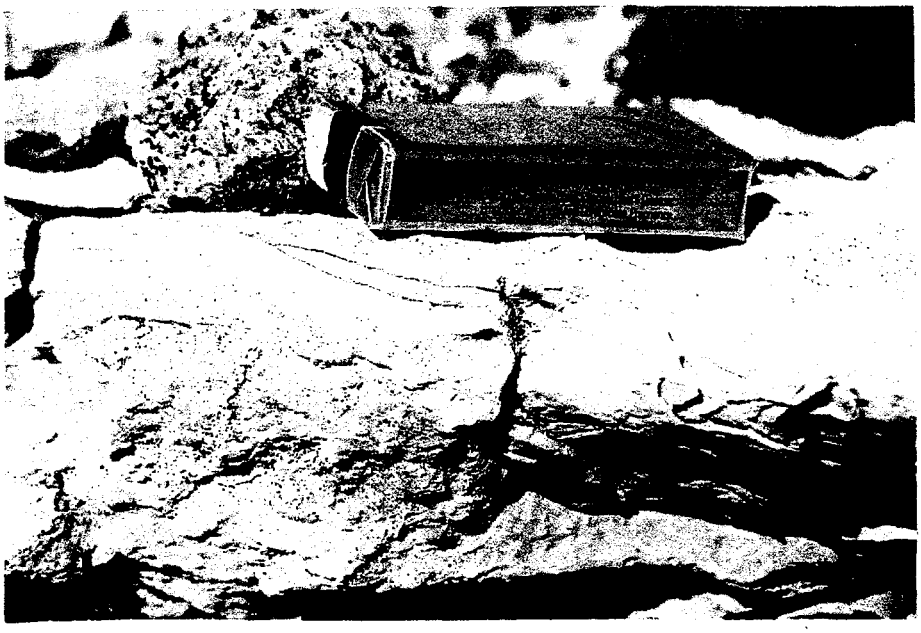

Example - M-textured, laminated calcretes or sinters.

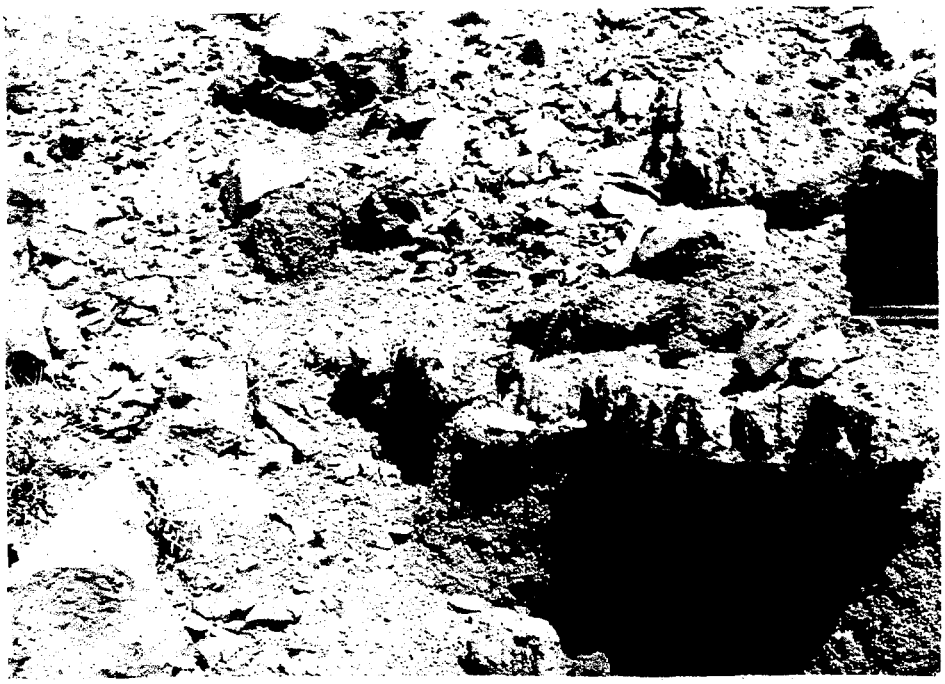

a) silica vein emplaced within locally altered unwelded tuff.

b) jasperoidal opal cementing (impregnating) unwelded tuff.

Example - localized hydrothermal oxidation and silicification (Solitario Canyon and Harper Valley).

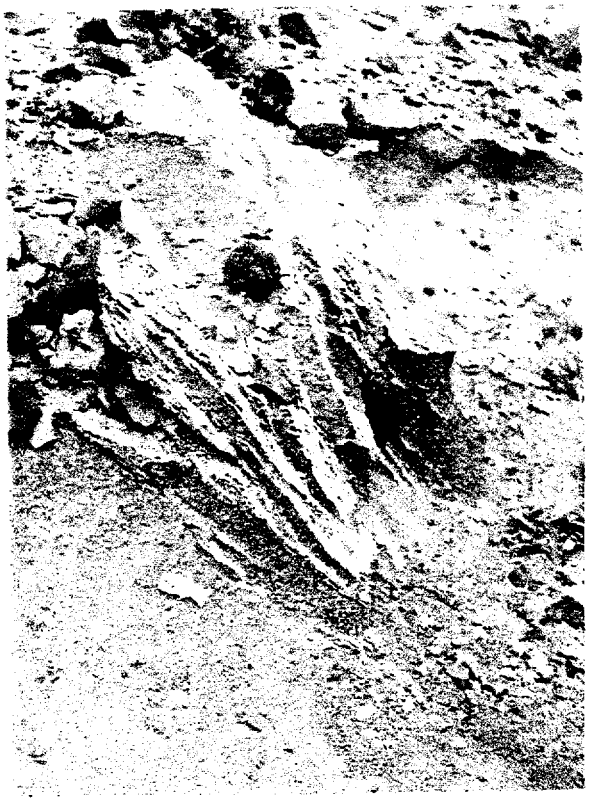

a) the host rock is the Yucca Mountain - Pah Canyon Member of the Paintbrush Tuff, Harper Valley.

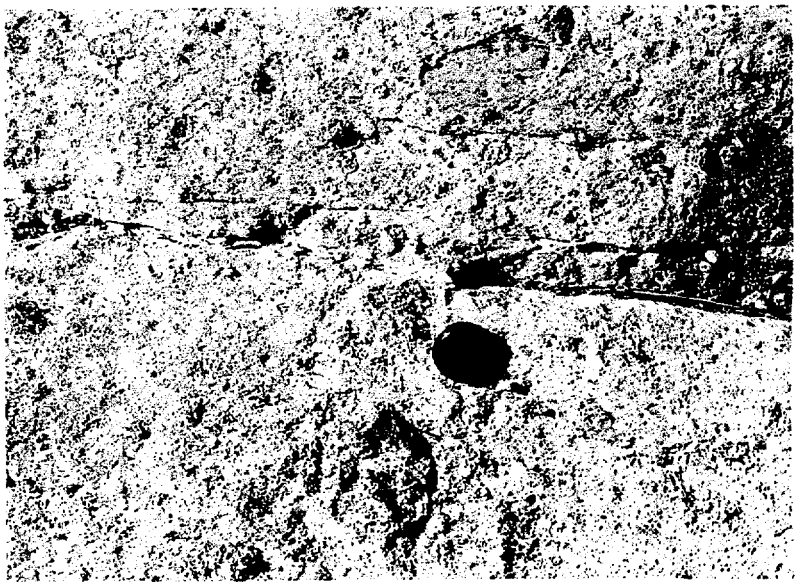

b) the host rock is the Ammonia Tanks Member of the Timber Mountain Tuff, around Stage Coach Road.

Example - calcitic veins emplaced within oxidized unwelded ignimbrites.

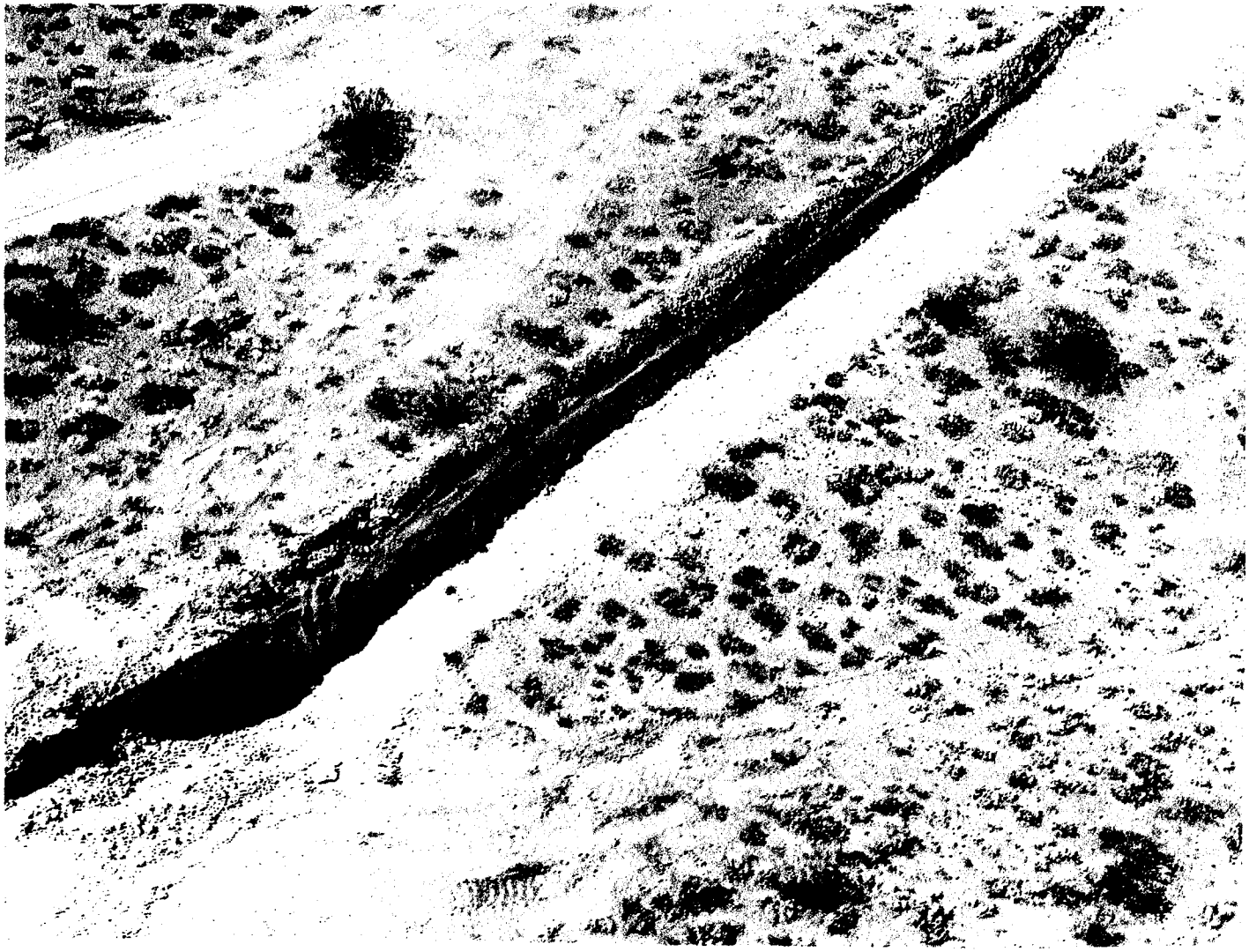

Example - the calcretes and associated bedrock veins (the Trench #14 exposure).

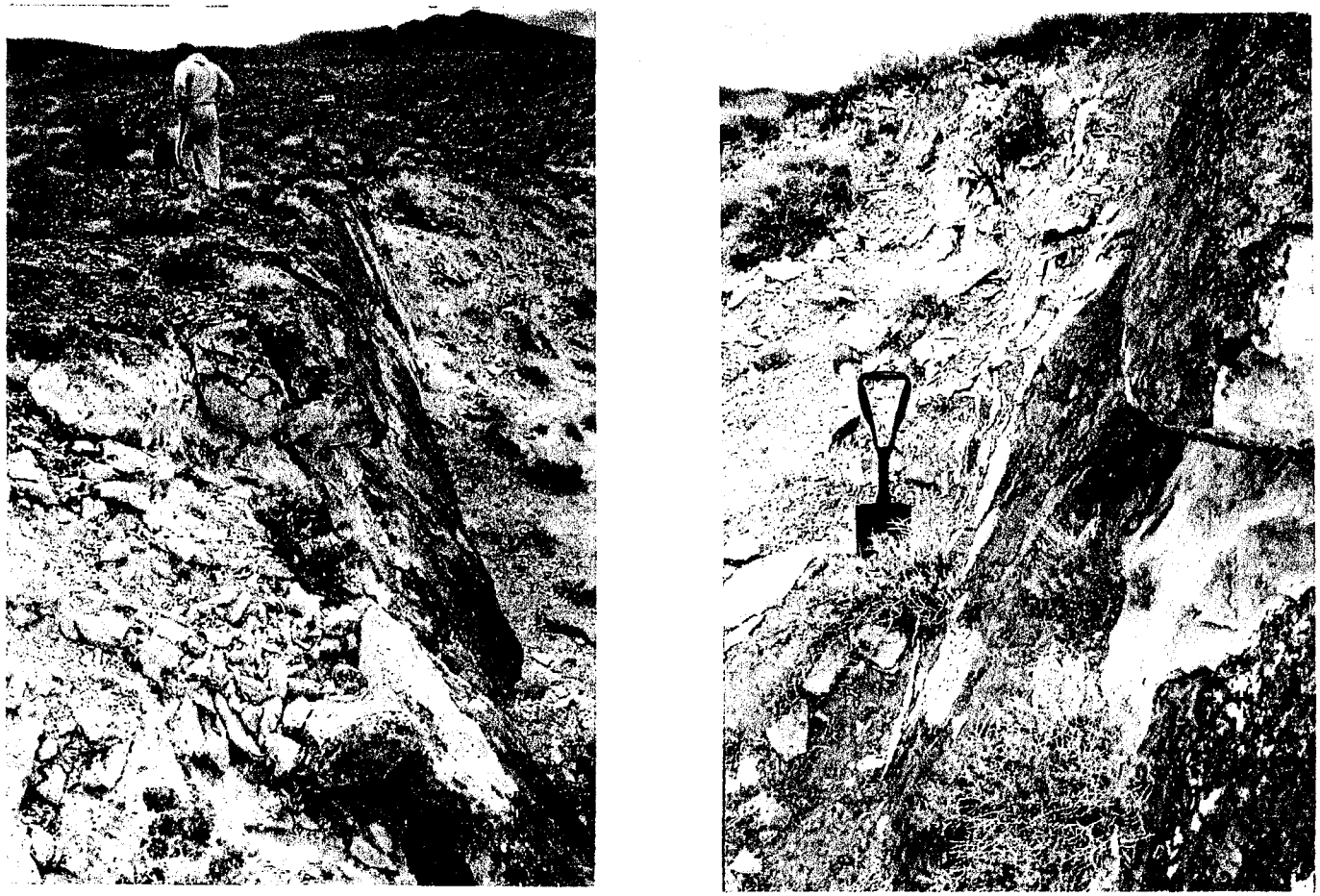

Note:

a) the 8-10 in thick vein, composed of micritic calcite intercaleted with opaline silica, occurs between bedrock and loose eolian sand.

Example - calcite-opaline silica vein (the so-called "Wailing Wall" fault).

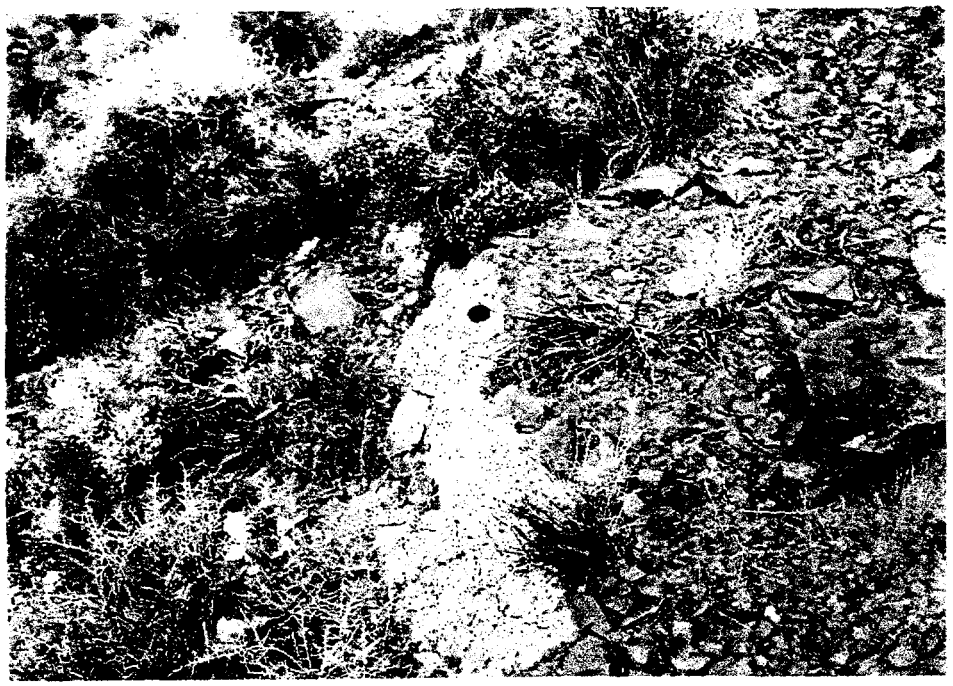

a) vein emplaced along the Solitario Canyon fault scarp.

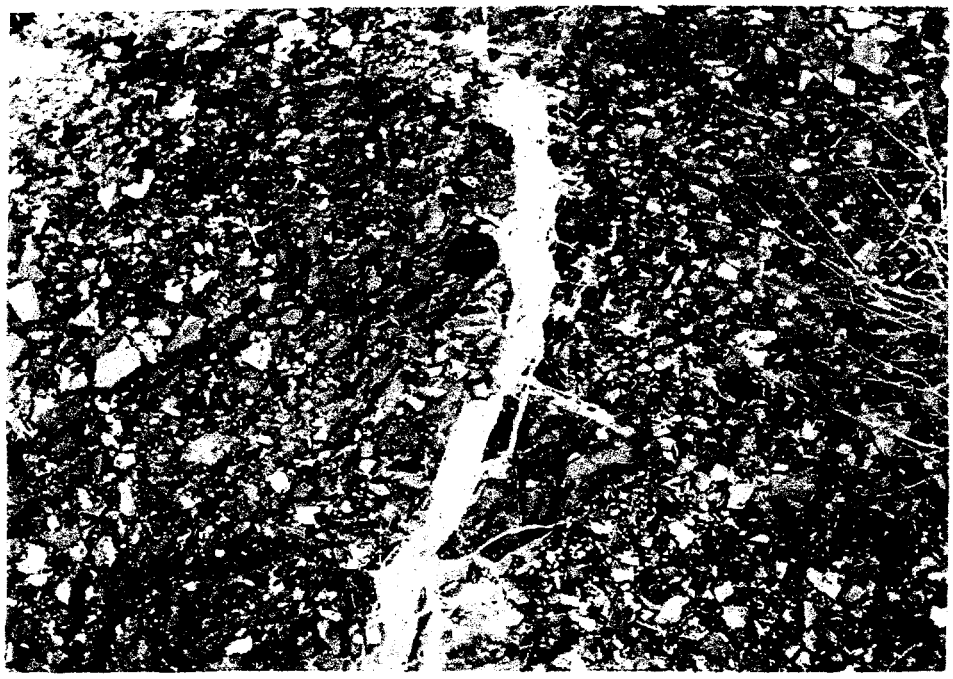

b) bedrock vein associated with explosive (?) fragmentation of bedrock (well pad WT#7).

Example - laminated calcite-opal veins.

a) calcretes and associated veins - sand ramps at Busted Butte.

b) silica tubes along fault-scarp contact between unwelded tuff and fine-grained eolian sand.

Example - "intrusions" of calcite and opaline silica into unconsolidated eolian sands.

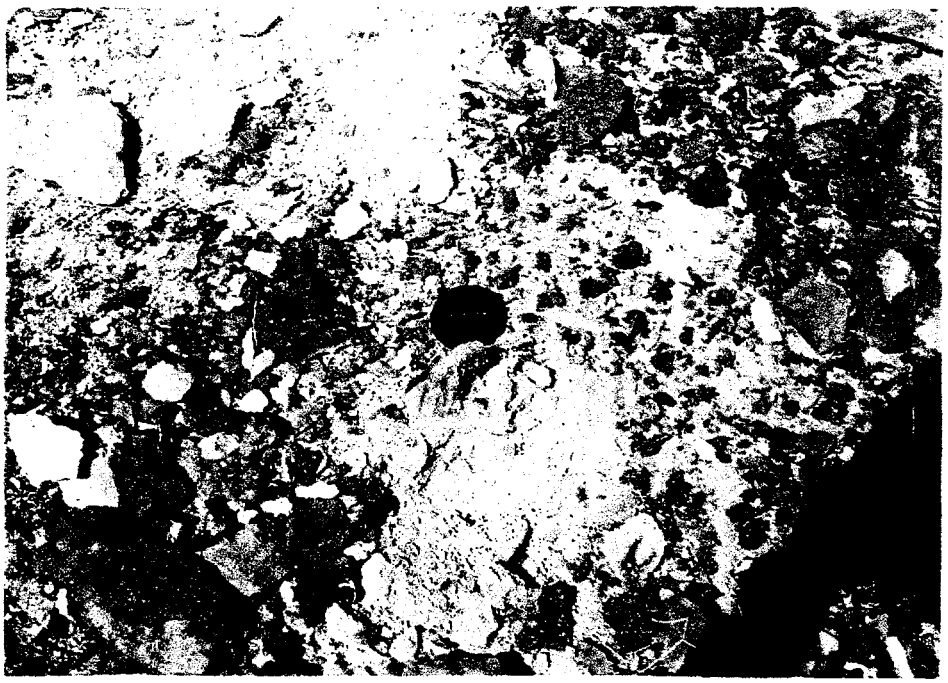

a) silica "tube" in a fine-grained eolian sand.

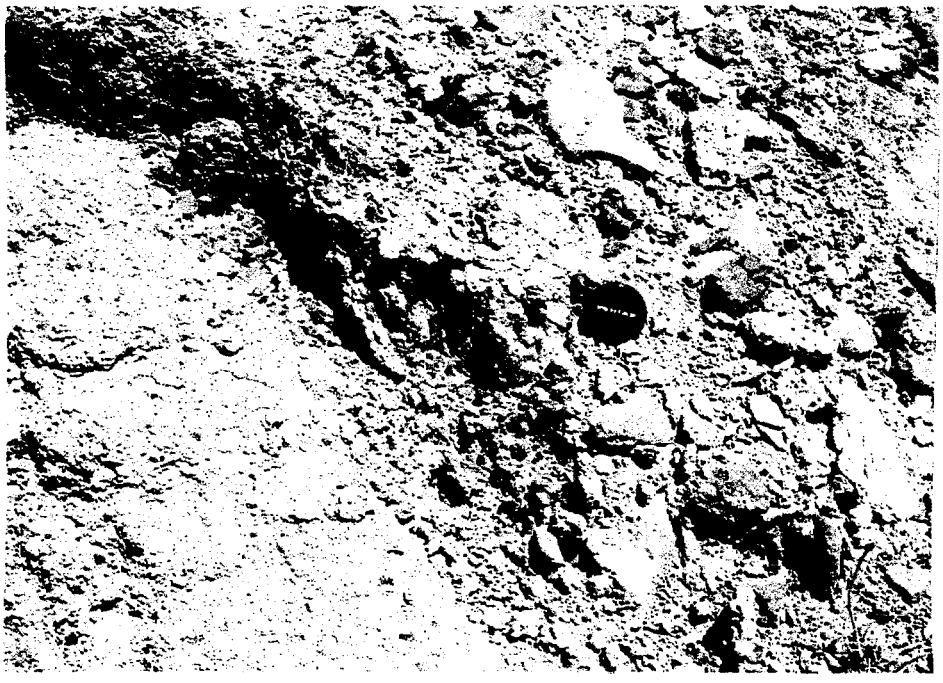

b) silica "tubes" along fault-scarp contact between unwelded tuff and fine-grained eolian sand.

Example - "intrusions" of calcite and opaline silica into unconsolidated eolian sands.

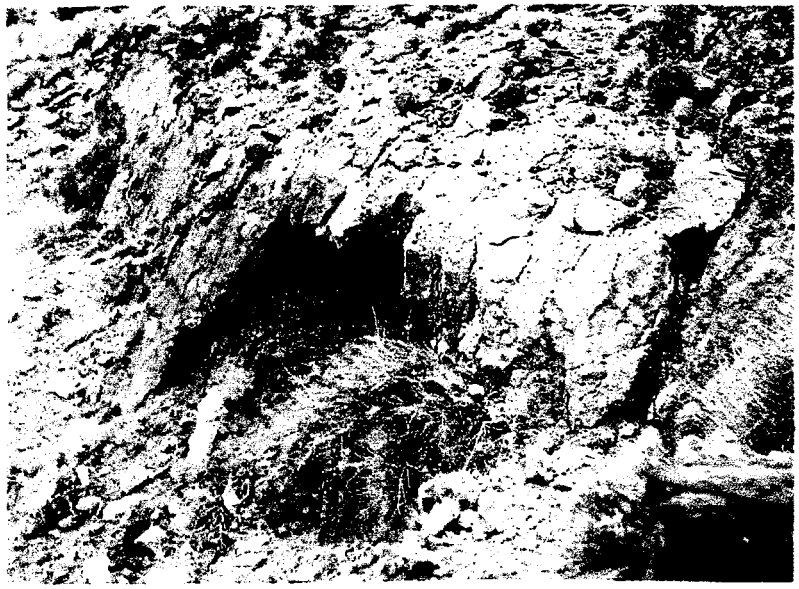

a) jasper opal vein and the associated bleaching of the Tiva Canyon footwall.

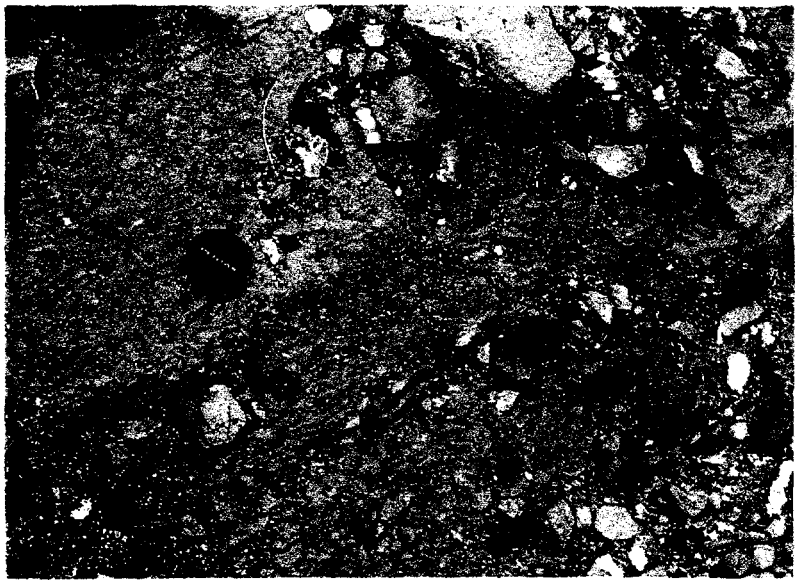

b) silicification and localized oxidation of the Pah Canyon hanging-wall.

Example - epigenetic hydrothermal alteration and silicification, the upper Harper Valley Fault.

a) silicification and carbonatization of the brecciated and altered Topopah Spring Member vitrophyre.

b) devitrified Topopah Spring Member with botryoidal opal.

Example - epigenetic hydrothermal alteration and silicification, the upper Harper Valley Fault.

a) vent oxidation - Pah Canyon Member of the Paintbrush Tuff.

b) breccia and associated devitrification - upper vitrophyre of the Topopah Spring Member of the Paintbrush Tuff.

Example - localized hydrothermal oxidation and devitrification (southern Yucca Mountain).

a) around Stage Coach Road.

Example - "mosaic" breccia.

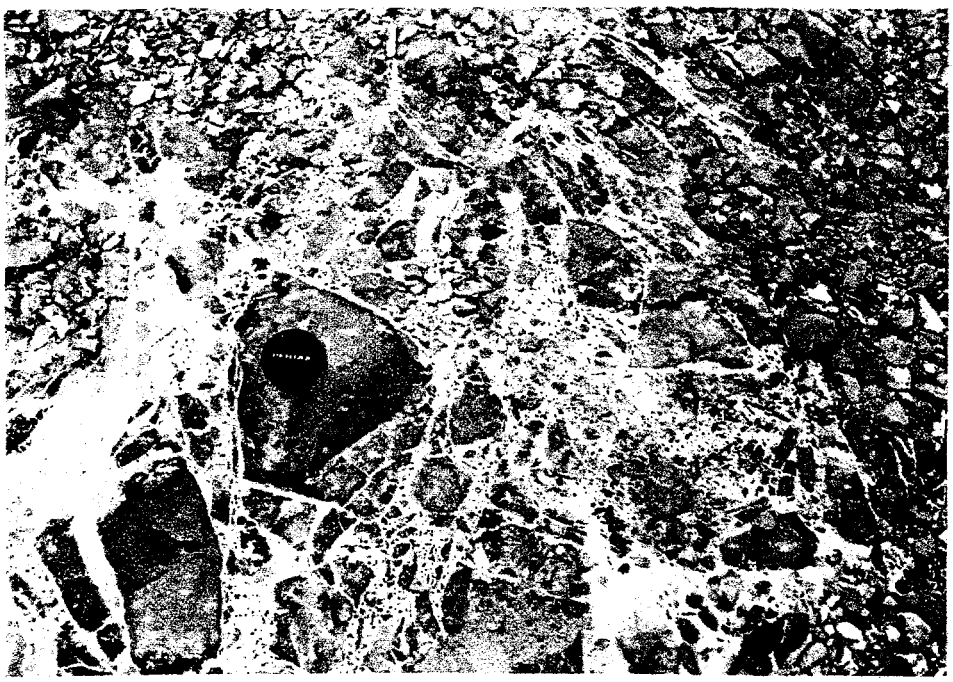

a) explosive breccia ?

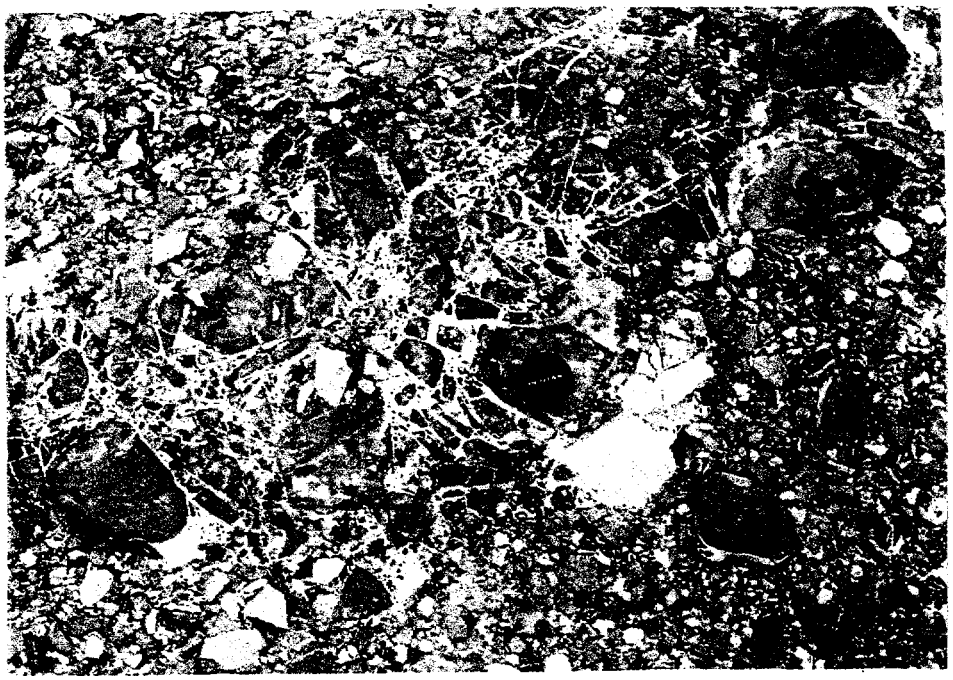

b) explosive breccia ?

Example - "mosaic" breccias (well pad WT-#7 - Solitario Canyon).

Figure 3-22

a) Solitario Canyon "explosive" breccia ?

b) Trench #14 "fragmentation" breccia.

Example - "mosaic" breccias.

Figure 3-23

Note:

a) host rock is unwelded - partially welded tuff between the Tiva Canyon and Topopah Spring Members of the Paintbrush Tuff.

Example - breccia dikes (north-east flank of Harper Valley).

Note:

a) host rock is unwelded - partially welded tuff between the Tiva Canyon and Topopah Spring Members of the Paintbrush Tuff.

Example - breccia dikes (eastern flank of Harper Valley).

Figure 3-25

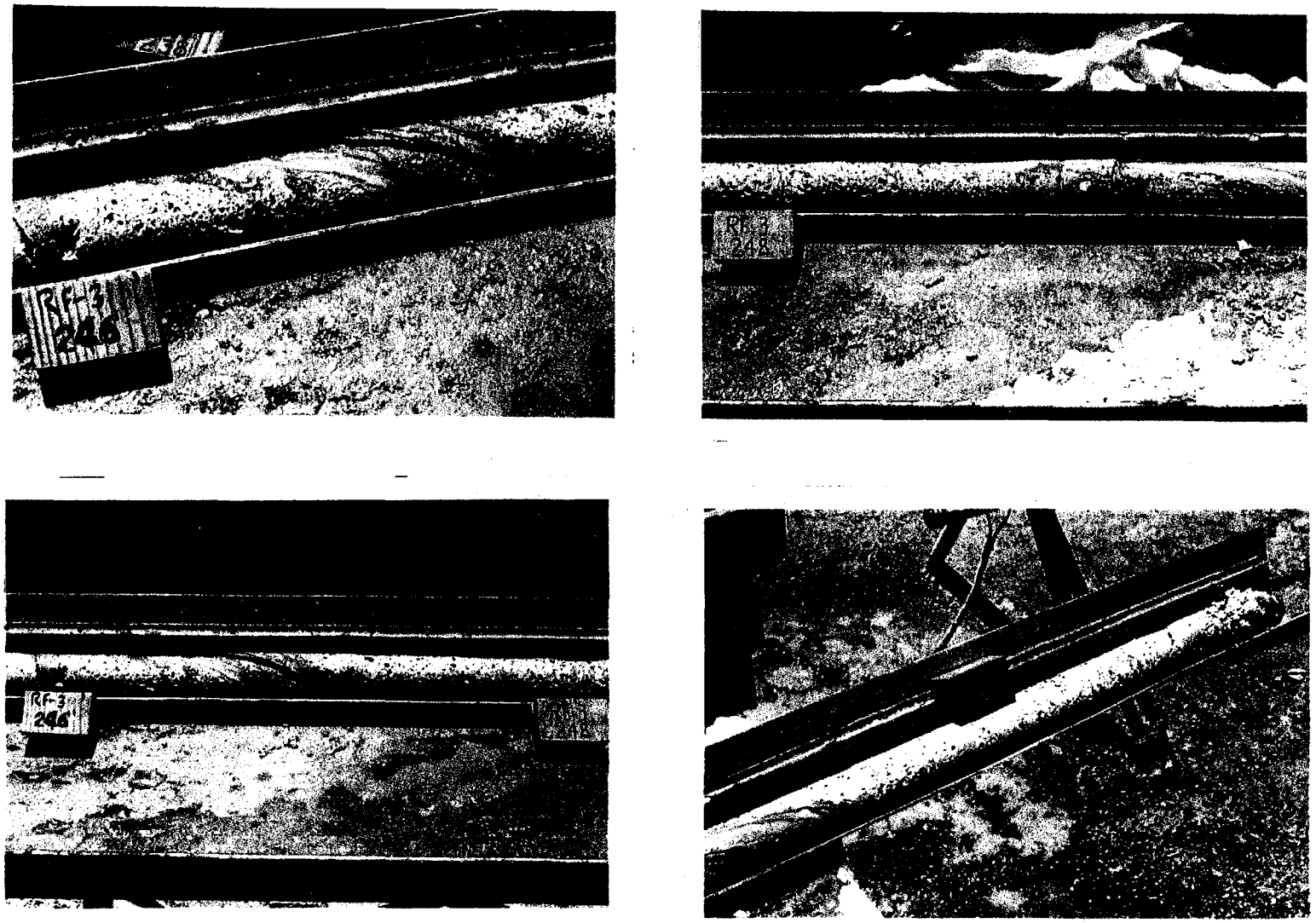

Example - travertine vein, Yucca Mountain vadose zone (a few hundred meters east of Trench #14).

Figure 4-1

Example - calcitic veins, Yucca Mountain vadose zone.

Figure 4-2

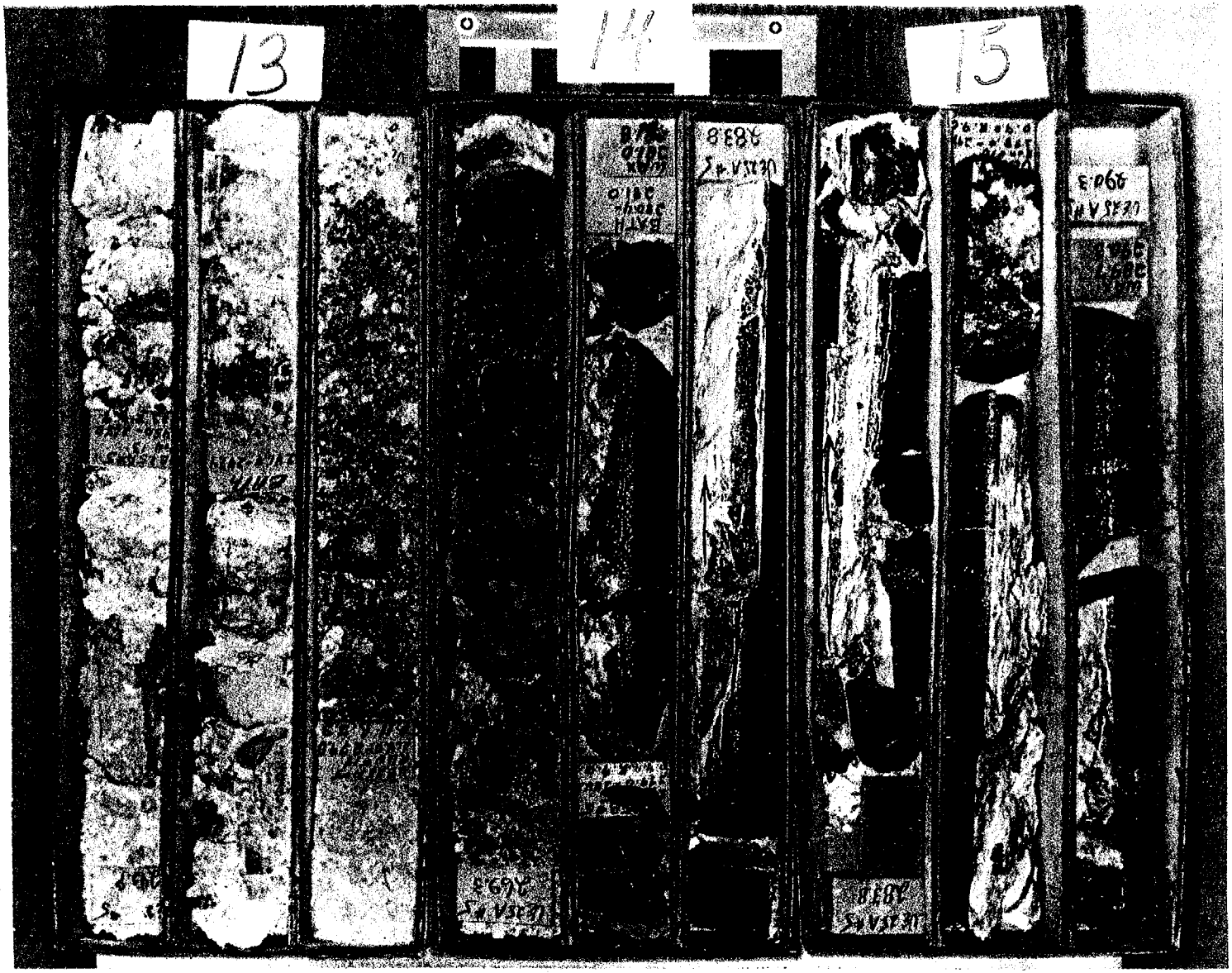

Example - calcitic veins, Yucca Mountain vadose zone.

Figure 4-3

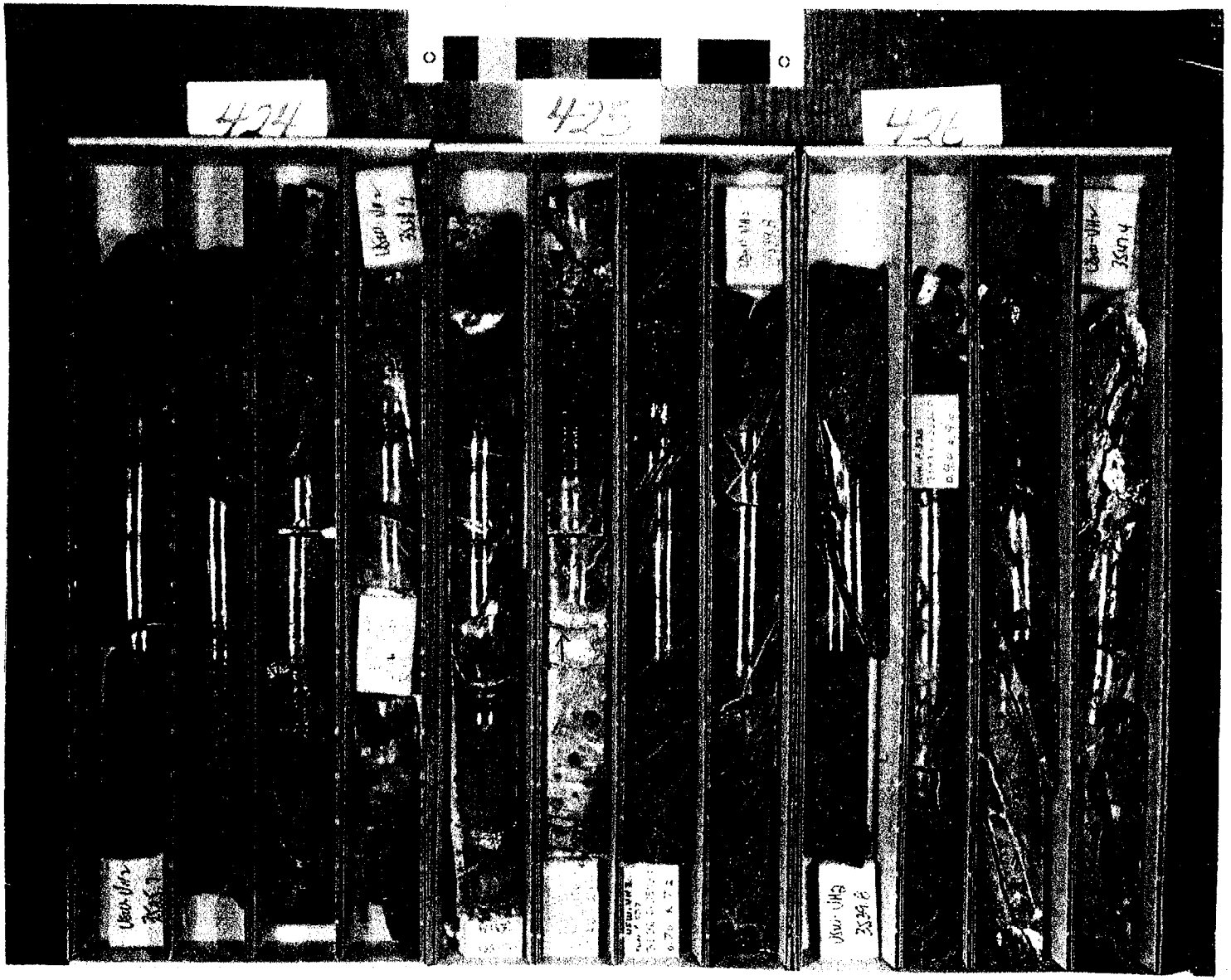

Example - fracture-based devitrification and mineralization of the Topopah Spring Member vitrophyre, Yucca Mountain vadose zone.

Figure 4-4

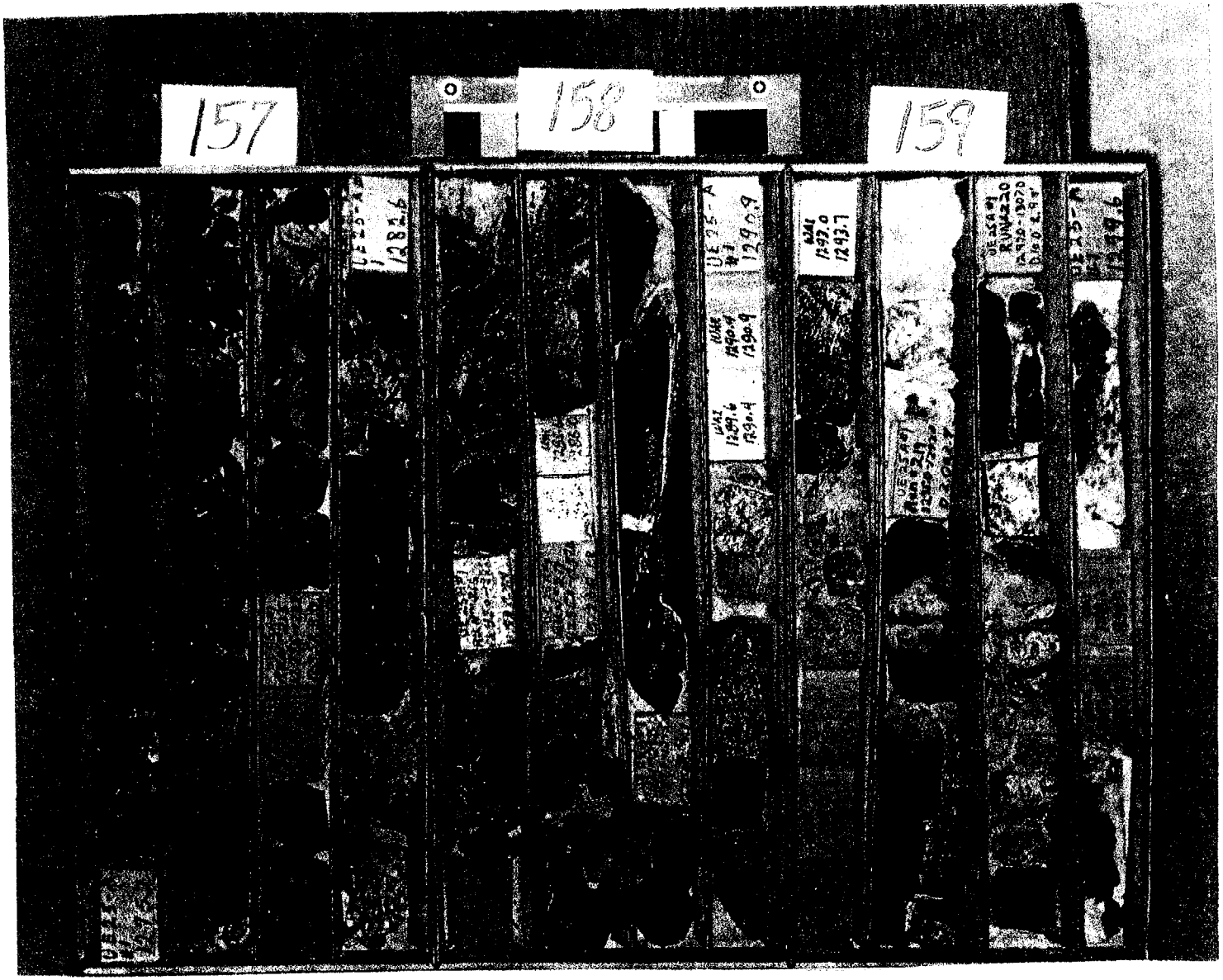

Example - fracture-based devitrification and mineralization of the Topopah Spring Member vitrophyre, Yucca Mountain vadose zone.

Figure 4-5

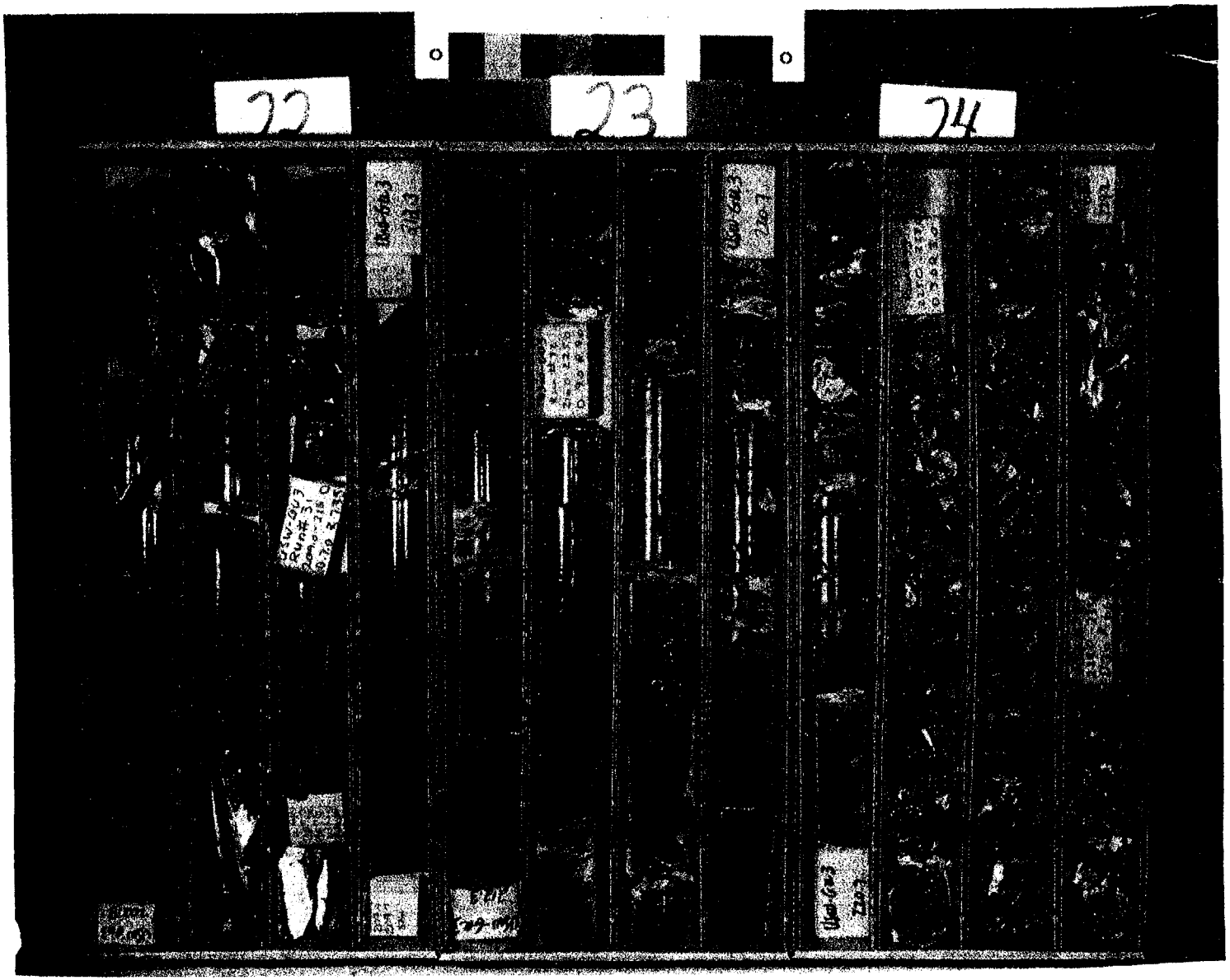

Example - fracture-based devitrification and mineralization of the devitrified Topopah Spring Member, Yucca Mountain vadose zone.

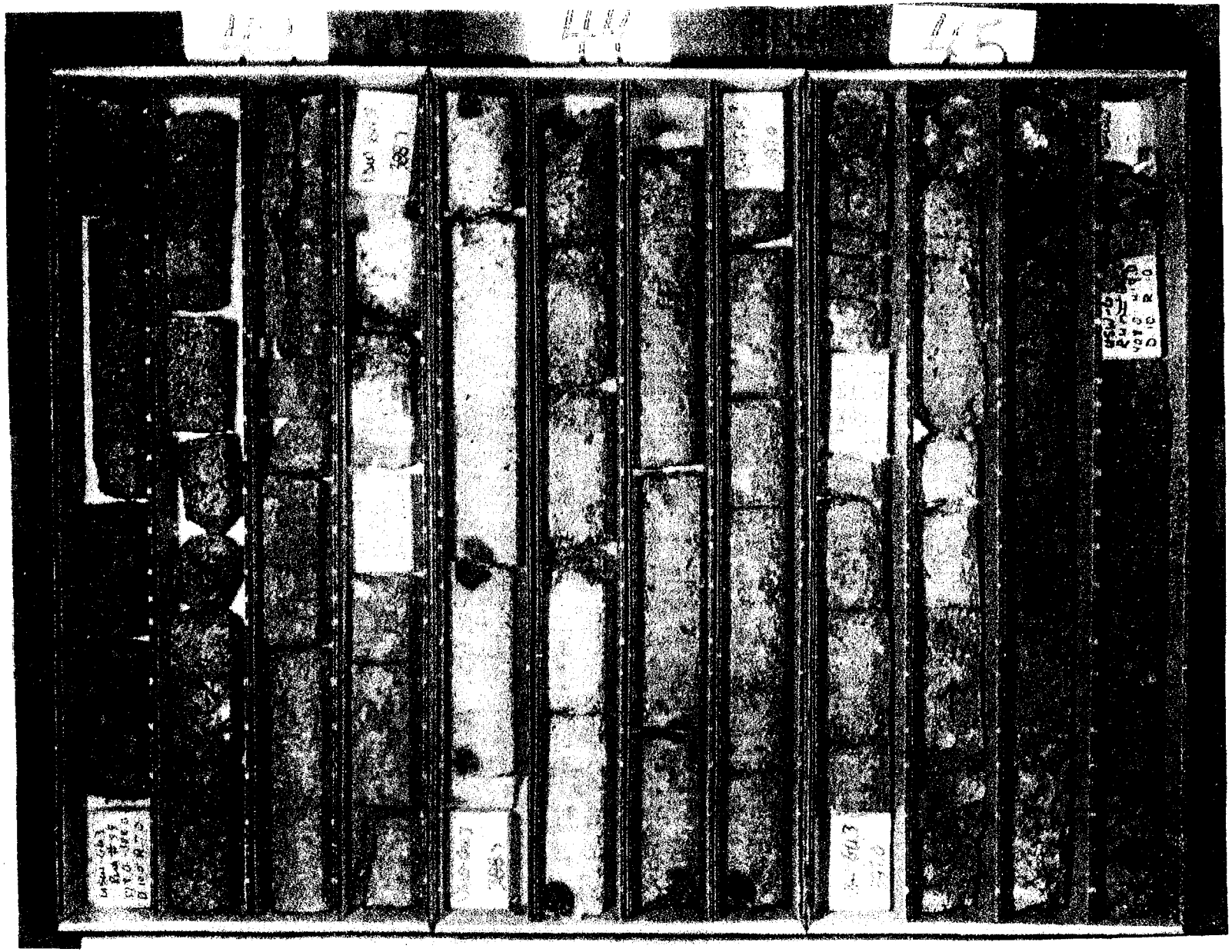

Example - hydrothermal oxidation of the hanging-wall of a fault encountered in USW GU-3 borehole, Yucca Mountain vadose zone.

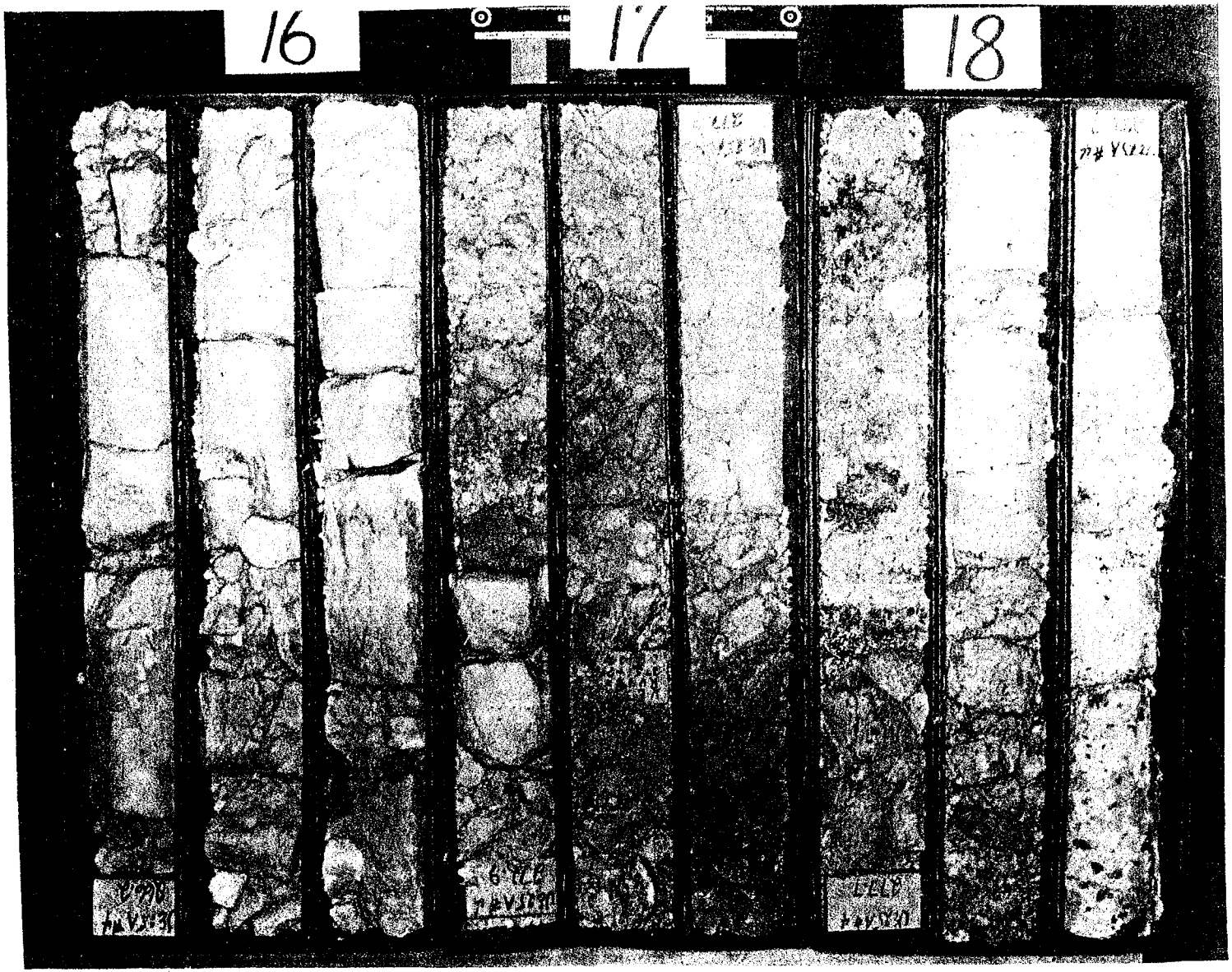

Example - hydrothermal oxidation of a fault encountered in UE-25A#4 borehole, Yucca Mountain vadose zone.

Figure 4-8

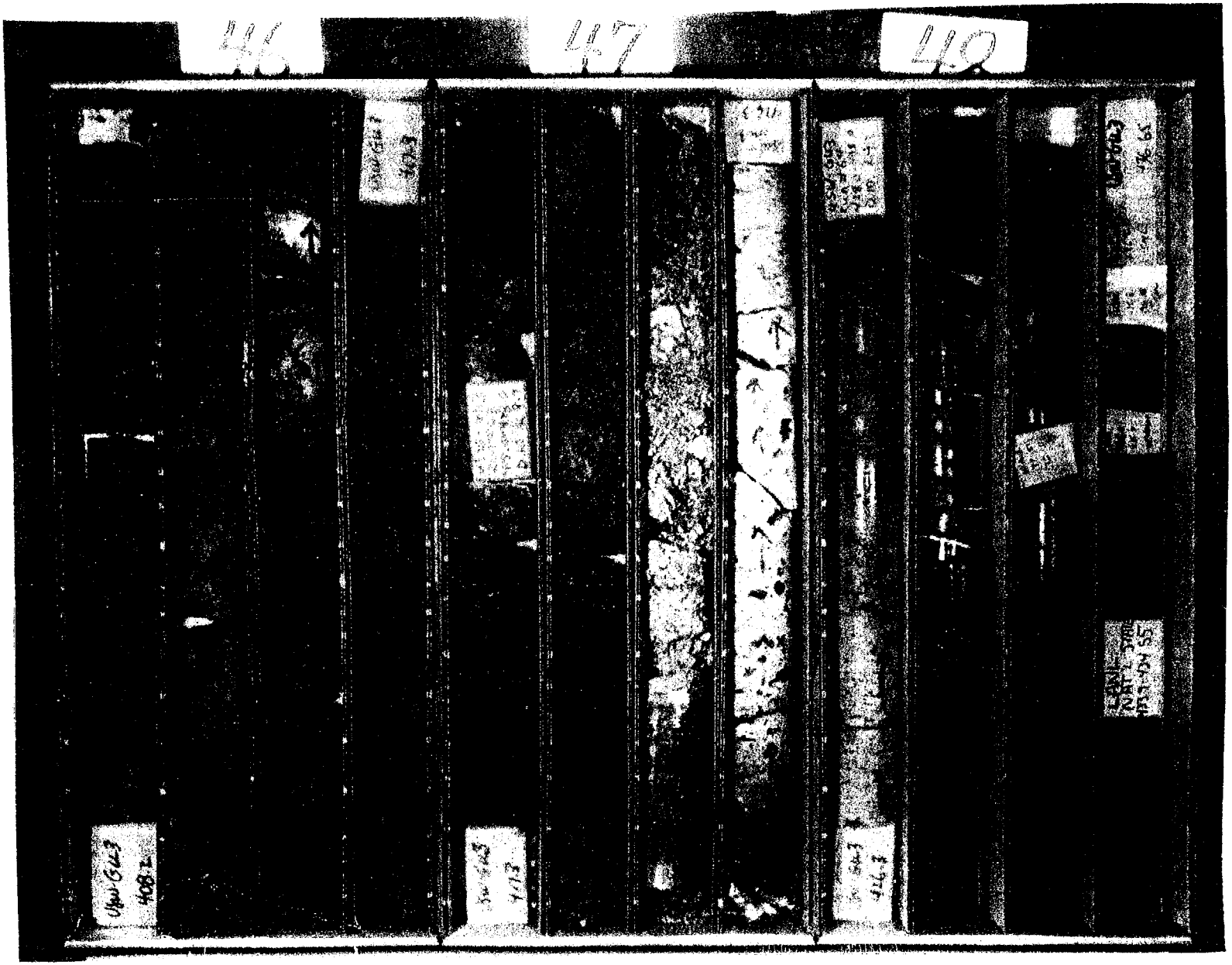

Example - hydrothermal bleaching of the footwall of a fault encountered in USW GU-3 borehole, Yucca Mountain vadose zone.

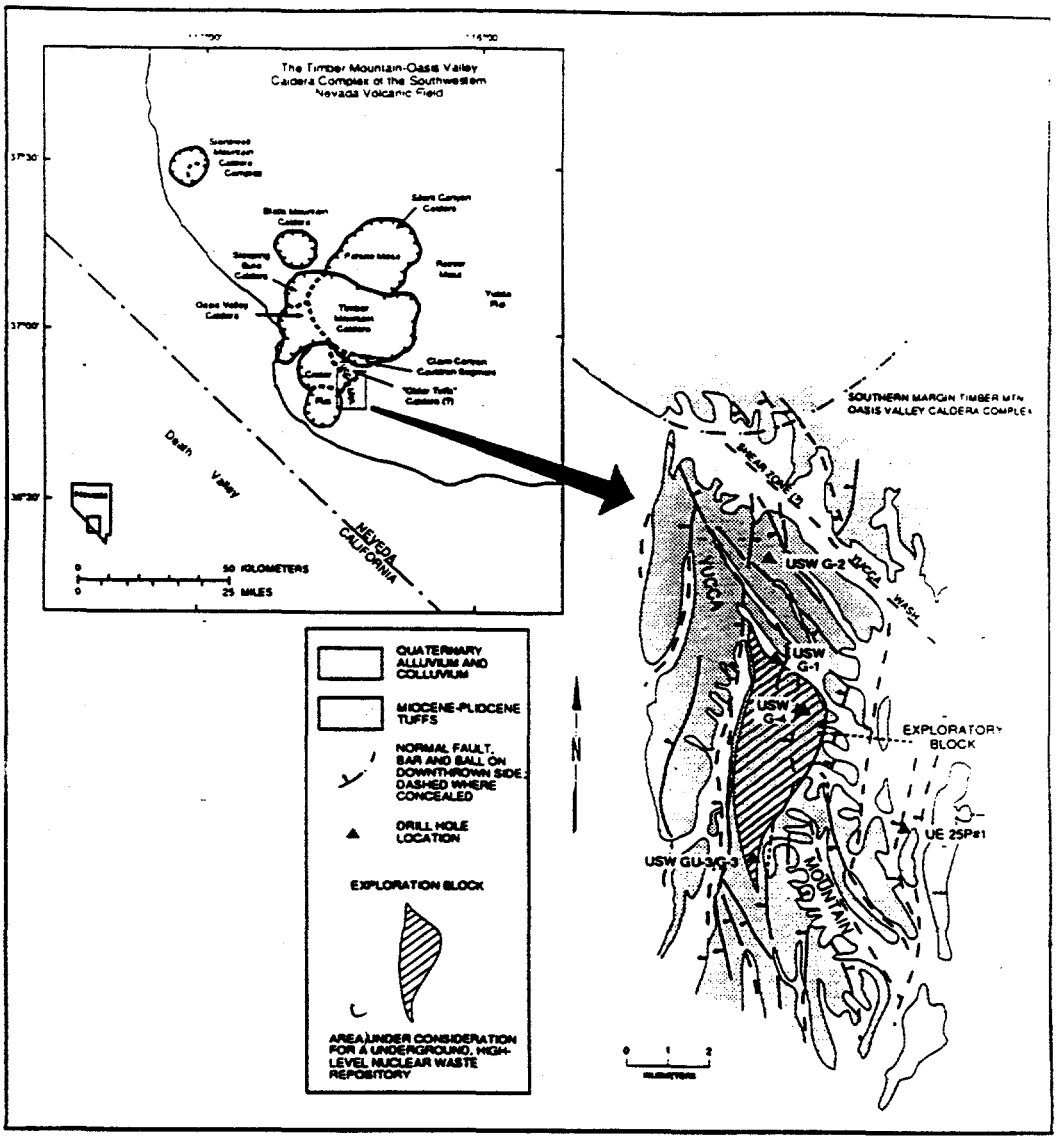

Location map of Yucca Mountain, Nevada. The candidate repository is diagonally shaded. Solid triangles indicate the locations of the exploratory drill holes. Inset map shows the location of Yucca Mountain with reference to the Timber Mountain-Oasis Valley caldera complex. From WoldeGabriel, 1991.

Table I. Qualitative Mineralogy as Determined by XRD for USW G-1 Fracture Samples

USW G-1 Sample	Smect-ite	Heul-andite	Stell-erite	Quartz	Cristob-alite	Opal-CT	Tridy-mite	Feld-spar	Rancie-ite	Lithio-phorite	Other
1104.3/1104.5	Trace	---	---	Major	Minor	---	Minor	Minor	---	---	Hematite[4]
1156.0/1156.4	Major	Trace[2]	---	Major	Minor	---	Minor	Minor	---	---	Hematite[5]
1165.5/1165.8	Major	Trace[2]	---	Major	---	---	Minor	Major	Minor[3]	Major	Hematite[5]
1225.6/1225.9	Major	Trace	Major	Minor	---	---	---	Minor	---	---	
1281.8/1282.0	Trace	Major	???[7]	Trace	Minor	---	---	Trace	---	---	Calcite[6]
1297.0/1297.2	Major	---	---	Minor	---	Major	---	Minor	Trace[3]	---	
1337.0/1337.5	Major	Major	---	Minor	---	Major	---	Minor	Minor[3]	---	
1356.0/1356.3	Trace	Major	---	Minor	---	Major	---	Minor	---	---	

Qualitative Mineralogy as Determined by XRD for USW G-2 Fractures

USW G-2 Sample	Smect-ite	Heul-andite	Morden-ite	Stell-erite	Quartz	Cristob-alite	Opal-CT	Tridy-mite	Feld-spar	Lithio-phorite	Other
1178.4/8.7	Trace	---	---	---	Major	---	---	Minor	Trace	---	Hematite[4]
1282.0/2.1	Trace	---	Trace[2]	---	Major	---	---	Major	Minor	---	Hematite[5]
1447 lithoph	Minor	---	Minor	---	Minor	Major	---	Minor	Major	---	Hematite[5]
1447 breccia	Minor	Minor	Minor	???[7]	Major	Major	---	Trace	Major	---	Hematite[4]
									---	Calcite[6]	
1449	Minor	Major	Major	Major	Minor	???[8]	---	---	Minor	---	
1456	Trace	Trace	Major	---	Minor	???[9]	---	Trace	Minor	---	
1488.2	Minor	---	Trace	???[7]	Major	---	---	???[8]	Minor	---	Hematite[4]
1505.0/5.2	Minor	Trace	Major	Major	Major	???[8]	---	???[8]	Trace	---	
1516.7/7.0	Trace	---	Major	Major	Minor	???[8]	---	---	Minor	---	
1534.4	Trace	Trace	Major	Trace	Minor	Minor	---	---	Minor	---	
1568.8/9.02a	Trace	Major	Minor	Major	Trace	Minor	---	---	---	---	
1568.8/9.01b	Trace	Major	Trace	Major	Major	Minor	---	---	---	---	
1581.0/2.2	Trace	Minor	Major	Major	Minor	???[8]	---	---	Minor	---	
1603.6/4.0	Minor	Major	Major	???[7]	Minor	???[8]	---	---	Trace	Major	Trace[3]
9.7/0.0	Minor	Major	Trace?	???[7]	Minor	Minor	---	---	Minor	---	
1.2/1.4	Major	---	Trace	---	Major	Major	---	---	Major	Minor	Trace[3]
1636.7/6.8	Major	Minor	---	---	Trace	---	---	---	---	---	
1643.8/4.0	Major	Minor	---	---	---	---	---	---	---	---	
1653.4	Major	Major	---	???[7]	Trace	---	Minor	---	Trace	---	
1669	Major	Major	Trace	---	---	---	Major	---	Trace	---	
1680.7	Minor	Major	---	---	Minor	---	Major[10]	---	---	---	Trace[3]
1687.6	Minor	Major	Trace	---	Minor	---	Major	---	Trace	---	

Qualitative Mineralogy as Determined by XRD for USW GU-3 Fracture Samples

USW GU-3 Sample	Smect-ite	Heul-andite	Morden-ite	Quartz	Cristob-alite	Opal-CT	Tridy-mite	Feld-spar	Rancie-ite	Lithio-phorite	Other
799.7/800.0	Minor	---	---	Major	???[9]	---	Minor	Minor	---	---	Hematite[5]
811.0/811.1	Major	---	Trace[2]	Major	Minor	---	Minor	Minor	---	---	Hematite[4]
818.6/819.0	Major	---	---	Major	???[9]	---	Minor	Minor	Trace[3]	Major	Hematite[5]
829.4/829.8a	Major	---	---	---	---	---	---	Trace	---	---	Calcite[5]
829.4/829.8b	Trace	---	---	Minor	Minor	---	---	Trace	---	---	Calcite[6]
846.0/846.2	---	---	---	Major	---	---	Minor	---	---	---	
876.0/876.2	Trace	---	---	Major	---	---	---	Minor	---	---	Hematite[4]
944.5/944.9	---	---	---	Major	---	---	Major	Minor	---	Trace	Hematite[4]
973.0/973.1	---	---	---	Major	---	---	Minor	Trace	---	---	
981.0/981.5	Major	---	---	Major	???[9]	---	Major	Minor	Trace[3]	Minor	
987.5/988.0	Minor	---	---	Major	Minor	---	Major	Major	---	Minor	Hematite[5]
1162.7/1163.0	Major	---	Minor	Minor	Trace	---	---	Minor	Trace[3]	---	Hematite[4]
1189.3/1189.6	Minor	Major	---	Major	---	Minor	---	Trace	Trace[3]	---	Erionite[5]
1210.2/1210.6	Major	---	Trace[2]	Minor	Minor	---	---	Minor	Trace[3]	---	Fluorite[6]
2.0/1232.1	Major	---	---	---	Minor	---	---	Trace	Trace[3]	---	Fluorite[6]

Qualitative mineralogy - fracture lining minerals in the lower Topopah Spring Member of the Paintbrush Tuff. Yucca Mountain. From Carlos et al., 1990.

Table 4 (cont'd.)

USW G-4 Sample	Smect-ite	Heul-andite	Morden-ite	Quartz	Cristob-alite	Opal-CT	Tridy-mite	Feld-spar	Rancie-ite	Lithio-phorite	Other
349.0/349.3	Trace	---	Major	---	Minor	---	Minor	Major	---	---	Hematite[4]
669.9/670.3	Trace	---	---	Trace	Trace	---	---	Trace	---	---	Calcite[6]
7.8/778.0	Trace	---	---	Major	???[9]	---	Major	Minor	---	---	Hematite[4]
810.7/811.2	Major	---	Major	Minor	---	---	---	Trace	---	---	
87.2/887.4	Minor	---	---	Major	???[9]	---	Minor	Major	---	---	Hematite[4]
984.0/984.4	Trace	---	---	Major	???[9]	---	Minor	Minor	---	---	Hematite[4]
1001.4/1001.8	Minor	---	---	Major	Minor	---	Trace	Major	---	---	Hematite[5]
1008.1/1008.3	Trace	---	Minor[2]	Major	Minor	---	---	Major	---	---	Hematite[5]
1038.0/1038.7	Major	---	Trace	Major	Minor	---	Major	Major	---	---	Hematite[4]
1072A type-1	---	---	---	Major	---	---	Minor	Minor	---	---	Hematite[4]
1072B type-2	Minor	---	Minor	Major	Minor	---	Minor	Major	---	---	Hematite[4]
1083 Fract#3	Major	---	---	Minor	Major	---	Major	Major	---	---	Hematite[4]
1148.2/1148.4	Major	---	---	Major	Minor	---	---	Major	---	---	
1160.1/1160.2	Trace	---	---	Major	Minor	---	Trace	Major	---	---	
1173.0/1173.2	Trace	---	Major	Minor	Minor	---	---	Major	---	---	
1201.6/1201.8	Trace	---	---	Major	???[9]	---	Minor	Major	---	Minor	Hematite[4]
1244.5/1244.8	Minor	---	---	Major	Minor	---	---	Major	---	---	Hematite[4]
1254 Fract#1	Trace	Major	Minor	Minor	Minor[10]	---	---	Major	---	---	
1254 Fract#3	---	Major	Trace	Minor	Minor[10]	---	---	Major	---	Minor	
1258.9/1258.1	Minor	Major	---	Minor	Minor[10]	---	---	Minor	Trace	Minor	
1309.0/1309.4	---	Major	---	---	---	---	---	---	---	---	
1341 Blue	Minor	Major	Trace	---	---	Minor	---	---	---	---	
1341 Beige	Minor	Minor	---	---	---	Minor	---	---	---	---	
1341 Cream	Major	Minor	---	---	---	Minor	---	---	---	---	
1350.1/1350.3	Major	Major	Trace	Trace	---	Trace	---	---	Trace	---	
1362.1/1362.3	Major	Minor	Trace	---	---	Minor	---	Trace	---	---	
1381.2/1381.5	---	Major	Trace	Trace	---	Major	---	---	---	---	

Ue25a#1 Sample	Smect-ite	Mica	Heul-andite	Morden-ite	Erion-ite	Phillip-site	Quartz	Opal-CT	Feld-spar	Rancie-ite
1242.7/1243.1	---	---	Major	Minor	---	---	Minor	Minor	---	---
1252.3	Trace	---	Minor	Major	---	---	Minor	Minor	Minor	---
1274.5	Major	Trace	Major	Trace	---	---	Minor	Minor	Minor	Trace[3]
1276.0/1276.2	Major	Trace	Minor	Minor	---	---	Minor	Minor	Minor	Trace[3]
1282.6	Major	---	Major	Trace	---	---	---	---	---	Trace?[3]
1296.2	Minor	Trace	Major	---	Major	---	---	---	---	---
1301.5/1302.0	Minor	---	Major	---	---	Major	Trace	---	---	Trace[3]
1309.0/1309.2	Minor	---	Major	---	---	---	---	Minor	Trace	Trace[3]
1318.4/1319.5	Trace	---	Major	Minor	---	---	Trace	Minor	---	---
1322.9/1323.2	Minor	---	Major	Minor	---	---	Trace	Minor	Minor	---
1339.5/1339.7	Minor	Trace	Major	Major	---	---	Trace	Trace	Trace	---
1361.8/1362.0	Minor	Trace	Major	Minor	---	---	Trace	Major	Minor	---

J-13 Sample	Smect-ite	Heul-andite	Morden-ite	Chab-azite	Quartz	Cristob-alite	Opal-CT	Tridy-mite	Feld-spar	Hemat-ite	Other
800	Major	---	---	---	Minor	???[9]	---	Major	Major	Trace	---
1101	---	Trace[2]	---	---	Major	---	---	---	Minor	Trace	Lithiophorite[6]
1102	---	---	---	---	Major	---	---	---	Trace	Trace	---
1345	Trace	Major	---	Major	Trace	---	Major	---	Trace	---	---
1456	Minor	Major	Minor	---	???	---	Major	---	???	---	---
1519	Trace	Major	Major	---	Minor	---	Minor	---	Minor	---	---

[1] Clinoptilolite/heulandite group mineral
[2] Zeolite -- unknown whether heulandite/clinoptilolite or mordenite
[3] Rancieite believed to be present based on chemistry and a single XRD reflection
[4] Trace amount [5] Minor amount [6] Major amount
Presence uncertain due to peak overlaps with heulandite and mordenite
[9] Presence uncertain due to peak overlaps with feldspar or tridymite
[10] Either poorly crystallized cristobalite or opal-C

Qualitative mineralogy - fracture lining minerals in the lower Topopah Spring Member of the Paintbrush Tuff. Yucca Mountain. From Carlos et al., 1990.

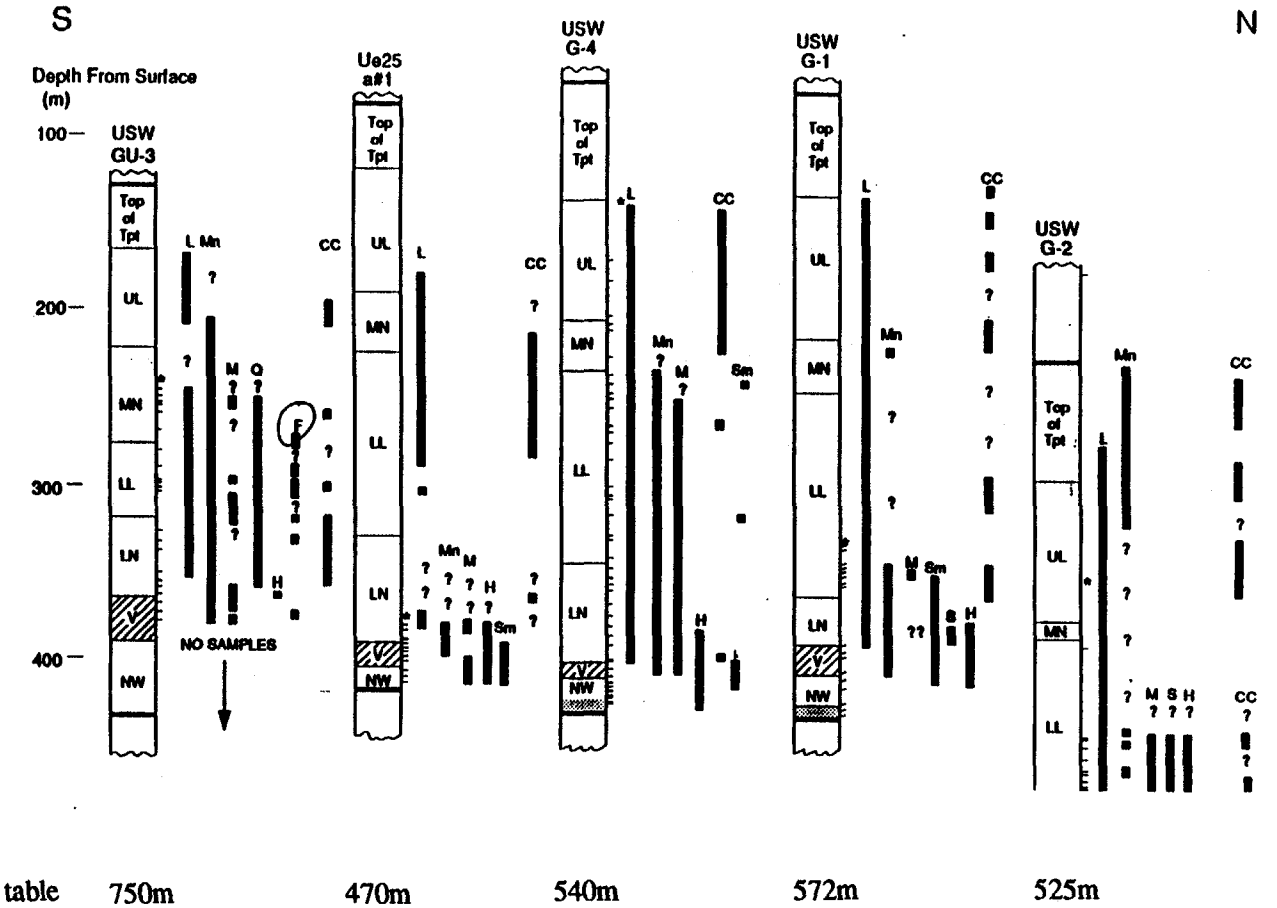

Explanation:

a) UL - upper lithophysal; MN - middle non-lithophysal; LL - lower lithophysal; LN - lower non-lithophysal; V - vitrophyre; NW - non-welded; and

b) fracture mineralogy is indicated by bars, L - lithophysal; MN - manganese; Q - quartz; H - heulandite; S - stellerite; SM - smectite; CC - calcite; F - fluorite, M - Mordenite.

Fracture lining minerals in the lower Topopah Spring Member of the Paintbrush Tuff. From Carlos et al., 1990.

Sample Identification Number	Depth Intervals (m)	Date of Collection	δD (‰)	$\delta^{18}O$ (‰)	Tritium (TU)
UE-25 UZ5-D-1	28.21 - 28.44	11-01-84	-93.5	---	59.9 ± 4.0
UE-25 UZ5-D-2	28.78 - 28.94	11-01-84	-91.5	---	
UE-25 UZ5-CF-51	29.81 - 29.96	11-01-84	---	---	65.0 ± 5.4
UE-25 UZ5-D-TP-3	30.40 - 30.59	11-01-84	-93.0	---	---
UE-25 UZ5-41-2	30.40 - 30.59	11-01-84	-88.0	-11.5	---
UE-25 UZ5-TP-3-2	30.40 - 30.59	11-01-84	-88.0	-11.5	---
UE-25 UZ5-10-2	31.30 - 31.55	11-01-84	-87.5	-11.7	---
UE-25 UZ5-D-4	31.93 - 31.55	11-01-84	-93.0	-11.6	---
UE-25 UZ5-D-TP-12	32.61 - 32.77	11-01-84	-85.0	-9.5	---
UE-25 UZ5-40-2A	32.61 - 32.77	11-01-84	-84.0	-10.4	---
UE-25 UZ5-TP-12-2	32.61 - 32.77	11-01-84	-84.0	-10.4	---
UE-25 UZ5-D-5	33.63 - 33.71	11-02-84	-92.0	---	39.1 ± 4.6
UE-25 UZ5-D-6	34.03 - 34.14	11-02-84	-93.5	---	---
UE-25 UZ5-D-7	34.74 - 34.90	11-02-84	-90.5	---	---
UE-25 UZ5-D-8	35.96 - 36.13	11-02-84	-87.5	---	---
UE-25 UZ5-D-9	36.45 - 36.53	11-02-84	-94.5	---	---
UE-25 UZ5-D-10	36.53 - 33.70	11-02-84	-92.5	---	---
UE-25 UZ5-D-11	37.18 - 37.34	11-02-84	-85.0	-10.6	4.0 ± 4.5
UE-25 UZ5-39-3A,B	37.18 - 37.34	11-02-84	-86.0	-10.7	---
UE-25 UZ5-TP-32	37.55 - 37.70	11-02-84	-86.0	-10.7	---
UE-25 UZ5-D-TP-19	44.80 - 46.33	11-02-84	-89.0	---	---
UE-25 UZ5-D-12	56.81 - 56.90	11-05-84	---	-12.2	---
UE-25 UZ5-D-15	68.64 - 68.75	11-06-84	-91.0	-11.7	---
UE-25 UZ5-D-16	70.10 - 70.24	11-06-84	-91.5	---	0.5 ± 4.3
UE-25 UZ5-D-TP-22	72.35 - 72.52	11-06-84	-77.0	---	---
UE-25 UZ5-D-TP-23	72.52 - 72.53	11-06-84	-90.5	---	---
UE-25 UZ5-D-TP-24	75.28 - 72.65	11-07-84	-92.5	---	---
UE-25 UZ5-D-18	78.69 - 78.85	11-07-84	-94.0	-12.2	0 ± 3.7
UE-25 UZ5-D-19	82.43 - 82.57	11-07-84	-89.0	---	---
UE-25 UZ5-D-TP-29	90.06 - 90.19	11-08-84	-93.0	-11.3	---
UE-25 UZ5-TP-9-1	94.12 - 94.27	11-08-84	-88.0	-11.8	---
UE-25 UZ5-TP-10-1	94.27 - 94.46	11-08-84	-87.5	-11.8	---
UE-25 UZ5-38-1A	98.26 - 98.35	11-08-84	-88.0	-11.8	---

Note:

a) samples of the interstitial fluids were obtained employing the direct distillation method.

Isotopic compositions of the vadose zone interstitial fluids. Yucca Mountain. From Yang (1989).

Sample Identification Number	Depth Intervals (m)	Date of Collection	δD (‰)	$\delta^{18}O$ (‰)	Tritium (TU)
UE-25 UZ4-T-1	1.00 - 2.25	10-01-84	---	---	18.7 ± 5.0
UE-25 UZ4-T-2	2.50 - 4.50	10-01-84	---	---	21.8 ± 5.0
UE-25 UZ4-T-3	5.50 - 6.50	10-01-84	---	---	6.6 ± 5.0
UE-25 UZ4-T-4	8.75 - 10.25	10-01-84	---	---	2.2 ± 5.0
UE-25 UZ4-T-5	11.00 - 11.75	10-01-84	---	---	2.5 ± 5.0
UE-25 UZ4-CF-25	24.71 - 24.81	10-02-84	---	---	28.0 ± 5.0
UE-25 UZ4-CF-24	25.54 - 25.63	10-02-84	---	---	3.0 ± 4.0
UE-25 UZ4-D-TP-8	33.53 - 33.63	10-02-84	-96.5	-12.3	22.0 ± 5.0
UE-25 UZ4-D-3	41.76 - 41.86	10-02-84	-91.5	-12.1	24.0 ± 5.0
UE-25 UZ4-D-6	44.91 - 45.00	10-02-84	---	---	37.5 ± 3.7
UE-25 UZ4-D-5	46.32 - 47.85	10-02-84	-90.0	-10.5	44.8 ± 4.8
UE-25 UZ4-D-TP-10	49.37 - 49.47	10-02-84	---	-11.1	45.0 ± 6.0
UE-25 UZ4-TP-6	95.59 - 95.74	10-05-84	---	---	0 ± 4.1

Note:

a) samples of the interstitial fluids were obtained employing the vacuum distillation method.

Isotopic compositions of the vadose zone interstitial fluids. Yucca Mountain. From Yang (1989).

Sample Identification Number	Depth Interval (m)	Triaxial Squeezing		Distillation	
		δD (‰)	$\delta^{18}O$ (‰)	δD (‰)	$\delta^{18}O$ (‰)
UE-25 UZ5-TP-3	30.40 - 30.59	-88.0	-11.5	-93.0	---
UE-25 UZ5-TP-4-2	31.55 - 31.67	-87.5	-11.7	-93.0	-11.55
UE-25 UZ5-TP-12	32.61 - 32.77	-84.0	-10.35	-85.0	-9.50
UE-25 UZ5-TP-32	37.18 - 37.34	-86.0	-10.65	-85.0	-10.55

Note:

a) samples of the interstitial fluids were obtained employing both the triaxial squeezing method and the direct distillation method.

Isotopic compositions of the vadose zone interstitial fluids. Yucca Mountain. From Yang (1989).

TABLE 5. Trace element data for Pore Water Samples from UZ#4							
Sample #	Pore wat	error	USGS		Pore wat	error	USGS
	6110926		(reported)#		6110923		(reported)#
pH			6.5				6.5
SO4(ppm)							190
Li	69~				85	10	
B							
Na(ppm)			48				53
Mg(ppm)	27	5	21		25	1	23
Al					<5		
Si(ppm)			74				78
Cl(ppm)			160				210
K			5				14
Ca(ppm)	120	10	120		110	10	130
Sc	<3	1			0.4		
Ti					<3		
Cr	<9	<3			0.4	0.1	
Mn	133	25	150		14	3	90
Fe	36	5	150		<20		<3
Co					<1		
Ni	40	10			<50	16	
Cu	40	10			10	1	
Zn	150	15			71	5	
Rb	23	2			12	2	
Sr	1020	110			1180	110	
Y	0.3	0.1			0.21	0.05	
Mo	1680	160			1400	30	
Cd					1.4	0.3	
Sb	1				0.7	0.2	
I	50				40		
Cs	0.5	0.1			0.44	0.05	
Ba	27	3			18	1	
La	<0.1				0.007	0.007	
Ce	<0.1				0.048	0.02	
Pr	<0.04				<0.006		
Nd	<2				<0.06		
Sm	<0.3				<0.008		
Eu	<0.06				<0.006		
Gd	<0.2				<0.003		
Tb	<0.03				0.013	0.005	
Dy	0.09	0.03			0.032	0.006	
Ho	<0.1				0.022	0.006	
Er	0.14	0.04			0.12	0.02	
Tm	0.05	0.02			0.04	0.01	
Yb	0.5	0.2			0.5	0.10	
Lu	0.14	0.05			0.16	0.05	
Hf	0.01				0.3	0.1	
Ta	0.5				<0.2		
W	600	200			330	50	
Re	0.2	0.09			0.2	0.1	
Pt	0.2	0.1			0.2	0.05	
Au	0.12	0.05			0.2	0.1	
Tl	0.2				0.2		
Pb	0.25	0.1			1.7	0.3	
Bi	<0.03				<0.1		
Th	0.0024	0.0006			<0.01		
U	0.45	0.05			0.13	0.03	
# Personal communication, Al Yang							

Note:

a) concentrations are in ppb unless noted; and

b) samples of the interstitial fluids were obtained employing the high-speed centrifugation method.

Chemical composition of the vadose zone interstitial fluids. Yucca Mountain. From Smith (1991).

Sample Identification Number	Interval Sampled (m)	pH (units)	Ca	Mg	Na	K	Fe	Mn	Zn	Sr	SiO_2	Cl	SO_4	$\delta^{13}C$ (‰)	^{14}C % modern	^{14}C apparent age (yr B.P.)
			(mg/L)				(µg/L)				(mg/L)					
UE-25 UZ4-17	91.32 - 91.41	7.8	127	21	65	16	5	57	25	1504	88	104	174	-----	-----	-----
UE-25 UZ4-19	91.53 - 91.62	7.8	107	18	68	15	11	65	19	1302	93	87	149	-----	-----	-----
UE-25 UZ4-23	96.49 - 96.56	7.4	80	15	48	--	17	66	552	983	89	85	123	-----	-----	-----
UE-25 UZ4-CF-11	96.01 - 100.58	---	--	--	--	--	--	--	---	---	--	--	---	-20.05	88.6	1,000
UE-25 UZ4-16	100.35 - 100.50	7.0	75	16	50	--	26	28	384	976	71	--	---	-----	-----	-----
UE-25 UZ5-CF-25	103.63 - 105.16	---	--	--	--	--	--	--	---	---	--	--	---	-26.70	55.1	4,900

Note:

a) cations and anions are not balanced in charge because not enough pore water was obtained for complete chemical analyses;

b) samples CF-11 and CF-25 were obtained employing the high-speed centrifugation method; and

c) samples 17, 19, 23, and 16 were obtained employing the triaxle squeezing method.

Chemical composition of the vadose zone interstitial fluids. Yucca Mountain. From Yang (1989).

TABLE 4 Trace element data for J-12 and J-13 Well waters

Sample #	J-12	error	J-13	error	SLRS-1*	cert. val
pH (field)	7.3		--			
pH (lab)	7.69					
F(ppm)	2.00					
Cl(ppm)	7.5					
NO3(ppm)	8.2					
SO4(ppm)	22.2					
HCO3(ppm)	117					
Li	50	10	40	10	1.5	
B	130	10				
Na(ppm)	41.8	1.3				10.4
Mg(ppm)	2.45	0.15	2.4	0.2		5.99
Al	1.2	0.6	0.5			23.5
Si(ppm)	25.6	1.1	30	5		
Cl(ppm)	7.5	0.5				
K	5.5	0.7				1.3
Ca(ppm)	15	0.2	14	5	25	25.1
Sc	<1		<3		0.34	
Ti	0.06		0.1		0.7	
V	4	1	5	1	0.73	0.66
Cr	0.37	0.12	0.33	0.03	0.26	0.36
Mn	0.15	0.06	<0.3		1.19	1.77
Fe	3	1	3	1	27.5	31.5
Co	<0.01		<0.01		0.023	0.043
Ni	0.03	0.01	0.05	0.01	0.7	1.07
Cu	0.2	0.06	0.8	0.2	2.8	3.56
Zn	2.7	0.5	2.4	0.5	0.95	1.3
As	9	3	8	3	0.53	0.55
Rb	9.2	1.1	6.5	1	0.83	
Sr	35	1	33	2	133	136
Y	0.0025	0.0006	0.0025	0.0006	0.28	
Mo	5	0.5	5.3	0.1	0.62	0.78
Pd	<0.01		<0.01			
Cd	<0.05		<0.05		0.011	0.015
Sb	0.15	0.01	0.21	0.01	0.57	0.63
I	2		2		2.22	
Te	<0.01		<0.03		<0.01	
Cs	0.56	0.02	0.95	0.16	0.0032	
Ba	1.75	0.35	1/6.8		21.5	22.2
La	0.0004		0.0003		0.04	
Ce	<0.005		0.0006		0.059	
Pr	<0.001		<0.001		0.01	
Nd	<0.001		<0.001		0.037	
Sm	<0.001		<0.001		0.02	
Eu	<0.001		<0.001		0.0014	
Gd	<0.001		<0.001		0.006	
Tb	<0.001		<0.001		0.0007	
Dy	<0.001		<0.001		0.0035	
Ho	<0.001		<0.001		0.0006	
Er	<0.001		<0.001		0.003	
Tm	<0.001		<0.001		0.0003	
Yb	<0.001		<0.001		0.0028	
Lu	<0.001		<0.001		0.0004	
Hf	0.001		<0.002			
Ta	<0.001		<0.001			
W	1.0	0.2	2.0	0.4	0.13	
Re	0.056	0.01	0.002/0.53		0.003	
Pt						
Au					0.0006	
Tl	0.01	0.004	0.008			
Pb	0.2	0.06	0.3	0.1	0.082	0.106
Bi	<0.001		<0.003		0.001	
Th	0.0001	0.00003	0.0004	0.0002	0.003	
U	0.55	0.13	0.4	0.14	0.25	0.28

* Riverine Water Reference Material for Trace Metals (National Research Council Canada)

Note:

a) concentrations are in ppb unless noted.

Chemical composition of the fracture-based fluids from below the water table. Yucca Mountain. From Smith (1991).

Test well designation	Land-surface altitude (m)	Approximate well depth (m)	Approximate depth to water (m)	Interval sampled (m)	Collection date	δD o/oo SMOW	$\delta^{18}O$ o/oo SMOW	$\delta^{13}C$ o/oo PDB	^{14}C percent modern	^{14}C Apparent age (yr B.P.)	HTO	$^{4}O_2$	Specific conductance (microsiemens per centimeter at 25° C) Onsite	Specific conductance (microsiemens per centimeter at 25° C) Laboratory
J-12	953.5	347	225	---	03/26/71	-97.5	-12.8	-7.9	32.2	9,100	<220	--	285	252
J-13	1,011.3	1,063	282	---	03/26/71	-97.5	-13.0	-7.3	29.2	9,900	<220	5.7	285	252
UE-25b#1	1,200.4	1,220	470	---	08/07/81	-99.5	-13.4	-10.7	--	--	--	1.8	318	319
UE-25b#1	1,200.4	1,220	470	---	09/01/81	-101	-13.4	-10.4	16.7	14,400	<200	--	300	281
UE-25b#1	1,200.4	1,220	470	(863-875)	07/20/82	-99.5	-13.5	-8.6	18.9	13,400	2	1.6	291	297
UE-25c#1	1,131.0	914	400	---	09/30/83	-102	-13.5	-7.1	15.0	15,200	<1	--	290	310
UE-25c#2	1,132.0	913	401	---	03/13/84	-100	-13.4	-7.0	16.6	14,400	<2	--	295	303
UE-25c#3	1,132.0	913	402	---	05/09/84	-103	-13.5	-7.5	15.7	14,900	2	--	298	309
UE-25p#1	1,114.0	1,800	381	(381-1,197)	02/09/83	-106	-13.5	-4.2	3.5	26,900	<10	--	628	639
UE-25p#1	1,114.0	1,800	361	(1,297-1,805)	05/12/83	-106	-13.8	-2.3	2.3	30,300	10	1.3	1,120	1,120
UE-29a#2	1,215.1	422	29	(247-354)	01/08/82	-93.5	-12.8	-13.0	62.3	3,800	37	5.4	240	255
UE-29a#2	1,215.1	422	29	(87-213)	01/15/82	-93.0	-12.8	-13.1	60.0	4,100	37	5.6	258	317
USW G-4	1,270.0	915	541	---	12/09/82	-103	-13.8	-9.1	22.0	12,160	--	6.4	312	307
USW H-1	1,302.2	1,829	572	(572-687)	10/20/80	-103	-13.4	--	19.9	13,000	<20	--	255	258
USW H-1	1,302.2	1,829	572	(687-1,829)	12/08/80	-101	-13.5	-11.4	23.9	12,000	<20	--	247	266
USW H-3	1,483.0	1,220	--	(822-1,220)	03/14/84	-101	-13.9	-4.9	10.5	18,100	2	<0.1	523	535
USW H-4	1,249.0	1,220	519	---	05/17/82	-104	-14.0	-7.4	11.8	17,200	<10	5.8	340	381
USW H-5	1,477.8	1,220	704	---	07/03/82	-102	-13.6	-10.3	18.2	13,700	<200	6.3	275	273
USW H-5	1,477.8	1,220	704	---	07/26/82	-102	-13.6	-10.3	21.4	12,400	<200	--	278	276
USW H-6	1,302.0	1,220	526	---	10/16/82	-106	-13.8	-7.5	16.3	14,600	<10	5.9	372	--
USW H-6	1,302.0	1,220	--	(753-835)	06/20/84	-105	-14.0	-7.3	10.0	18,500	4	--	360	392
USW H-6	1,302.0	1,220	--	(608-646)	07/06/84	-107	-14.0	-7.1	12.4	16,800	1	--	402	408
USW VH-1	954.5	762	184	---	02/06/81	--	--	--	--	--	--	--	370	410
USW VH-1	954.5	762	184	---	02/08/81	--	--	--	--	--	--	--	395	397
USW VH-1	954.5	762	184	---	02/11/81	-108	-14.2	-8.5	12.2	17,000	<20	--	388	402

Chemical composition of the fracture-based fluids from below the water table. Yucca Mountain. From Benson and McKinley (1985).

Test well designation	Onsite pH (units)	Laboratory pH (units)	Water temperature (°C)	Dissolved constituents													
				Ca	Mg	Na	K	HCO_3 (on-site)	HCO_3 (laboratory)	Cl	SO_4	SiO_2	Li	Sr	F	Dissolved solids (calculated)	Dissolved solids (180°C)
J-12	7.1	--	27.0	14	2.1	38	5.1	--	119	7.3	22	54	40	10	2.1	211	205
J-13	7.2	--	31.0	12	2.1	42	5.0	--	124	7.1	17	57	40	20	2.4	213	202
UE-25b#1	7.1	6.8	36.0	19	0.73	53	3.7	173	158	13	24	53	950	44	1.5	264	266
UE-25b#1	7.5	7.5	36.0	17	.59	46	3.5	139	134	8.5	22	52	220	38	1.6	218	225
UE-25b#1	7.1	7.7	37.2	18	.72	46	2.8	133	138	7.5	21	51	120	47	1.6	220	221
UE-25c#1	7.6	7.7	41.5	11.0	.34	56	2.0	151	140	7.4	23	56	120	30	2.1	229	--
UE-25c#2	7.7	7.8	40.5	12.0	.40	54	2.1	139	141	7.1	22	54	94	45	2.1	233	--
UE-25c#3	7.7	7.8	40.8	11.0	.40	55	1.9	137	143	7.2	22	53	110	44	2.0	229	--
UE-25p#1	6.8	7.7	44.3	37	10	92	5.6	--	282	13	38	49	230	180	3.4	418	394
UE-25p#1	6.6	7.2	56	100	39	150	12	--	569	28	160	41	590	450	4.7	812	784
UE-29a#2	7.2	7.6	25.1	10	.2	44	1.1	107	112	11	22	44	100	39	1.0	198	194
UE-29a#2	7.0	7.4	22.7	10	.3	44	1.3	107	110	8.8	21	44	110	33	.9	194	192
USW G-4	7.7	7.5	35.6	13	.2	57	2.1	139	143	5.9	19	45	67	17	2.5	215	216
USW H-1	7.7	7.8	33.0	4.5	<.1	51	2.4	--	115	5.7	18	47	40	5	1.2	--	176
USW H-1	7.5	8.0	34.7	6.2	<.1	51	1.6	--	122	5.8	19	40	40	20	1.0	--	188
USW H-3	9.2	9.0	26.5	.8	.02	120	1.1	--	274	5.5	31	43	220	1	5.5	347	--
USW H-4	7.4	7.9	34.8	17	.29	73	2.6	173	171	6.9	26	46	130	27	4.6	261	248
USW H-5	7.8	7.8	36.5	1.9	.01	60	2.1	126	124	6.1	16	48	62	9	1.4	--	220
USW H-5	7.9	8.0	35.3	2.0	<.01	60	2.1	127	124	6.1	16	48	71	4	1.4	--	206
USW H-6	8.1	8.3	37.8	4.1	.09	86	1.3	182	188	7.6	29	48	82	8	4.7	--	--
USW H-6	8.3	8.4	41.6	1.4	.02	88	1.3	217	183	7.2	25	47	71	3	3.9	269	--
USW H-6	8.3	8.3	37.2	4.7	.07	88	1.4	236	184	7.4	32	49	63	8	4.7	--	--
USW VH-1	7.9	8.0	35.2	11	1.6	79	1.9	167	158	11	44	50	90	70	2.7	280	287
USW VH-1	7.5	7.9	35.5	10	1.5	80	1.9	165	158	10	45	50	90	70	2.7	279	274
USW VH-1	7.5	8.0	35.5	9.9	1.5	78	1.8	162	158	10	44	49	90	60	2.7	275	277

Note:

a) concentrations of dissolved solids are reported in milligrams per liter, except Li and Sr which are reported in micrograms per liter.

Chemical composition of the fracture-based fluids from below the water table. Yucca Mountain. From Benson and McKinley (1985).

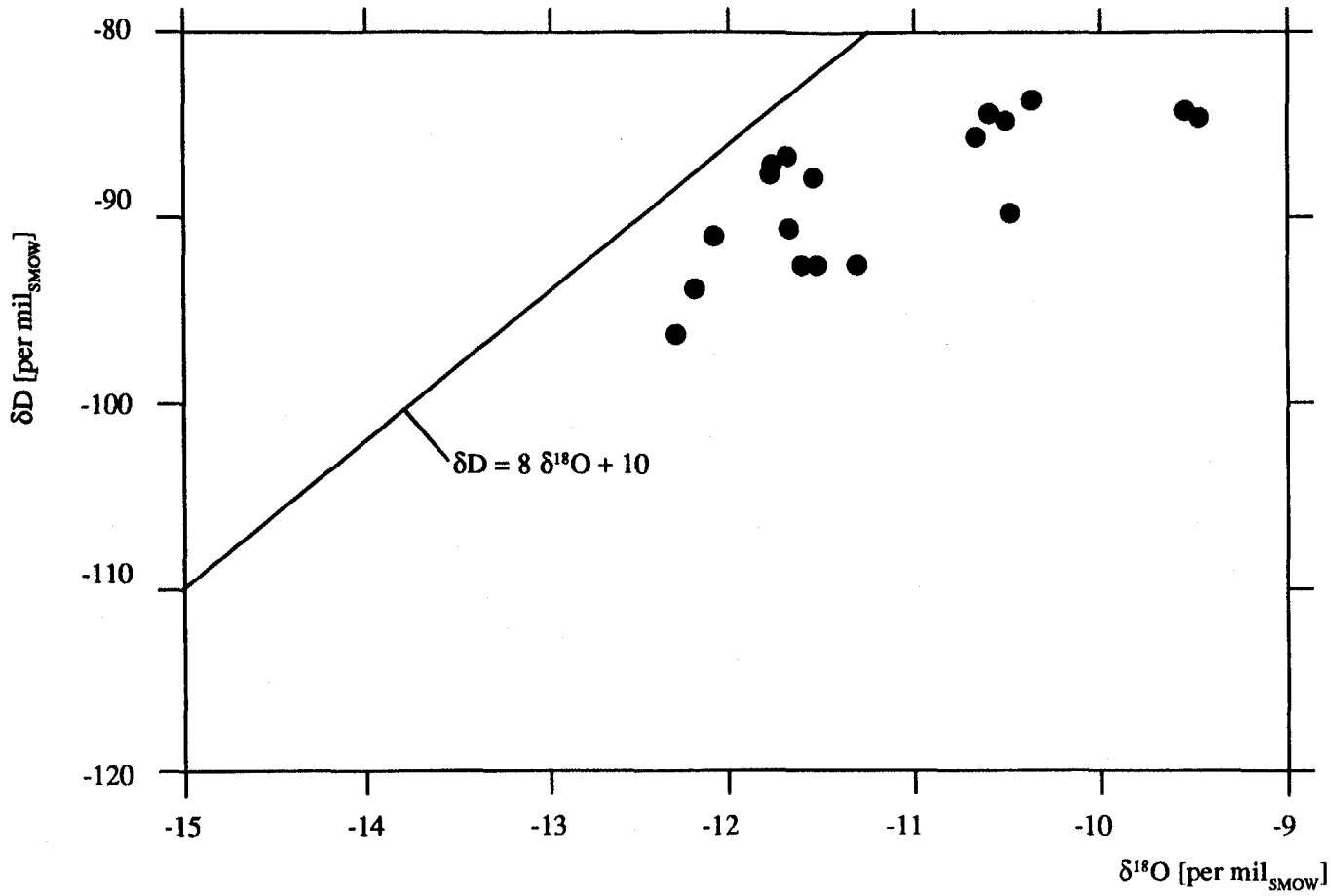

Note:

a) for the contemporary meteoric precipitation, weighted average values of the $\delta^{18}O$ ratio range from -11.7 to -11.3 per mil_{SMOW} (the corresponding altitudes range from 1250 to 1400m), Ingraham et al. (1990).

Isotopic composition of the vadose zone interstitial fluids, relative to the meteoric water line. Yucca Mountain.

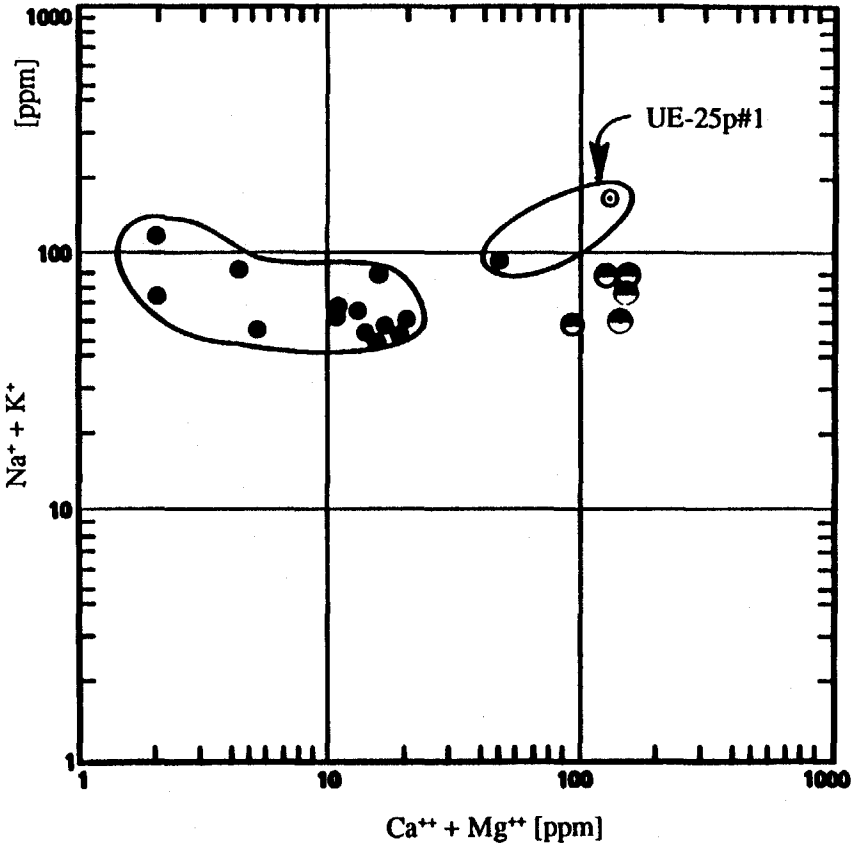

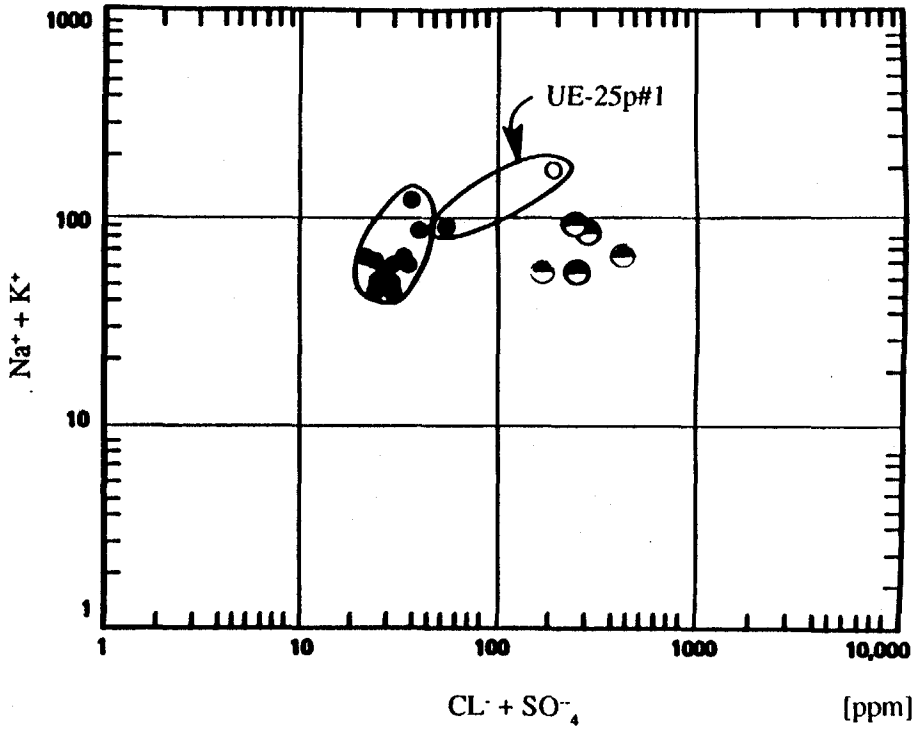

Explanation:

- ◓ - sample represents the vadose zone interstitial fluids;
- ● - sample represents the fracture-based fluids from the Tertiary ignimbrites; and
- ⊙ - sample represents the fracture-based fluids from the Paleozoic carbonates.

A comparison of chemical compositions of different fluid phases. Yucca Mountain.

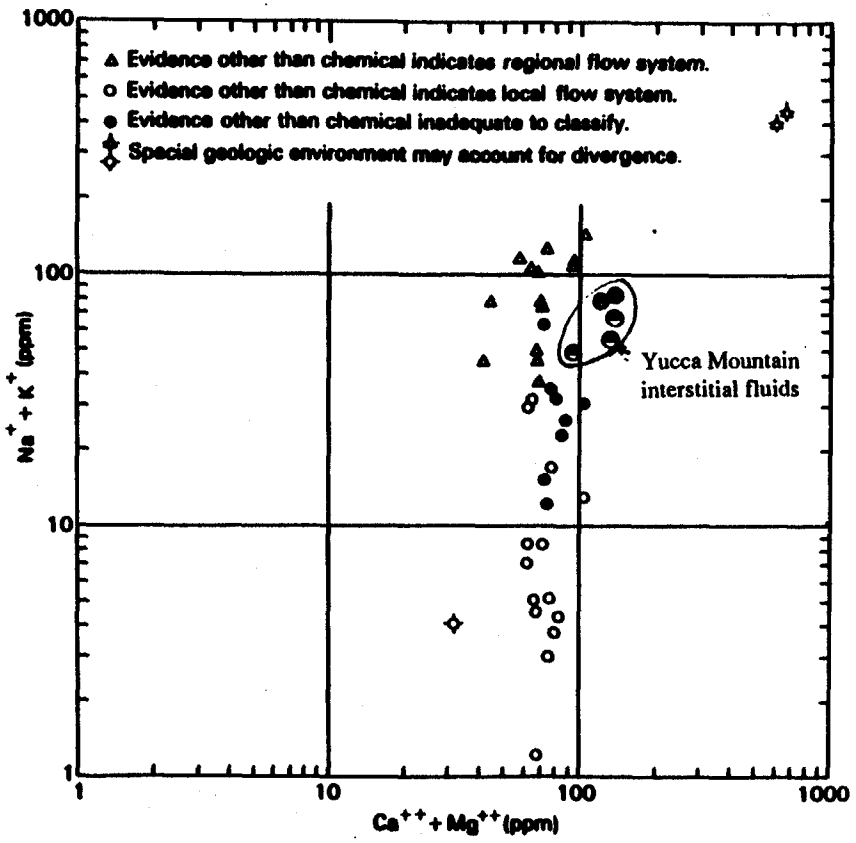

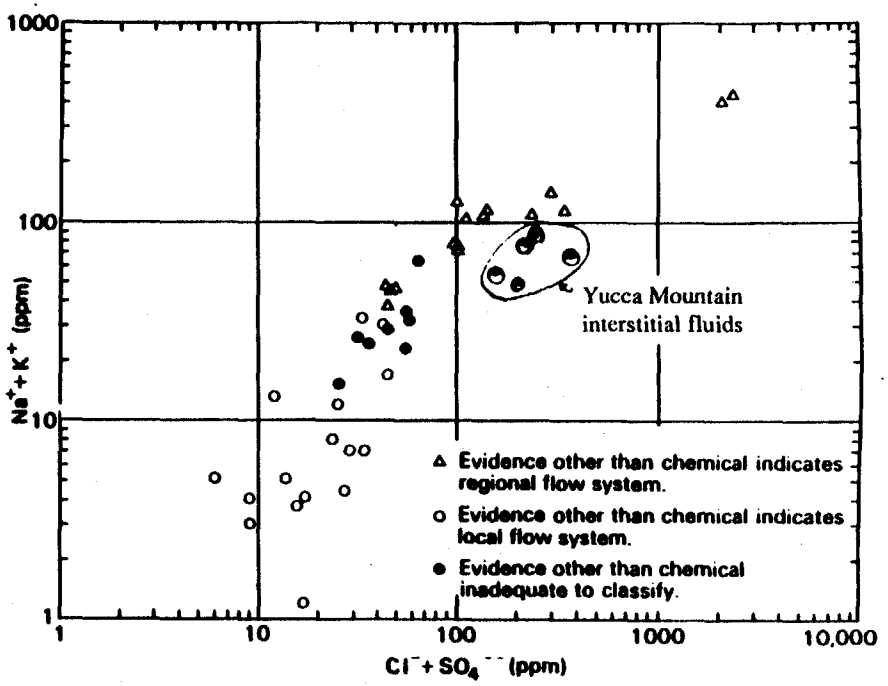

A comparison of chemical compositions of the vadose zone interstitial fluids and different fluid phases from the Paleozoic carbonates. Modified from Domenico (1972).

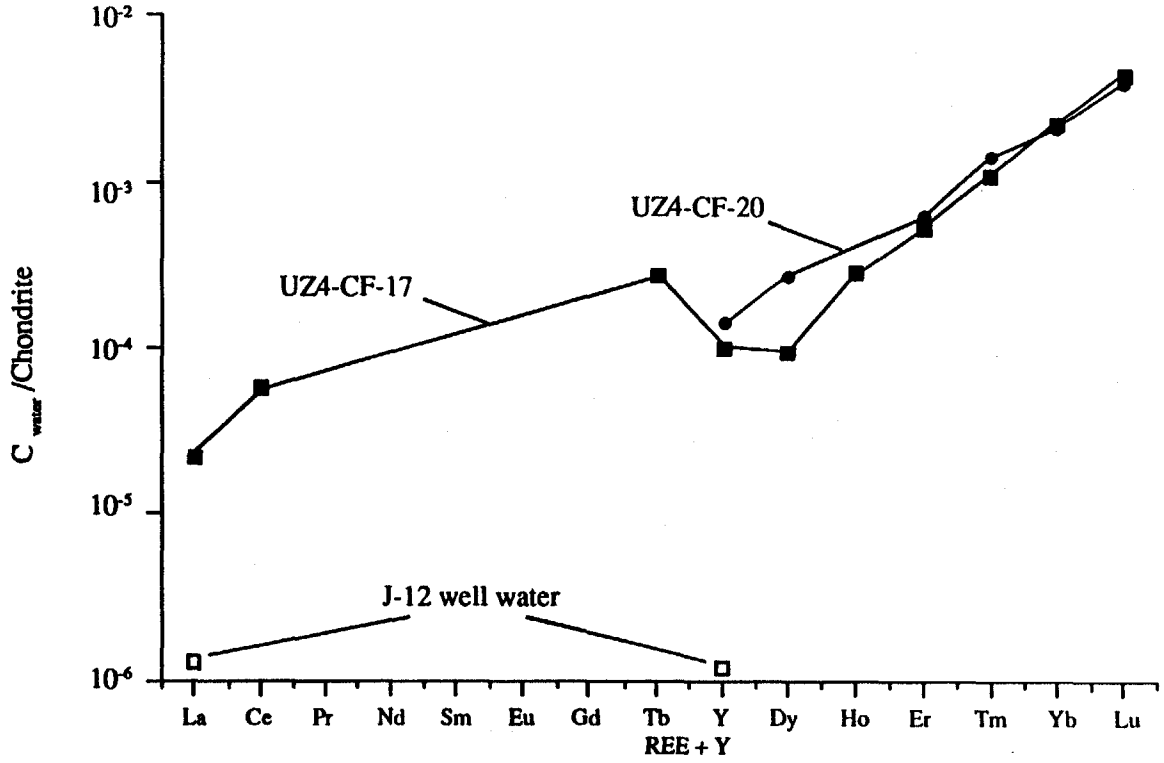

A comparison of the chondrite-normalized REE abundance patterns, the fracture-based fluids from below the water table and the vadose zone interstitial fluids. Modified from Smith (1991).

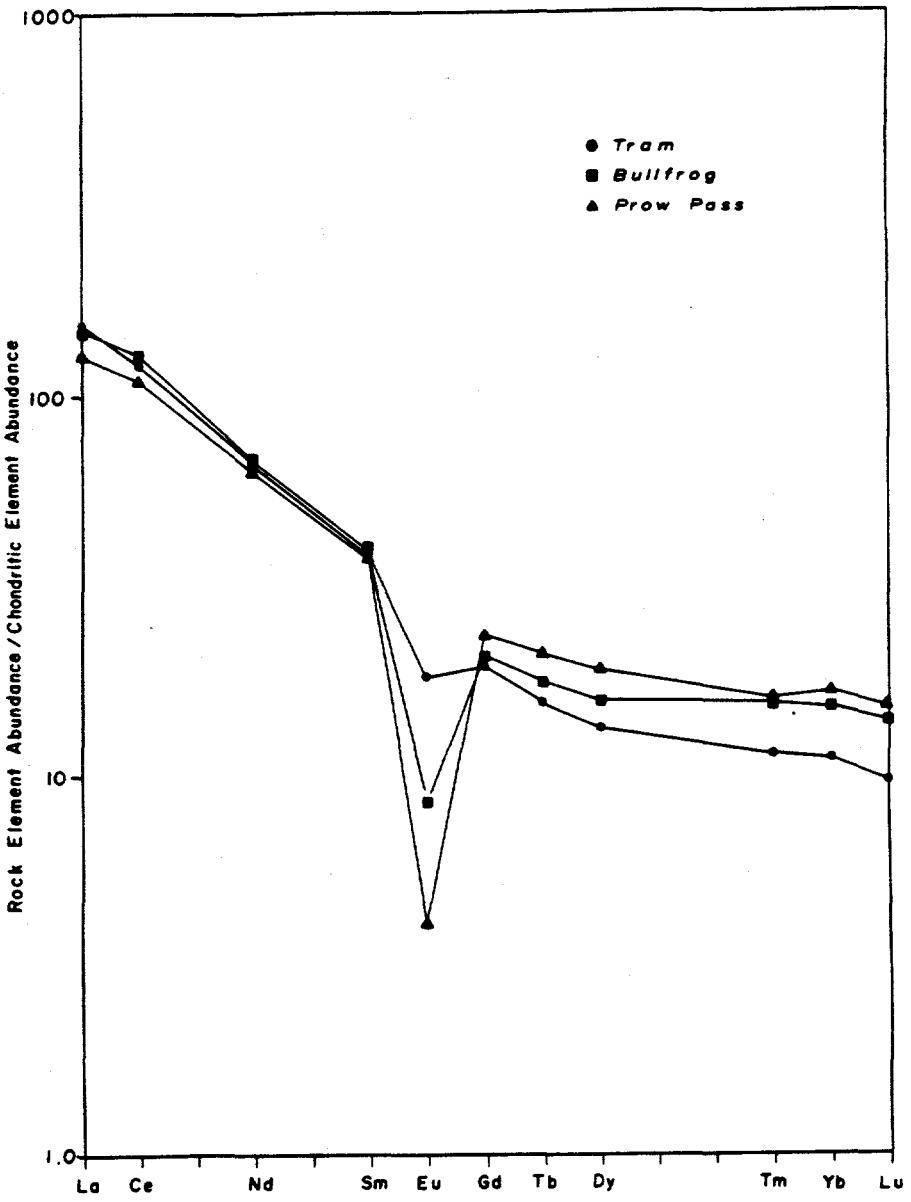

Note:

a) the data shown are average values from four samples of each tuff.

Chondrite-normalized REE abundance patterns, samples of the Crater Flat ignimbrites. Yucca Mountain. From Scott and Castellanos (1984).

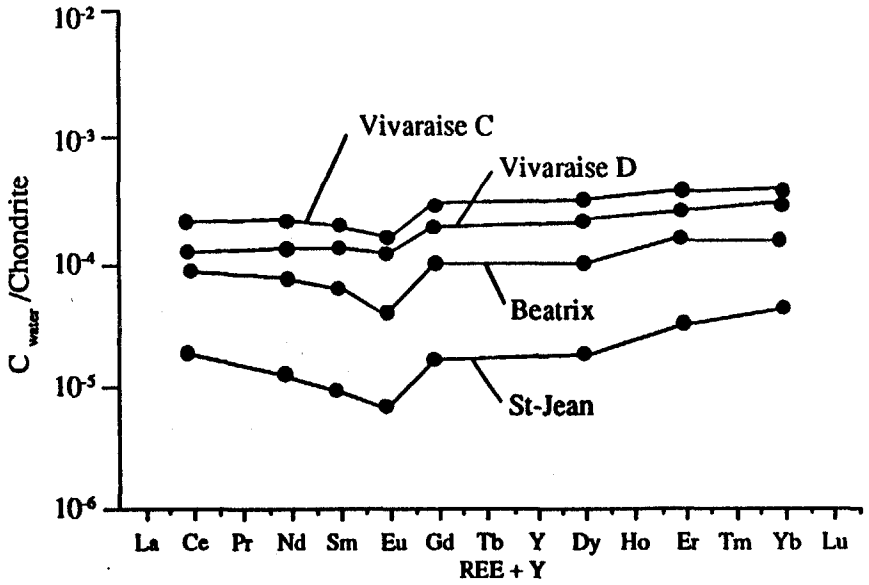

a) diluted fluids

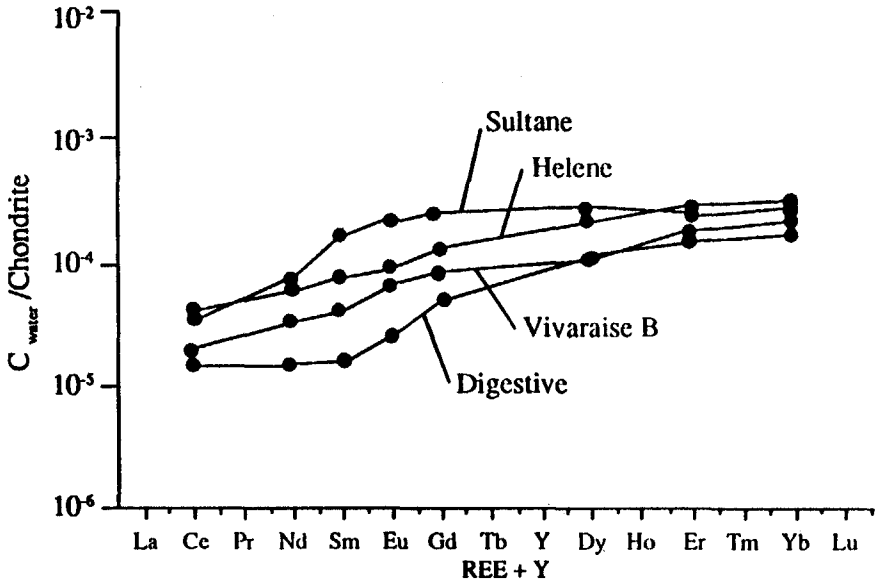

b) more concentrated fluids

	HCO^-_3	CL^-	Na^+	K^+
Vivaraise C	38	0.93	33.2	1.65
Vivaraise D	39.7	1.08	37.2	1.79
Beatrix	27.7	0.52	21.06	1.09
St-Jean	6.0	0.18	2.83	0.15
mean	27	0.67	23.57	1.17

	HCO^-_3	CL^-	Na^+	K^+
Sultane	46.4	1.34	42.4	2.00
Helene	74.2	2.08	68.6	3.17
Vivaraise B	75.1	2.23	67.2	3.03
Digestive	99.2	2.95	95.5	4.58
mean	73.7	2.15	68.42	3.20

Note:

a) concentrations are in 10^{-3} mol/L

Chondrite - normalized REE abundance patterns as a function of fluid chemistry. Vals-Les-Baines fluids. Modified from Michard et al. (1987).

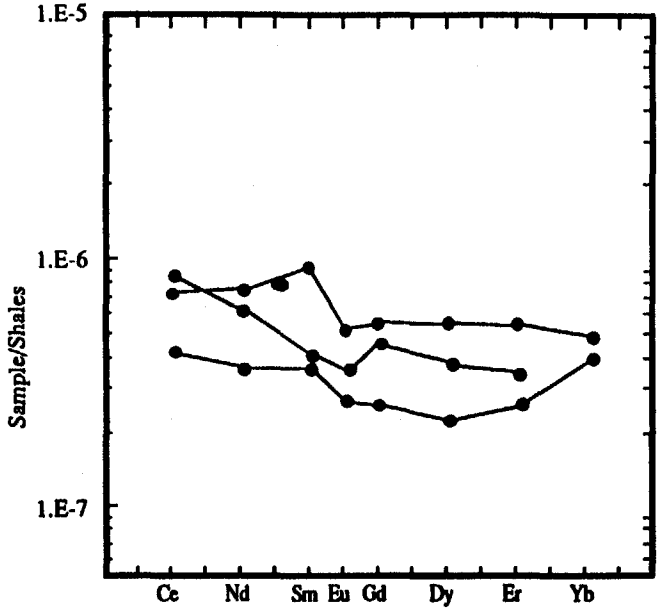

a) low alkalinity

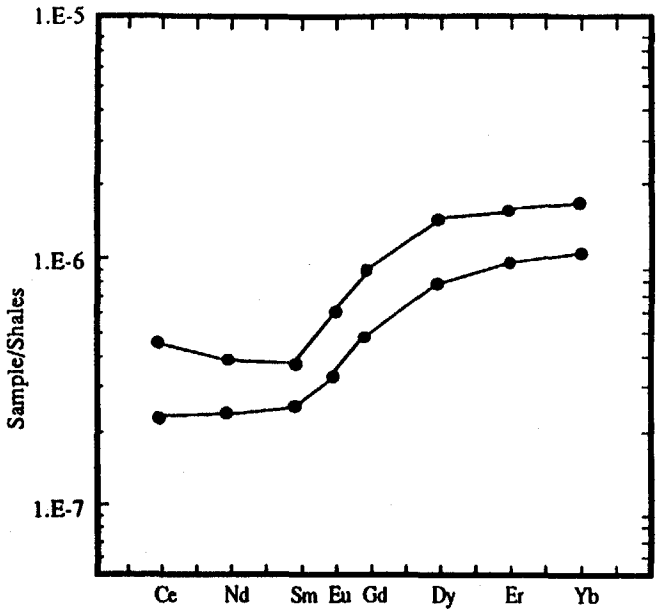

b) high alkalinity

Sample	Bu26	Bu04	Bu21
T(°C)	47	97	90
$T_{eq}^{(*)}$ (°C)	45	130	130
pH	9.50	8.40	8.15
Alkalinity (meq kg^{-1})	1.68	2.02	2.16
Ce (ng kg^{-1})	52	58	29
Nd	21.4	18	11
Sm	5.3	2.3	2.1
Eu	0.6	0.4	0.3
Gd	3.2	2.5	1.4
Dy	2.8	2.0	1.2
Er	1.7	1.1	0.8
Yb	1.3		1.2

Sample	Bu14	Bu13
T(°C)	84	75
$T_{eq}^{(*)}$ (°C)	130	
pH	7.25	6.65
Alkalinity (meq kg^{-1})	5.87	21
Ce (ng kg^{-1})	14.3	28.4
Nd	6.7	11
Sm	1.4	2.1
Eu	0.4	0.7
Gd	2.6	4.9
Dy	4.2	7.7
Er	3.1	5.1
Yb	3.2	5.2

Shale-normalized REE abundance patterns as a function of fluid chemistry. Hydrothermal solutions from Bulgaria. Modified from Michard and Albarede (1986).

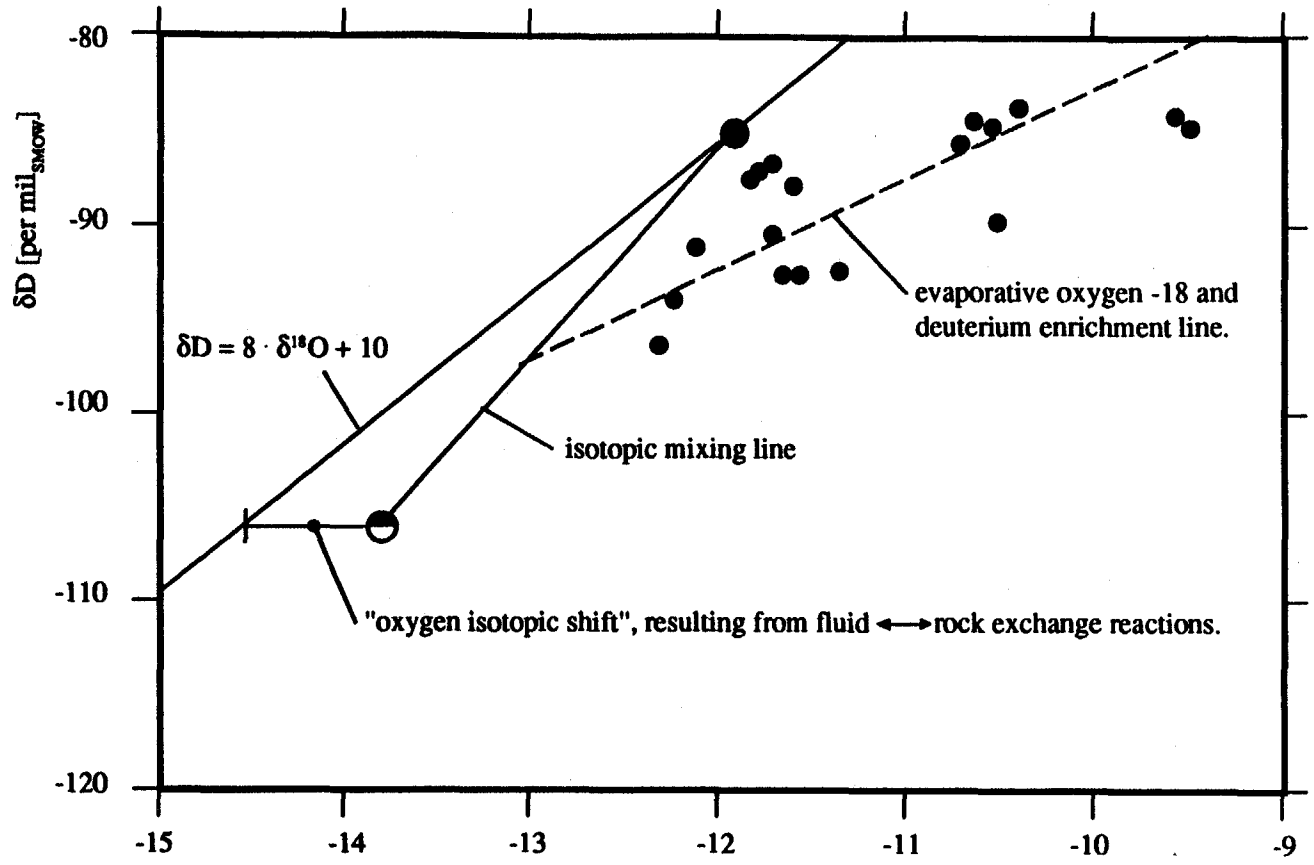

Explanation:

- isotopic composition of the vadose zone interstitial fluids;
- isotopic composition of the contemporary atmospheric precipitation, from Ingraham et al. (1990); and
- isotopic composition of the Paleozic carbonates - based fluids (well UE-25p#1), from Benson and McKinley (1985).

The origin of the vadose zone interstitial fluids, as interpreted for the Yucca Mountain vadose zone based on isotopic and chemical data.

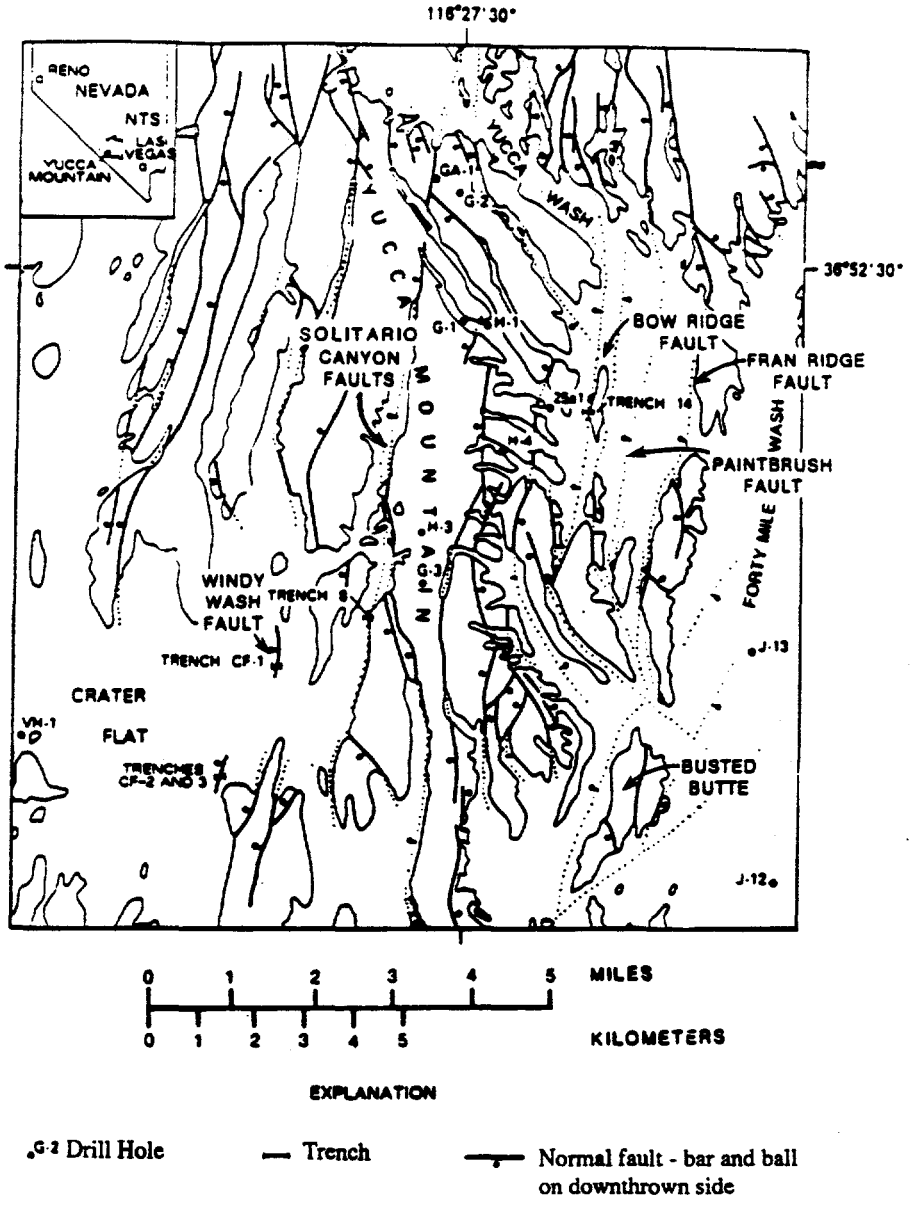

Location map for fault traces marked by the occurrance of the "mosaic" breccias. The Yucca Mountain area.

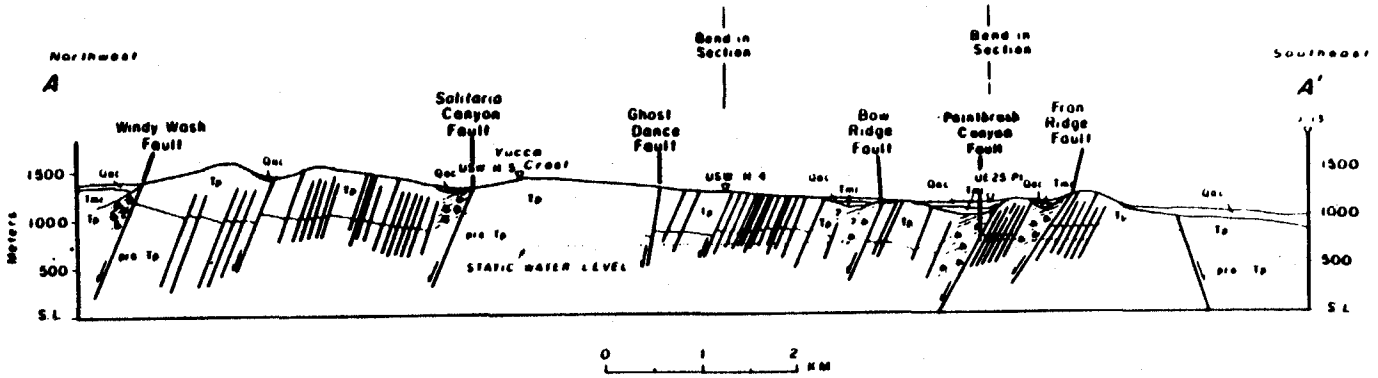

Explanation:

▲▲▲ - mapped extent of the Yucca Mountain "mosaic" breccias.

Geologic section across Yucca Mountain showing location and thickness of "mosaic" breccias. From Scott and Bonk, 1985.

		Ag	As	Au	Cu	Hg	Mo	Pb	Sb	Tl	Zn	Bi	Cd
Mean values - Yucca Mountain [ppm]		0.026	3.07	0.001	6.88	<0.10	0.10	0.25	0.25	0.50	1.00	0.25	0.10
silicified "mosaic" breccia	north wall	0.034	7.93	0.004	7.15	0.122	0.507	7.75	<0.247	<0.494	23.0	0.504	<0.099
from Trench #14	north wall	0.423	110.0	0.005	27.9	0.700	65.3	154.0	24.6	<0.497	33.2	<0.249	2.12
	south wall	0.031	7.31	0.002	4.52	0.147	0.422	5.31	<0.245	<0.49	19.0	<0.245	<0.090

Our surface geochemical sampling of faults and fracture zones does, however, show weakly anomalous bismuth, zinc, lead, and molybdenum. Statistical analysis indicates correlations among these elements. The anomalous samples could represent a very distal geochemical halo around a concentration of base metals in the deep subsurface.

From Castor and Tingley, 1990.

Note:

a) the average base metal concentrations for the Yucca Mountain area are from Castor et al. (1989);

b) the base metal concentrations from samples of the Trench #14 "mosaic" breccia are from Larson et al. (1988); and

c) the noticeably higher concentrations of the base metals, relative to the corresponding mean concentrations for the Yucca Mountain area, indicate that hydrothermal fluids were involved in formation of the Trench #14 "mosaic" breccias.

A comparison of the base-noble metal concentrations, the silicified "mosaic" breccia from Trench #14, relative to the local background.

(*expressed in parts per million*)

	Ag	As	Au	Cu	Hg	Mo	Pb	Sb	Tl	Zn	Bi	Ga	Se	Te
1)	0.423	110	0.005	27.9	0.799	65.3	154	24.6	<0.49	33.2	<0.249	1.90	<0.995	<0.497
1a)	0.129	10.0	0.002	6.49	0.202	1.11	15.0	0.763	<0.487	44.6	<0.243	1.15	<0.973	<0.487
1b)	-	-	-	-	0.036	-	-	-	-	-	-	-	-	-
2)	0.048	15.6	0.004	11.1	0.373	1.23	16.4	10.1	<0.488	90.8	<0.244	<0.488	<0.977	<0.488
2a)	-	-	-	-	0.085	-	-	-	-	-	-	-	-	-
3)	<0.015	5.89	0.001	2.71	0.349	1.80	10.7	2.90	<0.498	147	<0.249	<0.498	<0.996	<0.498
3a)	-	-	-	-	0.012	-	-	-	-	-	-	-	-	-
4)	0.048	11.2	0.001	4.11	0.553	2.29	14.8	6.36	<0.492	75.5	<0.246	<0.492	<0.984	<0.492
4a)	-	-	-	-	0.048	-	-	-	-	-	-	-	-	-
5)	0.049	11.2	0.002	2.95	2.02	1.58	46.6	2.89	<0.492	892	<0.246	<0.492	<0.983	<0.492
5a)	-	-	-	-	0.012	-	-	-	-	-	-	-	-	-
6)	0.141	14.1	0.001	14.4	3.08	2.54	78.6	8.69	<0.487	344	<0.244	<0.487	<0.975	<0.487
6a)	-	-	-	-	0.024	-	-	-	-	-	-	-	-	-
7)	0.054	1.77	0.001	2.35	0.160	0.759	3.27	<0.247	<0.494	50.0	<0.247	0.845	<0.987	<0.494
7a)	0.054	1.83	<0.0005	3.11	0.185	0.686	3.49	<0.245	<0.49	46.3	<0.245	0.799	<0.979	<0.49
7b)	0.049	1.57	0.001	1.68	0.170	0.637	2.93	<0.25	<0.5	49.4	<0.25	0.576	<0.999	<0.5
7c)	-	-	-	-	<0.050	-	-	-	-	-	-	-	-	-
8)	0.04	3.09	<0.0005	1.28	0.214	0.688	4.02	<0.245	<0.49	41.1	<0.245	0.606	<0.979	<0.49
8a)	0.055	3.05	<0.0005	1.31	0.184	0.712	4.02	<0.248	0.523	44.0	<0.248	0.684	<0.992	<0.496
8b)	0.053	3.51	0.001	1.57	0.177	0.883	4.31	<0.245	<0.491	44.7	<0.245	0.650	<0.982	<0.49
8c)	-	-	-	-	<0.050	-	-	-	-	-	-	-	-	-
9)	0.048	4.34	<0.0005	1.23	0.154	0.703	3.68	<0.247	<0.494	43.1	<0.247	0.535	<0.989	<0.494
9a)	0.051	3.84	<0.0005	1.17	0.178	0.698	3.60	<0.244	<0.488	38.8	<0.244	0.524	<0.976	<0.488
9b)	0.047	4.09	<0.0005	1.16	0.171	0.680	3.49	<0.246	<0.491	41.1	<0.246	0.559	<0.982	<0.491
9c)	-	-	-	-	<0.050	-	-	-	-	-	-	-	-	-

1) [x]3SW195B: north wall, fractured Tiva Canyon Member with weak silicification, ± drusy quartz in lithophysae, analysis from Weiss et al. (1989). **

1a) Split of hand-sample remaining from 3SW-195B. **

1b) [z] Later split of hand-sample remaining from 3SW-195B.

2) [x]3SW329: south wall, siliceous buff to white carbonate vein filling. *

2a) [z]Split of hand-sample remaining from 3SW329.

3) [x]3SW331: south wall, dark purplish, silicified breccia of Tiva Canyon Member between calcareous veins. *

3a) [z]Split of hand-sample remaining from 3SW331.

4) [x]3SW333: south wall, siliceous margin of 1-2 cm thick white calcareous vein. Margin is composed of buff to light brown silica vein material containing small, dark colored, silica-replaced fragments of Tiva Canyon Member. *

4a) [z]Split of hand-sample remaining from 3SW333.

5) [x]3SW335: north wall, silicified breccia of Tiva Canyon Member with bleached groundmass surrounding drusy quartz-lined lithophysal cavities, ~ 2 meters east of thick, white, calcareous vein. *

5a) [z]Split of hand-sample remaining from 3SW335.

6) [x]3LT029: south wall, silicified breccia of Tiva Canyon Member, purplish rock fragments in buff siliceous matrix. *

6a) [z]Split of hand-sample remaining from 3LT029.

7) 3SW433: dense, lithophysal Tiva Canyon Member, east side of Exile Hill. **

7a) Duplicate split of 3SW433. **

7b) Triplicate split of 3SW433. **

7c) [z]Split of hand-sample remaining from 3SW433.

8) 3SW435: dense, lithophysal Tiva Canyon Member, east side of Exile Hill. **

8a) Duplicate split of 3SW435. **

8b) Triplicate splits of 3SW435. **

8c) [z]Split of hand-sample remaining from 3SW435.

9) 3SW437: dense, lithophysal Tiva Canyon Member, east side of Exile Hill. **

9a) Duplicate split of 3SW437. **

9b) Triplicate split of 3SW437. **

9c) [z]Split of hand-sample remaining from 3SW437.

Except as noted, analyses by Geochemical Services Inc., using inductively-coupled plasma emission spectrography; * = 10 gram digestion; ** = 15 gram digestion. Values as reported by G.S.I.; number of significant figures does not indicate precision or accuracy of analyses.

[x] denotes analyses from Weiss et al. (1989b).

[z] denotes mercury analyses by the Nevada Mining and Analytical Laboratory, Nevada Bureau of Mines and Geology, using atomic absorption methods.

A comparison of the noble metal and the indicator-element concentrations, the silicified "mosaic" breccia from Trench #14, relative to the stratigraphically equivalent background. From Weiss et al. (1990).

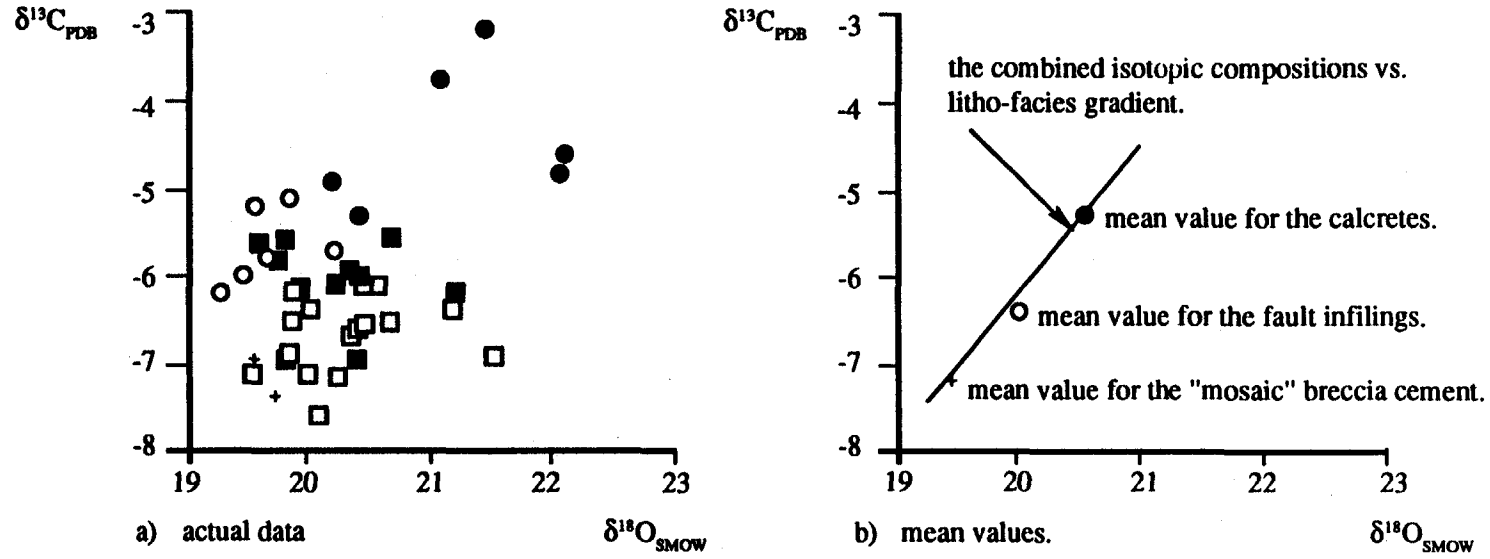

Explanation:

- ■ - sample represents the Trench 14 calcretes;
- ● - samples represents the Busted Butte calcretes;
- □ - sample represents the Trench 14 fault infiling;
- ○ - sample represents the Busted Butte fault infiling; and
- \+ - sample represents Trench 14 and Busted Butte "mosaic" breccia.

A comparison of the isotopic characters of carbon and oxygen, incorporated in samples of the "mosaic" breccia cement, the surficial veins, and the local calcretes. From Whelan and Stuckless (1990).

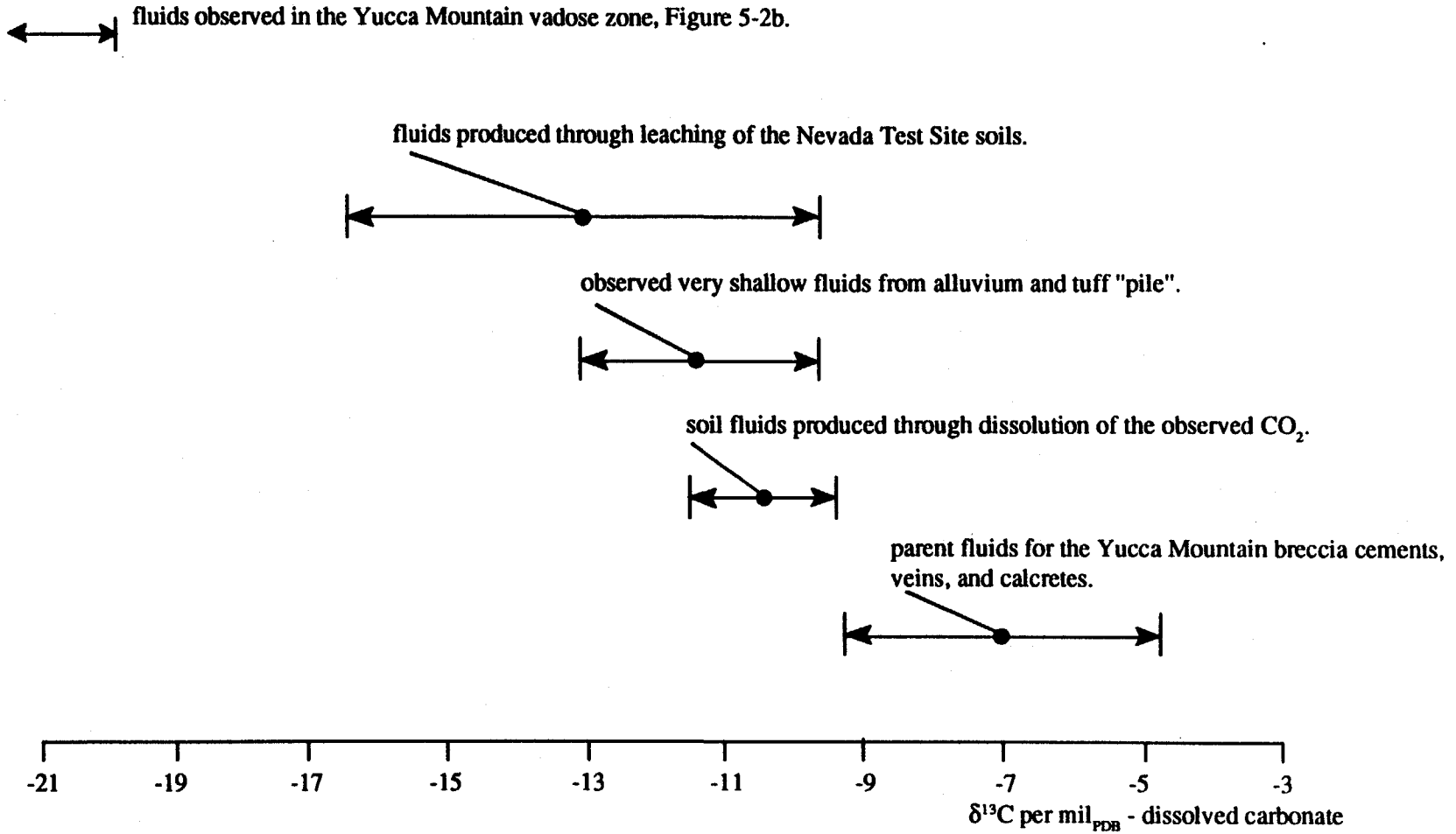

Note:

a) the isotopic data used in constructing this figure are explained and referenced in Figures 6-5b and 6-5c; and

b) carbonate gangue associated with hydrothermal ore deposits typically carry values of the $\delta^{13}C$ ratio ranging from -10 to about +10 per milPDB, Figures 8-8 and 8-9.

Carbon isotopic analyses of the origin of the authigenic breccia cements and the associated lithofacies.

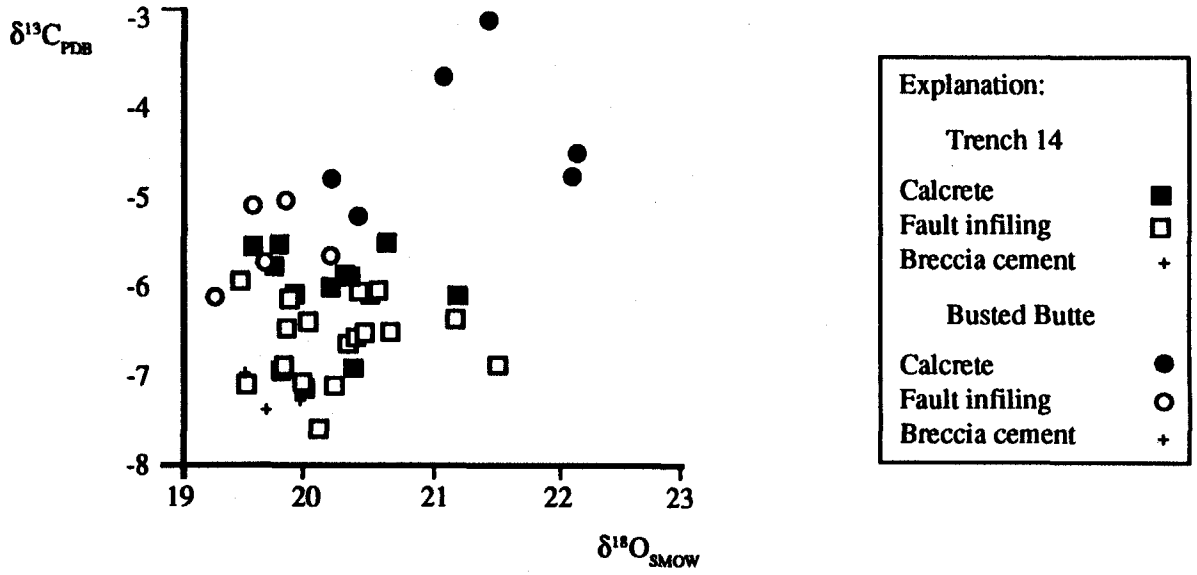

Note:

a) the observed range for the $\delta^{13}C$ ratio, from samples of the Yucca Mountain calcretes and surficial veins, is from -3.0 to -7.5 per mil_{PDB}, isotopic data are from Whelan and Stuckless, 1990;

b) for precipitation temperature T=15° Celcius, the equilibrium fractionation factor $10^3 ln\alpha_{CaCO_3 - HCO_3^-} = 1.75$ per mil_{PDB}; and

c) the interpreted range for the $\delta^{13}C$ ratio, for the parent fluids of the Yucca Mountain calcretes, surficial veins and breccia cements, is from -4.75 to -9.25 per mil_{PDB}.

Carbon isotopic analyses of the origin of the authigenic breccia cements and the associated lithofacies.

- A mean value of the $\delta^{13}C$ ratio for the CO_2 gas respired from the vadose zone, as observed at Yucca Mountain and Amargosa Narrows, is $\delta^{13}C$ = -18.36 and -20.0 per mil_{PDB}, respectively, Yang et al., 1986, Thorstenson et al., 1989, and White and Chuma, 1987 - the Yucca Mountain value is based on samples that carry PMC > 100 percent and were collected at a depth ranging from 0 to 12.8m.

- A mean value of the $\delta^{13}C$ ratio for soil gas, as observed at various locations throughout the Nevada Test Site, is $\delta^{13}C$ = -20.5 per mil_{PDB}, Boughton, 1986.

- The equilibrium isotopic fractionation factor $10^3 ln\alpha_{HCO_3^- - CO_2(g)} = 9.483 \cdot 10^3 \cdot T^{-1} - 23.89$, Turi (1986) - for 15° Celcius, the fractionation factor is ~9 per mil_{PDB}.

- Dissolution of the CO_2 gas respired from the vadose zone, with the observed range from -18.36 to -20.5 per mil_{PDB}, may be expected to yield the supergene pedogenic fluids with the $\delta^{13}C$ ratios ranging from -9.36 to -11.5 per mil_{PDB}.

- A mean value for the $\delta^{13}C$ ratio from samples of shallow alluvium-based fluids, as observed around Amargosa Narrows, is $\delta^{13}C$ = -11.3 per mil_{PDB} (range of the observed values is from -9.59 to -13.05 per mil_{PDB}), White and Chuma (1987).

- A value of the $\delta^{13}C$ ratio from samples of shallow tuff "pile" - based fluids, as observed in the Yucca Mountain borehole UE-29a#2 (depth to the water table is 29m, and PMC ranges from 60 to 62.3 percent), is $\delta^{13}C$ = -13.0 per mil_{PDB}, Benson and McKinley, 1985.

- A value of the $\delta^{13}C$ ratio for the Nevada Test Site soil water, as interpreted based on laboratory soil-leaching experiments, is $\delta^{13}C$ = -12.0 per mil_{PDB} (the observed range for leached water is from -9.6 to -16.4 per mil_{PDB}), Spencer (1990).

Carbon isotopic analyses of the origin of the authigenic breccia cements and the associated lithofacies.

The $\delta^{13}C$ range from -4.75 to -9.45 per mil_{PDB}, interpreted for the parent fluids of the Yucca Mountain calcretes and surficial veins, is too "heavy" to permit genetic association with the local supergene pedogenic fluids alone.

Note:

a) Quade and Cerling (1990) have proposed that, the Yucca Mountain calcite-silica deposits were precipitated during glacial maxima, when local climate was cooler than the contemporary climate;

b) the postulated climate was analogous to that presently encountered at altitudes 750 - 790m higher, in the lower pinyon-juniper-sagebrush zone;

c) it may reasonably be assumed that, during precipitation of the Yucca Mountain calcite-silica deposits, the local biomass have contained higher proportion of plants with the C-3 metabolic pathway and, consequently, the biogenically derived CO_2 was isotopically "lighter" than the contemporary CO_2; and

d) the depicted in Figure 6-5a isotopic discrepancy, between the parent fluids for the Yucca Mountain deposits and the local supergene pedogenic fluids, represents a minimum value.

Carbon isotopic analyses of the origin of the authigenic breccia cements and the associated lithofacies.

	DTV2.1		TR14-3B-SSL		TR14-3A-SSL	
	B1E-4	B1F-2	J-1	K-1	A-3	X-2
Weight percent						
SiO_2	49.5	49.7	75.6	68.4	62.4	63.9
TiO_2	0.00	0.00	0.03	0.06	0.00	0.00
Al_2O_3	0.61	2.44	0.13	0.23	0.26	0.54
Fe_2O_3	0.08	<0.05	<0.04	<0.03	0.00	0.00
MnO	0.00	0.00	0.00	<0.03	0.00	0.00
MgO	19.8	19.5	10.07	13.1	16.8	17.0
CaO	0.04	0.06	0.05	0.09	0.08	0.11
Na_2O	<0.05	0.00	0.00	0.00	<0.03	0.04
K_2O	0.05	0.08	0.00	<0.03	<0.02	0.04
Total	70.1	71.8	85.9	81.9	79.5	81.6
Si/Mg (molec.)	1.68	1.71	5.03	3.49	2.50	2.53

Note:

a) sample DTV2.1 represents the "mosaic" breccia from Busted Butte area; and

b) samples TR14-3B-SSL and TR14-3A-SSL represent the "mosaic" breccia from Trench #14 exposure.

Chemical compositions from samples of sepiolites, based on the microprobe analyses. From Levy and Naeser (1991).

SAMPLE	DF-	MINERAL	NUMBER GRAINS	ρ_s X 10^6 t/cm^2	FOSSIL TRACKS COUNTED	ρ_i X 10^6 t/cm^2	INDUCED TRACKS COUNTED	DOSIMETER DENSITY X 10^5 t/cm^2	TRACKS COUNTED	Ma	±σ
HD-41-4	6048	ZIRCON	12	2.03	470	10.1	1164	2.20	3093	14.17	1.6
1				0.70	13	5.94	55	"	"	8.3	5.1
2				0.65	3	4.90	34	"	"	9.3	7.0
3				1.15	16	10.8	75	"	"	7.5	4.1
4				2.13	79	8.37	155	"	"	17.9	4.9
5				3.89	36	17.7	82	"	"	15.4	6.2
6				1.30	24	7.99	74	"	"	11.4	5.3
7				1.24	23	5.18	48	"	"	16.8	8.5
8				1.51	21	7.02	65	"	"	11.3	5.7
9				5.45	101	15.6	144	"	"	24.6	6.4
10				0.76	6	5.47	76	"	"	9.7	4.8
11				2.95	41	24.2	168	"	"	8.6	3.0
12				3.72	66	16.2	188	"	"	16.1	4.2
HD-74-2	6050	ZIRCON	12	2.71	828	11.8	1799	"	"	16.2	1.5
1				1.47	34	9.68	112	"	"	10.7	4.2
2				0.32	9	4.41	51	"	"	6.2	4.5
3				0.35	13	3.02	56	"	"	8.2	5.0
4				0.89	37	4.70	98	"	"	13.3	5.1
5				14.5	268	17.0	157	"	"	59.7	12
6				9.07	168	41.1	381	"	"	15.5	2.9
7				4.17	116	21.7	302	"	"	13.5	2.9
8				0.62	19	7.52	87	"	"	7.7	3.9
9				1.86	43	15.0	174	"	"	8.7	3.0
10				2.18	40	12.1	112	"	"	12.5	4.6
11				2.76	64	12.4	144	"	"	15.6	4.7
12				0.73	17	10.8	125	"	"	4.8	2.5

ZETA (SRM 962) = 319.3 DF = LABORATORY NUMBER ANALYZED BY: C. W. NAESER

Note:

a) sample HD-41-4 represents "mosaic" breccia from Trench #14; and

b) sample HD-74-2 represents "mosaic" breccia from Busted Butte area.

Fission-track data from detrital zircons incorporated in samples of the "mosaic" breccias from Trench #14 and the Busted Butte area. From Levy and Naeser (1991).

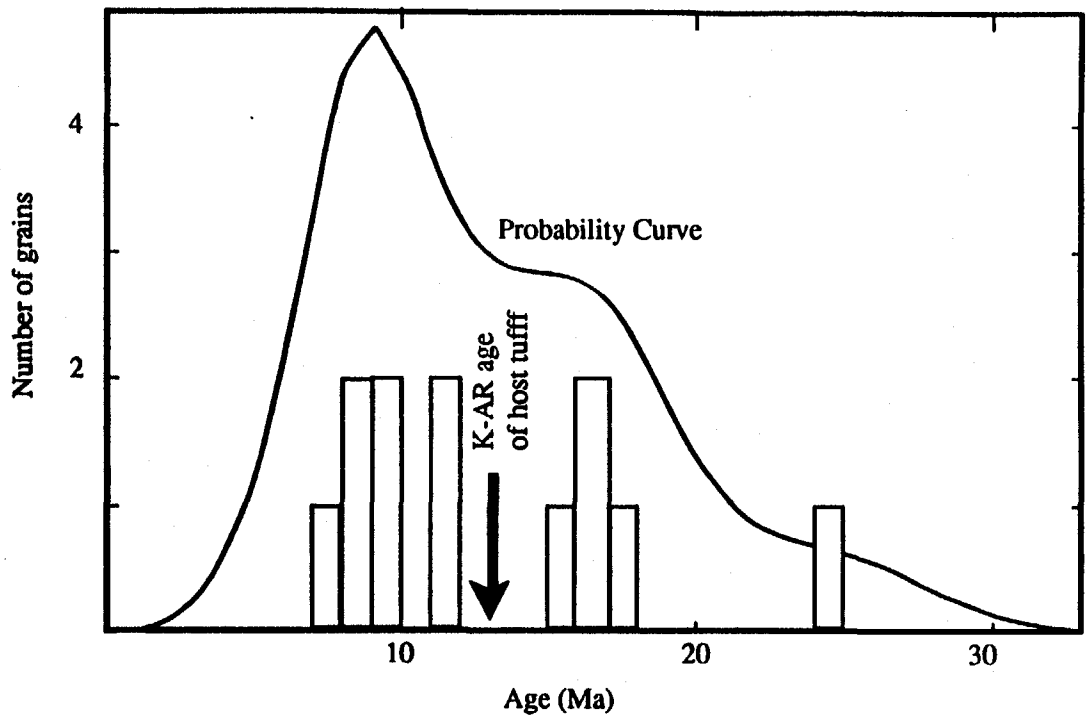

Note:

a) for sample HD-41-4, the host rock is the Tiva Canyon Member of the Paintbrush Tuff.

Probability density distribution and histogram of zircon ages from sample HD-41-4 of the "mosaic" breccia. From Levy and Naeser (1991).

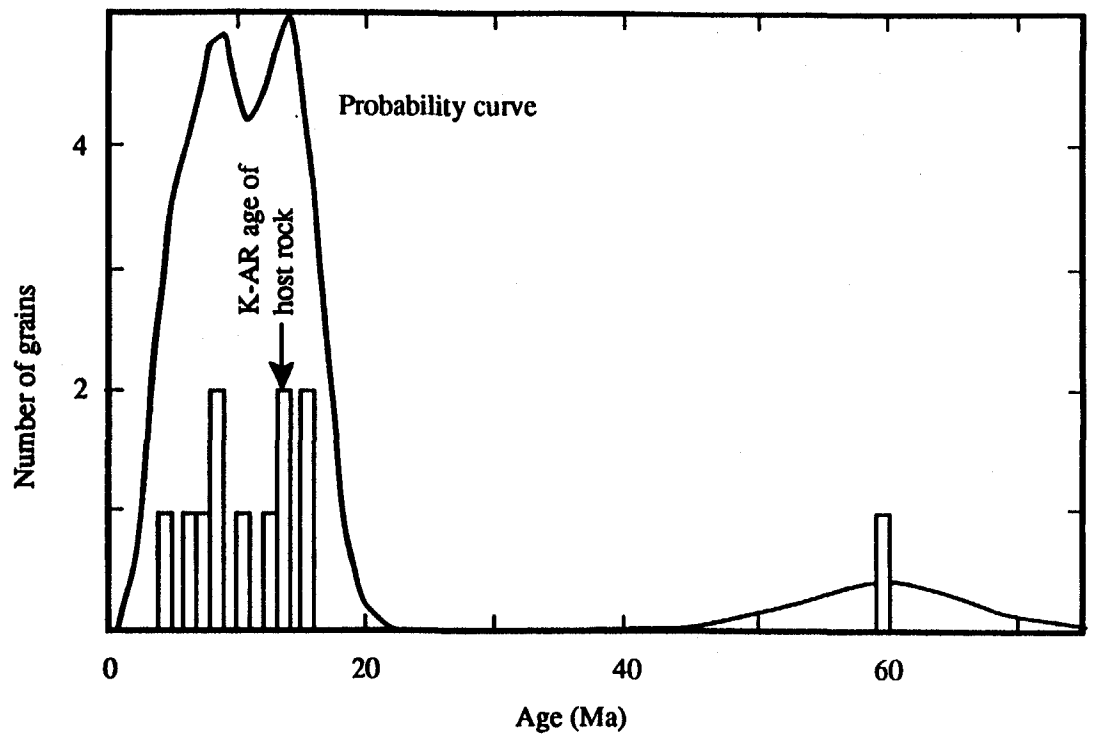

Probability density distribution and histogram of zircon ages from sample HD-74-2 of the "mosaic" breccia. From Levy and Naeser (1991).

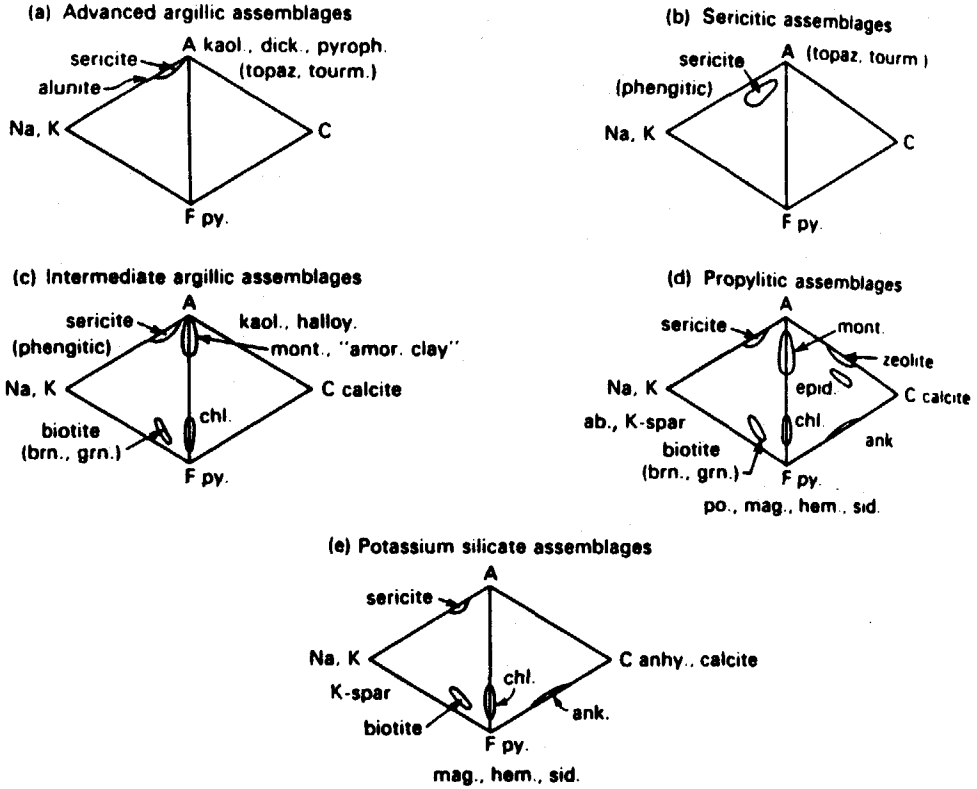

Explanation:

ab. = albite; ank. = ankerite; chl. = chlorite; dick. = dickite; epid. = epidote; halloy. = halloysite; hem. = hematite; K-spar = K-feldspar; kaol. = kaolinite; mag. = magnetite; mont. = montmorillonite; po. = pyrrhotite; py. = pyrite; pyroph. = pyrophyllite; sid. = siderite; tourm. = tourmaline.

Mineral assemblages in major types of the hydrothermal wall-rock alterations. From Meyer and Hemley, 1967.

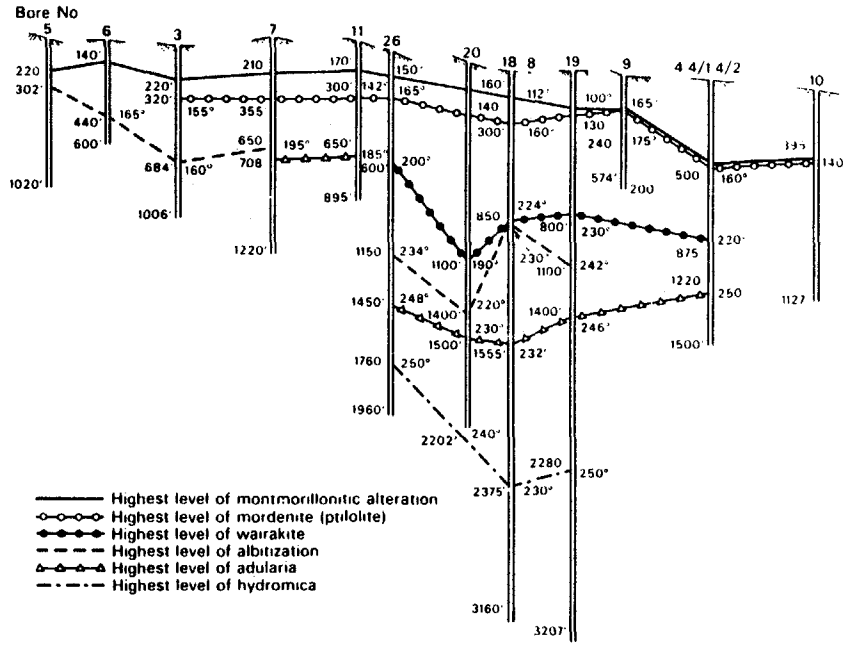

Depth and temperature related zonation of hydrothermal zeolitization. Wairakei, New Zealand. From Ellis, 1967.

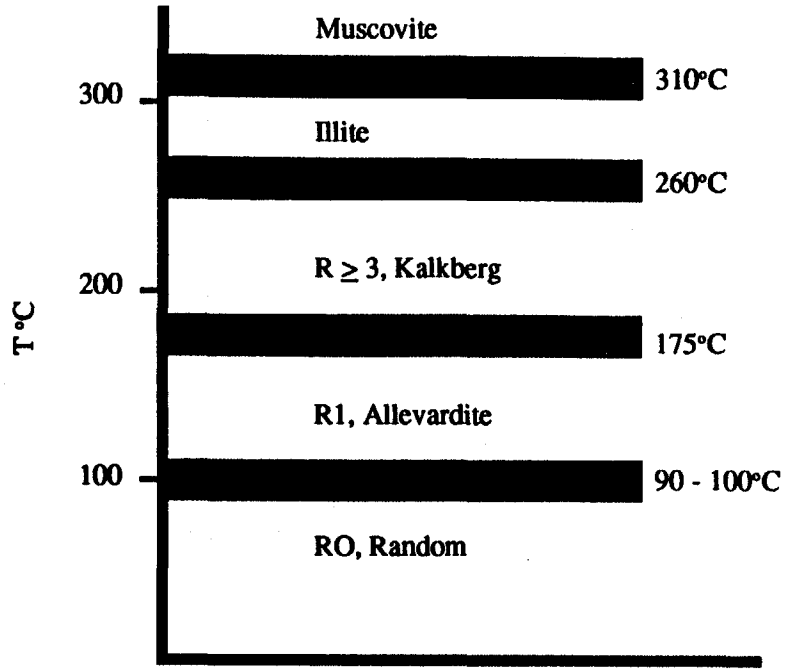

a) Relationship between temperature and the degree of the smectite → illite reaction, based on data from areas undergoing burial diagenesis and hydrothermal alteration.

Note:

a) over reaction times $>10^7$ years, the allevardite clays are formed at 90° to 100° C, but over reaction times $<10^6$ years these clays are formed at 130° to 150° C;

b) high K^+ concentrations tend to promote the illitization reaction, whereas low K^+ concentrations and the presence of Ca^{++}, Mg^{++}, and Na^+ cations inhibit this reaction; and

c) top of the allevardite clay bearing zone may be interpreted as having been formed at a temperature 130° to 150° C; top of the Kalkerberg clay and illite bearing zones may be interpreted as having been formed at 175° and 260° C; respectively.

Key for reconstructions of paleo-geothermal conditions, based on observed zonation of smectite - hydromice series. From Bish (1989).

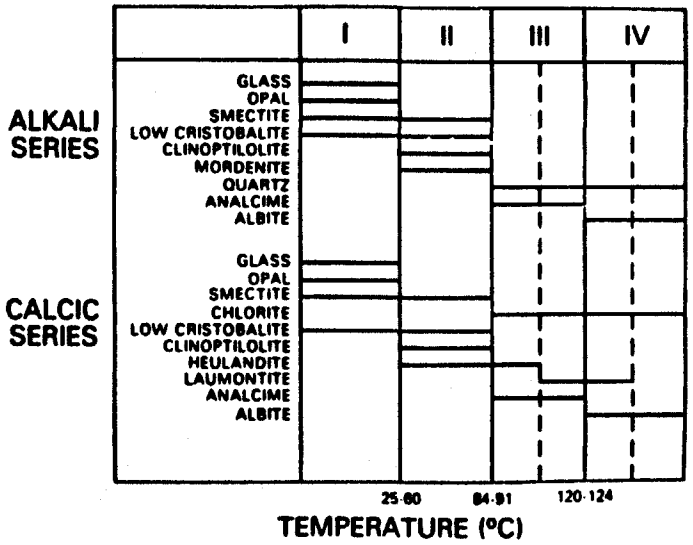

a) Zeolite zonation for marine tuffs with high (~10^4 ppm) concentrations of Na^+ cations in fluids.

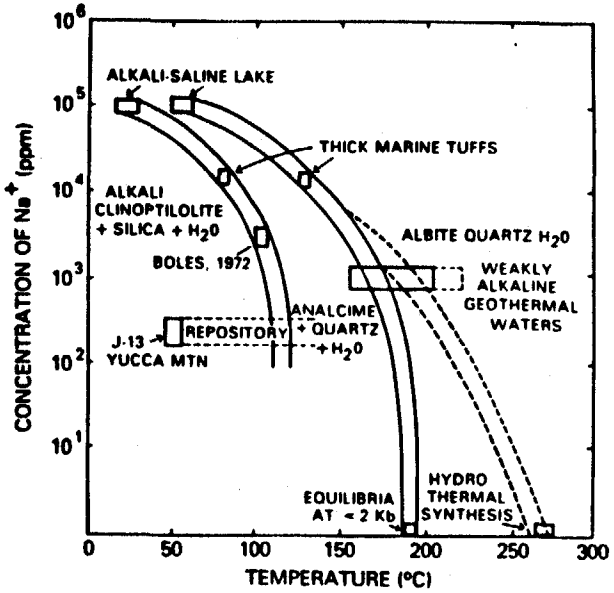

b) Zeolite zonations as a function of temperature and concentrations of Na^+ cations in fluids.

Note:

a) it may reasonably be assumed that, partially, zeolitic alteration of the Yucca Mountain ignimbrites was accomplished by fluids with cation concentrations similar to those of the "weakly alkaline geothermal waters";

b) top of the analcime zeolitic zone may be interpreted as having been formed at a temperature of about 110° Celsius; and

c) top of the albite zeolitic zone may be interpreted as having been formed at a temperature of about 130° Celsius.

Key for reconstructions of paleo-geothermal conditions, based on observed zonation of zeolitic alteration. From Smyth and Caporuscio, 1981.

Origin of Analcime.

Analcime crystallizes in many different environments, including hydrothermal solutions in volcanics, pegmatites, alteration of volcanic ash in saline alkaline lakes, deep-sea sediments, and as a primary mineral crystallizing from basaltic magma.

The temperature, pressure, and solution composition in which analcime crystallizes is well known from data obtained in geothermal areas in Iceland, Japan, and the USA. Geothermal wells, drilled through Tertiary basalt in Iceland, show that analcime crystallized at temperatures from 60° to 300°C, at depths from 72 to 1600 meters, and is dominant above 175°C (Kristmannsdóttir and Tómasson, 1978). Calcium-rich analcime is believed to have crystallized at 280° to 380°C in thermally metamorphosed aureoles in Miocene basalt and andesite tuff breccia in Japan (Seki and Oki, 1969; Seki et al., 1969). Analcime is found in low-temperature zone (below 120° - 150°C) surrounding the Kuroko ore (= black ore) derived from "Black Smoker" hydrothermal vents, under water in Miocene seafloor volcanics (Utada, 1988).

Liquid inclusions in calcite, associated with analcime, indicate that the zeolites crystallized at 133°C on the Keweenaw Peninsula, Michigan (Stoiber and Davidson, 1959). Cesium-bearing analcime crystallized at 170° C at 80 meters, and at 198°C at 124 meters, in obsidian-rich sands and gravels in the Upper and Lower Geyser Basins, in Yellowstone National Park (Keith et al., 1983).

Analcime crystallizes from late-stage hydrothermal fluids, estimated at 200° to 300° C, in nepheline syenite complexes on the Kola Peninsula, U.S.S.R. (Fersman, 1926).

Volcanic ash, which fell into an Eocene saline, alkaline lake in Wyoming, was first altered by the saline, alkaline solutions (SiO_2 = 10 ppm, K = 50 ppm, Na = 1000 ppm, pH 8) to heulandite and mordenite. Later, sodium carbonate brines (SiO_2 = 1000 ppm, K = 5000, Na = 100,000, pH 9 to 10) replaced heulandite and mordenite by analcime (Surdam and Parker, 1972; Ratterman and Surdam, 1981). High-alkaline brines in the lakes take up to 3.18 million years to produce beds of analcime from rhyolitic glass tuff (Hay and Guldman, 1987).

Analcime and other zeolites form a white, natural cement between volcanic fragments at surface conditions from a reaction between seawater spray altering nephelinite tuffs near Honolulu Oahu (Iijima and Harada, 1969).

Analcime can crystallize from magma only under special conditions (5 to 13 kb pressure and at 600° to 640° C) when water is present (Roux and Hamilton, 1976). The analcime crystals then must be brought quickly to the surface and quenched for them to survive. Analcime phenocrysts, found embedded in tuffs, can also be derived by metasomatic replacement of leucite (Gottardi and Galli, 1985). Additional information on the origin of analcime can be found in Gottardi and Galli (1985).

Origin of zeolitic species which have been identified in the Yucca Mountain ignimbrites. Analcime. From Tschernich (1992).

Origin of Chabazite.

Date from geothermal wells, in basalt in Iceland, show that chabazite crystallizes at depths from 50 to 400 meters and at temperatures from 55° to 75° C (Kristmannsdóttir and Tómasson, 1978). With increasing depth, empty cavities are first encountered followed by clay-chabazite-phillipsite-levyne > thomsonite-mesolite-scolecite > stilbite-heulandite-epistilbite-mordenite > laumontite > analcime-wairakite (Kristmannsdóttir and Tómasson, 1978). Mapping of zeolites exposed in basalt in eastern Iceland and Northern Ireland also showed that chabazite was the characteristic zeolite in the shallowest zone, and, therefore, it crystallized at a lower temperature and pressure than all the other zeolites in those areas (Walker, 1951, 1960a, 1960b). Mapping of chabazite into zones, based on crystal morphology (rhombohedra, complex twins, and phacolite) in Northern Ireland by Walker (1951), is not valid since several of these habits are commonly present at a single locality and the morphology of synthetic chabazite is related to pH rather than temperature or pressure (RWT).

Chabazite has been synthesized from silica-poor basaltic and phonolitic glass in a sodium hydroxide (NaOH) or postassium hydroxide (KOH) solution with low pH at a wide range of temperatures (50° to 100° C), but in silica-rich rocks like rhyolite, chabazite only crystallizes in a solution with high pH (Höller and Wirsching, 1988). The composition of the reacting solution influenced the morphology. In solutions with low pH concentration, all the habits can form, commonly in the same sample. In solutions with a high concentration of NaOH, simple rhombohedra (some with penetration twins and negative rhombohedral faces) were produced, while a high concentration of KOH in the solution produced lenslike phacolite disks or rosettelike aggregates (Höller and Wirsching, 1988). Surface morphology of the crystal is determined by the amount of time that crystal reacts with the solution. Poorly shaped cyrstals are first produced, which in time, develop into rhombohedra on the phacolite disks. In a KOH solution, chabazite commonly forms alone, but in NaOH it crystallizes with phillipsite and analcime (Höller and Wirsching, 1988). In rhyolite, phillipsite formed first, but over a longer period of time, it was converted to chabazite. These reactions simulate conditions found in the center of a saline-alkaline lake where a high pH (high-alkaline concentration) is present.

Origin of zeolitic species which have been identified in the Yucca Mountain ignimbrites. Chabazite. From Tschernich (1992).

Origin of Erionite.

Erionite, found in drill cores from rhyolite-derived sediments in geyser basins in Yellowstone National Park, crystallized at a temperature below 110°C (Honda and Muffler, 1970). Data from geothermal wells passing through olivine basalt in Iceland indicate that levyne (which commonly precedes erionite) crystallized in the temperature range from 55° to 70° C (Kristmannsdóttir and Tómasson, 1978). Crystallization of levyne, with a low Si/Al ratio and low potassium content, causes an increase in silica and potassium in the solution. The potassium ion is the precursor for the cancrinite cage, which is the building block for offretite and erionite (Gard and Tait, 1972). Offretite forms rather than the more silica-rich erionite because offretite has a Si/Al ratio nearest that of levyne. As the Si/Al increases in solution, intergrowths with erionite occur. In silica-rich environments, such as andesite and sedimentary ash beds, erionite is dominant.

Woolly erionite may be a result of low-temperature hydrothermal solutions dissolving locally abundant sedimentary erionite and redepositing it in cavities and seams in adjacent rhyolite (Gottardi and Galli, 1985).

Origin of zeolitic species which have been identified in the Yucca Mountain ignimbrites. Erionite. From Tschernich (1992).

Origin of Heulandite (= Clinoptilolite).

Data from geothermal wells, in basalt in Iceland, indicate that heulandite crystallizes at depths from 30 to 1200 meters, and at temperatures from 65° to 200° C (Kristmannsdóttir and Tómasson, 1978). With increasing depth, empty cavities are first encountered, followed by chabazite-phillipsite-levyne > thomsonite-mesolite-scolecite > stilbite-heulandite-epistilbite-mordenite > laumontite > analcime-wairakite (Kristmannsdóttir and Tómasson, 1978). Heulandite commonly crystallizes in a cavity in the order: heulandite-mordenite-quartz > stilbite > mesolite-scolecite > thomsonite > chabazite (RWT).

Regional mapping of zeolites in Iceland, Northern Ireland, India, and Brazil shows that heulandite is found in the lower, deeper, and, therefore, hotter zones (Walker, 1960a, 1960b; Sukheswala et al., 1972; Murata et al., 1987). At Boron, California, heulandite crystals on colemanite, and analcime on searlesite, indicate that the zeolites formed at a very low temperature, compatible with borate crystallization. Since borax beds that cover the zeolite-bearing basalt are only slightly converted to kernite (a reaction that occurs at 60° C), the zeolites must have crystallized below that temperature (William Wise, pers. comm.). Silica-rich heulandite (= clinoptilolite) commonly crystallizes at surface temperatures in volcanic tuff beds, saline alkaline lakes, and as an alteration of phillipsite in deep-sea sediments.

Origin of zeolitic species which have been identified in the Yucca Mountain ignimbrites. Heulandite (= Clinoptilolite). From Tschernich (1992).

Origin of Laumontite.

Laumontite has been considered an indicator mineral for high-temperature, depth zonation of zeolites in burial diagenesis, although it has been found to form at very low temperatures (McCulloh et al., 1981). Laumontite is very difficult to synthesize in the laboratory, requiring temperatures of 250°C and 1000 bars pressure, yet it crystallizes rapidly in natural conditions at low temperatures and pressures where the solutions are of the appropriate composition (McCulloh et al., 1981). Laumontite crystallizes rapidly from water in radiators at geothermal plants and coats rounded rocks, in a stream fed by water (pH 7.74) issued from Sespe Hot Springs in California, at temperatures from 89°C down to 43°C (McCulloh et al., 1981).

Laumontite, when associated with prehnite, appears to form at a high temperature, in a transition between the zeolite zone (low-temperature zone where zeolites are dominant) and green-schist zones (higher-temperature zones where the green minerals prehnite, pumpellyite, chlorite, and epidote are dominant). Data from geothermal wells in basalt in Iceland show laumontite crystallized at temperatures between 98° and 230° C (Kristmannsdóttir and Tómasson, 1978). Laumontite is encountered in rhyolite, at temperatures from 140° to 200° C, in boreholes in Yellowstone National Park, Wyoming (Bargar and Beeson, 1981; Bargar et al., 1981).

Regional surface mapping by Walker (1960b) shows that laumontite occurs in the deepest zone (mesolite-scolecite zone) in the Tertiary olivine basalts in eastern Iceland. The Langford Lodge borehole, drilled through 789 meters of zeolite-bearing basalt in County Antrim, Northern Ireland, encountered laumontite only below 549 meters (Walkerm 1960a) and laumontite is restricted to the bottom of zeolite-bearing tholeiitic basalt and andesite in Rio Grande do Sul, Brazil (Murata et al., 1987). In Iceland, local zones of high-temperature alteration surrounding volcanic centers consist of a highly altered inner zone containing an abundance of the high-temperature minerals, epidote, chlorite, anadradite, pyrite, and some laumontite surrounded by a zone rich in laumontite but lacking epidote and garnet (Walker, 1960b).

Laumontite, covered by prehnite in Bombay, India, and associated with prehnite and pumpellyite at other localities, probably indicates a high-temperature origin, yet the sequence of crystallization studied in vesicular basalt at many other localities shows that laumontite is commonly the last zeolite to crystallize in a sequence (even after thomsonite and chabazite), which indicates a falling temperature. Laumontite, which cements sandstone under surface conditions or forms from glass in saline lakes, clearly indicates that it can crystallize at very low temperature when the correct chemical conditions are present.

Origin of zeolitic species which have been identified in the Yucca Mountain ignimbrites. Laumontite. From Tschernich (1992).

Figure 7-4e

Origin of Mordenite.

Mordenite is commonly found in geothermal wells; therefore, the temperature and pressure needed for crystallization in natural conditions are well known. In Iceland, mordenite is found in basalt, tuffaceous breccia, and dolerite (scattered throughout the mesolite-scolecite, stilbite, and laumontite zones) at temperatures from 75° to 280°C and at depths from 25 to 1800 meters (Kristmannsdóttir and Tómasson, 1978). In the Katayama geothermal area, Japan, mordenite is found in rhyolite at depths from 118 to 514 meters and at temperatures from 60° to 170°C in the Ohaki-Broadlands geothermal are (Browne and Ellis, 1970); and it is found in pumice and rhyolite tuff taken at depths from 80 to 213 meters and at temperatures from 60° to 164°C, in the Wairakei geothermal area (Steiner, 1953).

Glass in volcanic ash that fell into saline, alkaline lakes was altered over a very long period of time (1000 to 10,000 years) by the solutions (SiO_2 = 10 ppm, K = 50 ppm, Na = 1000 ppm, pH 8 to 9) at 25° to 65°C to tiny crystals of heulandite and mordenite (Hoover, 1968; Papke, 1972; Surdam and Parker, 1972; Ratterman and Surdam, 1981).

Thin, capillary needles of mordenite commonly crystallize slowly in stagnant, water-filled cavities. If the water-filled cavities slowly dry out under natural conditions, the mordenite needles become stiff and unmatted specimens result. If the pockets remain partially filled with surface water, movement of the rock and water, during collecting or blasting, mats the mordenite fibers together.

Origin of zeolitic species which have been identified in the Yucca Mountain ignimbrites. Mordenite. From Tschernich (1992).

Origin of Phillipsite.

Data from geothermal wells, in basalt in Iceland, show that phillipsite crystallizes at temperatures from 60° to 85°C (Kristmannsdóttir and Tómasson, 1978). With increasing depth, empty cavities are first encountered followed by clay-chabazite-phillipsite-levyne > thomsonite-mesolite-scolecite > stilbite-heulandite-epistilbite-mordenite > laumontite > analcime-wairakite (Kristmannsdóttir and Tómasson, 1978). Mapping of zeolites, exposed in basalt in eastern Iceland and Northern Ireland, also showed that phillipsite is found with chabazite in the shallowest zone, and, therefore, at a lower temperature and pressure than all the other zeolites in those areas (Walker, 1951, 1960a, 1960b).

Phillipsite is deposited in the cement wall-work of Roman baths at Plombieres where the water from hot springs emerges at a maximum temperature of 70°C (Daubrée, 1879).

At Boron, California, phillipsite is found with other zeolites on searlesite and colemanite, indicating that the zeolites formed at very low temperatures compatible with borate crystallization. Since borax beds that cover the zeolite-bearing basalt are only slightly converted to kernite (a reaction that occurs at 60°C), the zeolites must have crystallized below that temperature (William Wise, pers. comm.).

In Searles Lake, San Bernardino County, the glassy ash layers, in contact with highly saline, alkaline pore fluid (pH 9.5 at 24°C), were altered to phillipsite (Hay and Guldman, 1987). Phillisite in the palagonite tuffs in Honolulu, on Oahu, formed at surface conditions from reaction of surface water with volcanic glass (Iijima and Harada, 1969). Phillipsite crystallizes on the seafloor at temperatures as low as 4°C.

Origin of zeolitic species which have been identified in the Yucca Mountain ignimbrites. Phillipsite. From Tschernich (1992).

Origin of Stilbite (= stellerite).

Data from geothermal wells, in basalt in Iceland, show that stilbite crystallizes at depths from 45 to 1200 meters and at temperatures from 75° to 200°C (Kristmannsdóttir and Tómassson, 1978). With increasing depth, empty cavities are first encountered, followed by chabazite-phillipsite-levyne > thomsonite-mesolite-scolecite > stilbite-heulandite-epistilbite-mordenite > laumontite > analcime-wairakite (Kristmannsdóttir and Tómasson, 1978). Stilbite commonly crystallizes in a single cavity in the order: heulandite-mordenite-quartz > stilbite > mesolite-scolecite > thomsonite > chabazite (RWT).

Origin of zeolitic species which have been identified in the Yucca Mountain ignimbrites. Stilbite (= stellerite). From Tschernich (1992).

Origin of Wairakite (Ca equivalent of analcime).

Data taken from geothermal wells, in New Zealand, Japan, Iceland, and the U.S.A., have established the temperature, pressure, and solution composition for crystallization of wairakite. Wairakite generally forms at temperatures from 60° to 300°C and at depths from 72 to 1600 meters. Most wairakite forms at temperatures above 175°C (higher than most zeolites) although it has been reported to crystallize at surface temperatures. In geothermal areas, in New Zealand, wairakite has crystallized from dilute alkaline solutions with near neutral pH, low CO_2, and low aluminum content (Browne et al., 1989). The fluid in the geothermal wells contains 1200 ppm of chloride (Browne and Ellis, 1970).

Origin of zeolitic species which have been identified in the Yucca Mountain ignimbrites. Wairakite. From Tschernich (1992).

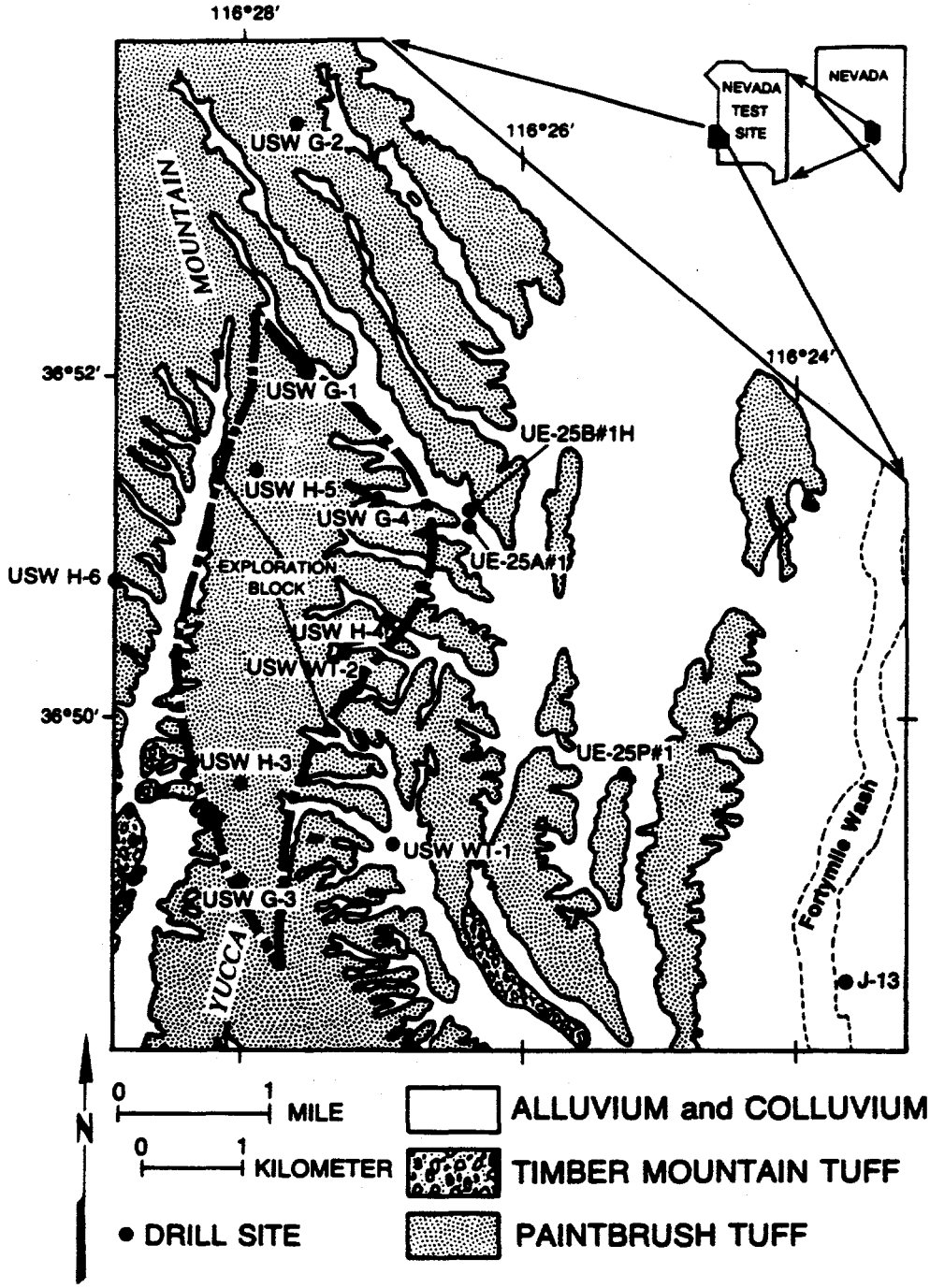

Map of Yucca Mountain showing the location of boreholes discussed in the text. From Bish and Chipera (1989).

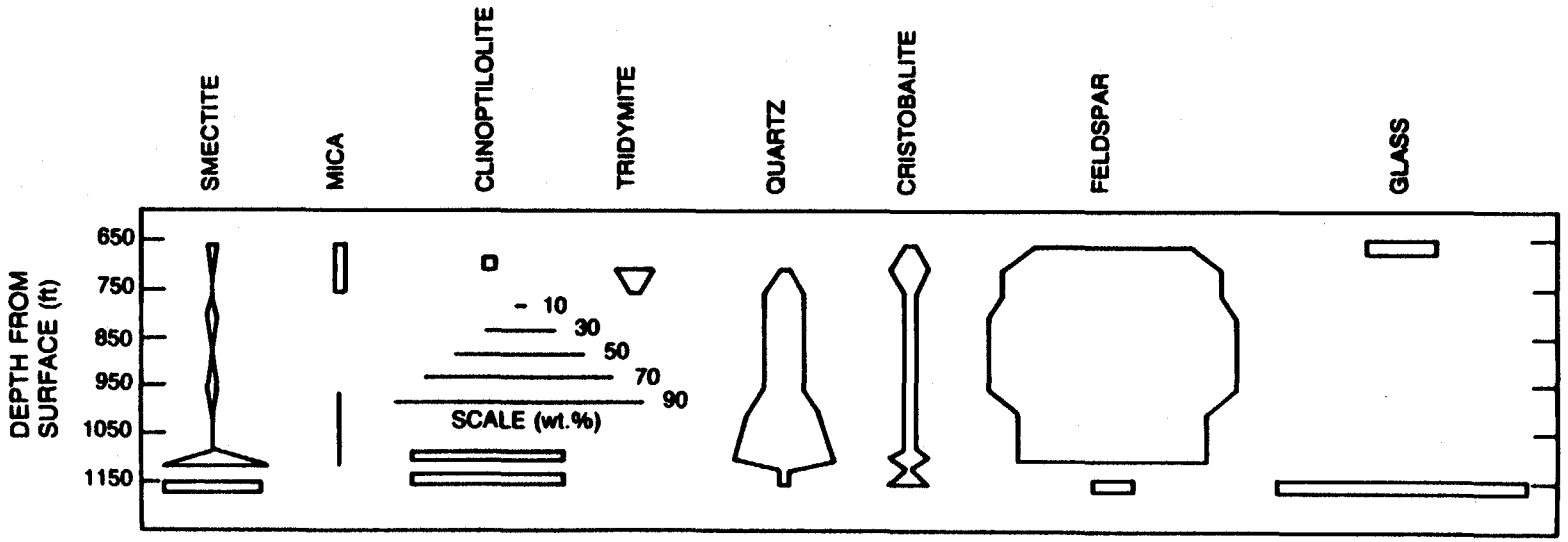

Note:

a) the contemporary water table is at a depth of ~738 ft. below land surface.

Relative abundances of glass and alteration minerals. Borehole J-12. From Bish and Chipera (1989).

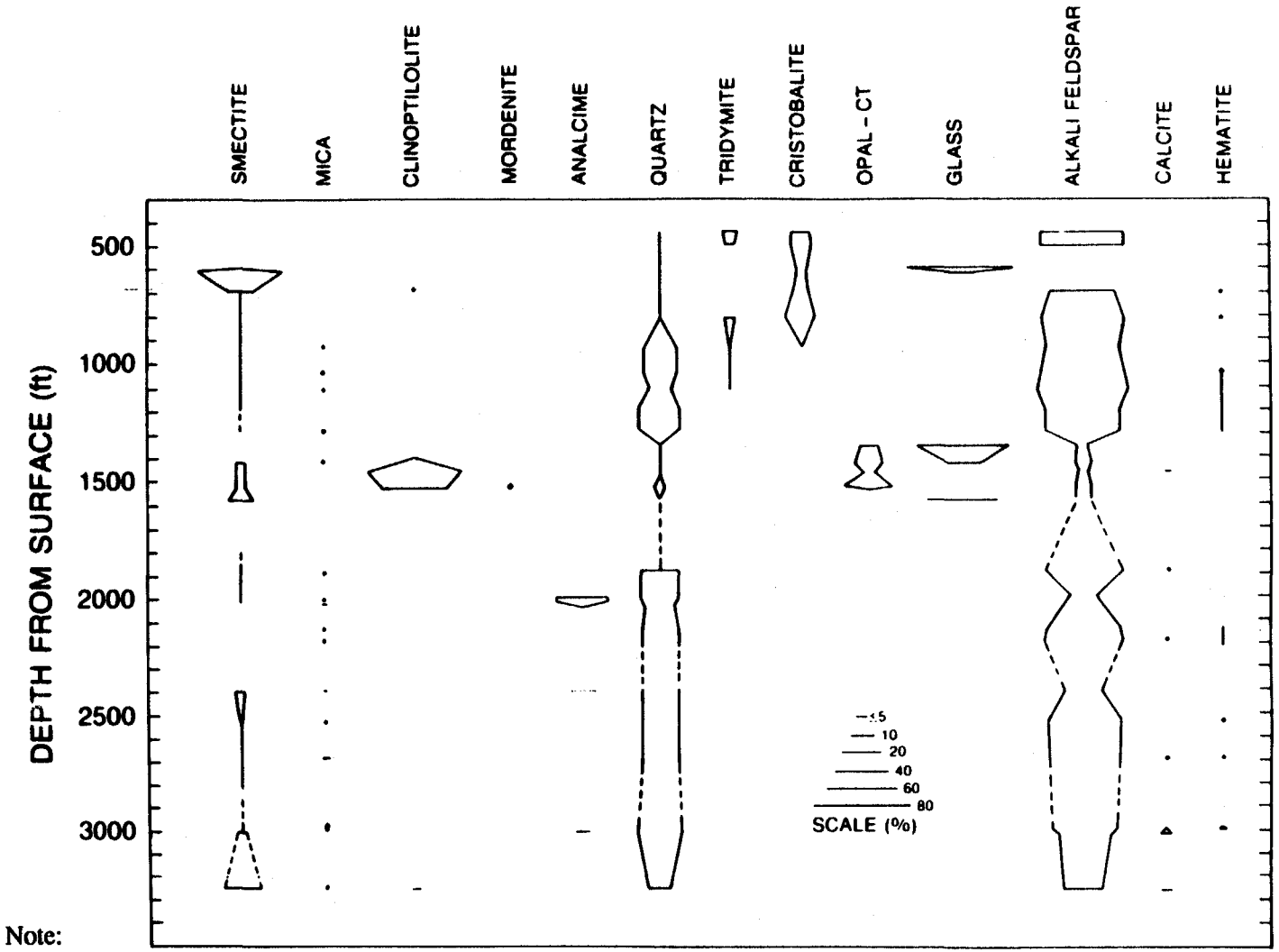

Note:

a) the contemporary water table is at a depth of ~925 ft below land surface; and

b) presence of analcime was reported by Broxton et al. (1986) within the Tiva Canyon Member of the Paintbruch Tuff, at a depth of 608 feet.

Relative abundances of glass and alteration minerals. Borehole J-13. From Bish and Chipera (1989).

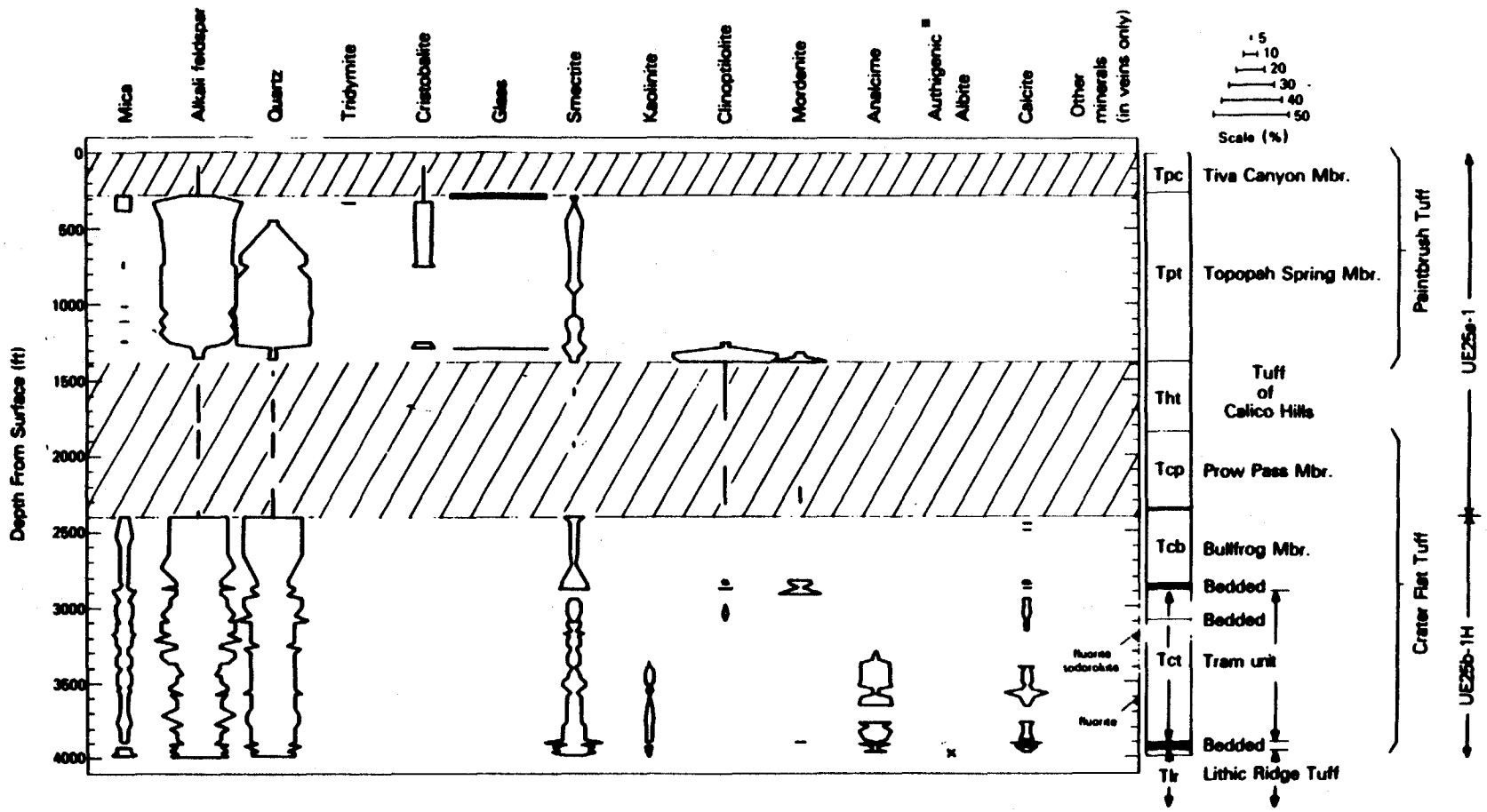

Note:

a) the contemporary water table is at a depth of ~1542 ft. below land surface.

Relative abundances of glass and alteration minerals. Boreholes UE-25a#1 and UE-25b#1. From Bish and Chipera (1989).

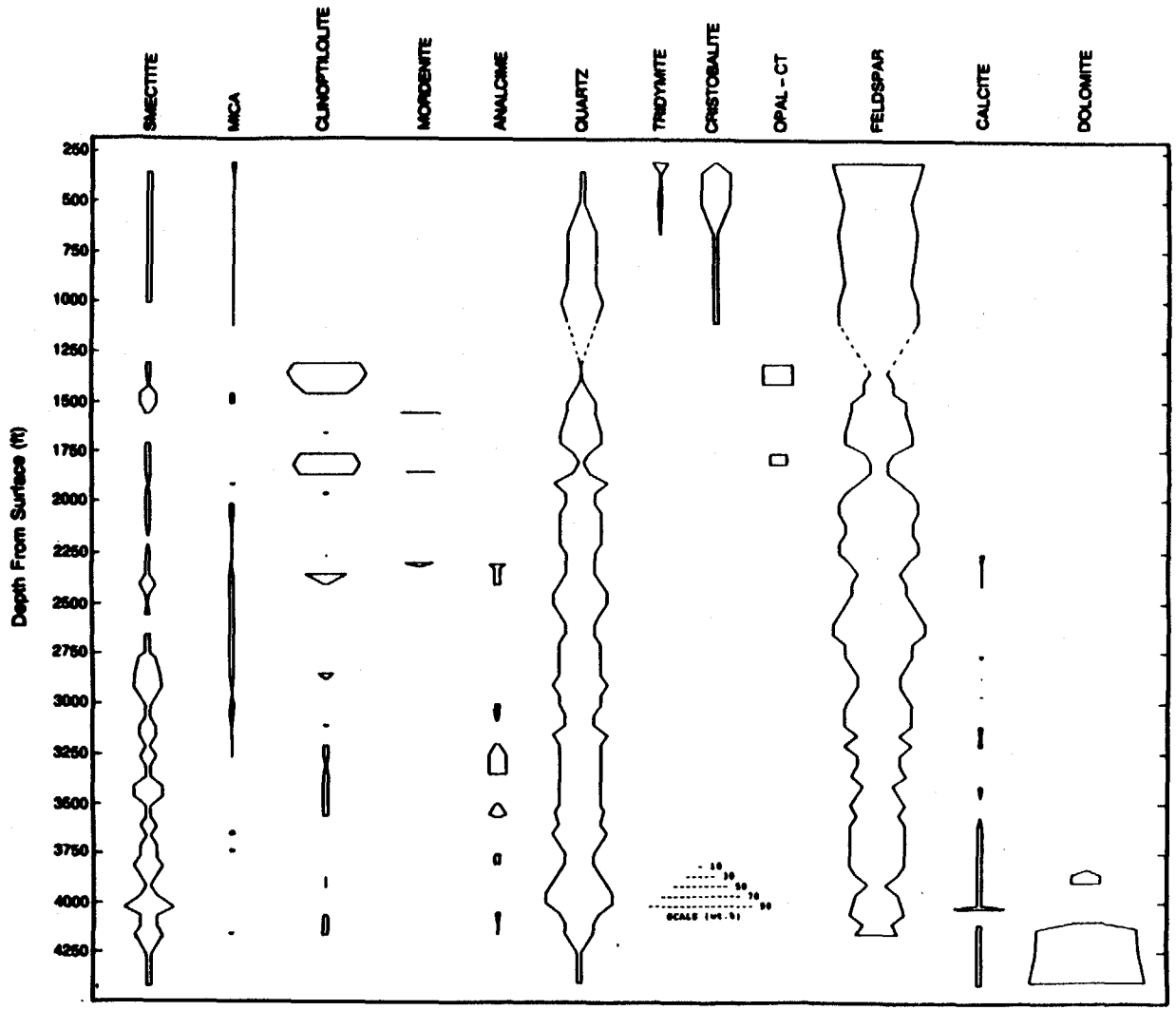

Note:

a) the contemporary water table is at a depth of ~1250 ft. below land surface.

Relative abundances of glass and alteration minerals. Borehole UE-25p#1. From Bish and Chipera (1989)

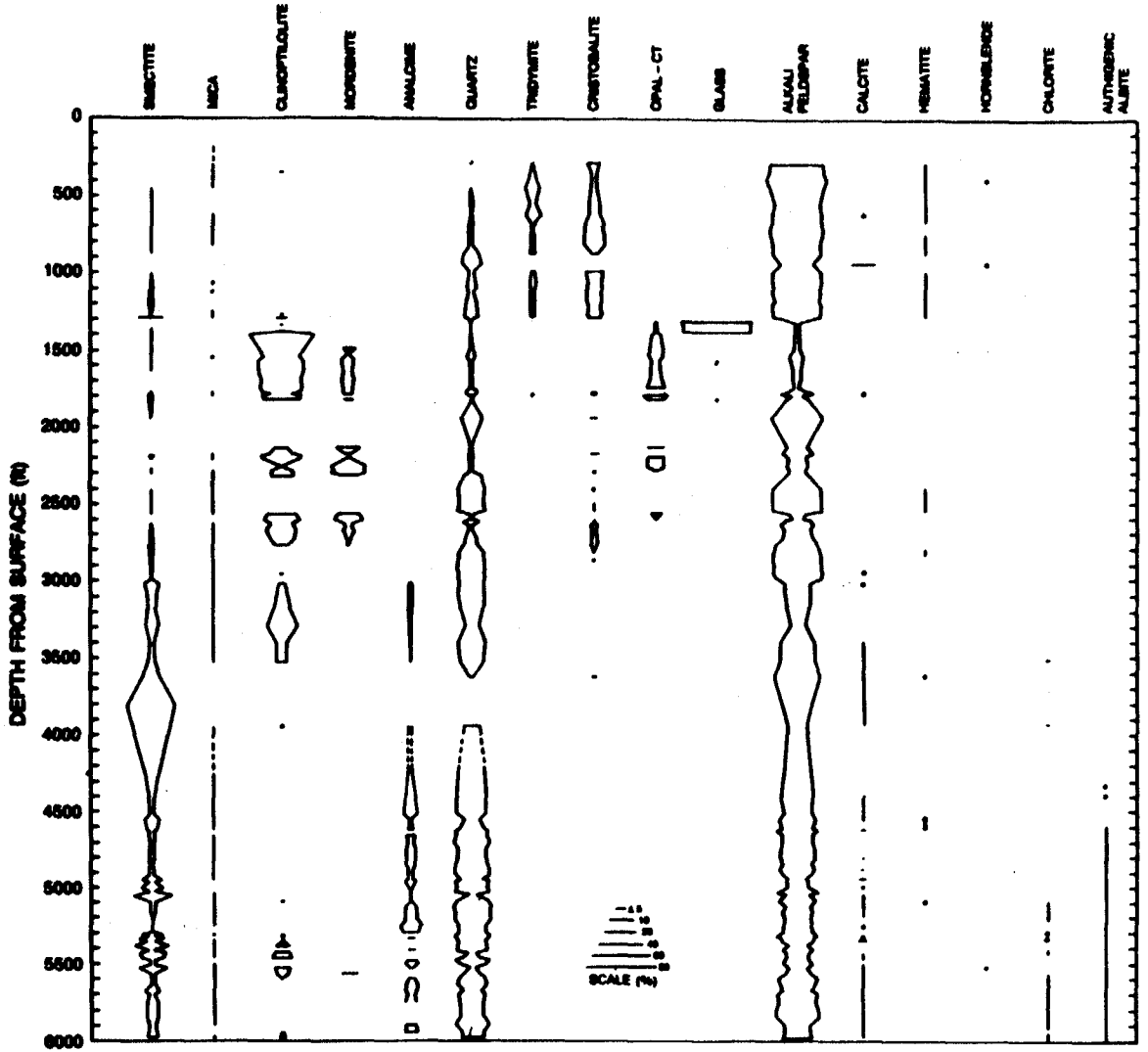

Note:

a) the contemporary water table is at a depth of ~1804 ft. below land surface.

Relative abundances of glass and alteration minerals. Borehole USW G-1. From Bish and Chipera (1989).

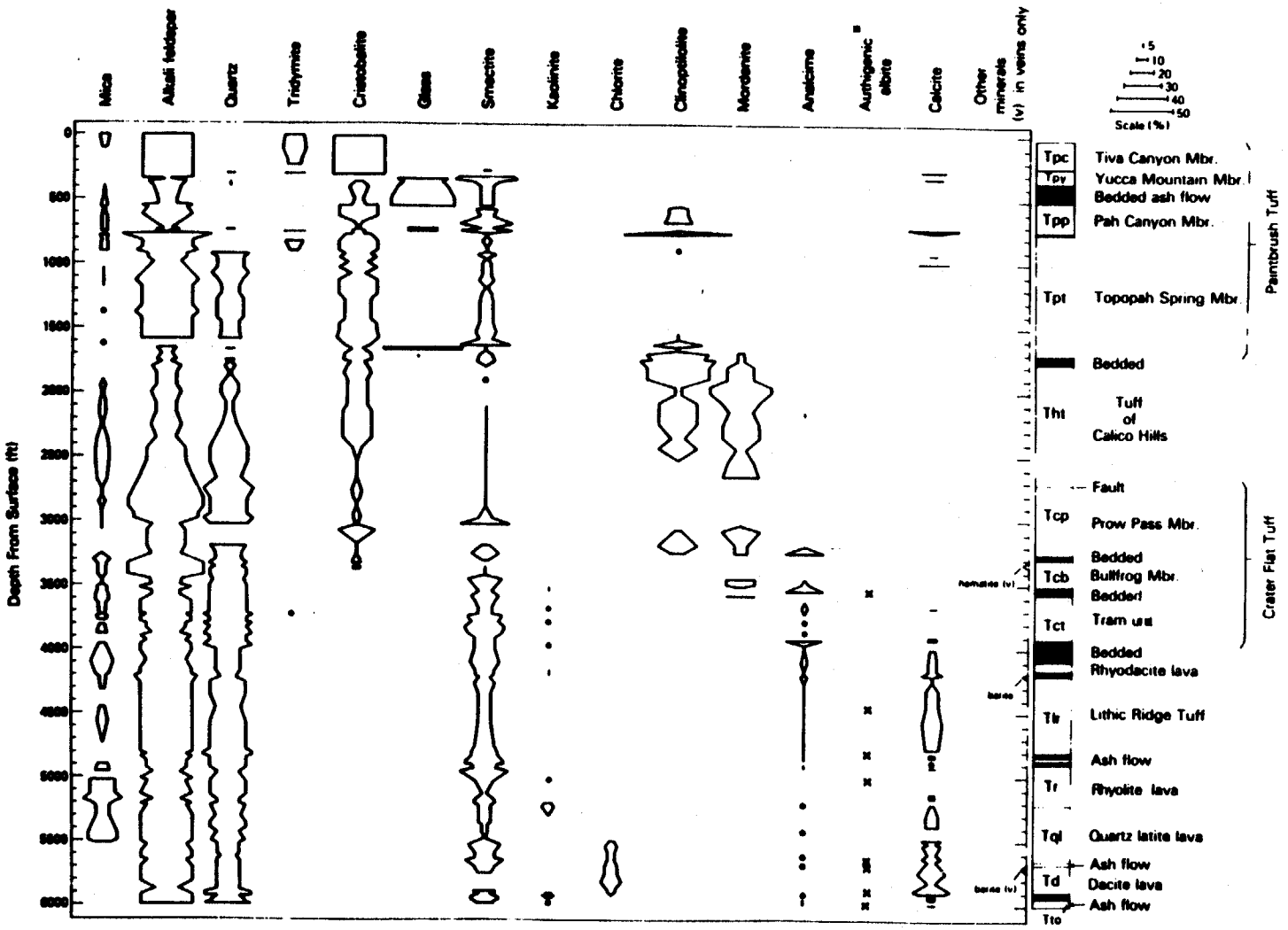

Note:

a) the contemporary water table is at a depth of ~1706 ft. below ground surface.

Relative abundances of glass and alteration minerals. Borehole USW G-2. From Bish and Chipera (1989).

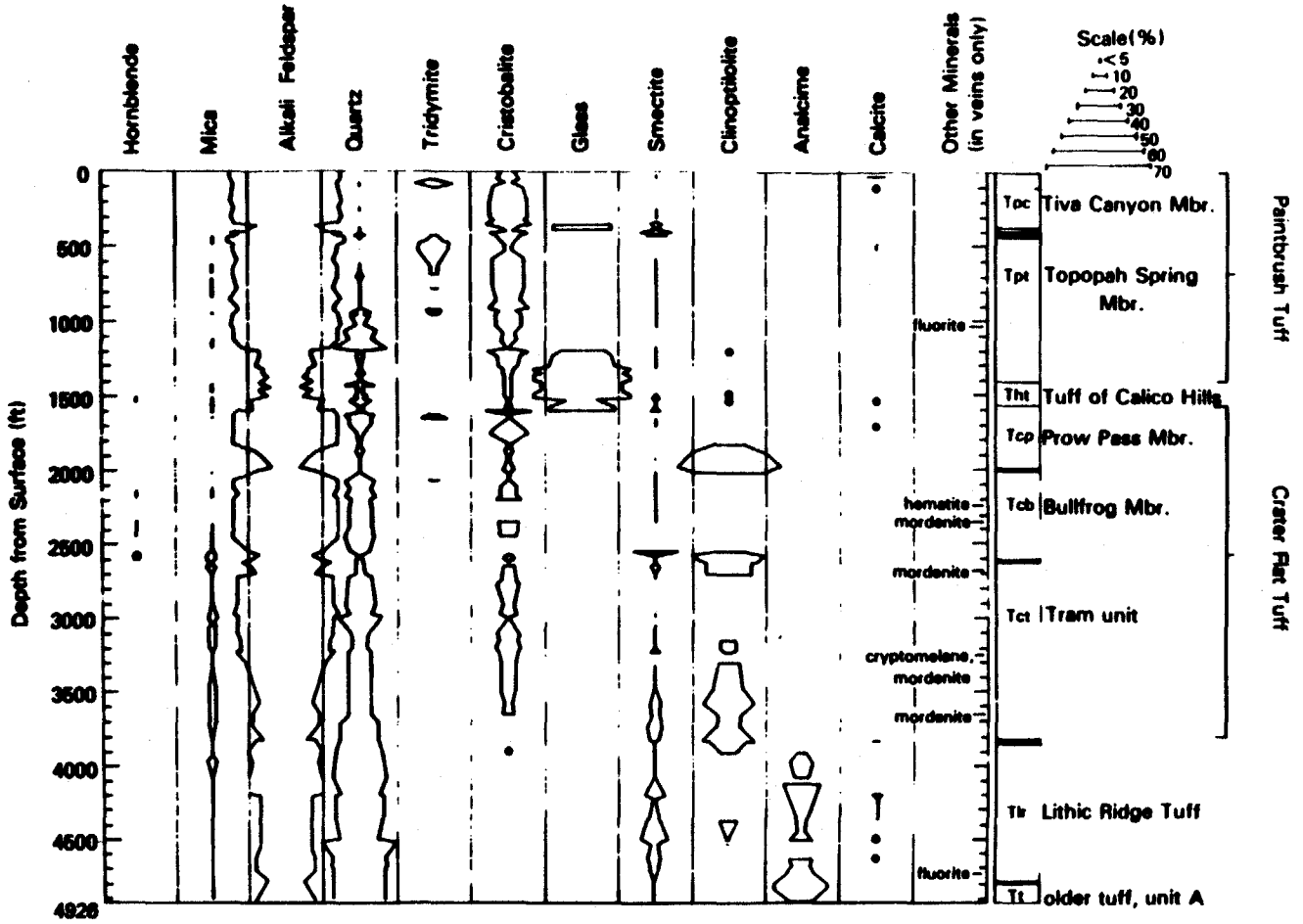

Note:

a) the contemporary water table is at a depth of ~2460 ft. below land surface.

Relative abundances of glass and alteration minerals. Boreholes USW G-3 and GU-3. From Bish and Chipera (1989).

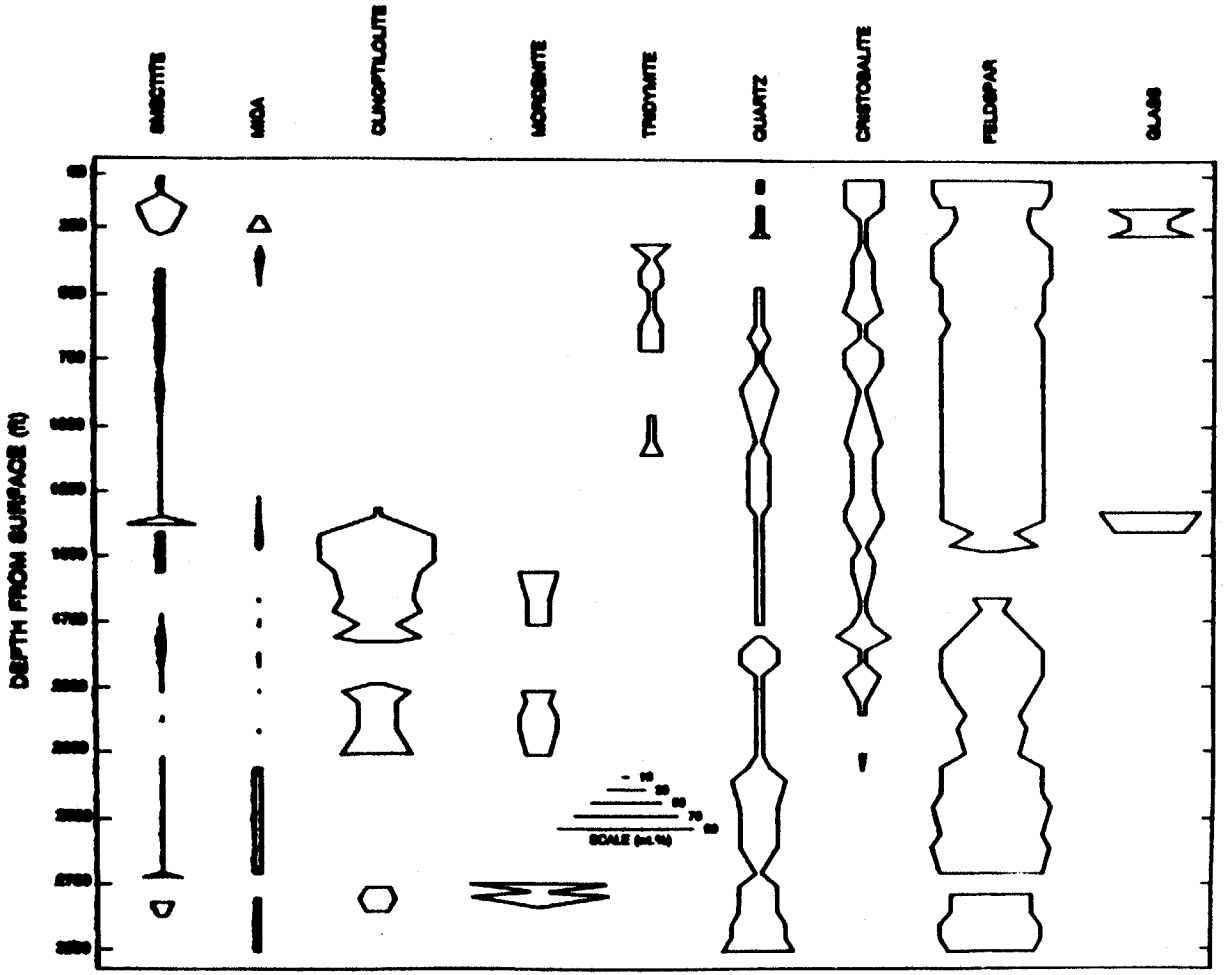

Note:

a) the contemporary water table is at a depth of ~1770 ft. below land surface.

Realtive abundances of glass and alteration minerals. Borehole USW G-4. From Bish and Chipera (1989).

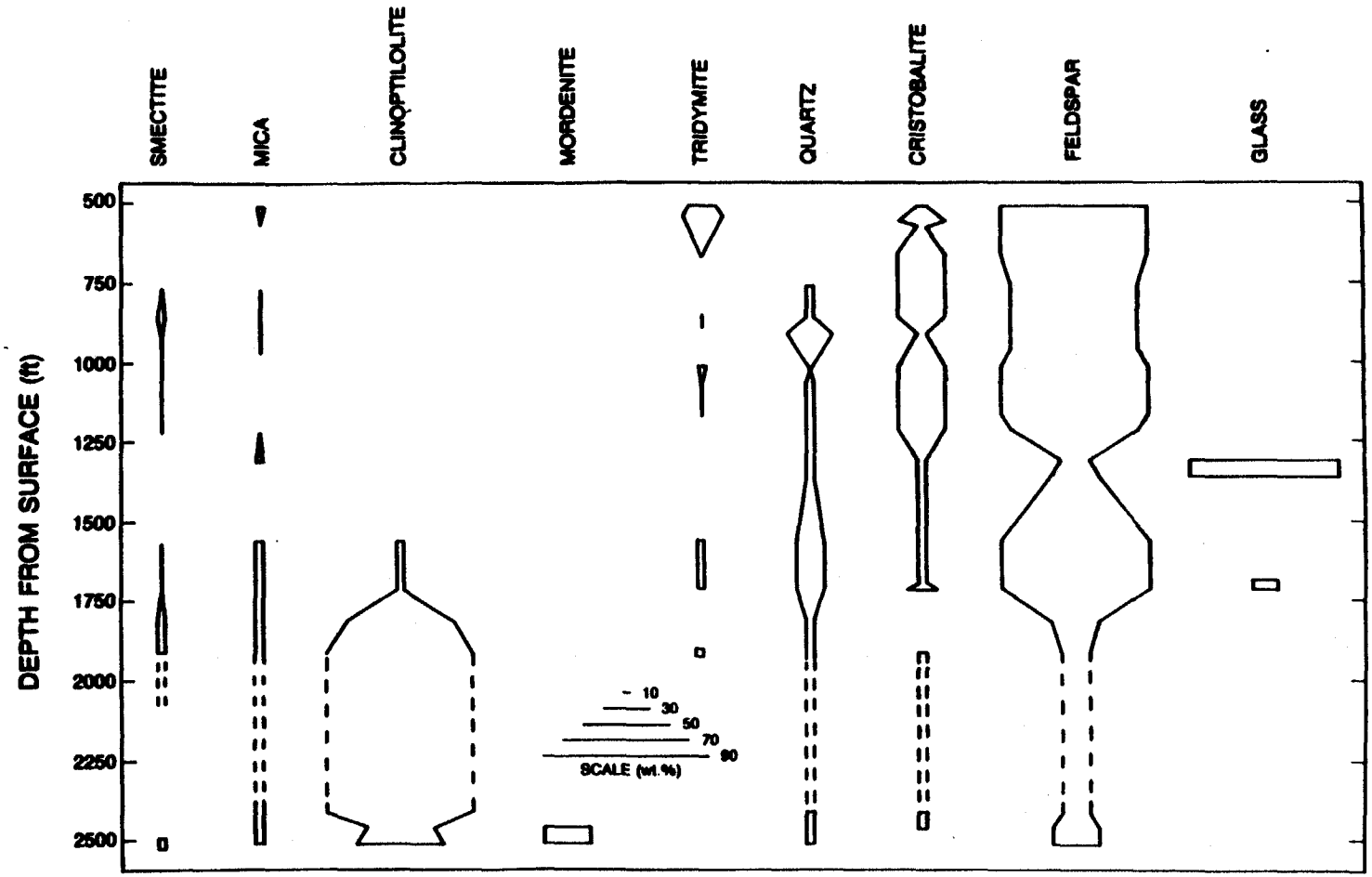

Note:

a) the contemporary water table is at a depth of ~2500 ft. below land surface.

Relative abundances of glass and alteration minerals. Borehole USW H-3. From Bish and Chipera (1989).

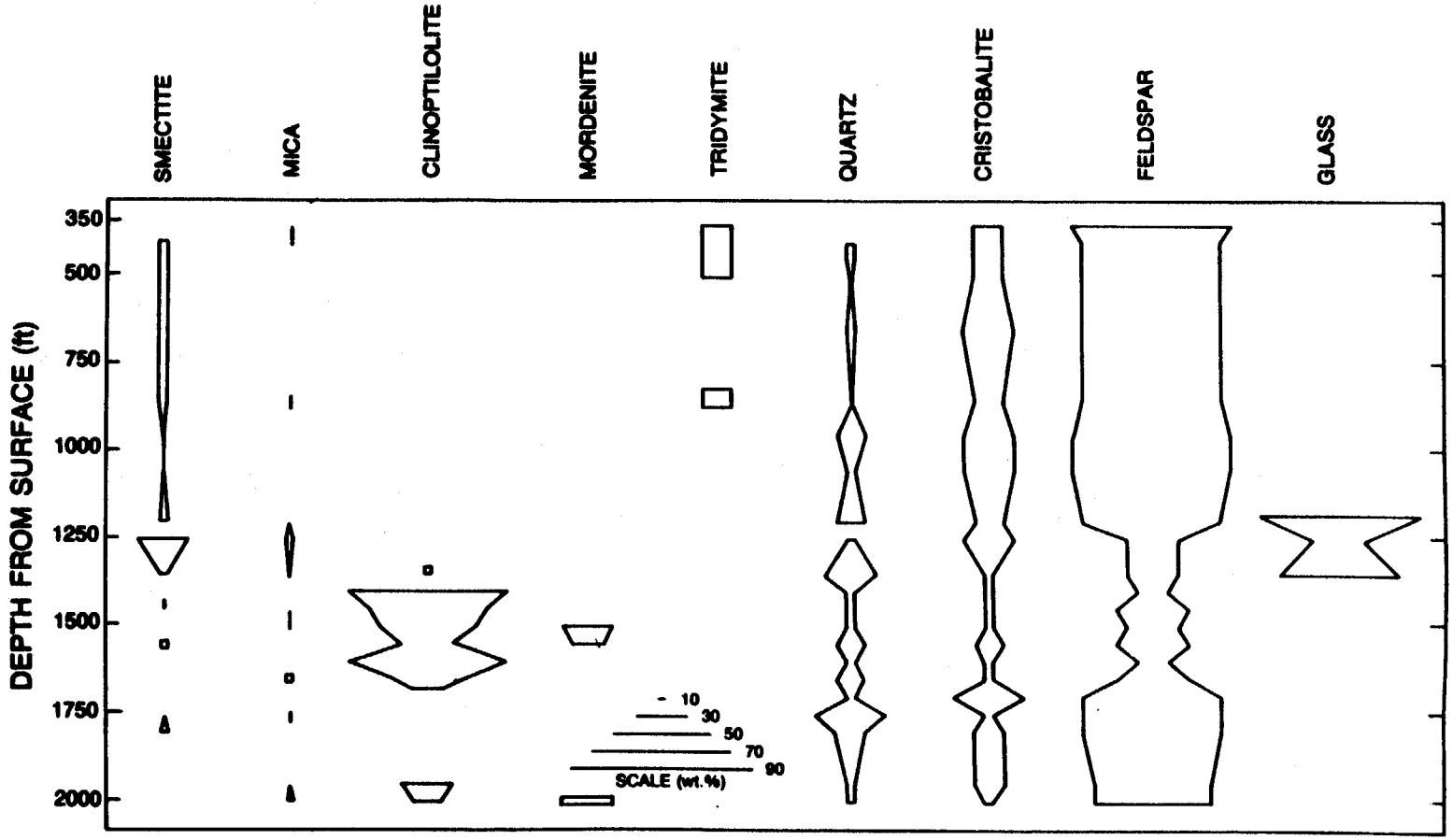

Note:

a) the contemporary water table is at a depth of ~1700 ft. below land surface.

Relative abundances of glass and alteration minerals. Borehole USW H-4. From Bish and Chipera (1989).

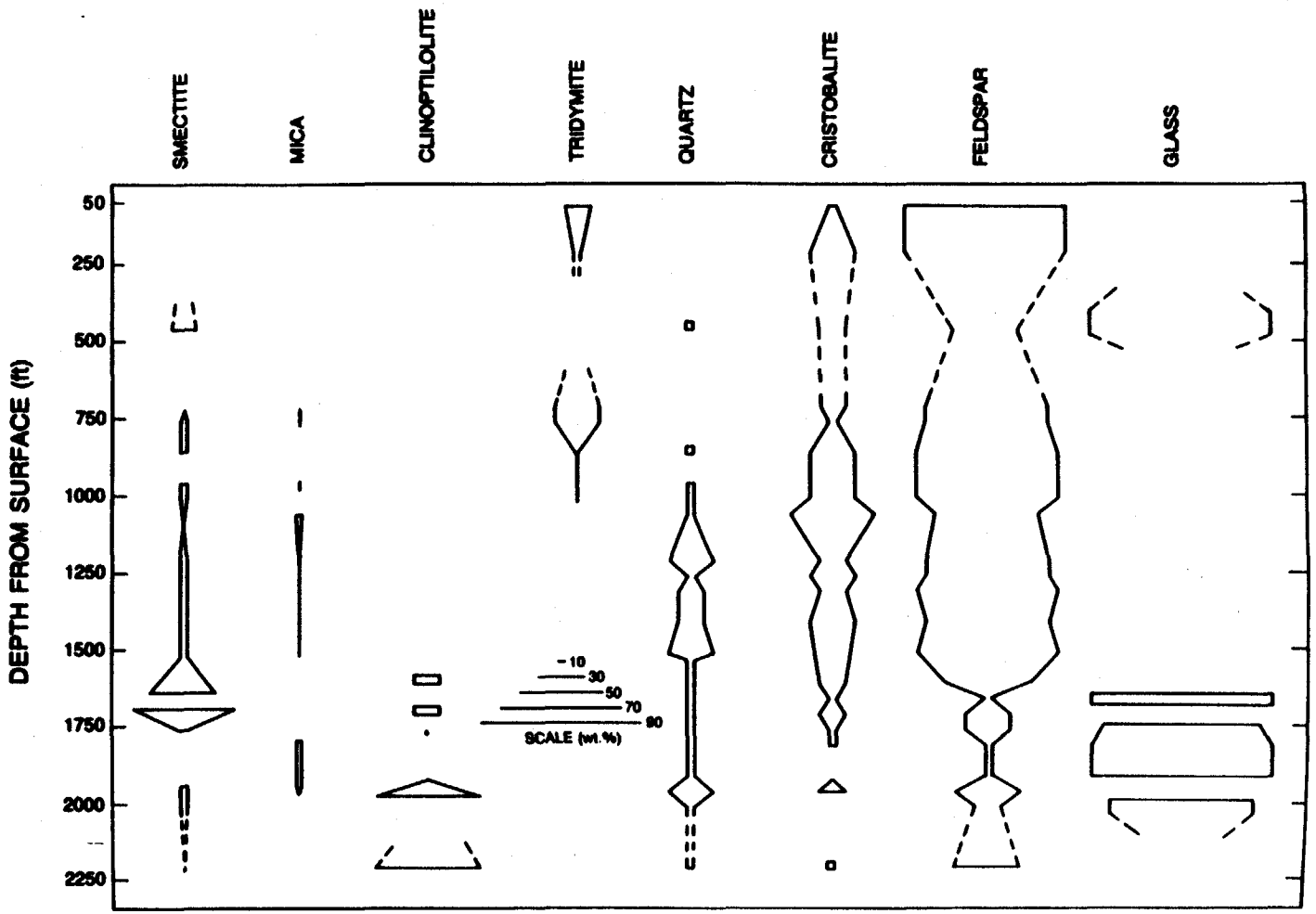

Note:

a) the contemporary water table is at a depth of ~2300 ft. below ground surface.

Relative abundances of glass and alteration minerals. Borehole USW H-5. From Bish and Chipera (1989).

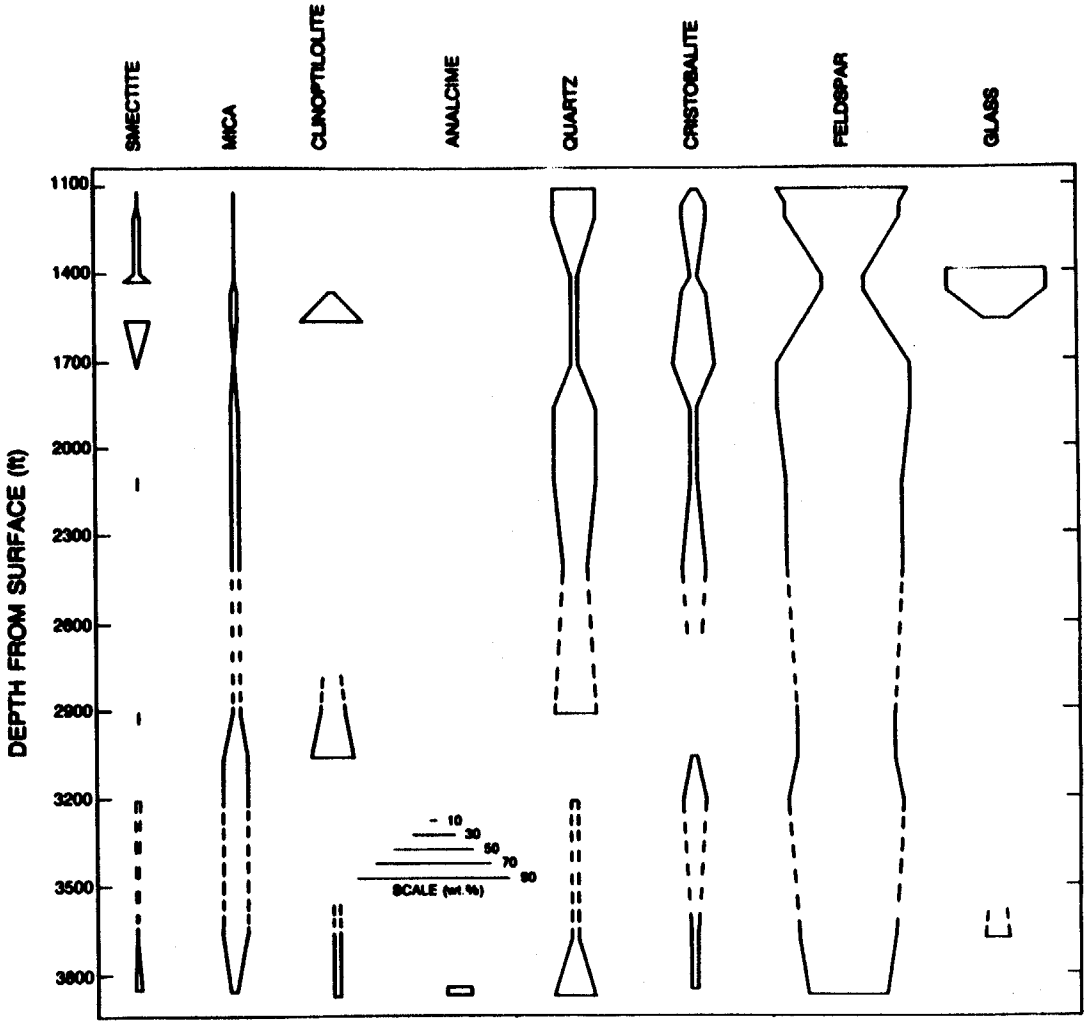

Note:

a) the contemporary water table is at a depth of ~1725 ft. below land surface.

Relative abundances of glass and alteration minerals. Borehole USW H-6. From Bish and Chipera (1989).

Sample No.	% Illite Layers	Type of Inter-stratification	EG-Smectite Thickness (Å)	(001) at Room Temperature (Å)
G1-1286	10	Random	16.85	13.1Å
3621 dark	20	"	16.9	12.2
3621 clear	15	"	16.9	11.8
3810 dark	20	"	16.9	12.2
3810 clear	20	"	16.85	11.9
3940 dark	20	"	16.7	11.9
3940 clear	25	"	16.8	12.1
4246 dark	20	"	16.75	13.7
4400	25	"	16.6	14.1
4556	20	"	16.65	14.3
4750	50-60	"	16.6	13.7, 11.3
4958	60	Allevardite	16.65	11.4
4998	30	Random	16.7	12.7
5339 dark	30	"	16.75	14.0
5339 clear	30	"	16.75	13.6
5534	40	"	16.75	11.9
5637	85-90	Kalkberg	16.5	10.5+Chl[a]
5898	80-90	"	16.55	11.0
5980	85-90	"	16.6	10.9+Chl[a]

[a]Chl = Chlorite.

Depth extent of the smectite → illite transformation. Borehole USW G-1. From Bish (1989).

Sample No.	% Illite Layers	Type of Inter-stratification	EG-Smectite Thickness (Å)	(001) at Room Temperature (Å)
G2-338	<5	Random	16.70	14.0
501	<5	"	16.70	14.4
675	~5	"	16.75	13.4
743	<5	"	16.70	12.4
921	<5	"	16.65	13.2
1032	<5	"	16.65	13.0
1382	<5	"	16.70	12.6
1634	~5	"	16.70	10.2
1745 clear	10	"	16.75	11.9
2667	10	"	-	10.3
3037	<5	"	16.60	13.5
3250	~5	"	16.55	10.2
3454 clear	10	"	16.55	12.3
3454 dark	15	"	16.60	10.1
3492	15	"	16.8	10.2
3512	20	"	16.65	10.1
3578	~5	"	16.65	10.2
3627	40-50	Minor ordering	16.55	10.1
3671	60	" "	16.60	10.2
3720 clear	~70	Allevardite	16.70	10.5
3720 dark	70	"	16.70	10.2
3724	~60	"	16.65	10.1
3750	60	"	16.60	10.1
3795	60	"	16.60	10.1
3833	60	Allevardite, some long-range order	16.60	10.1
3875	90	Kalkberg	16.60	10.1
3933	90	"	16.60	10.0
4005	70	Minor ordering	16.60	10.1
4090 clear	20	Random	16.60	13.0, 10.1
4090 dark	20	"	16.60	10.1, 13.4
4467	85	Kalkberg	16.55	10.2
4873	90	"	16.60	10.1
4885	90	Kalkberg + smectite	16.60	10.1
4949 clear	<5	Random	16.65	12.6
4949 dark	<5	"	16.60	10.5, 12.6
5171	>95	Illite		10.3
5369	Illite + discrete smectite/ 20% illite		16.6	10.16
5538	Illite + chlorite		10.1	
5657	Illite + chlorite		10.3	
5696	Illite + chlorite + smectite		16.65	10.5
5820	Randomly interstratified chlorite-smectite, 60-80% chlorite, minor ordering			
5931	>95	Illite	-	10.3

Depth extent of the smectite → illite transformation. Borehole USW G-2. From Bish (1989).

Figure 7-7b

Sample No.	% Illite Layers	Type of Inter-stratification	EG-Smectite Thickness (Å)	(001) at Room Temperature (Å)
G3-315.7	10-20	Random	16.7	13.5
332.5	10-20	"	16.75	13.9
414.3	10-20	"	16.8	13.0
1344.8	(poorly ordered, no higher orders of (001)		13.9	
1394.6	10-20	"	16.7	-[a]
1438.2	10-20	"	16.7	12.5
1493.7	10-20	"	16.7	-
2189.0	10-20	"	16.7	12.9
3170.5	10-20	"	16.7	12.5
3228.0	5-15	"	16.75	13.7
3264.4 clear	5-15	"	16.8	12.0
3264.4 dark	5-15	"	16.8	12.1
3310.9 clear	5-15	"	16.75	-
3310.9 dark	0-10	"	16.75	12.3
3315.1 super[b]	10-20	"	16.7	11.9
3315.1 clear	0-5	"	16.7	12.4
3315.1 dark	5-15	"	16.8	-
3799.0 clear	5-15	"	16.95	10.0
3799.0 dark	5-15	"	17.0	10.0
3847.5 clear	5-15	"	17.0	9.7
3847.5 dark	5-15	"	17.0	9.8
4288.9 clear	10-20	"	16.65	13.0
4288.9 dark	5-15	"	16.7	-
4439.0 clear	5-15	"	16.7	12.1
4439.0 dark	5-15	"	16.75	13.8
4706.9	10-20	"	16.65	14.2
4857.5 clear	15-25	"	16.80	12.0
4857.5 dark	5-15	"	16.70	13.8
4964.3 clear	15-25	"	16.7	14.1
4964.3 dark	15-25	"	16.65	13.0

[a]Not measured.

[b]Super = supernatant.

Depth extent of the smectite → illite transformation. Borehole USW G-3. From Bish (1989).

SAMPLE	PERCENT COLLAPSED LAYERS	COMPLEX THICKNESS (Å)	TYPE OF INTERSTRATIFICATION	COMMENTS
1420SW	15	16.7	Random	
2340	25	16.8	Random	Two clays, cannot decompose
2800 #1	25	16.9	Random	
#2	40	16.8	Random	
2850	35	16.8	Random	Two clays, cannot decompose
3090	40	16.8	Random	Two clays, can't decompose
3380	40	16.8	Random	Two clays ???
3520 #1	20	16.7	Random	
#2	55	??	Allevardite	Poor Resolution
3700 #1	15	16.7	Random	
#2	60	16.6	Allevardite	Poor Resolution
3760 #1	15	16.7	Random	
#2	??	??	Allevardite	Poor Resolution
3800 #1	20±10	??	Random	Poor Resolution
#2	75	16.6	Allevardite	
3913C#1	??	??	Random	Poor Resolution
#2	75	16.6	Allevardite	
3928C#1	20±10	??	Random	Poor Resolution
#2	65	16.7	Allevardite	
4050 #1	15	16.7	Random	
#2	70	16.7	Allevardite	
4080 #1	15	16.7	Random	
#2	70	16.6	Allevardite	Poor Resolution
4180 #1	15	16.7	Random	
#2	75	16.8	Allevardite	

Depth extent of the smectite → illite transformation. Borehole UE-25p#1. From Chipera and Bish (1989).

Drill Hole J-13

Depth (ft)	1335	1335	1335	1335	1421	1421	1421	1421
	Mol% Exchangeable Cations							
K	14.9	15.5	15.4	13.0	53.5	49.7	53.2	50.2
Na	23.1	21.1	17.5	28.5	20.6	22.7	22.8	22.8
Ca+Mg	62.0	63.5	67.1	58.5	25.8	27.5	24.0	27.0
Depth (ft)	1421	1421	1421	1421	1421	1457	1457	1457
	Mol% Exchangeable Cations							
K	51.0	48.9	50.1	53.4	55.4	30.3	38.7	36.0
Na	21.1	22.2	23.6	21.3	22.5	8.6	7.9	9.3
Ca+Mg	27.9	28.9	26.2	25.3	22.1	61.1	53.3	54.7
Depth (ft)	1457	1457	1457	1457	1457	1457	1519	1519
	Mol% Exchangeable Cations							
K	37.5	37.2	39.1	37.0	38.9	38.0	40.4	41.9
Na	10.7	10.3	9.0	10.9	12.1	7.4	11.4	13.5
Ca+Mg	51.8	52.5	51.8	52.1	49.0	54.6	48.2	44.6
Depth (ft)	1519	1519	1519	1519	1519	1519	1519	1519
	Mol% Exchangeable Cations							
K	37.1	34.2	39.6	39.5	42.4	40.5	43.1	43.1
Na	10.8	13.7	14.5	11.6	13.8	14.3	12.9	12.6
Ca+Mg	52.1	52.1	45.8	48.9	43.8	45.2	44.0	44.3

Depth (ft)	1546	1546	1612	1612
	Mol% Exchangeable Cations			
K	33.7	39.5	38.1	36.1
Na	5.4	10.2	6.8	6.8
Ca+Mg	60.9	50.3	55.1	57.1

Exchangeable cations content. Clinoptilolites in borehole J-13. From Broxton et al. (1986).

Drill Hole UE-25a#1

Depth (ft)	1279	1323	1323	1323	1323	1323	1323	1323
			Mol% Exchangeable Cations					
K	11.5	26.4	29.8	27.7	26.8	22.2	26.9	26.5
Na	12.7	11.5	12.3	12.1	13.0	13.2	15.4	13.4
Ca+Mg	75.8	62.1	57.8	60.2	60.3	64.5	57.7	60.0
Depth (ft)	1358	1358	1358	1381	1384	1384	1384	1384
			Mol% Exchangeable Cations					
K	29.2	35.7	30.4	28.1	32.4	28.0	24.1	25.5
Na	14.1	14.8	9.1	11.2	13.3	11.7	11.4	11.8
Ca+Mg	56.7	49.4	60.5	60.7	54.3	60.3	64.5	62.7
Depth (ft)	1384	1465	1465	1505	1584	1584	1584	1667
			Mol% Exchangeable Cations					
K	24.8	56.8	34.3	42.9	32.4	38.3	35.9	40.1
Na	11.2	10.7	16.3	16.6	20.1	17.4	10.0	18.4
Ca+Mg	63.9	32.5	49.3	40.6	47.4	44.3	54.1	41.5
Depth (ft)	1667	1667	1667	1667	1667	1667	1667	1667
			Mol% Exchangeable Cations					
K	39.7	41.3	43.4	40.6	39.6	43.5	41.0	40.5
Na	17.1	19.2	19.2	17.6	16.0	17.3	17.2	19.6
Ca+Mg	43.3	39.5	37.3	41.7	44.4	39.2	41.8	39.9
Depth (ft)	1667	1667	1667	1824	1824	1824	1824	2087
			Mol% Exchangeable Cations					
K	39.6	37.1	37.8	16.5	17.1	19.4	17.2	24.5
Na	16.0	17.8	20.1	15.6	22.1	20.3	24.8	6.9
Ca+Mg	44.4	45.1	42.1	67.9	60.8	60.3	58.0	68.5
Depth (ft)	2087	2087	2087	2087	2113	2220	2220	2220
			Mol% Exchangeable Cations					
K	24.6	22.9	21.7	29.2	45.7	25.0	23.3	22.1
Na	11.4	13.8	9.2	14.5	47.0	10.5	8.8	9.4
Ca+Mg	64.0	63.3	69.1	56.3	7.3	64.4	67.9	68.5
Depth (ft)	2220	2220	2220	2220	2220	2304	2304	2304
			Mol% Exchangeable Cations					
K	23.4	24.9	24.3	24.4	23.4	22.6	22.4	24.1
Na	9.1	7.9	9.5	9.4	13.0	21.7	20.9	21.6
Ca+Mg	67.5	67.2	66.2	66.2	63.5	55.7	56.6	54.3
Depth (ft)	2304	2304	2304	2304	2304	2304	2304	2304
			Mol% Exchangeable Cations					
K	20.1	24.5	24.4	24.6	24.5	25.2	23.1	23.6
Na	22.1	17.7	17.6	19.7	18.7	17.0	23.7	20.0
Ca+Mg	57.8	57.9	57.9	55.7	56.8	57.8	53.3	56.4

Exchangeable cations content. Clinoptilolites in borehole UE-25a#1. From Broxton et al. (1986).

Drill Hole UE-25b#1(H)

Depth (ft).	2832	2832	2832	2832	2832	2832	2832	2832
			Mol% Exchangeable					
K	13.3	16.0	15.5	15.4	17.8	17.4	16.4	13.5
Na	11.8	12.8	13.9	12.4	4.4	6.9	13.6	13.7
Ca+Mg	74.8	71.3	70.6	72.2	77.8	75.8	70.0	72.8
Depth (ft).	2832	2832	2832	2832	2832	2879	2879	2879
			Mol% Exchangeable Cations					
K	15.4	16.6	16.6	16.5	17.4	19.8	18.4	18.8
Na	15.7	11.3	6.8	9.5	9.7	4.7	9.6	12.2
Ca+Mg	68.9	72.1	76.5	73.9	72.9	75.5	72.0	69.1
Depth (ft)	2879	2879	2879	2879	2879	2879		
			Mol% Exchangeable Cations					
K	16.6	18.6	17.9	16.4	17.6	18.5		
Na	16.3	8.7	10.4	15.5	15.0	11.1		
Ca+Mg	67.1	72.7	71.7	68.1	67.3	70.5		

Exchangeable cations content. Clinoptilolites in borehole UE-25b#1. From Broxton et al. (1986).

Drill Hole UE-25p#1

Depth (ft)	1250	1250	1250	1250	1250	1250	1250	1250
			Mol% Exchangeable Cations					
K	34.3	36.0	34.5	36.0	37.2	38.5	36.6	36.4
Na	22.2	21.2	20.3	20.9	25.4	21.9	25.7	21.8
Ca+Mg	43.5	42.8	45.1	43.1	37.4	39.6	37.7	41.8
Depth (ft)	1250	1350	1350	1350	1400	1400	1400	1700
			Mol% Exchangeable Cations					
K	36.3	32.5	32.7	36.6	19.8	21.1	27.9	20.3
Na	23.2	23.1	19.1	15.9	26.6	30.1	25.4	28.9
Ca+Mg	40.5	44.4	48.2	47.5	53.6	48.8	46.7	50.9
Depth (ft)	1700	1700	1700	1700	1700	1700	1700	1700
			Mol% Exchangeable Cations					
K	16.9	17.7	18.1	16.1	17.0	16.8	17.6	18.7
Na	28.8	31.6	34.0	30.9	34.0	32.8	31.6	29.5
Ca+Mg	54.2	50.7	47.9	53.0	49.0	50.5	50.7	51.7
Depth (ft)	1700	1700	1800	1800	1800	1800	1800	1800
			Mol% Exchangeable Cations					
K	18.0	20.0	17.9	21.7	16.9	16.3	20.4	19.8
Na	31.4	33.3	35.6	29.9	28.4	27.4	30.8	30.8
Ca+Mg	50.6	46.7	46.5	48.4	54.8	56.3	48.7	49.4
Depth (ft)	1800	2760	2760	2760	3330	3330	3330	3330
			Mol% Exchangeable Cations					
K	23.2	8.0	7.5	7.2	3.7	5.2	5.6	4.7
Na	30.8	21.5	21.7	26.2	15.3	16.4	20.1	25.4
Ca+Mg	45.9	70.5	70.7	66.7	81.0	78.3	74.4	69.9
Depth (ft)	3330	3330	3330	3330	3330	3330	3330	3330
			Mol% Exchangeable Cations					
K	6.3	5.6	6.4	6.2	6.6	6.4	6.2	6.2
Na	20.4	17.2	20.0	20.5	18.2	13.8	14.7	24.4
Ca+Mg	73.3	77.3	73.6	73.4	75.1	79.8	79.0	69.4

Exchangeable cations content. Clinoptilolites in borehole UE-25p#1. From Broxton et al. (1986).

Drill Hole USW G-1

Depth (ft)	1286	1436	1561	1561	1561	1639	1774	1774
			Mol% Exchangeable Cations					
K	8.8	58.3	52.1	58.7	55.8	49.9	44.0	26.7
Na	20.4	34.4	42.3	36.4	38.9	43.1	45.2	57.4
Ca+Mg	70.9	7.3	5.6	4.9	5.3	7.0	10.9	15.9

Depth (ft)	1819	1819	2083	2166	2290	3598	3598	3598
			Mol% Exchangeable Cations					
K	43.7	37.0	37.8	36.6	33.5	8.2	6.2	6.0
Na	45.2	49.9	53.8	56.6	44.0	76.4	78.7	78.2
Ca+Mg	11.1	13.0	8.3	6.8	22.4	15.5	15.1	15.9

Depth (ft)	3706
Mol% Exchangeable Cations	
K	1.0
Na	76.2
Ca+Mg	22.8

Exchangeable cations content. Clinoptilolites in borehole USW G-1. From Broxton et al. (1986).

Drill Hole USW G-2

Depth (ft)	561	561	561	561	561	561	584	584
			Mol% Exchangeable Cations					
K	21.1	15.6	21.2	17.0	19.8	20.3	10.5	16.4
Na	5.4	5.1	6.6	6.3	5.9	4.6	0.5	4.1
Ca+Mg	73.5	79.3	72.2	76.7	74.4	75.1	89.0	79.4
Depth (ft)	584	584	584	584	584	657	657	657
			Mol% Exchangeable Cations					
K	12.8	15.3	15.0	9.4	8.6	21.2	24.8	26.5
Na	0.8	3.1	3.4	2.9	2.4	2.8	5.8	3.4
Ca+Mg	86.4	81.6	81.6	87.6	89.0	76.1	69.4	70.2
Depth (ft)	657	762	1691	1691	1745	1745	1745	1745
			Mol% Exchangeable Cations					
K	27.6	39.1	48.7	47.6	37.9	40.1	46.1	42.4
Na	8.1	5.7	18.7	17.1	21.2	24.7	17.8	24.6
Ca+Mg	64.3	55.2	32.6	35.3	40.9	35.2	36.1	33.0
Depth (ft)	1745	1745	2078	2078	2158	2158	2158	2158
			Mol% Exchangeable Cations					
K	38.6	40.8	39.9	41.2	38.0	35.1	36.9	35.5
Na	24.0	21.9	15.3	15.0	19.2	16.8	18.6	12.8
Ca+Mg	37.5	37.3	44.8	43.9	42.8	48.1	44.5	51.7
Depth (ft)	2158	2158	2325	2325	2430	2430	3067	3067
			Mol% Exchangeable Cations					
K	36.8	37.1	32.6	34.1	43.0	40.1	29.5	29.3
Na	10.5	16.4	22.5	20.1	14.9	16.2	67.8	67.8
Ca+Mg	52.7	46.5	44.9	45.8	42.1	43.7	2.8	2.9
Depth (ft)	3067	3067	3067	3067	3192	3192	3192	3192
			Mol% Exchangeable Cations					
K	28.9	29.9	27.6	7.8	21.9	23.8	18.3	19.9
Na	68.7	67.8	69.7	57.6	57.6	54.9	62.2	61.8
Ca+Mg	2.5	2.3	2.7	34.6	20.5	21.2	19.5	18.3
Depth (ft)	3192	3192	3192	3192	3250	3250		
			Mol% Exchangeable Cations					
K	20.0	23.0	22.7	26.3	0.5	1.5		
Na	58.4	56.9	53.4	57.3	74.0	74.9		
Ca+Mg	21.6	20.2	23.9	16.4	25.5	23.6		

Exchangeable cations content. Clinoptilolites in borehole USW G-2. From Broxton et al. (1986).

Drill Hole USW G-3

Depth (ft)	1195	1195	1195	1195	1195	1195	1874	1874
			Mol% Exchangeable Cations					
K	5.9	12.7	8.5	11.1	15.7	19.1	57.8	49.1
Na	17.5	19.0	14.5	15.5	12.2	17.1	26.1	33.3
Ca+Mg	76.6	68.3	77.1	73.4	72.1	63.7	16.0	17.6
Depth (ft)	1874	1874	1874	1874	1874	1874	1874	1986
			Mol% Exchangeable Cations					
K	54.9	55.1	57.4	55.7	52.1	55.3	58.1	68.4
Na	28.6	30.5	26.3	28.1	31.0	27.3	26.6	26.4
Ca+Mg	16.5	14.4	16.3	16.1	16.9	17.4	15.4	5.2
Depth (ft)	1986	1986	1986	1986	1986	1986	1986	1986
			Mol% Exchangeable Cations					
K	62.1	65.1	59.4	60.6	55.4	55.2	59.3	61.1
Na	32.4	29.9	34.6	34.2	39.2	39.6	35.8	33.2
Ca+Mg	5.5	5.1	6.0	5.2	5.4	5.1	4.8	5.7
Depth (ft)	1986	1993	2577	2577	2577	2577	2577	2577
			Mol% Exchangeable Cations					
K	60.2	58.3	23.9	25.6	23.5	26.5	27.4	24.2
Na	33.8	36.3	38.3	34.5	35.1	32.4	33.0	33.8
Ca+Mg	6.0	5.4	37.8	39.9	41.4	41.1	39.7	41.9
Depth (ft)	2577	2577	2615	2615	2656	2656	2695	3226
			Mol% Exchangeable Cations					
K	27.2	29.3	32.2	34.2	42.5	39.4	36.6	34.8
Na	33.5	31.2	52.1	51.0	38.7	42.9	44.3	44.7
Ca+Mg	39.3	39.5	15.7	14.8	18.8	17.8	19.1	20.5
Depth (ft)	3226	3475	3589	3589	3589	3672	3672	3672
			Mol% Exchangeable Cations					
K	33.3	38.3	57.0	52.3	48.4	42.6	41.8	46.1
Na	48.0	47.2	34.8	39.1	40.6	47.0	48.2	44.2
Ca+Mg	18.6	14.5	8.2	8.6	11.0	10.4	10.1	9.7
Depth (ft)	3672	3672	3672	3759	3759	3759	4423	4423
			Mol% Exchangeable Cations					
K	53.5	48.6	53.7	36.1	42.6	32.9	7.4	13.9
Na	38.1	41.0	36.9	53.1	48.0	57.7	61.0	59.1
Ca+Mg	8.5	10.5	9.3	10.8	9.4	9.4	31.6	27.0

Exchangeable cations content. Clinoptilolites in borehole USW G-3. From Broxton et al. (1986).

Drill Hole USW G-4

Depth (ft)	1432	1432	1470	1470	1470	1470	1470	1470
			Mol% Exchangeable Cations					
K	52.7	50.4	54.7	56.9	53.8	56.8	55.9	53.5
Na	34.6	37.6	38.2	34.4	37.6	35.7	36.0	36.7
Ca+Mg	12.7	11.9	7.1	8.7	8.6	7.5	8.1	9.8
Depth (ft)	1544	1544	1544	1544	1544	1707	1707	1707
			Mol% Exchangeable Cations					
K	50.9	48.9	49.8	51.3	49.9	52.9	53.2	56.8
Na	41.6	42.6	42.7	42.7	43.9	39.4	37.7	35.9
Ca+Mg	7.5	8.5	7.5	6.0	6.2	7.8	9.1	7.3
Depth (ft)	1707	1707	1762	1762	1762	1762	1762	1762
			Mol% Exchangeable Cations					
K	64.3	55.5	36.2	39.7	38.1	36.1	35.4	37.8
Na	28.3	35.3	49.3	44.6	47.4	48.9	49.2	47.0
Ca+Mg	7.4	9.1	14.5	15.7	14.5	15.0	15.4	15.1

Depth (ft)	1762	2132	2132	2132	2132	2132	2132	2132
			Mol% Exchangeable Cations					
K	40.8	32.2	35.2	30.4	33.6	34.0	25.9	29.3
Na	44.6	23.3	21.1	28.2	23.7	20.7	27.4	25.0
Ca+Mg	14.6	44.5	43.8	41.4	42.7	45.3	46.7	45.7
Depth (ft)	2132	2132	2132	2227	2227	2227	2227	2227
			Mol% Exchangeable Cations					
K	29.8	30.2	25.4	21.8	25.5	17.9	23.8	26.4
Na	22.8	26.4	28.8	28.5	20.1	28.9	24.9	29.9
Ca+Mg	47.4	43.4	45.8	49.6	54.4	53.2	51.3	43.7
Depth (ft)	2227	2227	2239	2239	2239	2239	2239	2239
			Mol% Exchangeable Cations					
K	22.6	28.8	21.4	19.5	24.9	25.4	28.4	22.2
Na	20.6	24.3	21.8	13.9	18.7	10.1	18.1	13.1
Ca+Mg	56.8	46.9	56.9	66.6	56.4	64.6	53.5	64.8
Depth (ft)	2239	2738	2738	2738	2738	2738	2738	2738
			Mol% Exchangeable Cations					
K	28.0	14.9	18.5	16.1	16.6	24.8	19.6	11.8
Na	15.7	20.0	14.3	20.1	20.5	23.1	14.5	16.5
Ca+Mg	56.4	65.1	67.2	63.8	62.8	52.1	65.9	71.7

Exchangeable cations content. Clinoptilolites in borehole USW G-4. From Broxton et al. (1986).

Drill Hole USW H-3

Depth (ft)	1800	1800	1800	1800	1800
			Mol% Exchangeable Cations		
K	39.7	39.3	43.9	41.8	38.1
Na	17.7	18.2	18.1	17.1	19.6
Ca+Mg	42.6	42.5	37.9	41.1	42.3

Drill Hole USW H-4

Depth (ft)	1420	1420	1420	1420	1420	1420	1455	1455
				Mol% Exchangeable Cations				
K	45.8	42.4	43.8	46.4	41.9	43.9	29.9	29.2
Na	14.7	12.1	14.2	13.1	15.6	14.6	13.2	10.2
Ca+Mg	39.5	45.5	42.1	40.5	42.5	41.5	56.9	60.6
Depth (ft)	1455	1455	1550	1550	1550	1550	1550	1550
				Mol% Exchangeable Cations				
K	29.5	23.3	54.8	53.4	41.7	52.8	52.3	53.8
Na	10.0	9.6	25.3	25.7	34.3	25.8	23.4	23.8
Ca+Mg	60.5	67.1	19.9	20.9	23.9	21.4	24.3	22.4
Depth (ft)	1980	1980	1980	1980	1980	1980	1980	
				Mol% Exchangeable Cations				
K	44.5	45.9	38.8	47.4	40.9	52.1	50.9	
Na	53.1	51.6	58.9	50.5	56.4	45.2	46.5	
Ca+Mg	2.3	2.5	2.3	2.1	2.7	2.6	2.6	

Exchangeable cations content. Clinoptilolites in borehole USW H-3 and H-4. From Broxton et al. (1986).

Drill Hole USW H-5

Depth (ft)	1666	1666	1917	1917	1917	1917	1917	1917
			Mol% Exchangeable Cations					
K	9.6	3.6	51.5	52.9	54.0	54.2	56.6	49.5
Na	11.2	4.4	31.9	33.0	30.8	31.3	30.6	33.3
Ca+Mg	79.1	92.0	16.6	14.1	15.2	14.5	12.7	17.2
Depth (ft)	1917	1917	1917	1917	1930	1930	1930	1930
			Mol% Exchangeable Cations					
K	51.3	49.3	51.5	52.8	49.7	48.9	51.3	41.7
Na	31.0	34.9	31.4	30.4	31.0	30.7	26.5	39.9
Ca+Mg	17.7	15.7	17.1	16.8	19.3	20.4	22.2	18.4
Depth (ft)	2200	2200	2200	2200				
	Mol% Exchangeable Cations							
K	39.7	42.0	43.7	49.1				
Na	46.3	45.9	40.6	36.2				
Ca+Mg	14.0	12.1	15.7	14.7				

Exchangeable cations content. Clinoptilolites in borehole USW H-5. From Broxton et al. (1986).

Drill Hole J-13

Sample Number	55.	56.	57.	58.	59.	60.	61.
Depth (ft)	1457	1519	1883	2001	2133	2982	2999
Ca+Mg	31.3	25.9	6.3	4.3	7.9	9.0	25.2
K	49.9	50.4	39.8	24.7	38.5	40.3	38.8
Na	18.8	23.7	53.9	71.0	53.6	50.8	36.0

Sample Descriptions:

55. Tuff of Calico Hills. Clinoptilolite-bearing nonwelded tuff in Zone II.
56. Tuff of Calico Hills. Clinoptilolite-bearing nonwelded tuff in diagenetic Zone II.
57. Prow Pass Member, Crater Flat Tuff. Devitrified partially welded tuff.
58. Prow Pass Member, Crater Flat Tuff. Analcime-bearing nonwelded tuff in diagenetic Zone III.
59. Bullfrog Member, Crater Flat Tuff. Devitrified partially welded tuff.
60. Tram Member, Crater Flat Tuff. Authigenic albite-bearing nonwelded tuff in diagenetic Zone IV.
61. Tram Member, Crater Flat Tuff. Analcime- and authigenic albite-bearing nonwelded tuff in diagenetic Zone IV.

Exchangeable cations content. Whole-rock samples from borehole J-13. From Broxton et al. (1986).

Drill Hole UE-25b#1(H)

Sample Number	40.	41.	42.	43.	44.	45.	46.
Depth (ft)	2832	2879	3393	3602	3767	3835	3963
Ca+Mg	32.0	42.8	30.4	29.6	30.1	28.0	27.9
K	33.0	38.7	30.9	32.3	35.2	32.5	32.9
Na	35.0	18.5	38.7	38.1	34.7	39.5	39.2

Sample Number	47.	48.	49.	50.	51.	52.	53.	54.
Depth (ft)	1700-1710	1730-1740	1790-1800	2280-2290	2650-2660	2760-2770	3430-3440	3560-3570
Ca+Mg	27.6	24.4	29.1	22.3	24.2	29.7	9.4	19.1
K	30.9	33.6	28.4	43.0	39.2	36.8	48.3	52.9
Na	41.4	42.1	42.6	34.6	36.6	33.5	42.2	28.1

Sample Descriptions:

40. Bullfrog Member, Crater Flat Tuff. Mordenite- and clinoptilolite-bearing nonwelded tuff in diagenetic Zone II.
41. Bullfrog Member, Crater Flat Tuff. Mordenite- and clinoptilolite-bearing nonwelded tuff in diagenetic Zone II.
42. Tram Member, Crater Flat Tuff. Analcime- and calcite-bearing nonwelded tuff in diagenetic Zone III.
43. Tram Member, Crater Flat Tuff. Analcime- and calcite-bearing nonwelded tuff in diagenetic Zone III.
44. Tram Member, Crater Flat Tuff. Analcime-, calcite-, and kaolinite-bearing nonwelded tuff in diagenetic Zone III.
45. Tram Member, Crater Flat Tuff. Analcime- and calcite-bearing nonwelded tuff in diagenetic Zone III.
46. Tuff of Lithic Ridge. Analcime- and calcite-bearing nonwelded tuff in diagenetic Zone III.
47. Prow Pass Member, Crater Flat Tuff. Clinoptilolite-bearing nonwelded tuff in diagenetic Zone II.
48. Prow Pass Member, Crater Flat Tuff. Clinoptilolite-bearing nonwelded tuff in diagenetic Zone II.
49. Prow Pass Member, Crater Flat Tuff. Clinoptilolite-bearing nonwelded tuff in diagenetic Zone II.
50. Bullfrog Member, Crater Flat Tuff. Analcime-bearing nonwelded tuff in diagenetic Zone III.
51. Bullfrog Member, Crater Flat Tuff. Analcime-bearing nonwelded tuff in diagenetic Zone III.
52. Bullfrog Member, Crater Flat Tuff. Analcime-bearing nonwelded tuff in diagenetic Zone III.
53. Older Tuff Sequence. Authigenic albite-bearing nonwelded tuff in diagenetic Zone IV.
54. Older Tuff Sequence. Authigenic albite-bearing nonwelded tuff in diagenetic Zone IV.

Exchangeable cations content. Whole-rock samples from borehole UE-25b#1. From Broxton et al. (1986).

Drill Hole USW G-2

Sample Number	1.	2.	3.	4.	5.	6.	7.
Depth (ft)	675	2430	2667	3067	3192	3454	3541
Ca+Mg	46.9	24.8	17.9	20.8	12.2	22.5	10.6
K	30.0	45.7	36.4	31.2	43.3	24.8	31.0
Na	23.1	29.5	45.7	47.9	44.5	52.7	58.4

Sample Number	8.	9.	10.	11.	12.	13.
Depth (ft)	3795	3933	4090	4805	5895	5992
Ca+Mg	19.4	11.3	51.6	10.2	47.2	14.7
K	53.4	44.9	21.7	49.9	23.5	35.6
Na	27.2	43.8	26.7	39.9	29.3	49.7

Sample Descriptions:

1. Pah Canyon Member, Paintbrush Tuff. Clinoptilolite- and smectite-bearing nonwelded tuff in diagenetic Zone I.
2. Tuff of Calico Hills. Clinoptilolite- and mordenite-bearing nonwelded tuff in diagenetic Zone II.
3. Tuff of Calico Hills. Clinoptilolite- and mordenite-bearing nonwelded tuff in diagenetic Zone II.
4. Prow Pass Member, Crater Flat Tuff. Mordenite-bearing tuff in diagenetic Zone II.
5. Prow Pass Member, Crater Flat Tuff. Clinoptilolite- and mordenite-bearing tuff in diagenetic Zone II.
6. Bullfrog Member, Crater Flat Tuff. Mordenite-bearing tuff in diagenetic Zone III.
7. Bullfrog Member, Crater Flat Tuff. Analcime-bearing tuff in diagenetic Zone III.
8. Tram Member, Crater Flat Tuff. Analcime- and kaolinite-bearing nonwelded tuff in diagenetic Zone III.
9. Tram Member, Crater Flat Tuff. Analcime-bearing tuff in diagenetic Zone III.
10. Rhyodacite Lava. Analcime- and calcite-bearing lava in diagenetic Zone III.
11. Tuff of Lithic Ridge. Authigenic albite- and analcime-bearing nonwelded tuff in diagenetic Zone IV.
12. Bedded Tuff. Calcite- and chlorite-bearing bedded tuff in diagenetic Zone IV.
13. Older Tuff Sequence. Calcite- and chlorite-bearing nonwelded tuff in diagenetic Zone IV.

Exchangeable cations content. Whole-rock samples from borehole USW G-2. From Broxton et al. (1986).

Drill Holes USW GU-3 and USW G-3

Sample Number	14.	15.	16.	17.	18.	19.	20.
Depth (ft)	1498	1598	1986	2577	3207	3589	3854
Ca+Mg	7.9	9.0	9.8	23.8	16.1	22.1	17.8
K	43.4	42.4	36.9	37.7	39.0	33.5	30.5
Na	48.7	48.5	53.4	38.5	44.9	44.4	51.7

Sample Number	21.	22.	23.	24.	25.
Depth (ft)	4008	4263	4568	4786	4869
Ca+Mg	15.2	14.5	26.2	15.8	12.5
K	40.8	31.5	22.7	38.0	23.1
Na	44.0	54.0	51.1	46.2	64.3

Sample Descriptions:

14. Tuff of Calico Hills. Vitric nonwelded tuff in diagenetic Zone I.
15. Prow Pass Member, Crater Flat Tuff. Vitric nonwelded tuff in diagenetic Zone I.
16. Prow Pass Member, Crater Flat Tuff. Clinoptilolite-bearing nonwelded tuff in diagenetic Zone II.
17. Bullfrog Member, Crater Flat Tuff. Clinoptilolite-bearing nonwelded tuff in diagenetic Zone II.
18. Tram Member, Crater Flat Tuff. Clinoptilolite-bearing partially welded tuff in diagenetic Zone II.
19. Tram Member, Crater Flat Tuff. Clinoptilolite-bearing nonwelded tuff in diagenetic Zone II.
20. Tuff of Lithic Ridge. Clinoptilolite-bearing nonwelded tuff in diagenetic Zone II.
21. Tuff of Lithic Ridge. Analcime-bearing nonwelded tuff in diagenetic Zone III.
22. Tuff of Lithic Ridge. Analcime-bearing nonwelded tuff in diagenetic Zone III.
23. Tuff of Lithic Ridge. Analcime-bearing nonwelded tuff in diagenetic Zone III.
24. Older Tuff Sequence. Analcime-bearing nonwelded tuff in diagenetic Zone III.
25. Older Tuff Sequence. Analcime-bearing nonwelded tuff in diagenetic Zone III.

Exchangeable cations content. Whole-rock samples from borehole USW G-3. From Broxton et al. (1986).

Drill Hole USW G-4

Sample Number	26.	27.	28.	29.	30.	31.	32.
Depth (ft)	1314	1470	1544	2131	2226	2716	2792
Ca+Mg	52.6	9.0	8.5	25.2	24.9	26.4	32.5
K	9.5	48.1	43.9	35.6	40.3	26.5	19.3
Na	38.0	42.9	47.6	39.2	34.8	47.1	48.2

Sample Number	33.	34.	35.	36.	37.	38.	39.
Depth (ft)	1279	1323	1381	1505	1667	2087	2304
Ca+Mg	9.1	45.7	42.0	30.3	29.5	23.7	30.8
K	39.7	31.8	24.9	43.8	42.9	45.7	39.7
Na	51.2	22.5	33.1	25.9	27.6	30.7	29.5

Sample Descriptions:

Sample Descriptions:

26. Topopah Spring Member, Paintbrush Tuff. Smectite- and clinoptilolite-bearing tuff at top of Topopah Spring vitrophyre in diagenetic Zone I.
27. Tuff of Calico Hills. Clinoptilolite-bearing nonwelded tuff in diagenetic Zone II.
28. Tuff of Calico Hills. Clinoptilolite- and mordenite-bearing nonwelded tuff in diagenetic Zone II.
29. Prow Pass Member, Crater Flat Tuff. Clinoptilolite- and mordenite-bearing nonwelded tuff in diagenetic Zone II.
30. Prow Pass Member, Crater Flat Tuff. Clinoptilolite- and mordenite-bearing nonwelded tuff in diagenetic Zone II.
31. Bullfrog Member, Crater Flat Tuff. Mordenite-bearing nonwelded tuff in diagenetic Zone II.
32. Tram Member, Crater Flat Tuff. Mordenite-bearing nonwelded tuff in diagenetic Zone II.
33. Topopah Spring Member, Paintbrush Tuff. Vitric basal vitrophyre.
34. Topopah Spring Member, Paintbrush Tuff. Clinoptilolite-bearing nonwelded tuff in diagenetic Zone II.
35. Tuff of Calico Hills. Clinoptilolite-bearing nonwelded tuff in diagenetic Zone II.
36. Tuff of Calico Hills. Clinoptilolite-bearing nonwelded tuff in diagenetic Zone II.
37. Tuff of Calico Hills. Clinoptilolite-bearing nonwelded tuff in diagenetic Zone II.
38. Prow Pass Member, Crater Flat Tuff. Clinoptilolite-bearing nonwelded tuff in diagenetic Zone II.
39. Bullfrog Member, Crater Flat Tuff. Clinoptilolite- and mordenite(?)-bearing nonwelded tuff in diagenetic Zone II.

Exchangeable cations content. Whole-rock samples from borehole USW G-4. From Broxton et al. (1986).

Drill Hole J-13

Depth (ft)	1421	1421	1421	1421	1427	1427	1427	1427
Unit[a]	Tpt	Tpt	Tpt	Tpt	Tpt	Tpt	Tpt	Tpt
				Mol% Exchangeable Cations				
K	52.0	53.3	52.8	50.7	44.4	44.0	44.8	44.5
Na	45.9	44.1	44.8	46.5	53.8	54.2	54.0	54.3
Ca+Mg	2.1	2.6	2.4	2.8	1.8	1.8	1.1	1.1

Depth (ft)	1507	1507	1507	1575	1575
Unit[a]	Tht	Tht	Tht	Tht	Tht
			Mol% Exchangeable Cations		
K	51.7	51.1	52.0	48.4	48.2
Na	45.3	45.7	45.3	47.4	47.6
Ca+Mg	3.0	3.1	2.6	4.2	4.2

Explanation:

Tpt - Topopah Spring Member; and
Tht - Tuff of Calico Hills.

Major cations content. Volcanic glass from borehole J-13. From Broxton et al. (1986).

Drill Hole UE-25a#1

Depth (ft)	226	226	251	251	251	251	251	277
Unit[a]	Tpc	Tpc	Tb	Tb	Tb	Tb	Tb	Tb
			Mol% Exchangeable Cations					
K	44.4	45.3	54.6	48.9	51.0	45.9	48.4	50.9
Na	52.1	51.2	41.5	47.6	45.7	47.4	48.5	45.5
Ca+Mg	3.5	3.5	3.9	3.5	3.3	6.7	3.1	3.6

Depth (ft)	277	277	277	277	277	277	277	277
Unit[a]	Tb	Tb	Tb	Tb	Tb	Tb	Tb	Tb
			Mol% Exchangeable Cations					
K	46.4	51.0	59.4	61.4	51.6	57.6	58.1	49.0
Na	47.2	42.9	39.6	37.4	47.3	41.4	40.7	48.4
Ca+Mg	6.4	6.1	1.0	1.2	1.1	1.1	1.2	2.6

Depth (ft)	277	277	1279	2113
Unit[a]	Tb	Tb	Tpt	Tcp
	Mol% Exchangeable Cations			
K	54.1	48.5	43.5	45.7
Na	43.4	49.2	53.4	47.0
Ca+Mg	2.5	2.3	3.0	7.3

Explanation:

Tpc - Tiva Canyon Member;
Tpt - Topopah Spring Member; and
Tcp - Prow Pass Member.

Major cations content. Volcanic glass from borehole UE-25a#1. From Broxton et al. (1986).

Drill Hole USW G-2

Depth (ft)	331	331	331	331	331	331	331	331
Unit[a]	Tpy	Tpy	Tpy	Tpy	Tpy	Tpy	Tpy	Tpy
			Mol% Exchangeable Cations					
K	40.9	38.3	39.4	37.5	37.2	38.0	35.8	35.7
Na	57.0	59.9	58.8	60.6	60.9	60.1	62.4	62.5
Ca+Mg	2.1	1.9	1.8	1.9	1.9	2.0	1.8	1.8

Depth (ft)	331	358	358	358	358	358	547	547
Unit[a]	Tpy	Tb	Tb	Tb	Tb	Tb	Tpp	Tpp
			Mol% Exchangeable Cations					
K	37.9	40.4	38.5	36.8	35.7	37.2	46.6	46.5
Na	60.3	58.1	60.1	61.6	62.4	61.1	48.7	49.1
Ca+Mg	1.9	1.5	1.4	1.6	1.8	1.7	4.7	4.4

Depth (ft)	547
Unit[a]	Tpp
Mol% Exchangeable Cations	
K	45.8
Na	50.4
Ca+Mg	3.9

Explanation:

Tpy - Yucca Mountain Member; and
Tpp - Pah Canyon Member.

Major cations content. Volcanic glass from borehole USW G-2. From Broxton et al. (1986).

Drill Hole USW GU-3

Depth (ft)	356	356	356	1195	1227	1227	1227	1227
Unit[a]	Tpc	Tpc	Tpc	Tpt	Tpt	Tpt	Tpt	Tpt
	Mol% Exchangeable Cations							
K	45.2	47.8	26.7	52.0	49.6	50.5	48.8	51.7
Na	54.4	51.8	64.9	46.5	47.7	46.4	46.3	46.2
Ca+Mg	0.4	0.4	8.4	1.6	2.7	3.0	5.0	2.1

Depth (ft)	1227	1227	1227	1227	1227	1303	1303	1303
Unit[a]	Tpt	Tpt	Tpt	Tpt	Tpt	Tpt	Tpt	Tpt
	Mol% Exchangeable Cations							
K	50.8	52.0	51.2	52.4	50.2	50.6	50.7	50.1
Na	47.4	46.3	45.9	43.5	47.5	47.0	46.5	47.0
Ca+Mg	1.8	1.7	2.9	4.1	2.3	2.4	2.8	2.9

Depth (ft)	1303	1303	1303	1394	1394	1394	1537	1537
Unit[a]	Tpt	Tpt	Tpt	Tpt	Tpt	Tpt	Tht	Tht
	Mol% Exchangeable Cations							
K	49.7	50.8	52.4	46.4	46.8	44.6	47.8	50.0
Na	47.8	47.0	44.8	50.0	49.6	52.1	47.4	45.3
Ca+Mg	2.5	2.2	2.8	3.6	3.7	3.4	4.9	4.7

Depth (ft)	1537	1537	1537	1571
Unit[a]	Tht	Tht	Tht	Tcp
	Mol% Exchangeable Cations			
K	48.7	47.5	50.0	47.2
Na	46.4	48.4	45.3	49.5
Ca+Mg	4.9	4.1	4.7	3.3

Explanation:

Tpc - Tiva Canyon Member;
Tpt - Topopah Spring Member;
Tht - Tuff of Calico Hills; and
Tcp - Prow Pass Member.

Major cations content. Volcanic glass from borehole USW GU-3. From Broxton et al. (1986).

Depth (ft) Unit[a]	1432 Tht	1432 Tht	1432 Tht
	Mol% Exchangeable Cations		
K	47.2	47.1	47.6
Na	48.7	47.9	48.3
Ca+Mg	4.1	5.0	4.1

Drill Hole USW H-4

Depth (ft) Unit[a]	1312 Tht	1312 Tht	1312 Tht	1312 Tht	1312 Tht	1312 Tht
			Mol% Exchangeable Cations			
K	47.9	48.8	52.0	47.4	49.9	50.4
Na	48.5	47.9	44.5	49.0	46.3	46.1
Ca+Mg	3.5	3.3	3.5	3.6	3.8	3.5

Explanation:

Tht - Tuffs of Calico Hills.

Major cations content. Volcanic glass from boreholes USW G-4 and H-4. From Broxton et al. (1986).

Depth (ft)	450	450	450	450	1610	1762	1762	1762
Unit[a]	Tpc	Tpc	Tpc	Tpc	Tpt	Tht	Tht	Tht
			Mol% Exchangeable Cations					
K	42.9	41.2	41.3	40.6	47.4	47.6	46.3	45.6
Na	56.0	57.5	57.2	57.8	48.8	48.4	49.9	50.6
Ca+Mg	1.0	1.3	1.5	1.6	3.8	4.0	3.8	3.9

Depth (ft)	1762	1800	1800	1966	1966	1966
Unit[a]	Tht	Tht	Tht	Tcp	Tcp	Tcp
			Mol% Exchangeable Cations			
K	46.8	48.4	47.5	50.1	51.9	50.7
Na	49.5	47.4	48.5	46.1	44.8	46.1
Ca+Mg	3.6	4.2	4.0	3.9	3.3	3.2

Explanation:

Tpc - Tiva Canyon Member;
Tpt - Topopah Spring Member;
Tht - Tuff of Calico Hills; and
Tcp - Prow Pass Member.

Major cations content. Volcanic glass from borehole USW H-5. From Broxton et al. (1986).

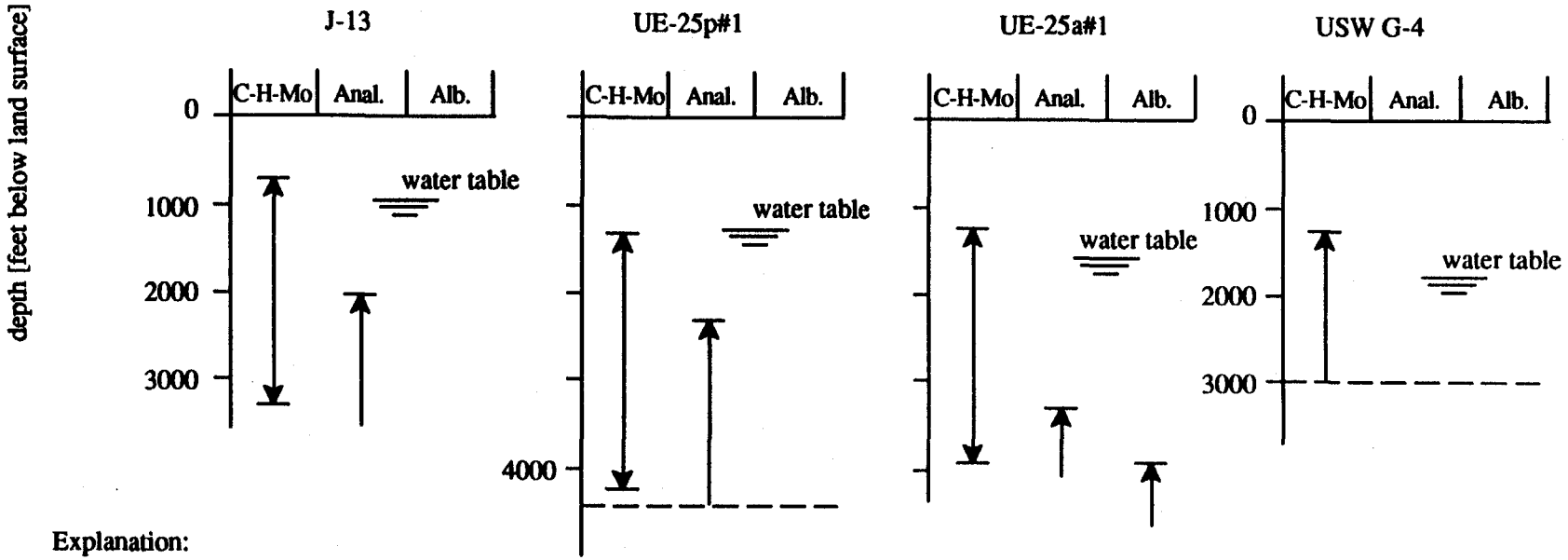

Explanation:

C-H-Mo - the clinoptilolite-heulandite-mordenite zeolitic zone;
Anal. - the analcime zeolitic zone; and
Alb. - the albite zeolitic zone.

Note:

a) the depth of occurrance of zeolitic zones, as shown, is from Bish and Chipera (1989); and

b) position of the contemporary water table, as shown, is from Sass et al. (1987).

Mineralogy of the Yucca Mountain zeolites, based on the x-ray powder diffraction patterns.

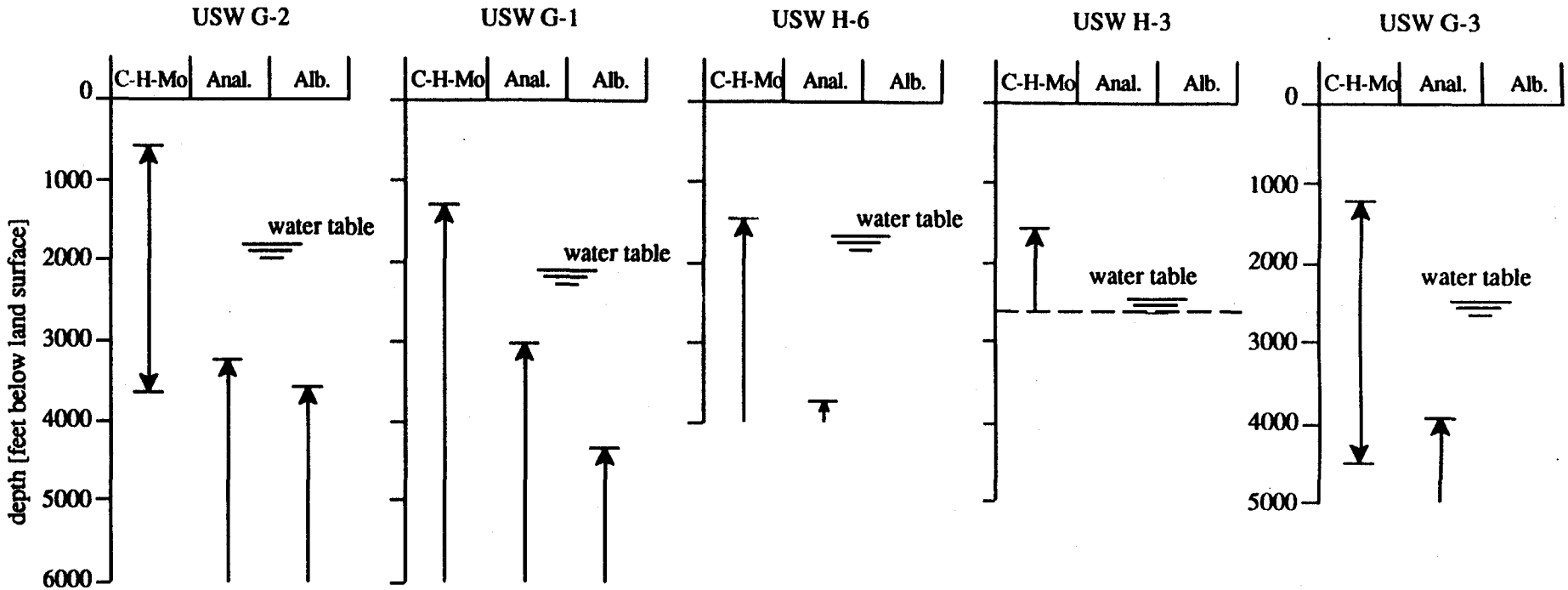

Explanation:

C-H-Mo - the clinoptilolite-heulandite-mordenite zeolitic zone;
Anal. - the analcime zeolitic zone; and
Alb. - the albite zeolitic zone.

Note:

a) the depth of occurrance of zeolitic zones, as shown, is from Bish and Chipera (1989); and

b) position of the contemporary water table, as shown, is from Sass et al. (1987).

Mineralogy of the Yucca Mountain zeolites, based on the x-ray powder diffraction patterns.

Figure 7-11b

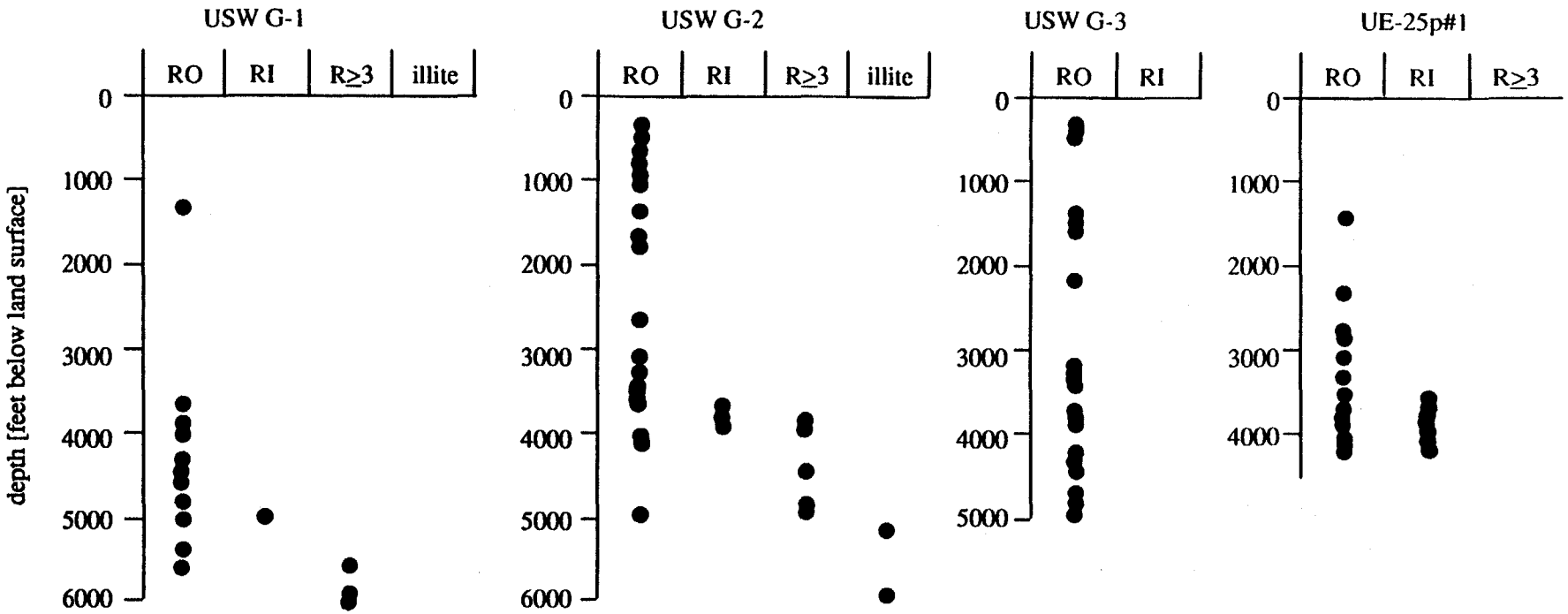

Explanation:

RO - the random type of the illite/smectite interstratification;
RI - the allevardite type of the illite/smectite interstratification; and
R≥3 - the kalkberg type of the illite/smectite interstratification.

Mineralogy of the Yucca Mountain clays, based on the x-ray powder diffraction patterns. Based on data from Chipera and Bish (1988) and Bish (1989).

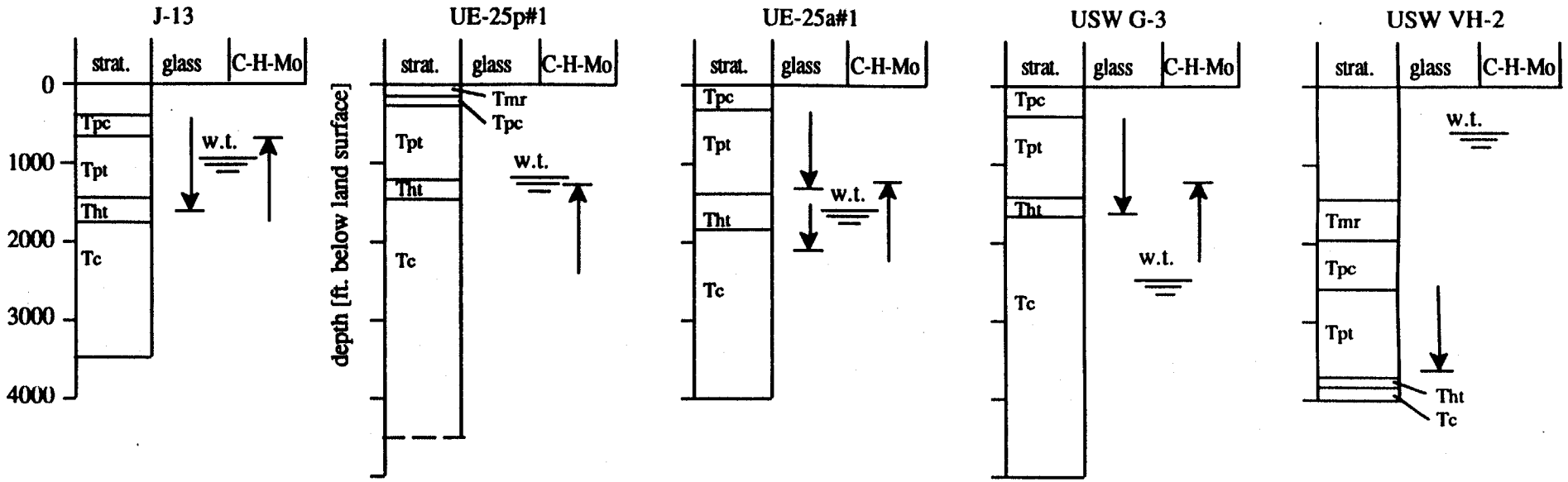

Explanation:

a) Tmr - the Timber Mountain Tuff;
b) Tp - the Paintbrush Tuff, Tpc - Tiva Canyon Member, and Tpt - Topopah Spring Member;
c) Tht - Calico Hills;
d) Tc - the Crater Flat Tuff and older volcanics;
e) glass - the deepest known occurrence of glass; and
f) C-H-Mo - the highest known occurrence of the clinoptilolite + heulandite + mordenite zone.

Position of the zeolitic zone I and II interface, relative to the local stratigraphy and the contemporary water table.

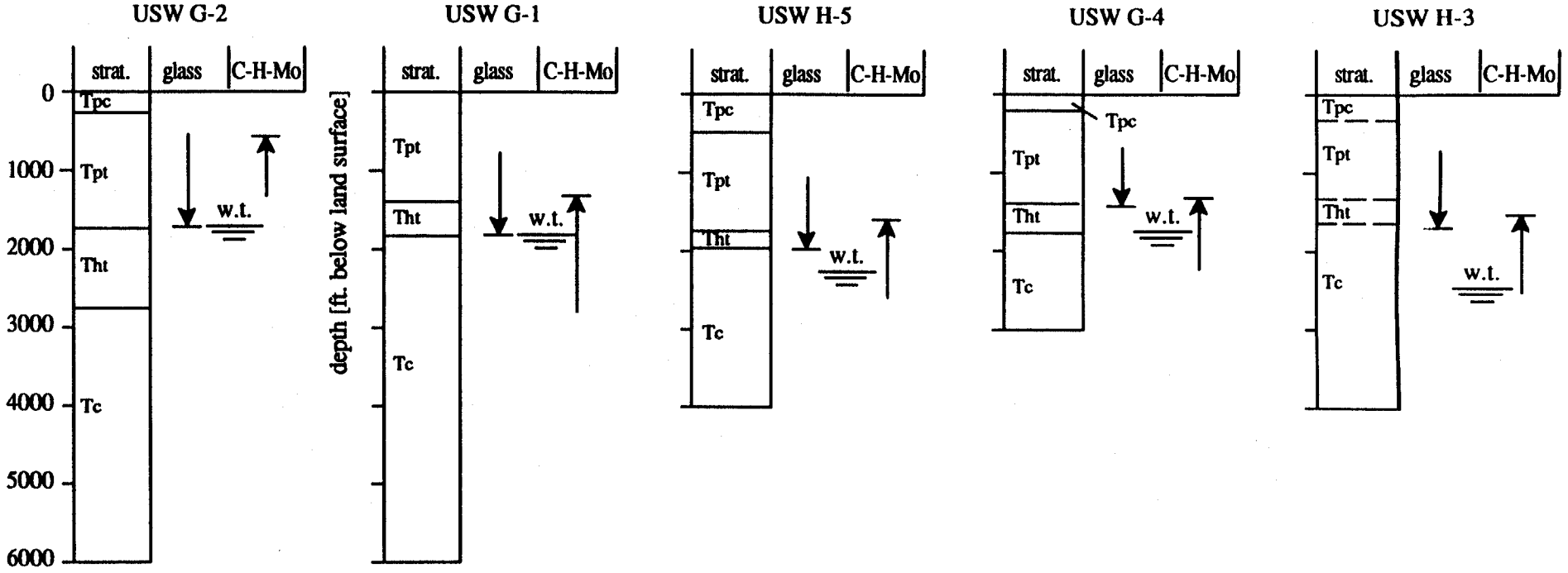

Explanation:

a) Tmr - the Timber Mountain Tuff;
b) Tp - the Paintbrush Tuff, Tpc - Tiva Canyon Member, and Tpt - Topopah Spring Member;
c) Tht - Calico Hills;
d) Tc - the Crater Flat Tuff and older volcanics;
e) glass - the deepest known occurrence of glass; and
f) C-H-Mo - the highest known occurrence of the clinoptilolite + heulandite + mordenite zone.

Position of the zeolitic zone I and II interface, relative to the local stratigraphy and the contemporary water table.

Figure 7-13b

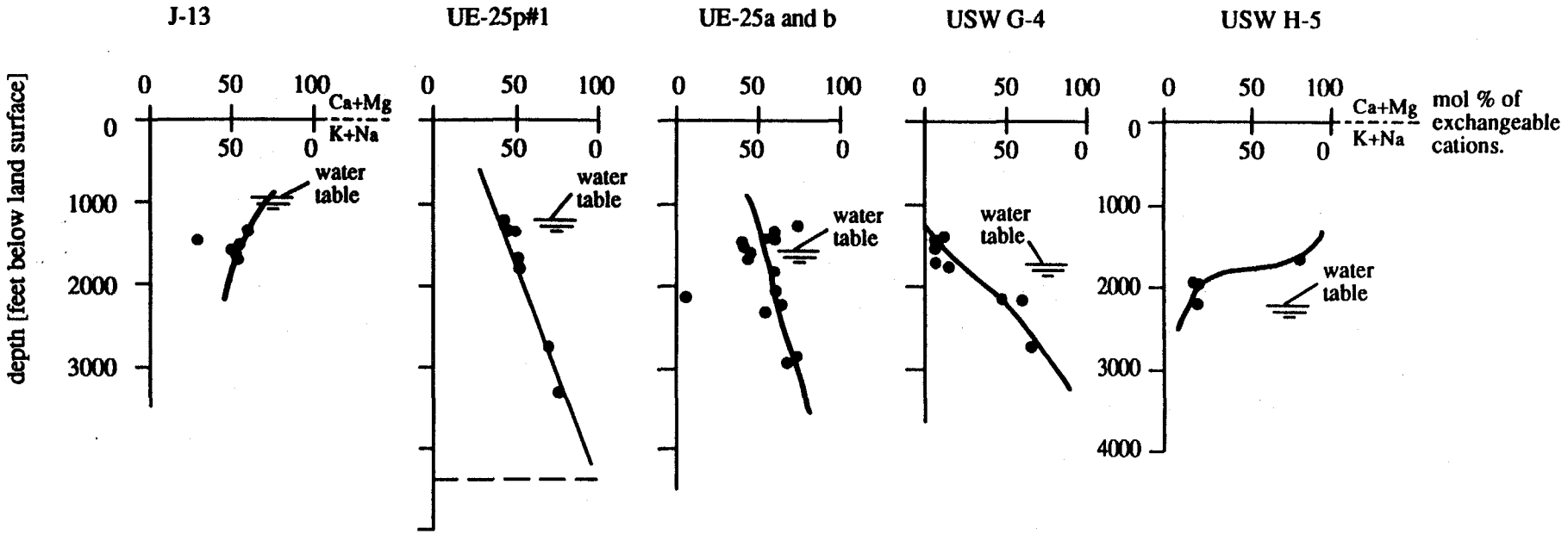

Note:

a) mol % of exchangeable cations, as determined by electron microprobe analyses, are from Broxton et al., (1986); and

b) calcic series zeolites have been identified in boreholes J-13 (heulandite + chabazite), UE-25p#1 (heulandite + laumontite + erionite), UE-25a#1 (heulandite + erionite) and G-4 (heulandite), Carlos et al. (1990) and Bish and Chipera (1989).

Chemical composition of the Yucca Mountain clinoptilolites, expressed as mol % of exchangeable cations, as a function of depth.

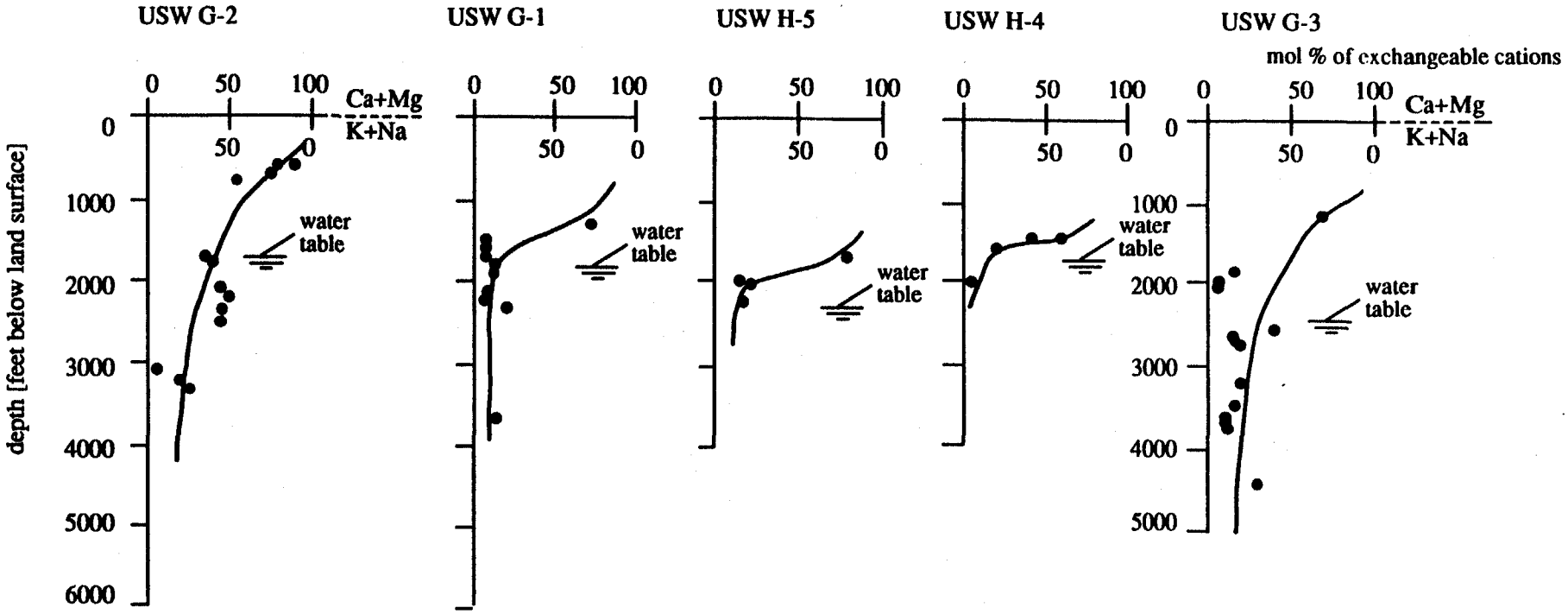

Note:

a) mol % of exchangeable cations, as determined by electron microprobe, are from Broxton et al. (1986); and

b) calcic series zeolites were identified in boreholes USW G-2 (heulandite + stellerite, at a depth from 1447 to 1687 feet), USW G-1 (heulandite + stellerite, at a depth from 1156 to 1356 feet), and USW G-3 (heulandite + erionite, at a depth of 1189 feet), Carlos et al. (1990).

Chemical composition of the Yucca Mountain clinoptilolites, expressed as mol % of exchangeable cations, as a function of depth.

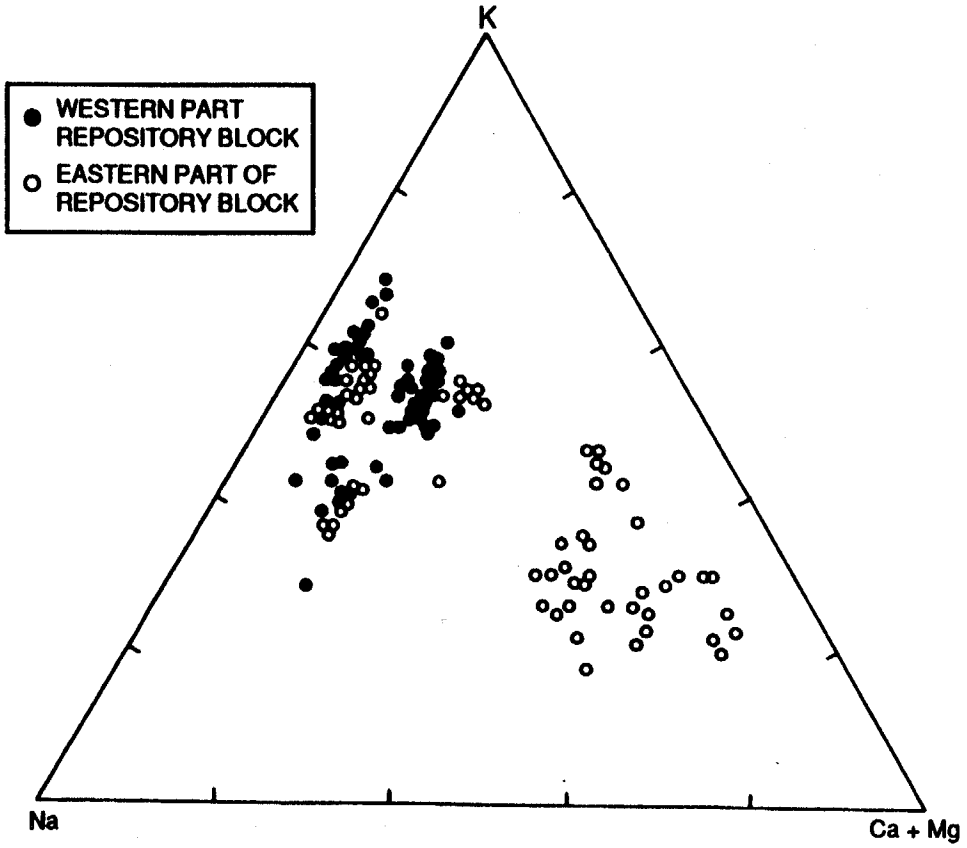

Triangular diagram showing the alkali metal and the alkali earth elements compositions, samples of the Yucca Mountain clinoptilolites. From Broxton et al. (1986).

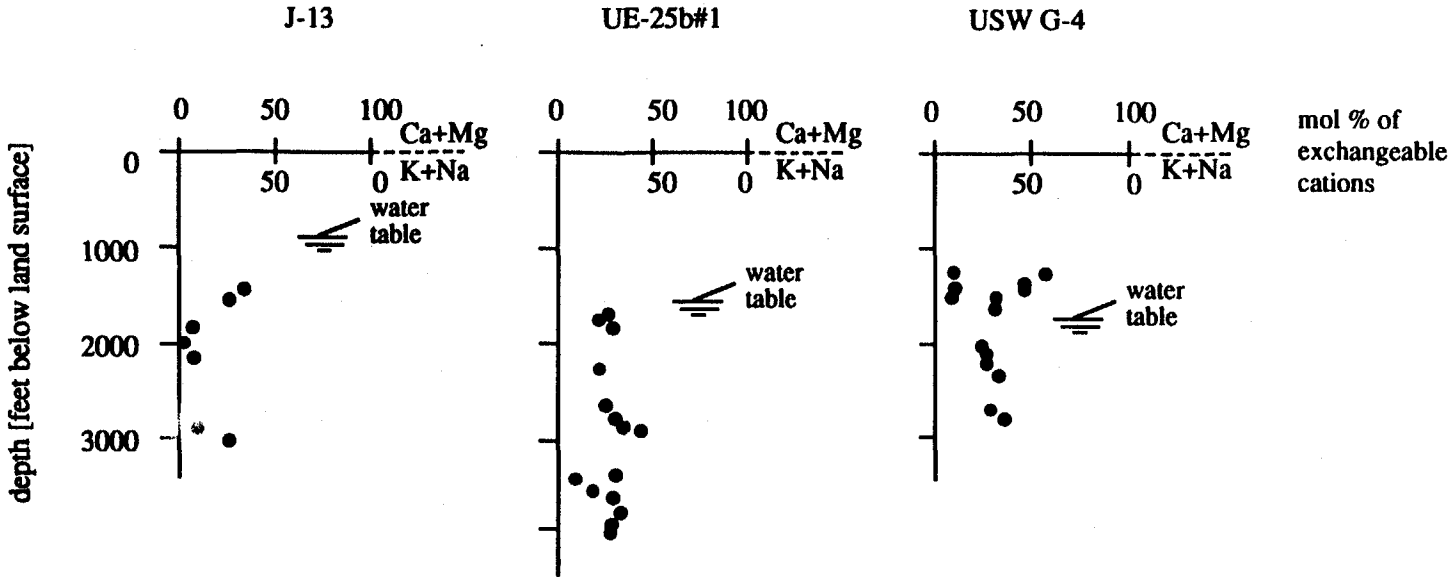

Note:

a) mol % of exchangeable cations [as determined employing a combination of x-ray flourescence, atomic absorption, and plasma-source emission spectrophotometry] are from Broxton et al. (1986).

Chemical composition of the Yucca Mountain ignimbrites (whole-rock samples), expressed as mol % of exchangeable cations, as a function of depth.

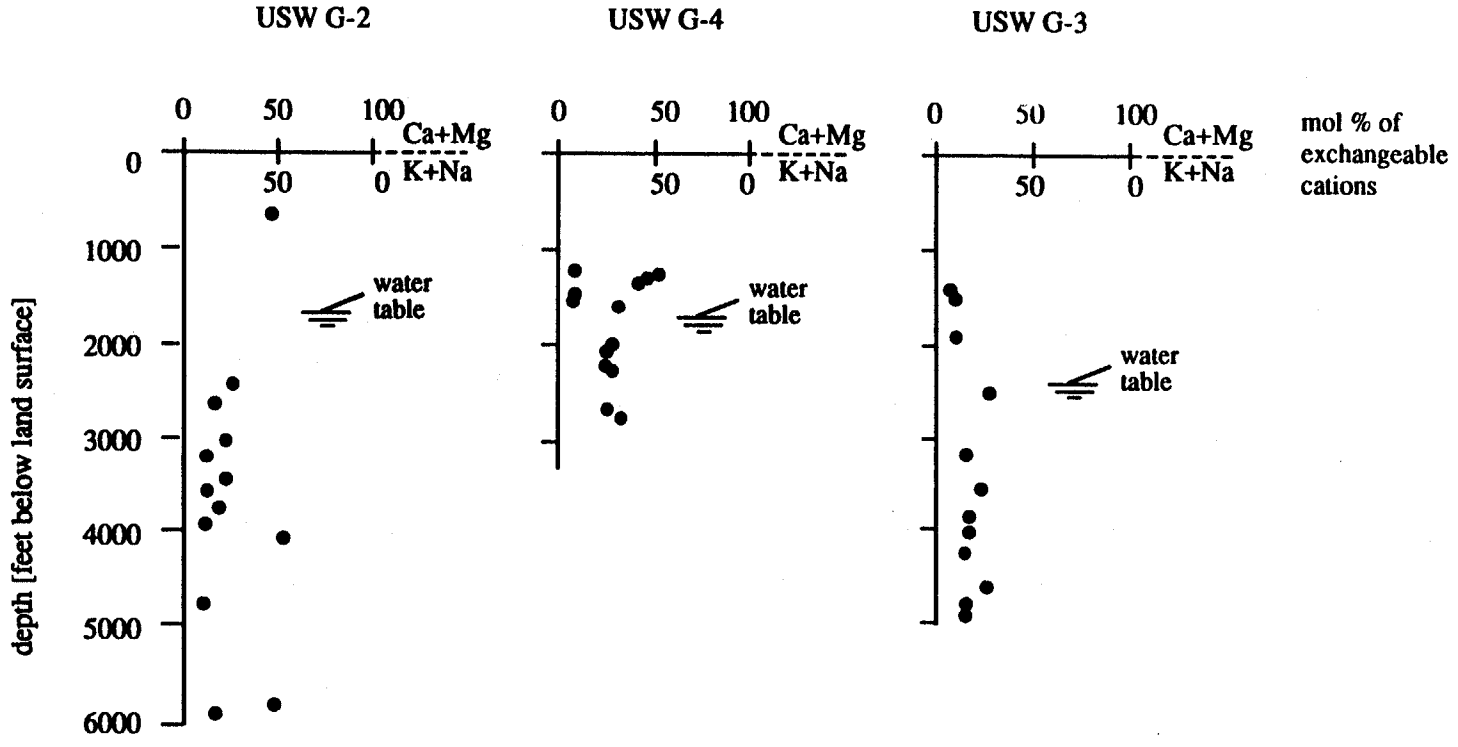

Note:

a) mol % of exchangeable cations [as determined employing a combination of x-ray flourescence, atomic absorption, and plasma-source emission spectrophotometry] are from Broxton et al. (1986).

Chemical composition of the Yucca Mountain ignimbrites (whole-rock samples), expressed as mol % of exchangeable cations, as a function of depth.

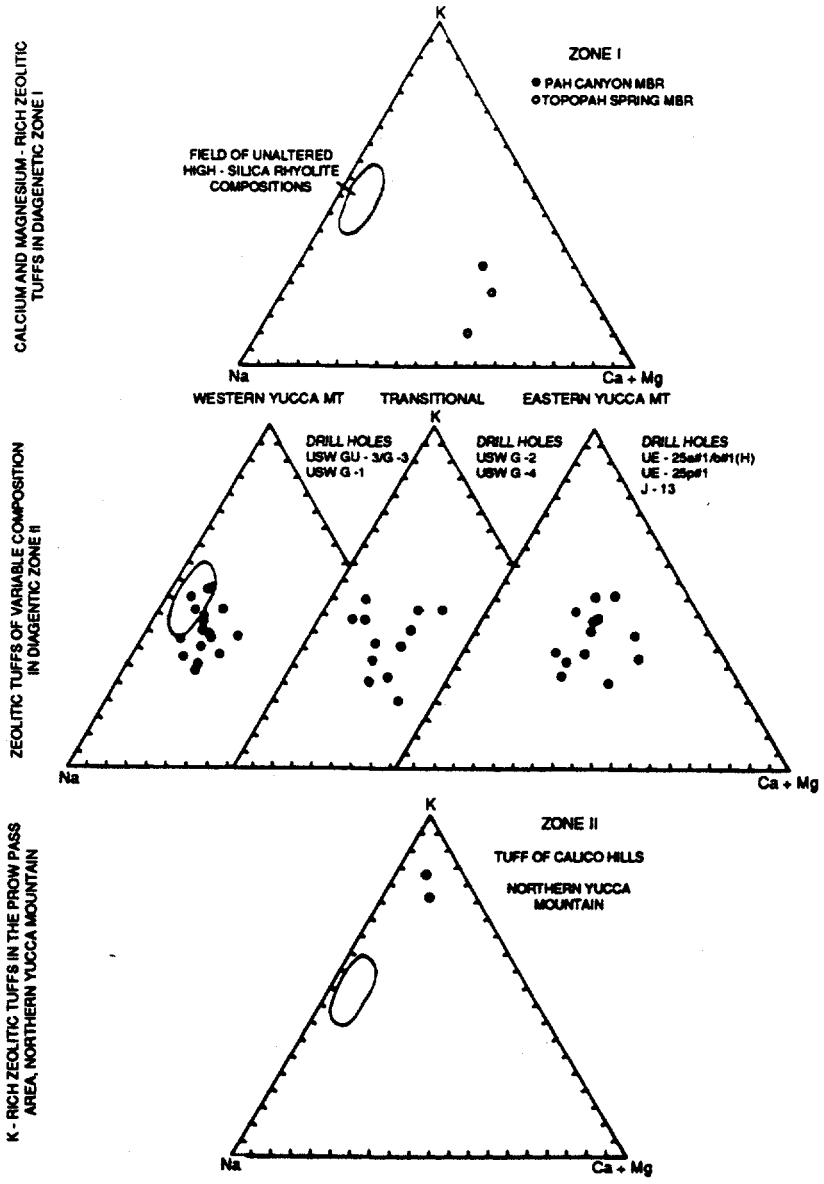

Triangular diagrams showing the relative alkali metal and alkali earth elements compositions, whole-rock samples of the Yucca Mountain ignimbrites. From Broxton et al. (1980).

Figure 7-16c

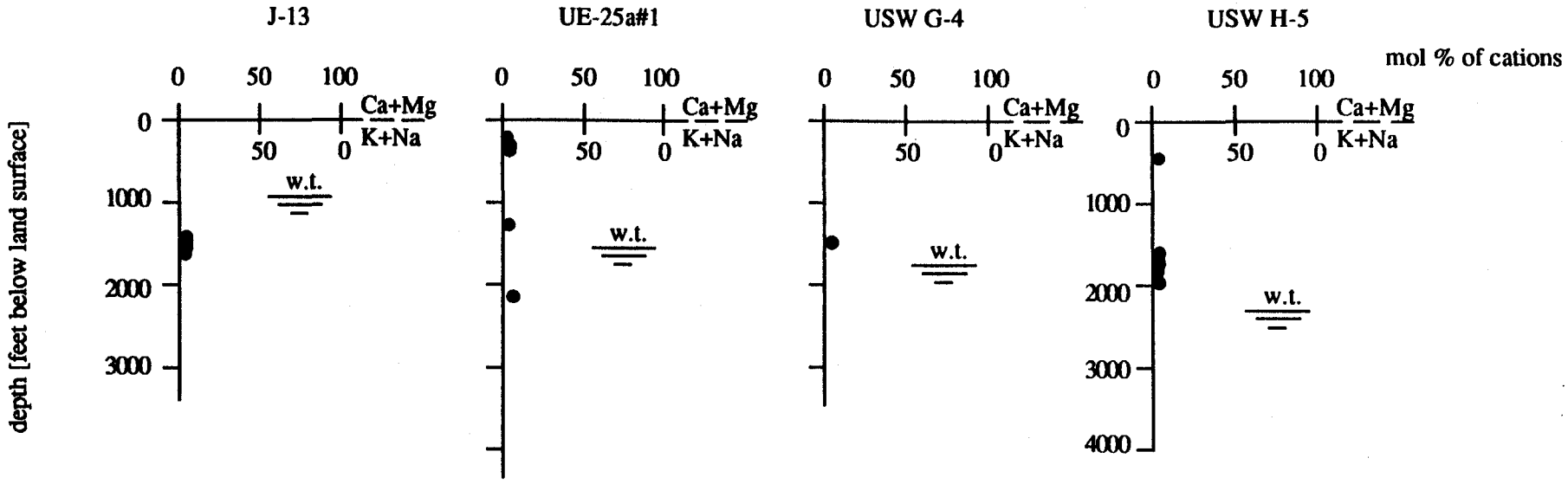

Note:

a) mol % of major cations, as determined employing the electron microprobe method, are from Broxton et al. (1986); and

b) samples of volcanic glass are from Tpc - the Tiva Canyon Member, Tpt - the Topopah Spring member, Tht - the Tuff of Calico Hills, and Tcp - the Prow pass Member.

Chemical composition of the Yucca Mountain volcanic glasses, expressed as mol % of major cations, as a function of depth.

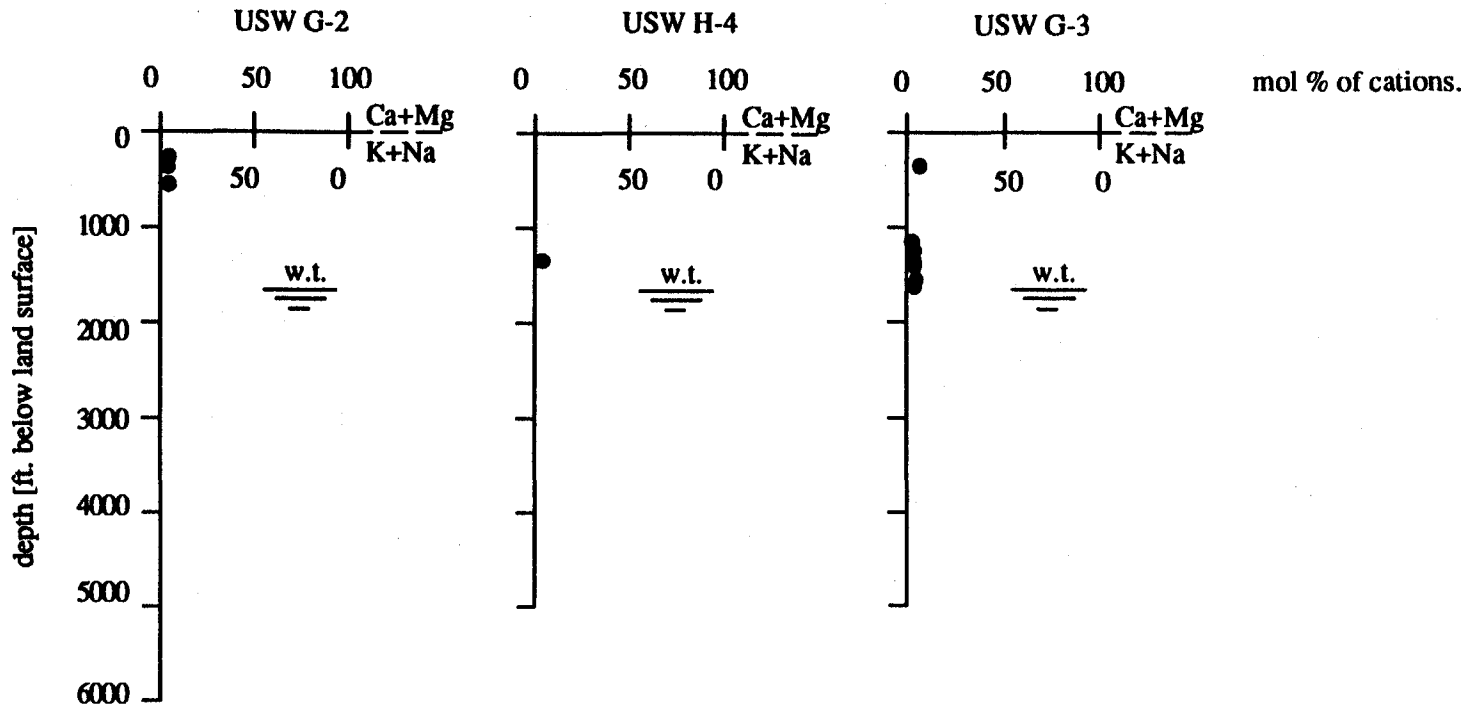

Note:

a) mol % of major cations, as determined employing the electron microprobe method, are from Broxton et al., (1986); and

b) samples of volcanic glass are from Tpc - the Tiva Canyon Member, Tpy - the Yucca Mountain Member, Tpp - the Pah Canyon Member, Tpt - the Topopah Spring Member, Tht - Tuffs of Calico Hills, and Tcp - the Prow Pass Member.

Chemical composition of the Yucca Mountain volcanic glasses, expressed as mol % of major cations, as a function of depth.

Explanation:

FIELD OF COMPOSITIONS FOR THE
PAH CANYON MBR. (n =3)
TOPOPAH SPRING MBR. (n = 40)
TUFF OF CALICO HILLS (n = 25
PROW PASS MBR. (n = 5)

FIELD OF COMPOSITIONS FOR THE
TIVA CANYON MBR. (n = 17)
YUCCA MOUNTAIN MBR. (n = 1)

n = NUMBER OF ANALYSIS

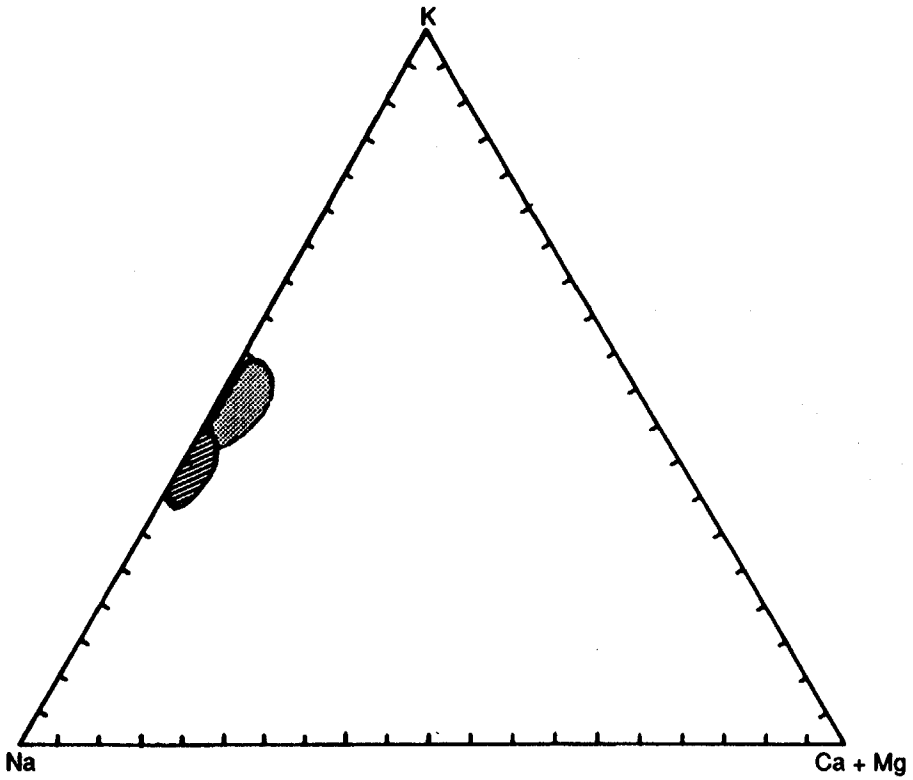

Triangular diagram showing the relative alkali metal and alkali earth elements compositions, samples of glasses from various Yucca Mountain ignimbrites. From Broxton et al. (1986).

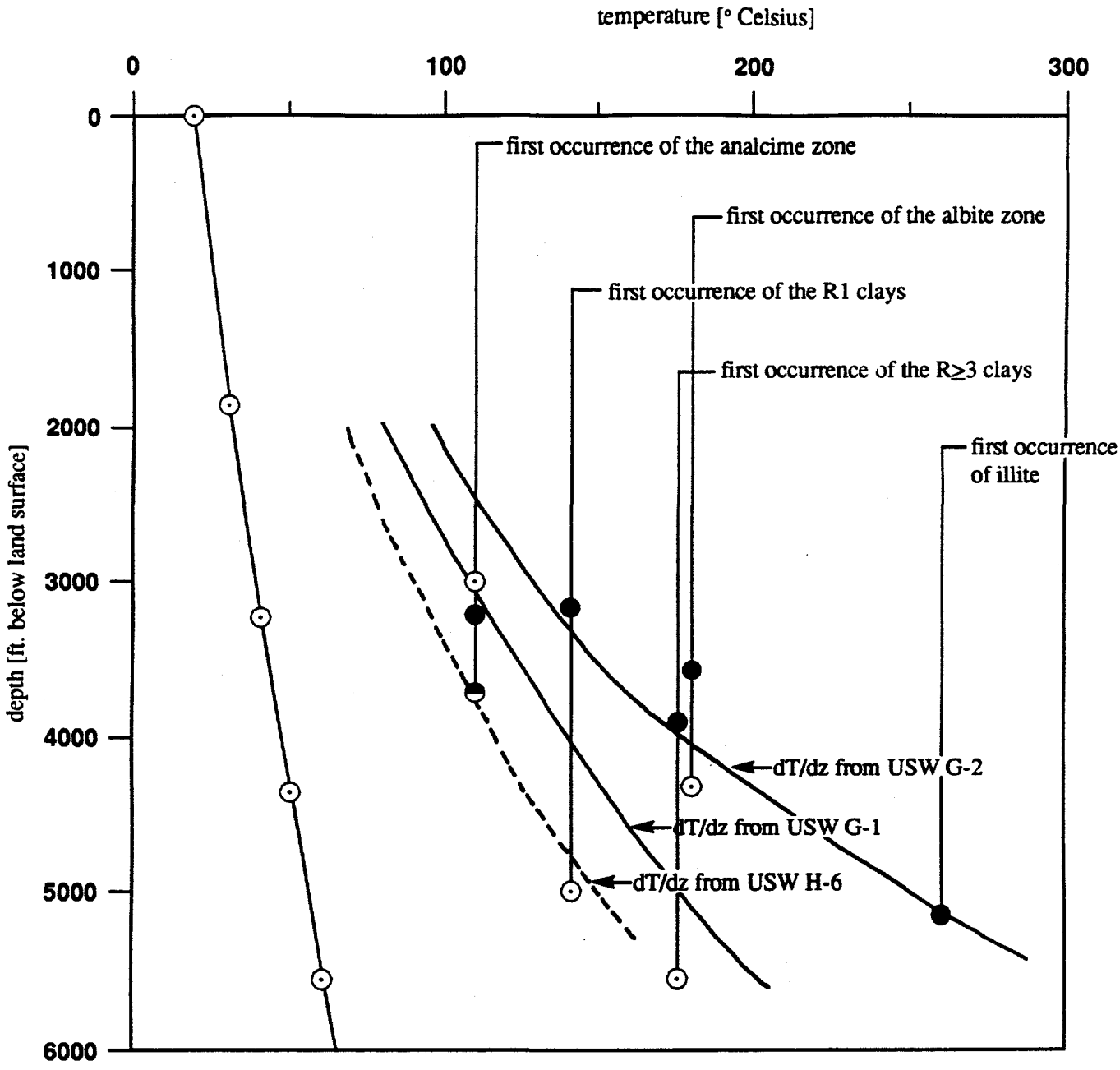

Explanation:

- ⊙ - USW G-1 borehole;
- ● - USW G-2 borehole;
- ◓ - USW H-5 borehole;
- - contemporary geothermal gradient in USW G-1, from Sass et al. (1987).

Paleo-geothermal reconstructions, based on the observed zonation of zeolitization and illitization, northwestern Yucca Mountain.

Figure 7-18

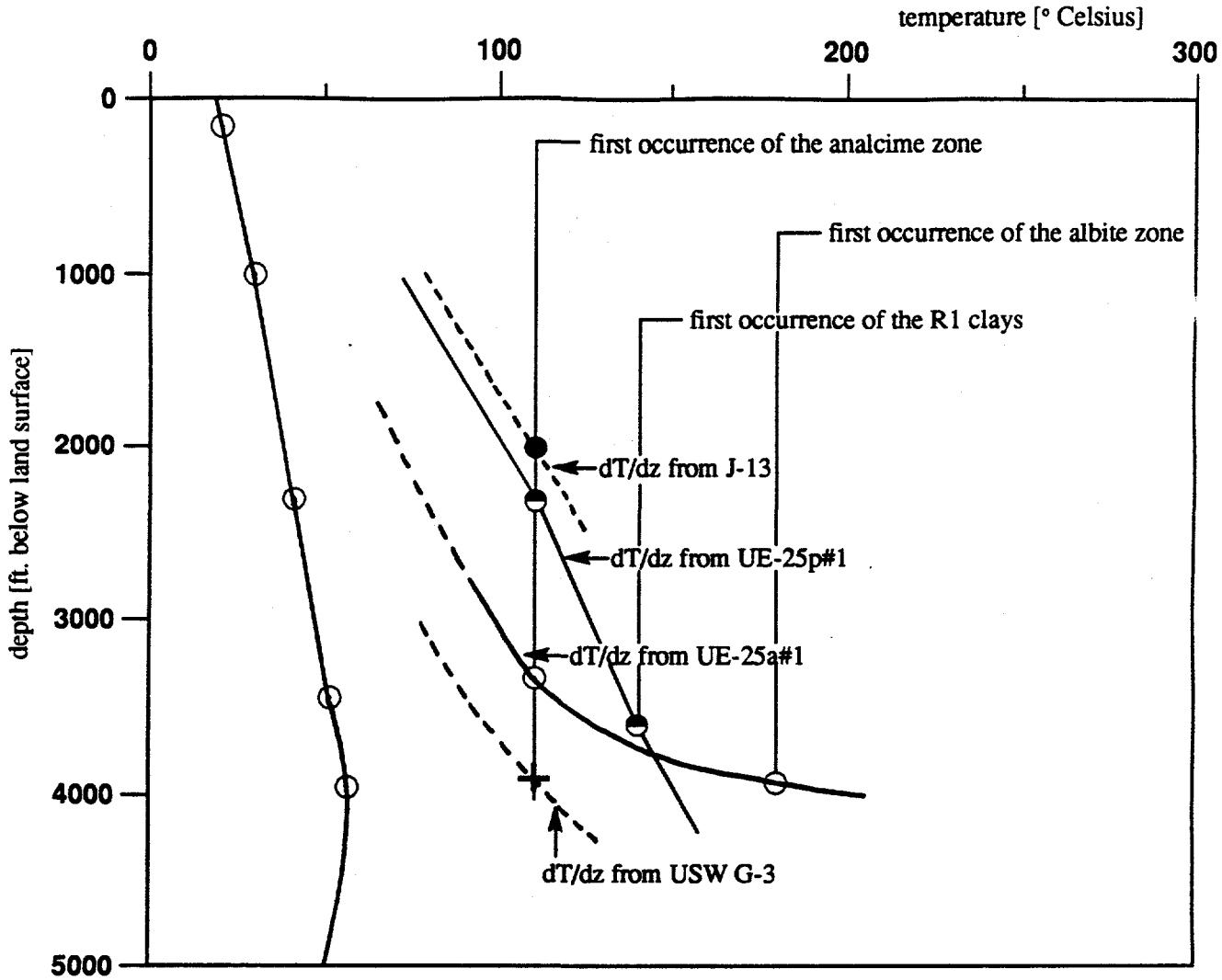

Explanation:

- ● - J-13 well;
- ◓ - UE-25p#1 borehole;
- ⊙ - UE-25a#1 borehole;
- ✚ - USW G-3 borehole; and
- - contemporary geothermal gradient in UE-25p#1

Note:

a) Chemistry of the zeolitic assemblage from the southeastern sector differs from that of zeolitic assemblage from the northwestern sector. The former zeolites tend to be more calcic in composition; the latter zeolites tend to be more of sodic-potassic composition. Also, the former zeolites include more exotic calcic species, such as: laumontite, heulandite, erionite, and chabasite.

Paleo-geothermal reconstructions, based on the observed zonation of zeolitization and illitization, southeastern Yucca Mountain.

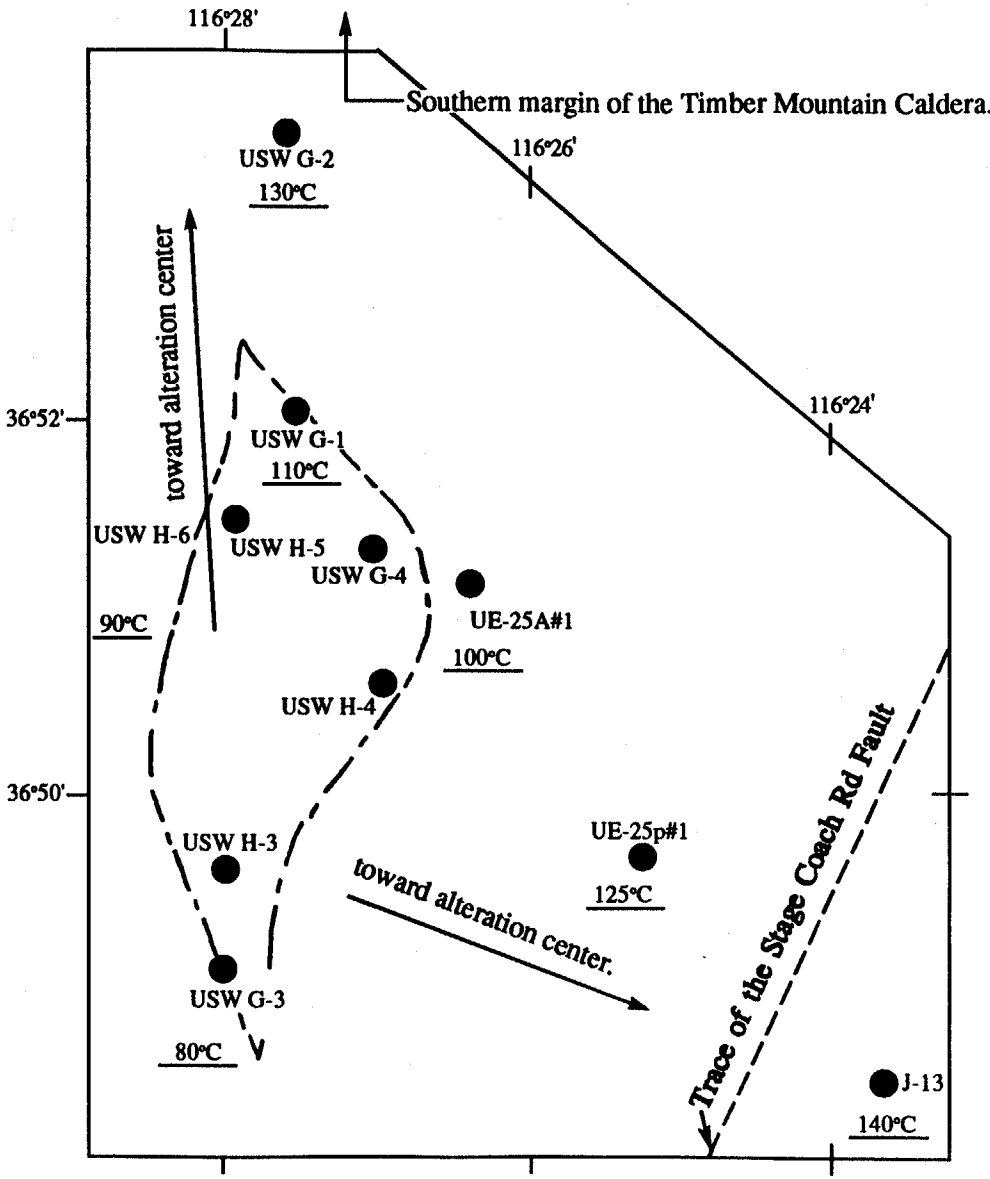

Distribution of the interpreted alteration temperatures at a depth of 3000 feet, Yucca Mountain.

Borehole #	Sample depth [ft]	Host ignimbrite	Type of the S/I interstratification	K/Ar age $x10^6$ years B.P.	Source
USW G-1	3940	Lithic Ridge Tuff	random	14.9 ± 0.30	WoldeGabriel
do	3940	do	random	15.88 ± 0.34	do
do	5637	pre-Lithic Ridge Tuff	Kalkberg	10.9 ± 0.6	Aronson and Bish
USW G-2	3875	Crater Flat Tuff	Kalkberg	11.0 ± 0.6	Aronson and Bish
do	5171	below the Lithic Ridge Tuff	illite	11.0 ± 0.6	do

K/Ar ages from samples of the Yucca Mountain clays (illite/smectite fractions). From Aronson and Bish (1987), and WoldeGabriel (1991).

Sample I.D.	Depth (m)	Mineral Type	Depth to Water Table (m)	Size Fraction (μm)	Weight (g)	K_2O Wt.%	^{40}Ar§ (10^{-11} mol/g)	^{40}Ar§ (%)	Age† (m.y.)
USW G-1 1561a	475.8	Clinoptilolite	572.4	1-3	0.1254	4.96	1.5890	8	2.23±0.13
USW G-1 1561b	475.8	"	"	1-3	0.1340	4.96	1.4195	10	1.99±0.11
USW G-1 1819	554.4	"	"	1-3	0.1961	4.91	3.8120	18	5.39±0.13
USW G-1 1819*	554.4	"	"	1-3	0.1632	3.55	3.5555	20	6.95±0.19
USW G-1 1819**	554.4	"	"	1-3	0.1540	3.20	3.4468	16	7.48±0.20
USW G-1 1819***	554.4	"	"	1-3	0.1708	3.97	4.8006	20	8.39±0.16
USW G-1 2190.8-2190.9 (LANL #207)	667.5	"	"	1-3	0.1760	4.86	4.8638	26	6.94±0.12
USW G-1 3288.5-3288.6 (LANL #216)	1002.2	"	"	1-3	0.1535	4.85	7.4387	35	10.62±0.20
USW G-1 3940a	1200.9	Illite/smectite	"	0.1-0.35	0.1810	2.66	5.5607	16	14.49±0.30
USW G-1 3940b	1200.9	"	"	"	0.1676	2.64	5.8210	22	15.88±0.34
USW G-2 1691-1691.5 (LANL #208)	515.4	Clinoptilolite	524.2	1-3	0.1540	4.13	2.4051	10	4.05±0.11
USW G-2 2430	740.7	" ††	"	1-3	0.1672	3.47	2.3181	18	4.64±0.15
USW G-2 3191.5-3192.0 (LANL #217)	972.9	"	"	1-3	0.1500	3.73	5.6810	28	10.56±0.20
USW GU-3 1674	571.2	" ††	"	1-3	0.1697	3.99	1.4192	8	2.47±0.18
USW GU-3 2013.15-2013.4 (LANL #209)	613.6	"	607.0	1-3	0.1573	4.64	2.6030	20	3.89±0.11
USW G-3 3589a	1094.1	" ††	"	1-3	0.1569	6.12	8.3841	34	9.50±0.18
USW G-3 3589b	1094.1	"	"	1-3	0.1800	5.66	8.1800	15	10.01±0.17
USW G-4 1381	420.9	" ††	"	1-3	0.1895	4.79	2.9145	10	4.22±0.14
USW G-4 1685.2-1685.4 (LANL #214)	513.6	Clinoptilolite	541.5	1-3	0.1560	5.42	3.5747	23	4.58±0.09
USW G-4 1734.3-1734.6 (LANL #210)	528.6	"	"	1-3	0.1548	3.28	1.8382	5	3.89±0.15
USW G-4 1763.2-1763.5 (LANL #211)	537.4	"	"	1-3	0.1672	3.09	1.9660	10	4.41±0.23
USW G-4 1779.6-1779.9 (LANL #212)	542.2	"	"	1-3	0.1623	7.13	7.7166	44	7.50±0.12
USW G-4 1788.4-1788.7 (LANL #213)	545.2	"	"	1-3	0.1629	3.85	7.2223	35	7.31±0.12
UE25P#1 1740-1760 (LANL #215)	530.4-545.6	"	383.9	1-3	0.1527	4.72	5.7606	18	8.47±0.19

§ Radiogenic
† Determined from decay constants and isotopic abundance of ^{40}K according to Steiger and Jager, 1977.
†† Undialyzed samples.
* NaCl exchanged - 48 h
** $BaCl_2$ exchanged - 48 h
*** $BaCl_2$ exchanged - 72 h.

Note:

a) depth of the water table in USW G-3 and USW GU-3, as reported by WoldeGabriel, is in error. Sass et al. (1987) and Carlos et al. (1990) reported this depth to be 750m.

K/Ar ages of clinoptilolites and clays from the Yucca Mountain ignimbrites. From WoldeGabriel (1991).

Sample I.D.	Stratigraphic Units	Depth (m)	Size Fraction (μm)	Authigenic Minerals
G-1 1561	Calico Hills	475.8	1-3	CPT, MOR, Opal CT
G-1 1819	Prow Pass Member	554.4	1-3	CPT, MOR, Opal CT
USW G-1 2190.8-2190.0 (LANL #207,P_1)	Prow Pass Member	667.5	1-3	CPT, MOR, Opal CT
USW G-1 3288.5-3288.6 (LANL #216,P_1)	Bullfrog Member	1002.2	1-3	CPT, MOR, Quartz, FEL
G-1 3940	Lithic Ridge Tuff	1200.9	0.1-0.35	I/S (10% illite layer)
G-2 2430	Calico Hills	740.7	1-3	CPT, Opal CT, minor MOR
USW G-2 1691-1691.5 (LANL #208,P_1)	Calico Hills	515.5	1-3	CPT, MOR, Opal CT
USW G-2 3191.5-3192.0 (LANL #217,P_1)	Tram Member	972.9	1-3	CPT, MOR, Quartz, FEL
GU-1874 1874	Prow Pass Member	571.2	1-3	CPT, MOR, Opal CT
USW G-3 2013.1-2013.4 (LANL #209,P_1)	Bullfrog Member	613.6	1-3	CPT, Opal CT
G-3 3589	Tram Member	1094.1	1-3	CPT, Quartz, I/S, FEL
G-4 1381	Topopah Spring Mem.	420.9	1-3	CPT, Opal CT
USW G-4 1685.2-1685.4 (LANL #214,P_1)	Calico Hills	513.6	1-3	CPT, Opal CT, Cristobalite
USW G-4 1734.3-1734.6 (LANL #210,P_1)	Calico Hills	528.5	1-3	CPT, MOR, Opal CT
USW G-4 1763.2-1763.5 (LANL #211,P_1)	Prow Pass Member	537.4	1-3	CPT, Opal CT, minor MOR
USW G-4 1779.6-1779.9 (LANL #212,P_1)	Prow Pass Member	542.2	1-3	CPT, Cristobalite
USW G-4 1788.4-1788.7 (LANL #213,P_1)	Prow Pass Member	545	1-3	CPT, Cristobalite, FEL
UE25P#1 1740-1750 (LANL #215,P_1)	Prow Pass Member	530.4	1-3	CPT, Opal CT

Note:

The representative radiometric ages for the Yucca Mountain ignimbrites are;

- for the Topopah Member of the Paintbrush Tuff ~ 13.1 x 10^6 years B.P.;
- for the Calico Hills Tuffs ~ 13.4 x 10^6 years B.P.;
- for the Crater Flat Tuff ~13.5 x 10^6 years B.P.; and
- for the Lithic Ridge Tuff ~13.9 x 10^6 years B.P.

Stratigraphic location of the K/Ar dated clinoptilolites. From WoldeGabriel (1991).

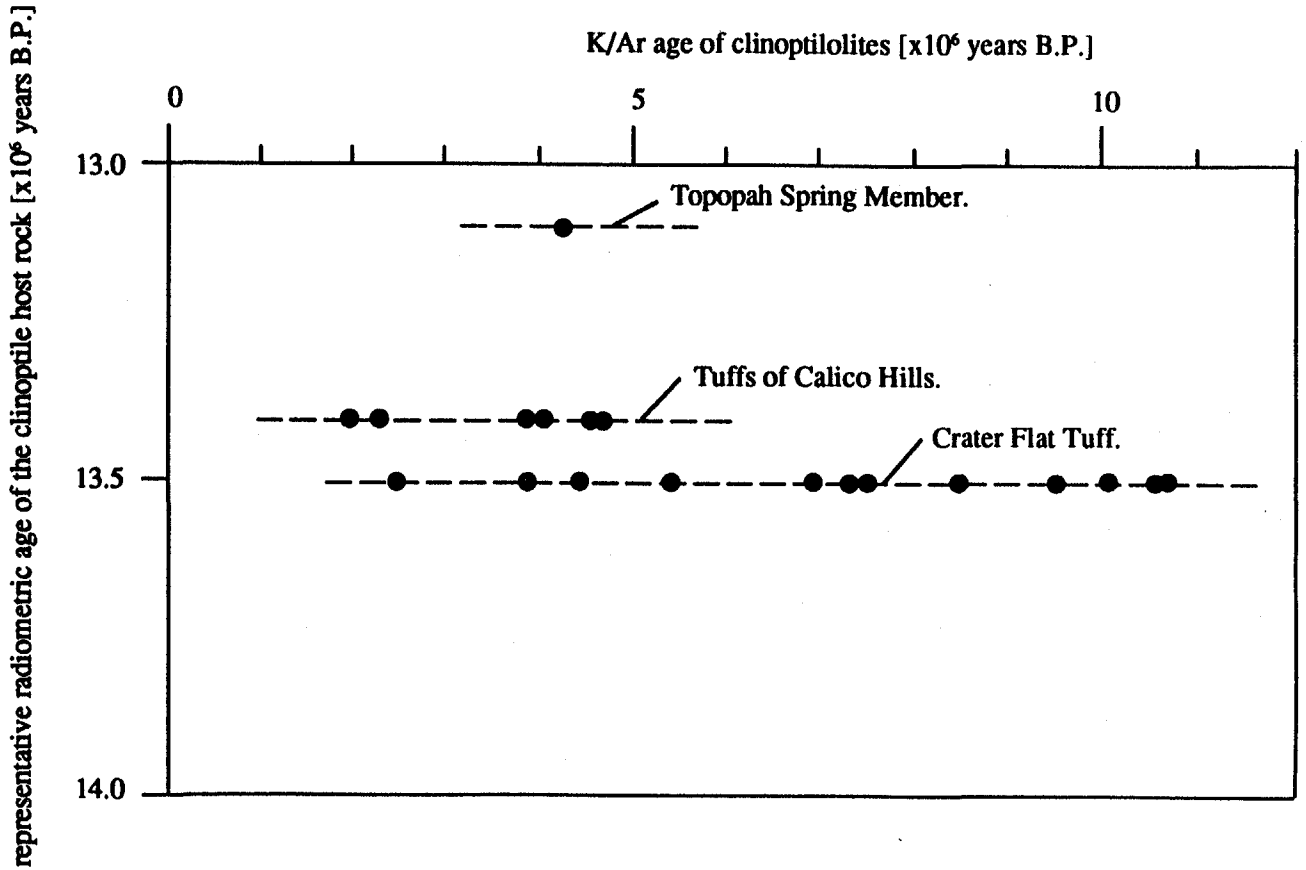

Relationship between the K/Ar ages of clinoptilolites and the representative ages of the corresponding host rock.

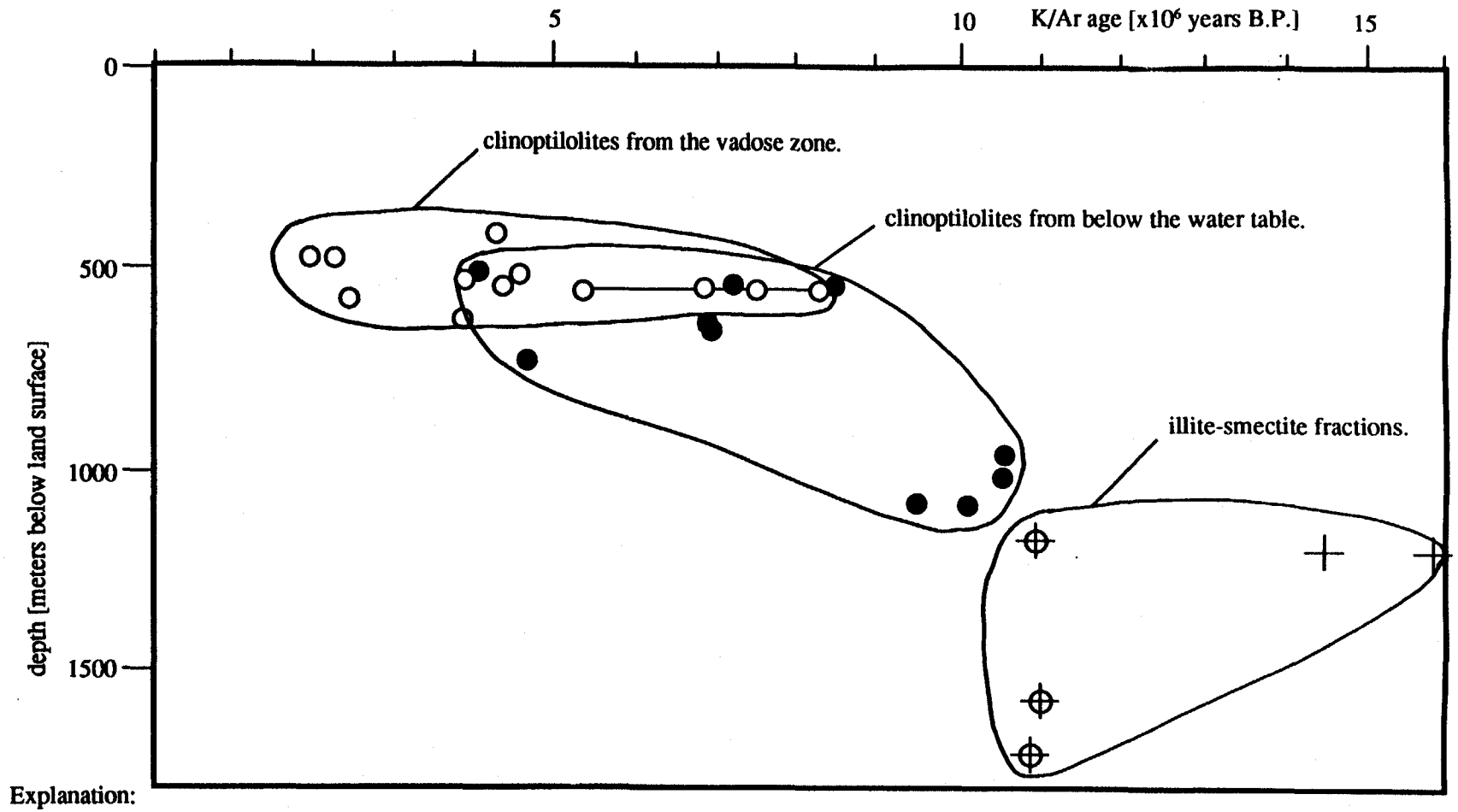

Explanation:

- ○ - sample represents clinoptilolites from the vadose zone;
- ● - sample represents clinoptilolites from below the water table;
- ┼ - sample represents illite/smectites with the RO type of interstratification; and
- ⊕ - sample represents illite/smectite with the R1 and R≥3 type of interstratification.

K/Ar ages of clinoptilolites and hydrothermal clays as a function of depth, Yucca Mountain. Based on radiometric data from Aronson and Bish (1987) and WoldeGabriel (1991).

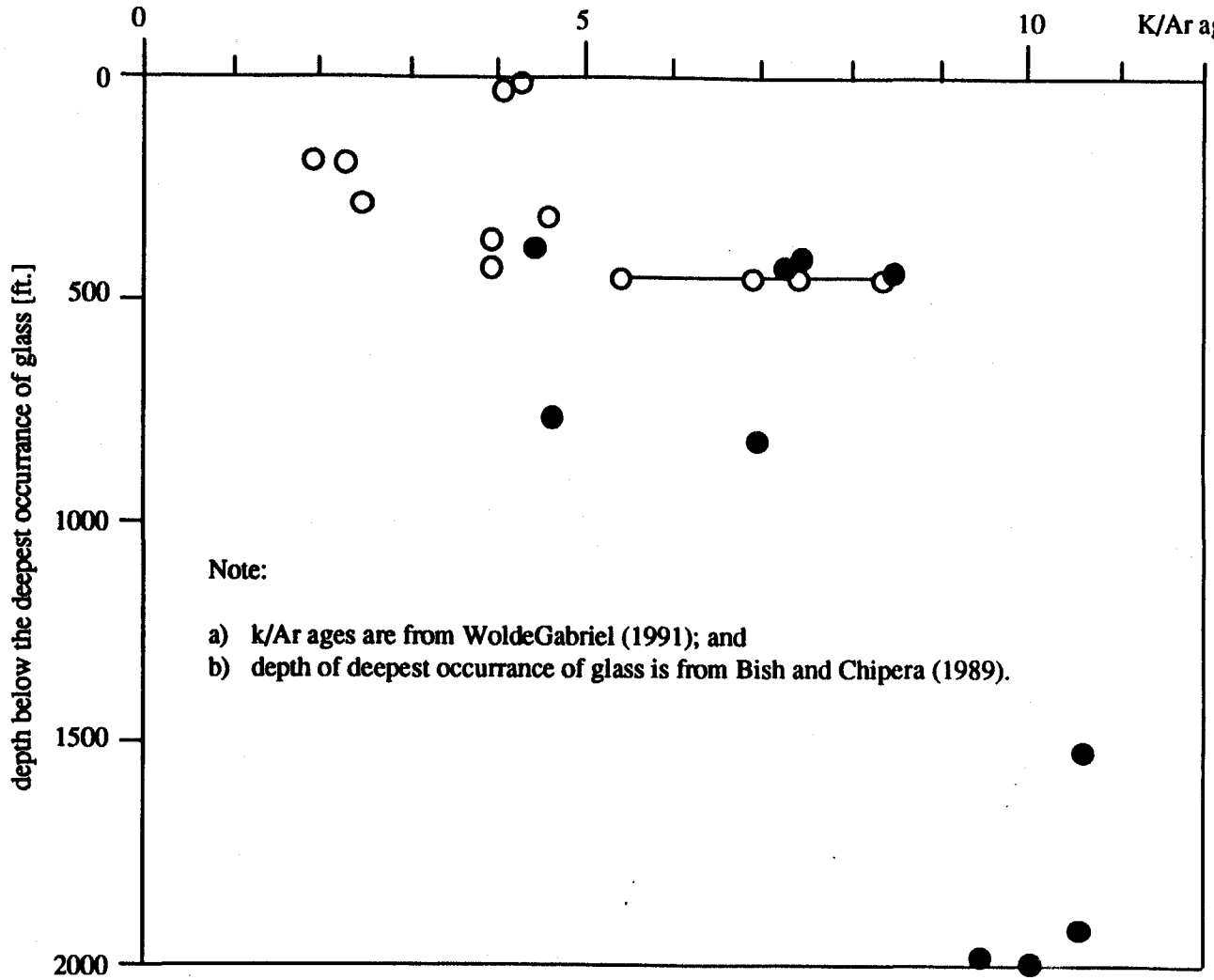

Explanation:

○ - sample represents clinoptilolites from the vadose zone; and

● - sample represents clinoptilolites from below the water table.

K/Ar of the Yucca Mountian clinoptilolites as a function of availability of vitric material.

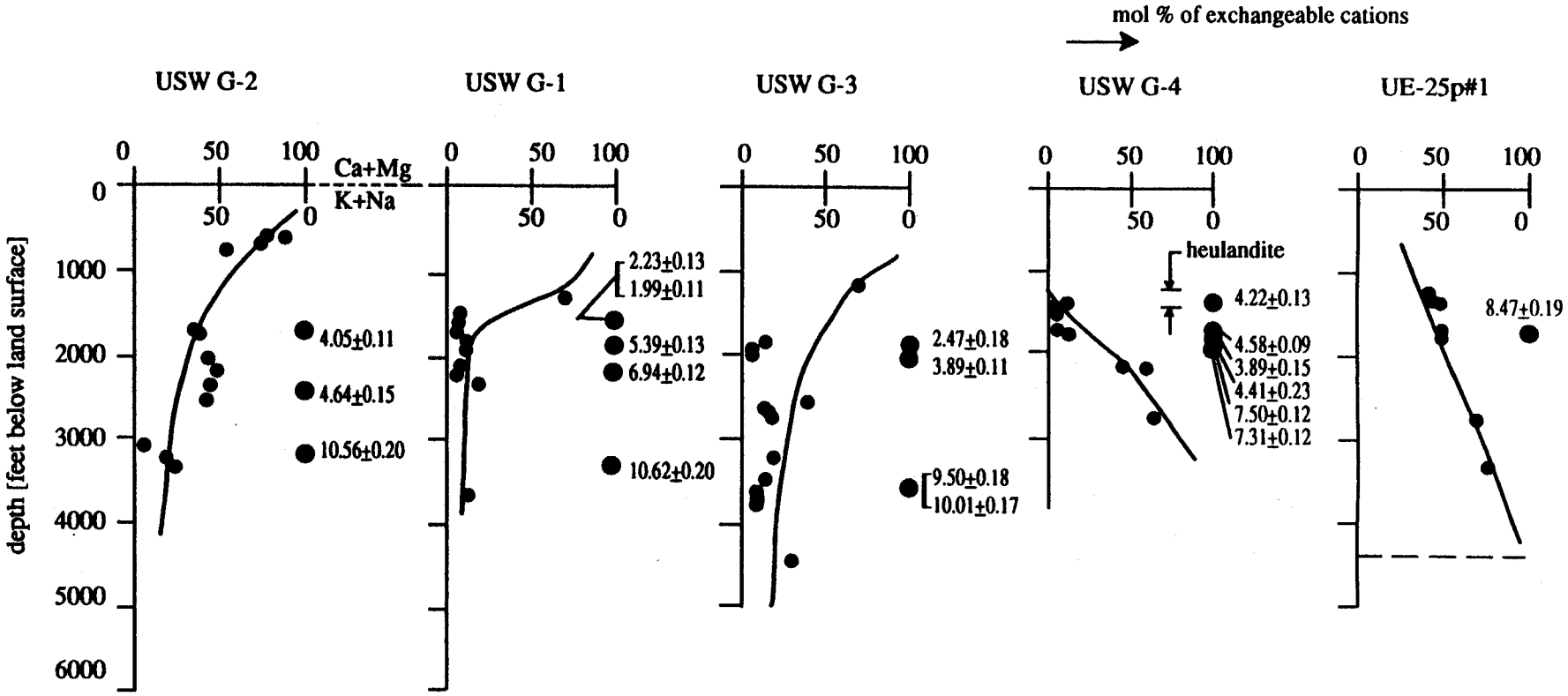

Note:

a) mol % of exchangeable cations are from Broxton et al. (1986);

b) K/Ar ages are from WoldeGabriel (1990);

c) Carlos et al. (1990) have reported that, in borehole USW G-4, heulandite occurs at a depth from 1254 to 1381 feet; evidently, the Ca+Mg zeolitic zone extends, at least, to a depth of 1254 feet; and

d) the representative Ca+Mg cations content is given by the mol % vs. depth curve.

K/Ar ages of the Yucca Mountain clinoptilolites, as a function of depth and mol % of exchangeable cations.

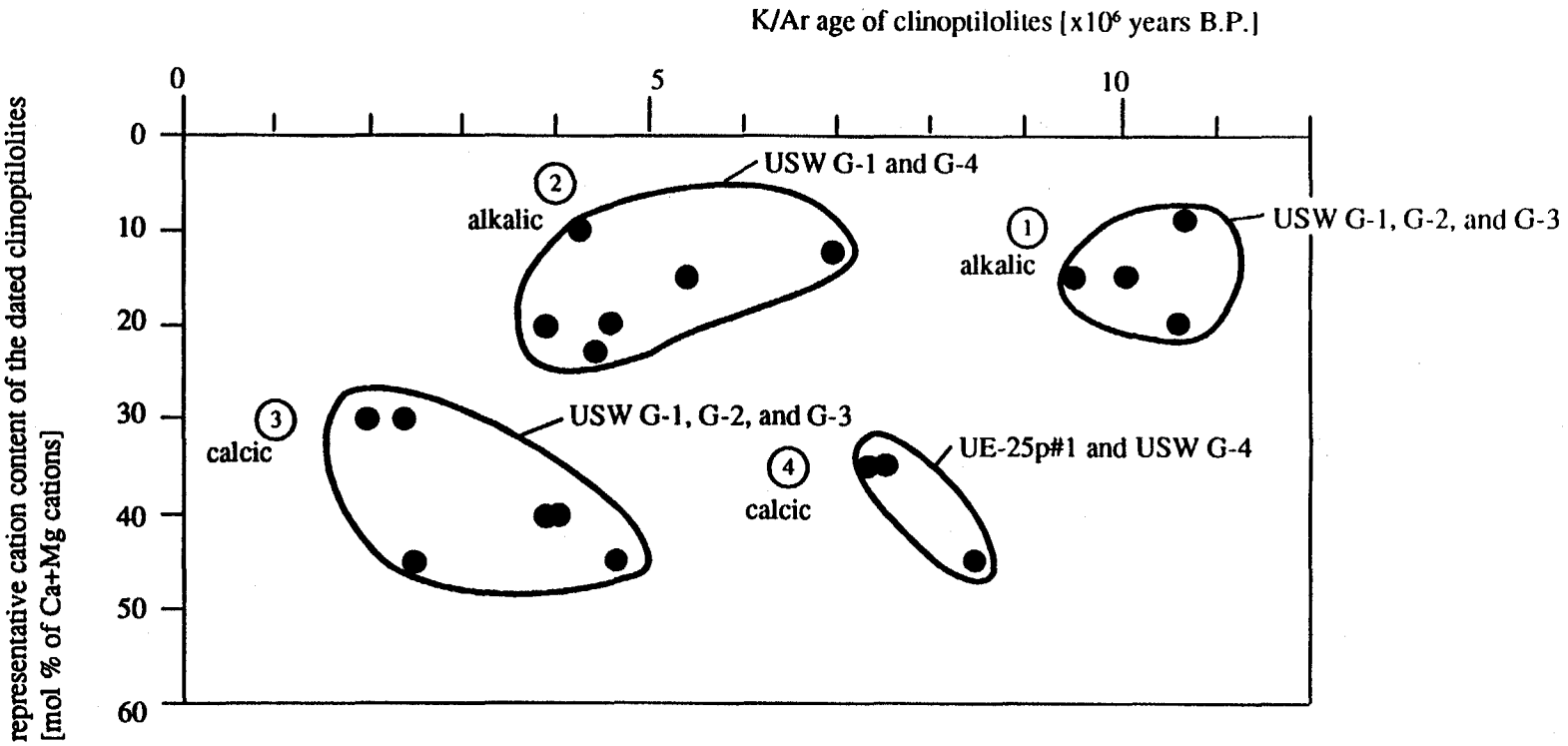

Relationship between the K/Ar ages of clinoptilolites and the representative Ca + Mg cation contents of these clinoptilolites.

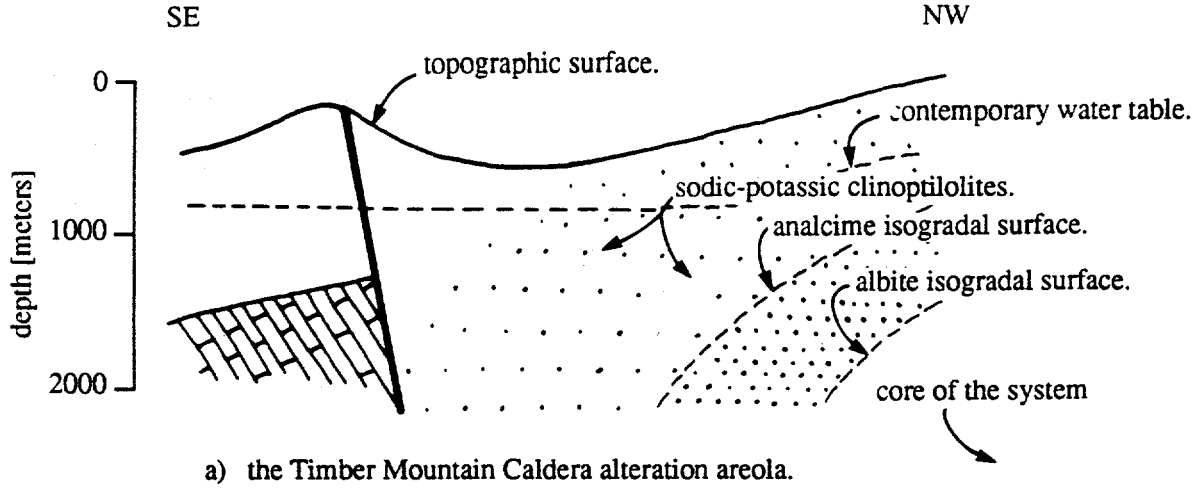

a) the Timber Mountain Caldera alteration areola.

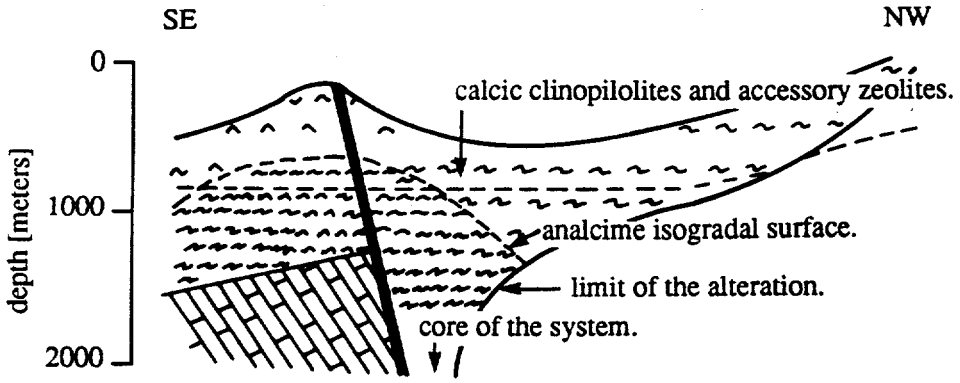

b) the alteration areola of the fault-based hydrothermal system.

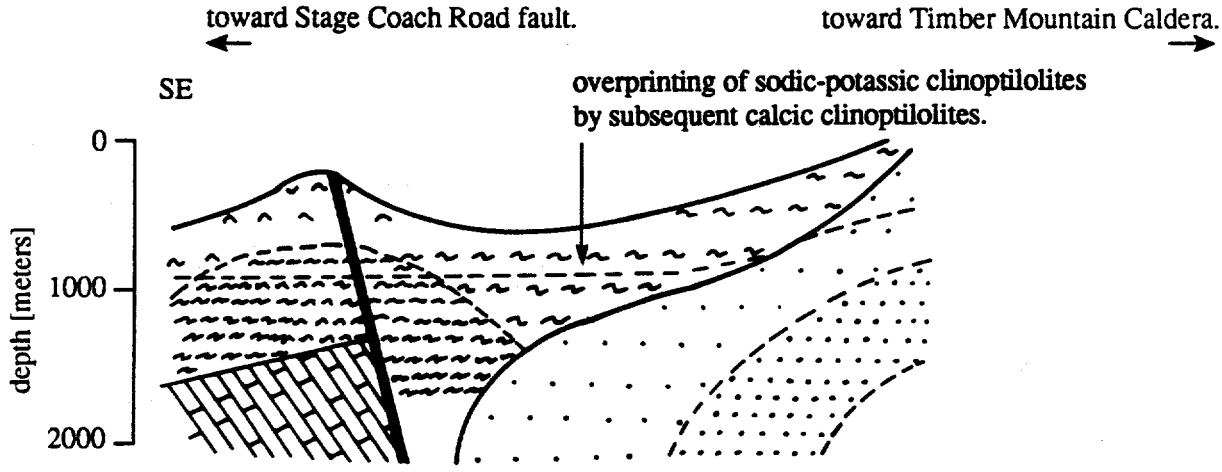

c) the presently observed juxtaposition of the alteration areolas.

Interpretation of the observed spatial distribution of the chemico-temporal characteristics of the Yucca Mountain alteration minerals.

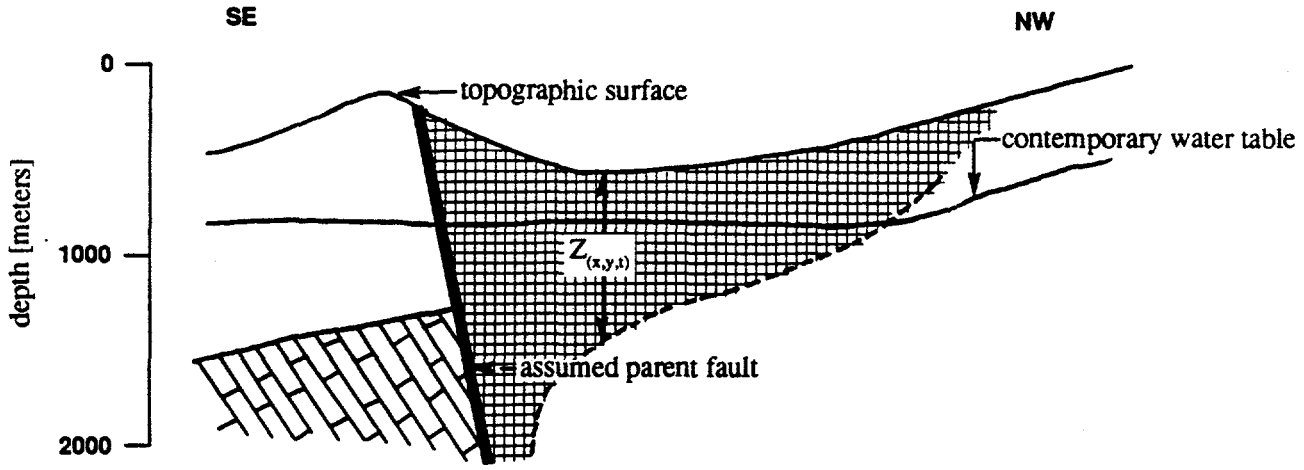

a) schematic diagram showing principal elements of the fault-based upwelling.

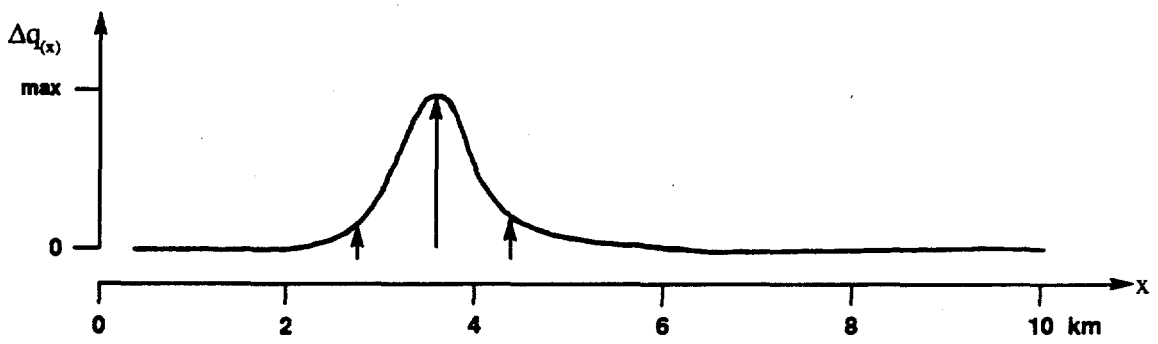

b) spatial distribution of the upward fluid flux increase - $\Delta q_{(x)}$.

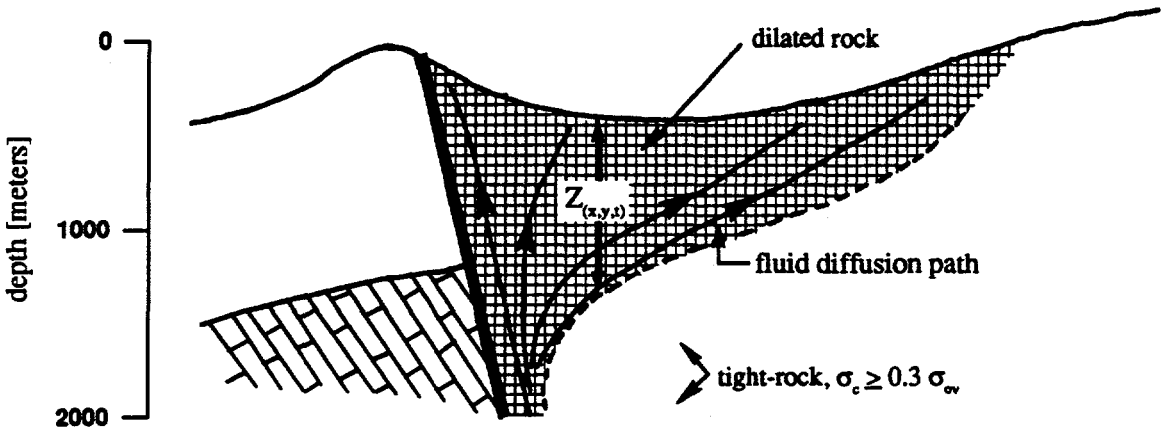

c) spatial distribution of the fluid diffusion path.

Explanation for the observed spatially selective development of the Yucca Mountain metasomatism and calcic zeolitization.

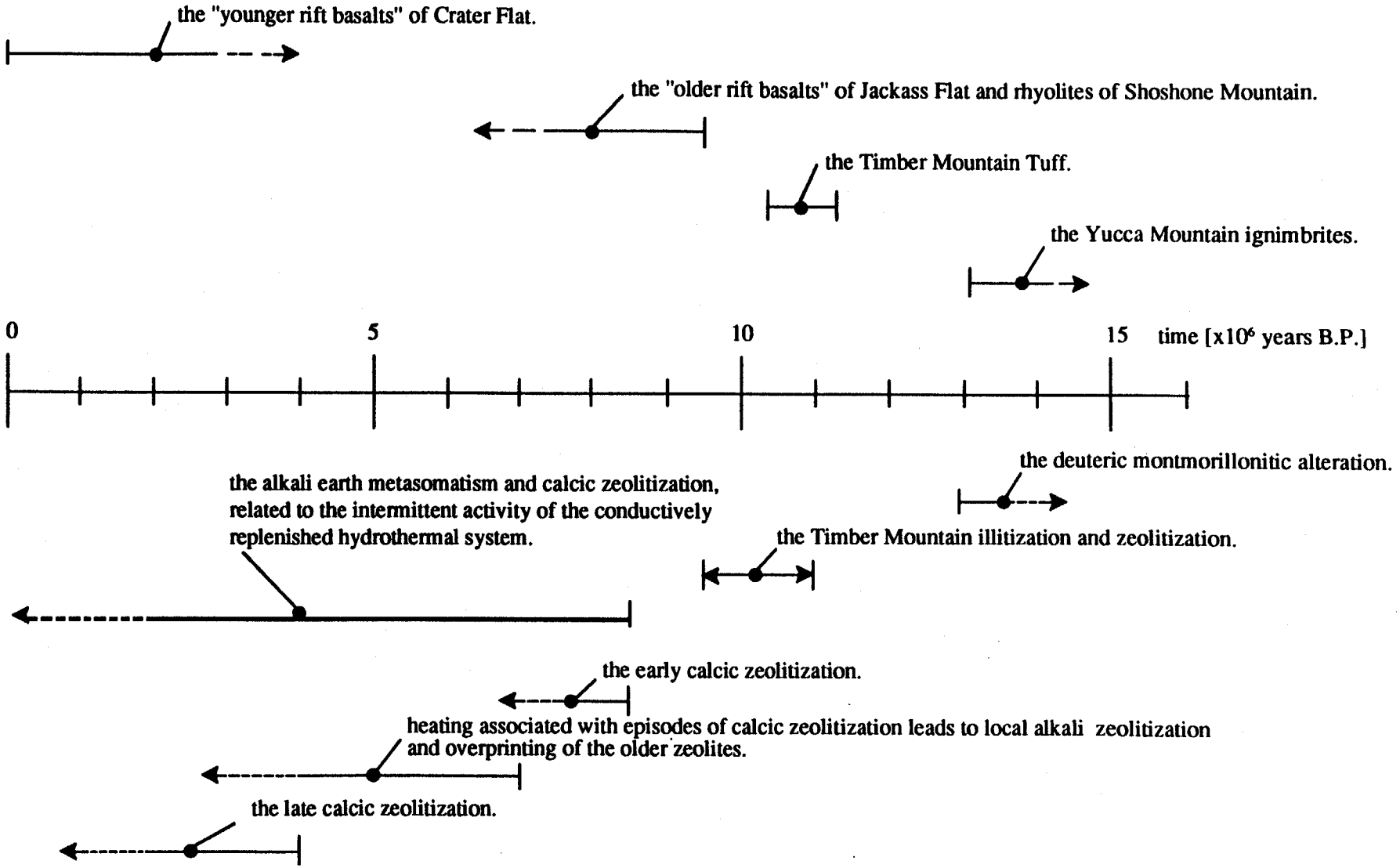

The interpreted history of illitization and zeolitization, based on radiometric ages of the local igneous events, of the local smectite/illite fractions, and of the local clinoptilolites. Yucca Mountain.

Sample No.	Percent[1] Carbonate	Fraction	Uranium (ppm)	Activity Ratios $\frac{^{234}U}{^{238}U}$	$\frac{^{230}Th}{^{232}Th}$	$\frac{^{230}Th}{^{234}U}$
			Crater Flat Area			
368[3]	90	Acid leach	3.62 ±0.07	1.28 ±0.02	34.3 ±1.7	1.06 ±0.04
		Residue	1.96 ±0.04	1.19 ±0.02	23.6 ±1.4	2.30 ±0.09
386	45	Acid leach	7.08 ±0.14	1.23 ±0.02	6.81 ±0.17	0.451 ±0.018
		Residue	8.48 ±0.17	1.20 ±0.02	4.34 ±0.17	1.10 ±0.04
387	58	Acid leach	7.26 ±0.15	1.13 ±0.02	4.23 ±0.17	0.479 ±0.19
		Residue	8.68 ±0.17	1.07 ±0.02	2.54 ±0.10	1.03 ±0.04
			Yucca Mountain			
395	48	Acid leach	5.56 ±0.11	1.34 ±0.02	3.09 ±0.15	0.529 ±0.021
		Residue	14.5 ±0.3	1.28 ±0.02	5.55 ±0.22	0.722 ±0.036

1 Percent carbonate in whole sample.
2 Isochron-plot ages after Szabo and others (1981).
3 Represents a resample of TSV-115 which gave an age of >20,000 years (Szabo and others, 1981).

Uranium concentrations and activity ratios. Samples of calcretes and surficial veins. Yucca Mountain. From Szabo and O'Malley, 1985.

Sample No.	Material	Percent[1] Residue	Fraction	Uranium (ppm)	Activity Ratios $\frac{^{234}U}{^{238}U}$	$\frac{^{230}Th}{^{232}Th}$	$\frac{^{230}Th}{^{234}U}$
			Yucca Mountain Area				
113	Calcr	75	S	2.78 ±0.04	1.03 ±0.02	0.687 ±0.027	0.146 ±0.006
			R	4.17 ±0.06	0.986 ±0.015	0.620 ±0.002	0.837 ±0.025
115	Calcr	80	S	10.6 ±0.2	1.46 ±0.03	16.7 ±1.7	0.422 ±0.017
			R	9.44 ±0.14	1.51 ±0.02	22.4 ±0.9	1.19 ±0.04
106	Ttrav	70	S	9.53 ±0.14	1.26 ±0.19	4.53 ±0.14	0.660 ±0.026
			R	3.66 ±0.05	1.33 ±0.02	2.43 ±0.07	0.860 ±0.034
			Crater Flat				
199	TTrav	30	S	1.81 ±0.03	2.16 ±0.03	2.57 ±0.08	0.290 ±0.012
			R	1.58 ±0.02	1.17 ±0.02	2.81 ±0.08	1.47 ±0.06

Explanation:

a) TTrav - tufaceous travertine;

b) Calcr - calcrete;

c) S - acid soluble fraction; and

d) R - acid insoluble residuum.

Uranium concentrations and activity ratios. Samples of calcretes and surficial veins. Yucca Mountain. From Szabo et al., (1981).

Sample No.	Percent[1] Carbonate	Fraction	Uranium (ppm)	Activity Ratios $\frac{^{234}U}{^{238}U}$	$\frac{^{230}Th}{^{232}Th}$	$\frac{^{230}Th}{^{234}U}$
412-1	38	Acid leach	5.7 ±0.1	0.975±0.013	10.9±0.7	1.11±0.03
		Opal	15.3 ±0.3	1.029±0.013	21.9±0.3	1.01±0.03
412-3	1	Opal	15.7 ±0.3	1.232±0.017	279±20	1.10±0.03
412-7	12	Opal	16.8 ±0.3	1.133±0.014	130±6	1.11±0.03

Note:

Samples 412-1, 412-3, and 412-7 are from Trench #14.

Uranium concentrations and activity ratios. Samples of calcretes and surficial veins. Yucca Mountain. From Szabo and O'Malley, 1985.

Sample depth (m)	Fraction	Percent carbonate	Uranium (ppm)	Activity Ratios $\frac{^{234}U}{^{238}U}$	$\frac{^{230}Th}{^{232}Th}$	$\frac{^{230}Th}{^{234}U}$
280	Calcite	>99	0.500 ±0.010	1.032 ±0.015	12.0 ±2.4	1.023 ±0.041
302	Calcite	n.d.	n.d.	n.d.	n.d.	n.d.
346.7	Calcite	64	0.405 ±0.008	1.167 ±0.018	4.29 ±0.21	0.915 ±0.037
	Residue	0	6.85 ±0.14	1.135 ±0.017	2.43 ±0.10	0.965 ±0.049
346.8	Calcite	n.d.	n.d.	n.d.	n.d.	n.d.
348.7	Calcite	>99	0.073 ±0.006	1.02 ±0.03	4.6 ±0.5	0.73 ±0.06
348.8-A	Calcite	97	0.136 ±0.004	0.937 ±0.028	10.7 ±1.6	1.010 ±0.040
348.8-B	Calcite	63	33.3 ±0.7	1.026 ±0.015	94 ±15	0.093 ±0.037
	U Opal	0	57.8 ±1.2	1.031 ±0.015	232 ±34	1.027 ±0.031
359-A	Calcite	61	1.21 ±0.06	1.020 ±0.015	261 ±80	0.795 ±0.032
359-B	Calcite	75	0.644 ±0.013	0.965 ±0.014	36 ±11	0.811 ±0.032
	U Opal	0	27.0 ±0.5	1.068 ±0.016	234 ±70	1.04 ±0.04
361	Calcite	n.d.	n.d.	n.d.	n.d.	n.d.

n.d. not determined
n.a. not applicable

Uranium concentrations and activity ratios. Samples of calcitic veins from borehole USW G-2. Yucca Mountain. From Szabo and Kyser, 1985.

Sample depth (m)	Fraction	Percent carbonate	Uranium (ppm)	Activity Ratios $\frac{^{234}U}{^{238}U}$	$\frac{^{230}Th}{^{232}Th}$	$\frac{^{230}Th}{^{234}U}$
63	Calcite	95	0.558 ±0.011	2.26 ±0.03	35 ±4	1.00 ±0.03
	Residue	n.a.	0.66 ±0.04	1.37 ±0.10	7.6 ±1.5	1.94 ±0.19
131	Calcite	52	3.02 ±0.06	1.43 ±0.02	84 ±40	0.216 ±0.009
	U Opal	n.a.	35.0 ±0.7	1.13 ±0.02	473 ±190	1.15 ±0.05
147	Calcite	n.d.	n.d.	n.d.	n.d.	n.d.
159	Calcite	n.d.	n.d.	n.d.	n.d.	n.d.
318	Calcite	95	0.0836 ±0.0017	0.991 ±0.020	2.58 ±0.13	1.10 ±0.06
	Residue	n.a.	1.88 ±0.11	0.73 ±0.07	4.89 ±0.73	1.27 ±0.13
331	Calcite	87	0.36 ±0.01	1.06 ±0.04	10 ±5	0.24 ±0.02
	U Opal	n.a.	14.9 ±0.4	1.05 ±0.03	153 ±61	1.13 ±0.06

n.d. not determined
n.a. not applicable

Uranium concentrations and activity ratios. Samples of calcitic veins from borehole USW G-3. Yucca Mountain. From Szabo and Kyser, 1985.

Sample depth (m)	Material	Uranium (ppm)	Activity Ratios $\frac{^{234}U}{^{238}U}$	$\frac{^{230}Th}{^{232}Th}$	$\frac{^{230}Th}{^{234}U}$
34	Calcite	0.767 ±0.015	1.17 ±0.02	2.37 ±0.07	1.02 ±0.04
87	Fault gouge	5.18 ±0.10	1.09 ±0.02	0.989 ±0.030	1.06 ±0.04
283	Calcite	5.03 ±0.10	1.47 ±0.02	22.2 ±0.7	1.04 ±0.04
611	Calcite	3.43 ±0.07	1.29 ±0.02	72 ±3	1.19 ±0.05

Uranium concentrations and activity ratios. Samples of calcitic veins from borehole UE-25a#1. Yucca Mountain. From Szabo and Kyser, 1985.

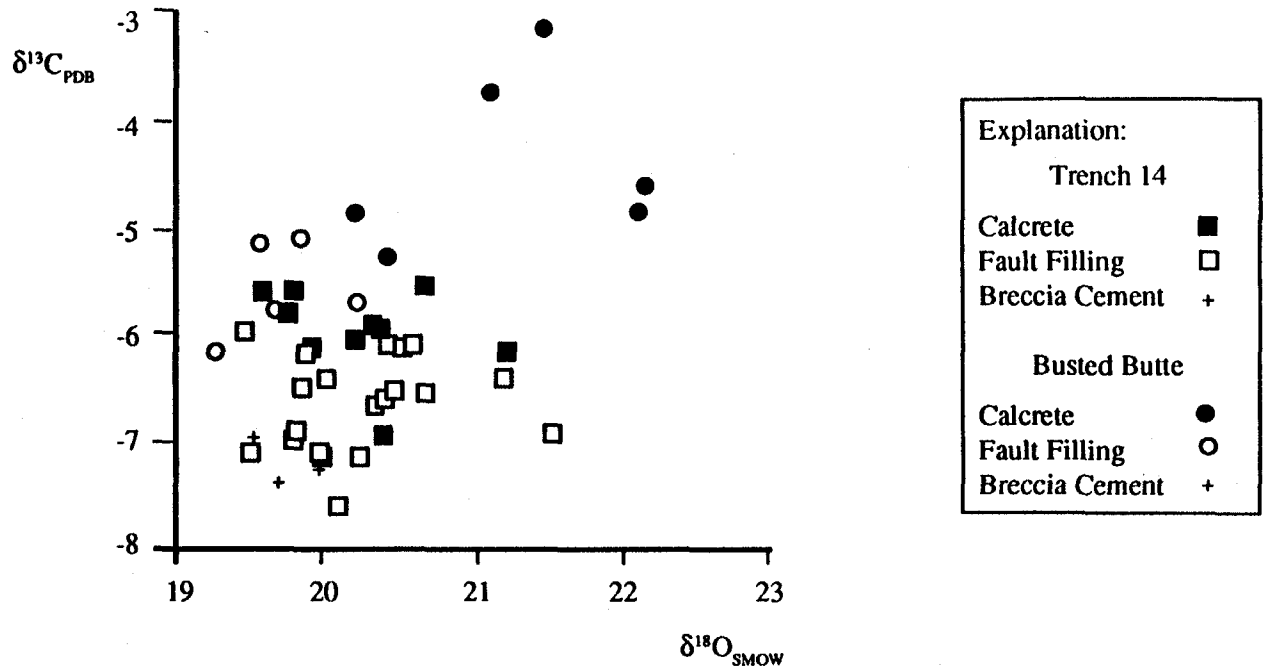

Note:

a) the observed range for the $\delta^{13}C$ ratio, from samples of the Yucca Mountain calcretes and surficial veins, is from -3.0 to -7.5 per mil_{PDB}, isotopic data are from Whelan and Stuckless, 1990;

b) for precipitation temperature T = 15°Celsius, the equilibrium fractionation factor $10^3 ln\alpha_{CaCO_3 - HCO_3^-} = 1.75$ per mil_{PDB}; and

c) the interpreted range for the $\delta^{13}C$ ratio, for the parent fluids of the Yucca Mountain calcretes and surficial veins, is from **-4.75 to -9.25** per mil_{PDB}.

The interpreted range of values for the $\delta^{13}C$ ratio - the parent fluids for the Yucca Mountain calcretes and surficial veins.

Figure 8-3

Sample #	Drill Hole	Depth (m)	Type[a]	$\delta^{13}C$[b]	$\delta^{18}O$[c]
HD-280	G-1	585	vein	-9.5	14.2
HD-281	G-1	595	vein	-2.3	11.0
	G-2[d]	280		-8.4	19.2
	G-2[d]	302		-7.9	19.3
	G-2[d]	347		-7.4	18.2
	G-2[d]	347		-7.4	18.3
	G-2[d]	349		-7.5	18.2
	G-2[d]	349		-6.9	18.1
	G-2[d]	359		-6.8	18.0
HD-272A	G-2	441	vug	-5.7	14.7
HD-272B	G-2	"	vug	-8.3, -8.3	15.6, 15.6
HD-272D	G-2	"	vein	-3.6	14.5
HD-273A	G-2	464	vug 1	-4.2	14.7
HD-273B	G-2	"	vug 2	-7.9	17.3
HD-273C	G-2	"	vug 3	-6.0	15.1
HD-273D	G-2	"	vug 4	-7.9	17.1
HD-273E	G-2	"	vein 1	-6.9	15.5
HD-273F	G-2	"	vein 2	-7.3	15.7
HD-274A	G-2	476	vug 1	-1.5	14.4
HD-274B	G-2	"	vug 2	-0.9	13.8
HD-274C	G-2	"	vug 3	-4.7	15.9
HD-274D	G-2	"	vug 4	-7.6	18.3
HD-274E	G-2	"	vug 5	-8.2	18.3
HD-275B	G-2	477	vug 2	-2.0	14.8
HD-275C	G-2	"	vug 3	-0.3	14.0
HD-261A	G-2	1280	vein	0.0	4.2
HD-261B	G-2	"	cement	-0.6	7.8
HD-262A	G-2	1459	vein	-1.5	7.8
HD-262B	G-2	"	cement	-1.0	8.1
HD-263A	G-2	1637	vein	1.0	9.4
HD-263B	G-2	"	cement	0.4	7.8
HD-264A	G-2	1640	vein 1	1.9	12.9
HD-264B	G-2	"	vein 2	0.7	6.2
HD-264C	G-2	"	cement	-0.4	8.9
HD-265A	G-2	1756	vein 1	-0.4	8.6
HD-265B	G-2	"	vein 2	-0.8	7.1
HD-265C	G-2	"	cement	-0.5	9.7
HD-266A	G-2	1794	cement	1.3	10.5
	G-3[d]	63		-7.1	20.2
	G-3[d]	131		-5.1	20.2
	G-3[d]	147		-5.6	20.0
	G-3[d]	159		-5.4	20.3
HD-276A	GU-3	295	vein?	-4.0	18.7

Explanation:

a) numbered sequences are from early to late.

b) $\delta^{13}C$ vs. PDB.

c) $\delta^{18}O$ vs. SMOW.

d) analyses reported by Szabo and Kyser[6].

e) unpublished data from B.A. Carlos.

The results of carbon and oxygen isotopic analyses, the Yucca Mountain calcitic phases. From Whelan and Stuckless (1991).

Sample #	Drill Hole	Depth (m)	Type[a]	$\delta^{13}C$[b]	$\delta^{18}O$[c]
HD-276B	GU-3	"	vein?	-5.2	19.2
HD-277A	GU-3	296	vein	-5.4	19.4
HD-267A	G-3	313	vein 1	-4.3	18.9
HD-267B	G-3	"	vein 2	-4.8	19.2
	G-3[d]	318		-5.1	19.1
	G-3[d]	331		-4.5	18.7
HD-278A	GU-3	347	vein 1	-5.7	18.9
HD-278B	GU-3	"	vein 2	-6.3	19.0
HD-278C	GU-3	"	veinlet 3	-6.5	19.1
HD-279A	GU-3	358	vein 1	-6.0	18.9
HD-279B	GU-3	"	vein 2	-5.7	19.4
HD-268A	G-3	1310	vein	2.2	10.9
HD-268B	G-3	"	vein	2.1	10.6
HD-268C	G-3	"	vein'	2.4	11.3
HD-268D	G-3	"	vein	2.3	9.5
HD-269A	G-3	1346	vein 1	0.5	9.7
HD-269B	G-3	"	vein 2	-2.0	11.7
HD-270A	G-3	1464	vein	1.7	7.5
HD-255A	b1	942	vein	3.8	5.3
HD-256A	b1	953	vein A	2.4	5.8
HD-256B	b1	"	vein B	1.8	5.8
HD-257A	b1	971	vein 1	4.2	11.7
HD-257B	b1	"	vein 2	4.4	11.4
HD-258A	b1	1098	vein	2.0	6.0
HD-259A	b1	1116	vein 1	1.6	5.7
HD-259B	b1	"	vein 2	0.6	4.4
HD-259C	b1	"	cement	2.1	6.8
HD-260A	b1	1216	vein 1	1.3	5.5
HD-260B	b1	"	vein 2	2.1	4.6
HD-260A	b1	"	cement	1.0	8.8
	G-4[e]	77		-6.8	17.0
HD-674A	G-4	108	vug 1	4.9	16.0
HD-674B	G-4	"	vug 2	0.6	16.5
HD-679A	G-4	265	vug 1	-7.1	16.8
HD-679B	G-4	"	vug 2	-1.2	14.7
	G-4[e]	"		-0.8	14.1
	G-4[e]	353		-3.6	17.1
HD-681A	G-4	401	vein	-9.1	16.0
	G-4[e]	"		-9.0	15.2
	G-4[e]	587		-6.7	17.4
	G-4[e]	663		-7.9	17.6
HD-687A	G-4	810	vein	-8.2	13.6
	G-4[e]	"		-8.0	13.1
HD-689A	G-4	842	vein	-5.7	13.3
	G-4[e]	"		-6.4	13.2

Explanation:

a) numbered sequences are from early to late.

b) $\delta^{13}C$ vs. PDB.

c) $\delta^{18}O$ vs. SMOW.

d) analyses reported by Szabo and Kyser[6].

e) unpublished data from B.A. Carlos.

The results of carbon and oxygen isotopic analyses, the Yucca Mountain calcitic phases. From Whelan and Stuckless (1991).

Sample No.	Uranium (ppm)	Thorium (ppm)	Activity Ratios $\frac{^{234}U}{^{238}U}$	$\frac{^{230}Th}{^{232}Th}$	$\frac{^{230}Th}{^{234}U}$	U-Series Age (k.a.)
			Total Dissolution			
1	0.564 ±0.011	0.75 ±0.04	1.07 ±0.02	2.05 ±0.06	0.868 ±0.035	209±25
2	0.668 ±0.013	0.86 ±0.04	1.08 ±0.02	2.00 ±0.06	0.793 ±0.032	165±16
3	0.609 ±0.012	0.88 ±0.04	1.09 ±0.02	1.84 ±0.06	0.819 ±0.033	177±18
4	0.693 ±0.014	1.05 ±0.05	1.11 ±0.02	1.82 ±0.06	0.859 ±0.034	198±22
			Carbonate Leach			
3	0.39 ±0.02	0.57 ±0.06	1.11 ±0.02	1.79 ±0.05	0.733 ±0.037	138±14
4	0.68 ±0.03	0.71 ±0.07	1.07 ±0.02	1.97 ±0.06	0.691 ±0.035	125±12
			Acid-Insoluble Residue			
3	0.74 ±0.04	0.95 ±0.10	1.03 ±0.02	1.90 ±0.05	0.769 ±0.038	n.a.
4	1.06 ±0.05	3.7 ±0.4	0.811 ±0.024	1.63 ±0.05	2.41 ±0.12	n.a.

n.a. not applicable

Uranium concentrations and activity ratios, the travertine veins from Furnace Creek Wash area. From Szabo and O'Malley, 1985.

Sample No.	Uranium (ppm)	Activity Ratios $\frac{^{234}U}{^{238}U}$	$\frac{^{230}Th}{^{232}Th}$	$\frac{^{230}Th}{^{234}U}$
	Caliche Nodules - Main Hectorite Whiting Pit			
79-3-7P[1]	1.51 ±0.03	1.196 ±0.012	213 ±64	0.921 ±0.027
80-10-20F[1]	0.431 ±0.015	1.206 ±0.009	55 ±11	0.952 ±0.038
	Travertine Vein[2]			
81-3-19F[3]	1.25 ±0.02	1.522 ±0.022	176 ±53	1.11 ±0.03
AM-9[4]	1.24 ±0.02	1.486 ±0.022	242 ±50	1.13 ±0.03

[1] Collected by R. L. Hay, 3.2 km south of IMV Plant, near center; east of edge SE 1/4 Sec. 6, T. 26N., R.5 E., (Calif. part of Ash Meadows 15 min. quad.).
[2] Vein location is SW 1/4, NW 1/4, sec. 23, T.17S, R5OE
[3] Collected by K. Kyser.
[4] Collected by T. J. Winograd.

Uranium concentrations and activity ratios, the Amargosa Basin calcareous deposits. From Szabo and O'Malley, 1985.

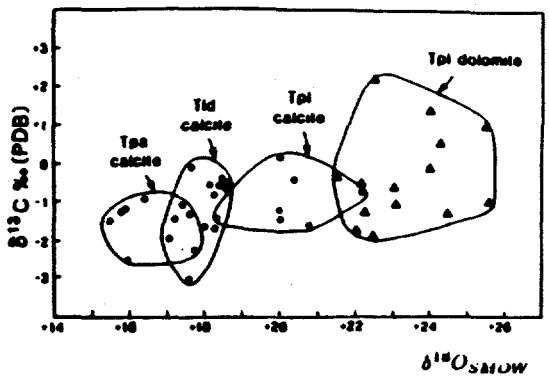

Note:

a) the overlapping $\delta^{13}C$ vs $\delta^{18}O$ fields indicate that, all four of the distinguished lithofacies were precipitated from common hypogene parent fluids;

b) the Tpa and Tld calcites represent proximal parts of the spring-fed depositional basin, while the Tpl calcites and dolomites represent the corresponding distal parts, as discussed by Hay et al. (1986);

c) the observed isotopic composition vs lithofacies gradients may reasonably be taken as recording alteration of i) mineral precipitation environment [mainly the mineral precipitation temperature]; and simultaneously ii) the isotopic composition of the former pristine deep-seated fluids;

d) the observed oxygen -18 content vs lithofacies gradient, from 15.5 to 26 per mil_{SMOW}, may reasonably be taken to indicate that, for distal lithofacies, both the mineral precipitation temperature and the degree of oxygen -18 evaporative enrichment were respectively lower and higher than those for the proximal lithofacies;

e) the observed carbon -13 content vs lithofacies gradient, from -3 to +2.5 per mil_{PDB}, may reasonably be taken to indicate that, for the distal lithofacies, the diffusional carbon -13 enrichment (resulting from CO_2 degassing) was higher than that for the proximal lithofacies;

f) it is totally unreasonable to propose that, the isotopically "heavier" fluids [ones involved in precipitation of the distal lithofacies] were supergene pedogenic fluids;

g) both the lithologic data and the isotopic data, as reported by Hay et al. (1986), provide direct and clear testimony that, after being discharged at the topographic surface, the pristine hypogene fluids undergo, as expected, the progressive alteration of their initial stable isotopic contents; and

h) for dispositional sites with a fairly constant altitude, it may reasonably be presumed that the isotopic composition vs lithofacies gradients are the characteristic and diagnostic feature for hypogene deposits.

Isotopic character of oxygen and carbon contained in the Amargosa Basin calcareous deposits. From Hay et al. (1986).

Figure 8-6a

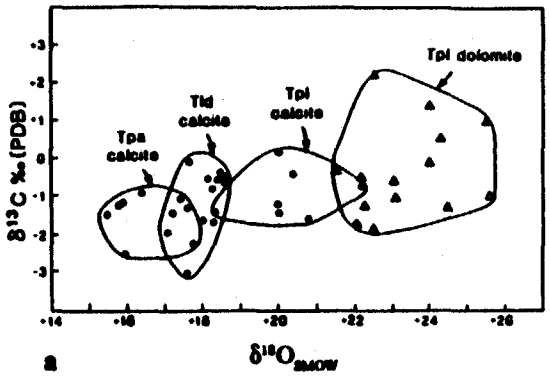

a) Composition of carbonate minerals in bedded claystones and carbonate rocks. Dolomite is represented by triangles and calcite by circles, which are closed for limestones of Tld. Tpa samples are of chalky limestones, most of which are soft; Tld samples are mostly of dense nodular and fenestral limestone; and Tpl samples include both carbonate rocks and carbonate minerals disseminated in claystones.

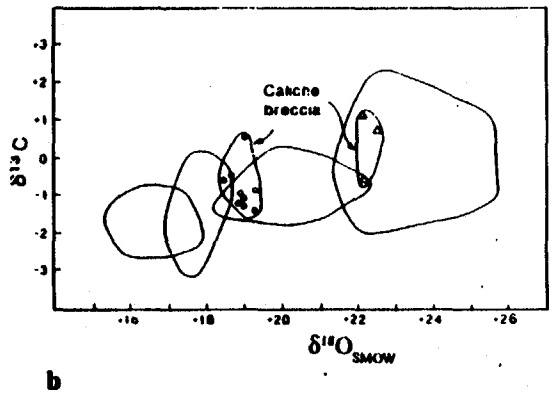

b) Composition of calcite and dolomite in caliche breccia. Solid circles represent caliche breccia from East Playa, and open circles represent samples from the westernmost caliche breccia. Dolomite is from caliche breccia of East Playa.

Explanation of the lithologic notations as employed by Hay et al. (1986). From Hay et al. (1986).

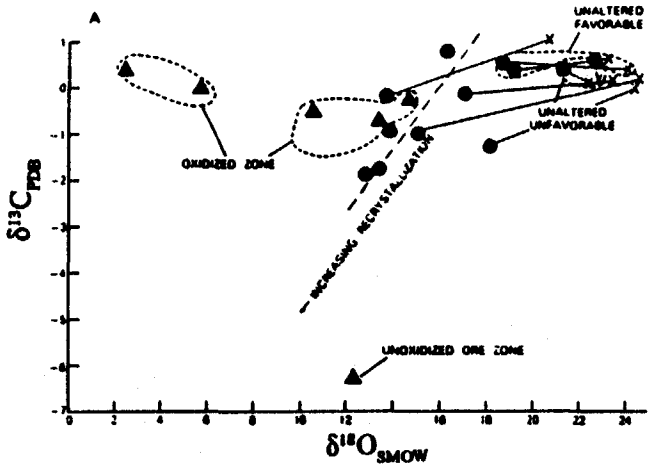

a) the Carlin disseminated gold deposit of Nevada.

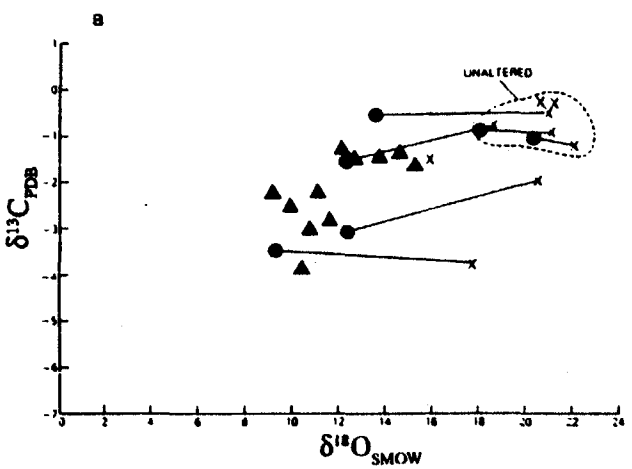

b) the Cortez disseminated gold deposit of Nevada.

Explanation:

- ▲ - sample represents altered host rock and calcite veins in oxidized and unoxidized zones;
- ● - sample represents calcite veins;
- x - sample represents dolomite; and

tielines connect coexisting calcite and dolomite

Note:

a) calcitic veins from the oxidized zone at Carlin, and all the veins at Cortez, have oxygen - isotopic compositions similar to that of the calcite component in the altered host rock; and

b) other veins were derived from low-temperature groundwater.

Isotopic characters of carbon and oxygen contained in carbonate gangue veins from the Carlin and Cortez gold deposits. From Rye, 1985

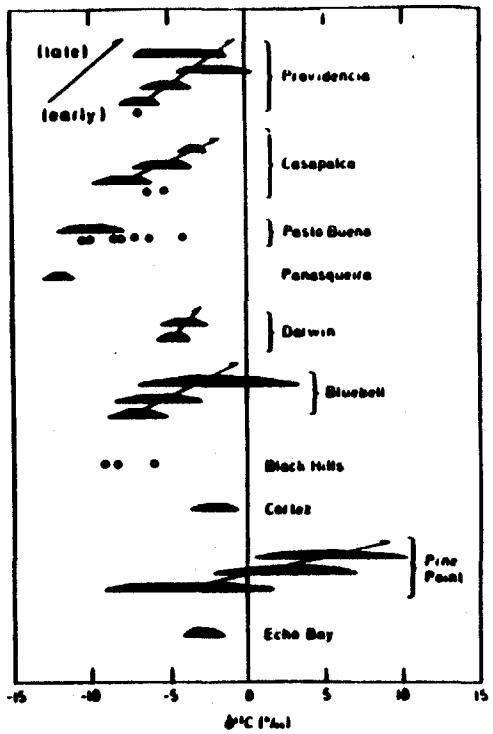

Explanation:

- carbonate gangue minerals; and
- fluid inclusion

Note:

a) relict fluids entrapped in fluid inclusions from samples of the carbonate gangue minerals, associated with various hydrothermal ore deposits, yield values of the $\delta^{13}C$ ratio ranging from -4 to about -10 per mil_{PDB};

b) for individual ore deposits, the different generations of the carbonate gangue minerals are arranged from early to late, as shown by arrows;

c) the observed trend toward the isotopically "heavier" carbon (with decreasing age of the carbonate gangue minerals) may be taken to indicate that, as the volcanic activity and the resulting geothermal circulations decay, the contribution of CO_2 from deep-seated igneous sources also decays; and

d) observations that hydrothermal ore forming fluids carry values of the $\delta^{13}C$ ratio ranging from -2 to about -10 per mil_{PDB} may be taken to indicate the deep-seated (igneous) origin of the dissolved carbon, Hoefs (1987).

The isotopic character of carbon contained in samples of the carbonate gangue minerals associated with various hydrothermal ore deposits. From Hoefs, (1987).

		Rock (‰)		Water (‰)		Temperature		
		$\delta^{13}C$	$\delta^{18}O$	$\delta^{13}C$	$\delta^{18}O$	measured	^{13}C	^{18}O
Spring travertine								
Reds Meadow Spring		+1.7	+15.8	−3.6	−14.7	48	76	15
Hot Creek		+1.5	−7.2	−1.5	−15.8	92	113	54
Dome Spring A		+2.6	+15.9	−5.7	−15.7	58	42	11
Dome Spring B		+1.8	+15.9	−5.7	−15.7	58	50	11
Mammoth Rock Spring		−0.3	+14.2	−9.7	−14.9	18	31	25
Layton Spring A		+3.5	—	−9.3	−13.7	33	6	—
Layton Spring B		+1.9	—	−9.3	−13.7	33	17	—
Layton Spring C		+1.3	—	−9.3	−13.7	33	22	—
Little Hot Creek		−0.7	—	−3.4	−15.2	83	119	—
Big Alkali Lake Spring		−0.3	+13.2	−6.0	−15.8	50	70	22
Colton Spring		+0.1	+14.4	−3.0	−14.2	93	112	24
Little Alkali Lake Spring		—	+16.7	−4.9	−15.9	48	—	7
Vein calcite in the hydrothermal reservoir								
RDO-8	317 m	−5.3	−5.4	−4.9	−14.3	164	205	211
	405 m	−7.0	−7.1	−4.9	−14.3	175	307	251
	503 m	−4.1	−3.3	−4.9	−14.3	173	167	173
	521 m	−3.2	−2.0	−4.9	−14.3	171	146	154
	541 m	−6.1	−8.4	−4.9	−14.3	198	244	288
	547 m	−5.8	−7.6	−4.9	−14.3	200	229	264
	568 m	−6.5	−8.5	−4.9	−14.3	196	268	292
	611 m	−4.6	−3.9	−4.9	−14.3	198	182	183
	613 m	−5.7	−7.4	−4.9	−14.3	189	222	259
44–16	2500 m	−3.0	−1.9	−4.8	−14.9	205	230	125

Isotopic character of carbon contained in the Long Valley travertines and hydrothermal calcitic veins. From White et al. (1990).

- The results of plant surveys indicate that, for the Yucca Mountain area (mean altitude ~ 1200m), representative proportion of plants having the C-3 metabolic pathway is ~ 85 percent, Quade et al. (1989).
- A mean value for the $\delta^{13}C$ ratio for CO_2 produced by plants having the C-3 metabolic pathway is -26 per mil_{PDB}.
- A mean value for the $\delta^{13}C$ ratio for CO_2 produced by plants having the C-4 metabolic pathway is -12 per mil_{PDB}.
- A mean value for the $\delta^{13}C$ ratio for CO_2 produced by the local plants is -24 per mil_{PDB}.
- Dissolution of the locally produced biogenic CO_2 will yield fluids with values of the $\delta^{13}C$ ratio of about -15 per mil_{PDB} (for 15° C, the fractionation factor is ~ 9 per mil_{PDB}.)

Isotopic character of carbon dissolved in supergene pedogenic fluids, interpreted based on the observed proportion of C-3 plants and assuming that these fluids acquire CO_2 solely from the biosphere.

- A mean value of the $\delta^{13}C$ ratio for the CO_2 gas respired from the vadose zone, as observed at Yucca Mountain and Amargosa Narrows, is **$\delta^{13}C$ = -18.36 and -20.0 per mil$_{PDB}$**, respectively, Yang et al., 1986, Thorstenson et al., 1989, and White and Chuma, 1987 - the Yucca Mountain value is based on samples that carry PMC > 100 percent and were collected at a depth ranging from 0 to 12.8m.

- A mean value of the $\delta^{13}C$ ratio for soil gas, as observed at various locations throughout the Nevada Test Site, is **$\delta^{13}C$ = -20.5 per mil$_{PDB}$**, Boughton, 1986.

- The equilibrium isotopic fractionation factor $10^3 \ln\alpha_{HCO_3^- - CO_2(g)} = 9.483 \bullet 10^3 \bullet T^{-1} - 23.89$, Turi (1986) - for 15°Celsius, the fractionation factor is ~ 9 per mil$_{PDB}$.

- Dissolution of the CO_2 gas respired from the vadose zone, with the observed range from -18.36 to -20.5 per mil$_{PDB}$, may be expected to yield supergene pedogenic fluids with the $\delta^{13}C$ ratios ranging from **-9.36 to -11.5 per mil$_{PDB}$**.

Isotopic character of carbon dissolved in supergene pedogenic fluids, interpreted based on the observed $\delta^{13}C$ ratios from samples of the Nevada Test Site vadose zone gases.

- A mean value for the $\delta^{13}C$ ratio from samples of shallow alluvium - based fluids, as observed around Amargosa Narrows, is $\delta^{13}C$ = **-11.3 per mil$_{PDB}$** (range of the observed values is **from -9.59 to -13.05 per mil$_{PDB}$**), White and Chuma (1987).

- A value of the $\delta^{13}C$ ratio from samples of shallow tuff "pile" - based fluids, as observed in the Yucca Mountain borehole UE-29 a#2 (depth to the water table is 29m, and PMC ranges from 60 to 62.3 percent), is $\delta^{13}C$ = **-13.0 per mil$_{PDB}$**, Benson and McKinley, 1985.

- A value of the $\delta^{13}C$ ratio for the Nevada Test Site soil water, as interpreted based on laboratory soil-leaching experiments, is $\delta^{13}C$ = **-12.0 per mil$_{PDB}$** (the observed range for leached water is from **-9.6 to - 16.4 per mil$_{PDB}$**), Spencer (1990).

- A value of the $\delta^{13}C$ ratio for the vadose zone interstitial fluids, as observed at Yucca Mountain, ranges from **-20.05 to - 26.70 per mil$_{PDB}$**, Yang (1989) and Figure 5-2b.

Isotopic character of carbon dissolved in supergene pedogenic fluids,based on direct measurements and on soil-leaching experiments.

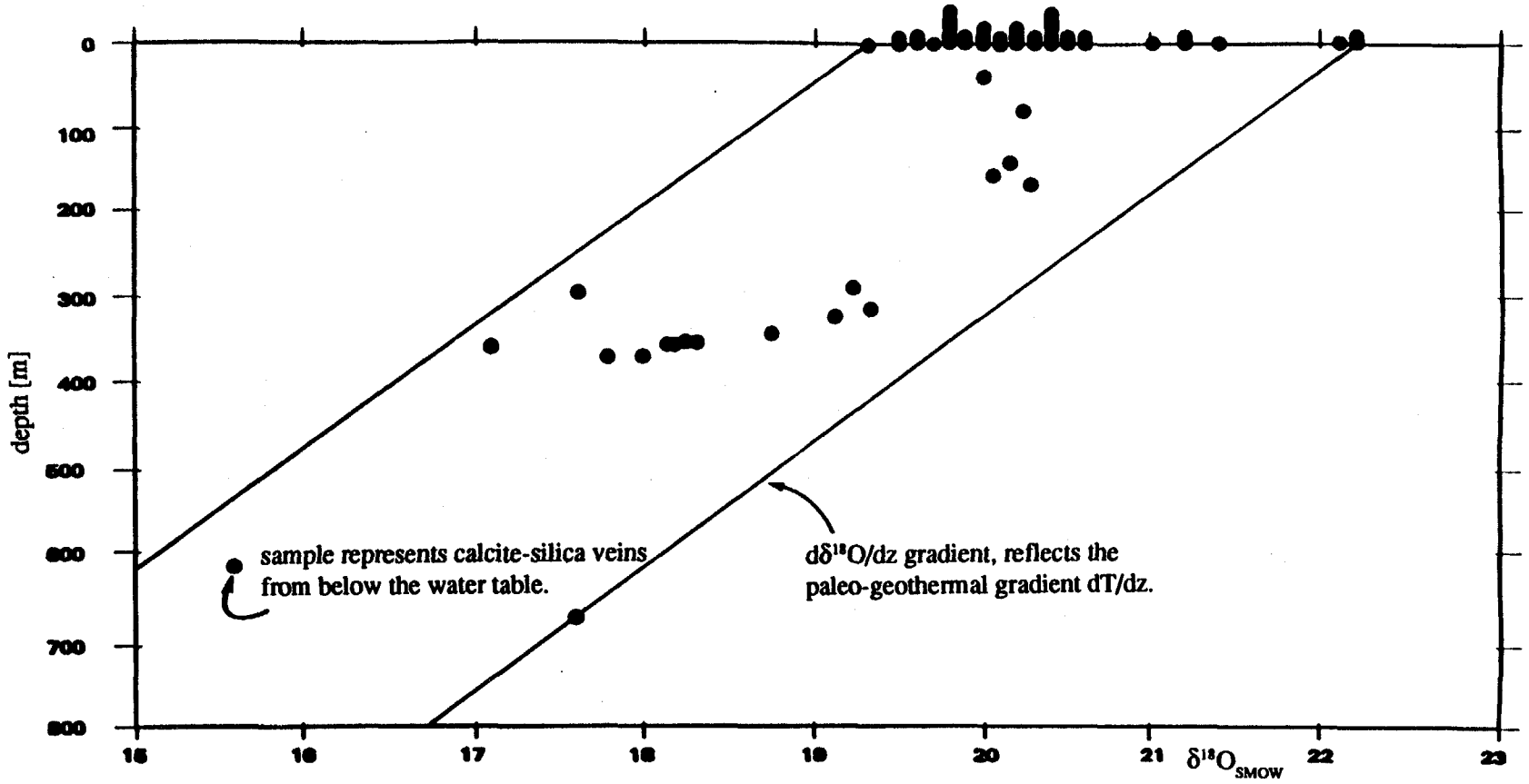

Note:

a) the oxygen -18 data, as shown in this figure, represent the Yucca Mountain calcites that are the most enriched in oxygen -18; and

b) presumably, for these calcites, the precipitation temperatures were at a minimum.

Isotopic character of oxygen contained in the Yucca Mountain calcite-silica subsurface veins. Data from Szabo and Kyser (1990) and Whelan and Stuckless (1990).

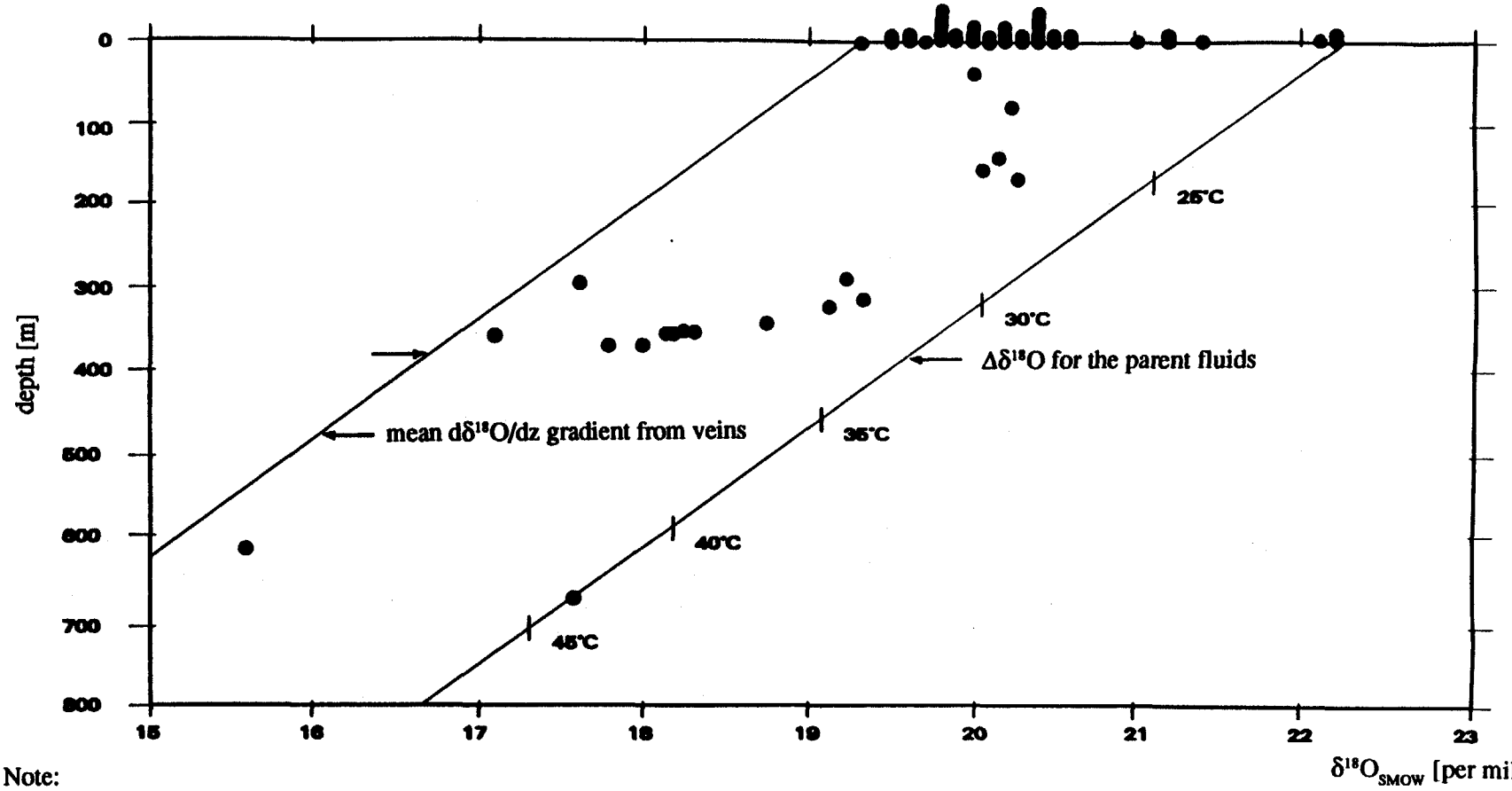

Note:

a) in performing this reconstruction, it has been assumed that: i) at the topographic surface, the precipitation temperature for calcretes and veins was T ~20° Celsius; ii) the constant depth variability of the oxygen -18 content, from samples of the calcite-silica deposits, reflects the spatio-temporal variability of the oxygen -18 content in the parent fluids, $\Delta\delta^{18}O$ ~3 per mil; and iii) the non-equilibrium isotopic fractionation effects are absent and, therefore, $10^3 \ln\alpha_{CaCO^3 - H_2O} = 2.78 \cdot 10^6/T^2 - 2.82$ - where T is precipitation temperature in ° Kelvin; and

b) value of the paleo-geothermal gradient is dT/dz ~35° Celsius per 1km increase in depth - the corresponding contemporary geothermal gradient ranges from 20 to 24° Celsius per 1km increase in depth.

Reconstruction A - the Yucca Mountain paleo-geothermal gradients, based on the oxygen -18 content of samples of the local calcite-silica deposits.

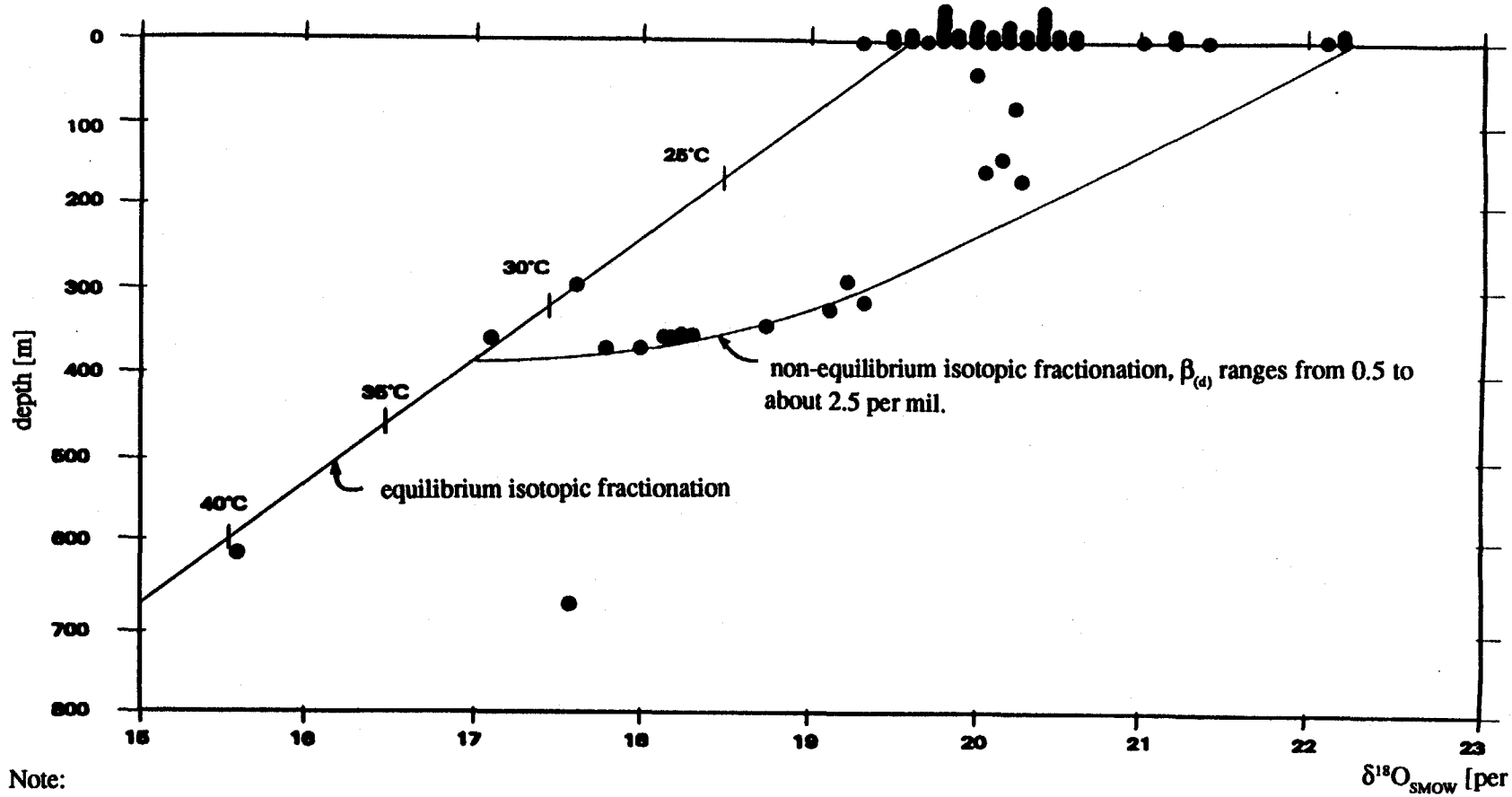

Note:

a) in performing this reconstruction, it has been assumed that: i) at the topographic surface, the precipitation temperature for calcretes and veins was T ~20° Celsius; ii) the oxygen -18 content of the parent fluids, for spatio-temporal different samples, was the same; iii) the constant depth variability of the oxygen -18 content, from samples of the calcite-silica deposits, is attributable to the non-equilibrium isotopic fractionation effects, such that combined $10^3 \ln\alpha_{CaCO^3 - H_2O} = 2.78 \cdot 10^6/T^2 - 2.82 + \beta_{(d)}$; and iv) the non-equilibrium fractionation is caused by a rapid, and depth variant escape of CO_2 from the parent solution - the CO_2 degassing rate decreases depthward, and $CaCO_3$ acquires its oxygen from both H_2O and CO_2; and

b) value of the paleo-geothermal gradient is dT/dz ~33° Celsius per 1km increase in depth - the corresponding contemporary geothermal gradient ranges from 20 to 24° Celsius per 1km increase in depth.

Reconstruction B - the Yucca Mountain paleo-geothermal gradients, based on the oxygen -18 content of samples of the local calcite-silica deposits.

Figure 8-11c

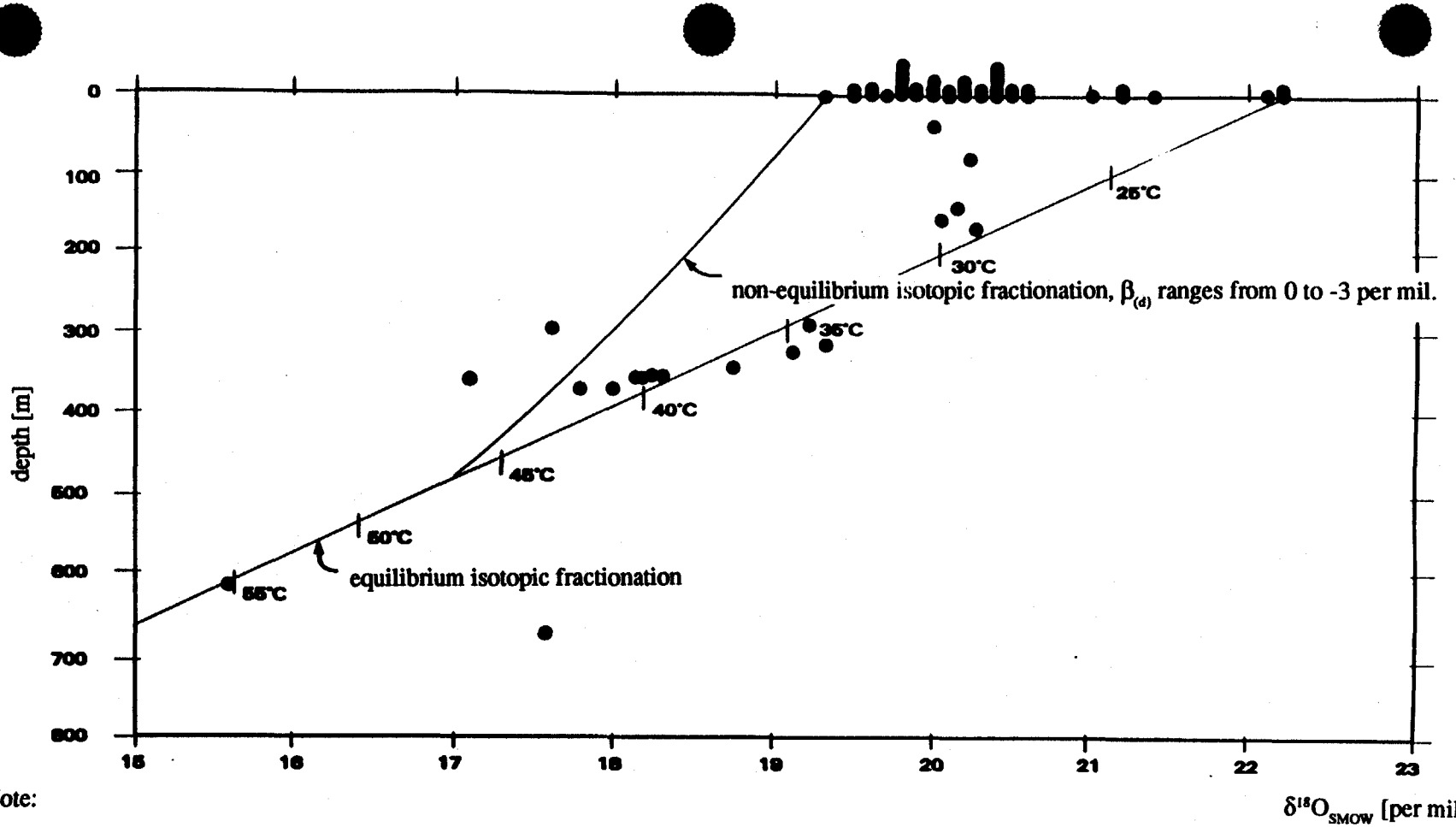

Note:

a) in performing this reconstruction, it has been assumed that: i) at the topographic surface, the precipitation temperature for calcretes and veins was T ~20° Celsius; ii) the oxygen -18 content of the parent fluids, for spatio-temporally different samples, was the same; iii) the constant depth variability of the oxygen -18 content, from samples of the calcite-silica deposits, is attributable to the non-equilibrium isotopic fractionation effects, such that combined $10^3 \ln\alpha_{CaCO^3 - H_2O} = 2.78 \cdot 10^6/T^2 - 2.82 - \beta_{(d)}$; and iv) the non-equilibrium fractionation is caused by a rapid upward movement of the parent fluids - the $CaCO_3$ nucleation occurs prior to its deposition and, consequently, the deposited $CaCO_3$ records, temperatures that are higher than those prevailing at the actual deposition sites; and

b) value of the paleo-geothermal gradient is dT/dz ~58° Celsius per 1km increase in depth - the corresponding contemporary geothermal gradient ranges from 20 to 24° Celsius per 1km increase in depth.

Reconstruction C - the Yucca Mountain paleo-geothermal gradients, based on the oxygen -18 content of samples of the local calcite-silica deposits.

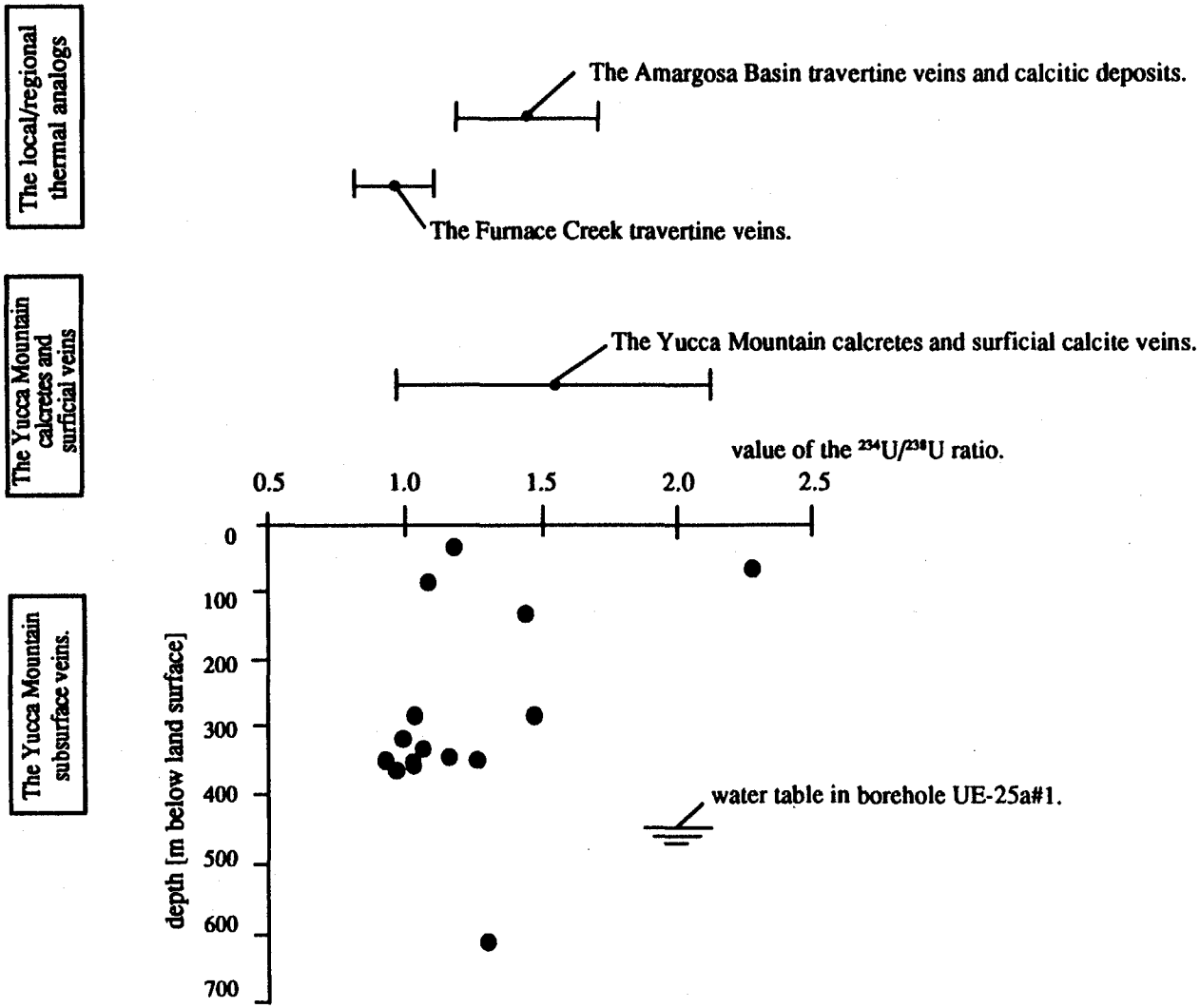

The uranium comparative analyses, isotopic character of uranium contained in: a) the Yucca Mountain subsurface calcite veins; b) the Yucca Mountain calcretes and surficial calcitic veins; and c) the local travertine veins and associated surficial deposits.

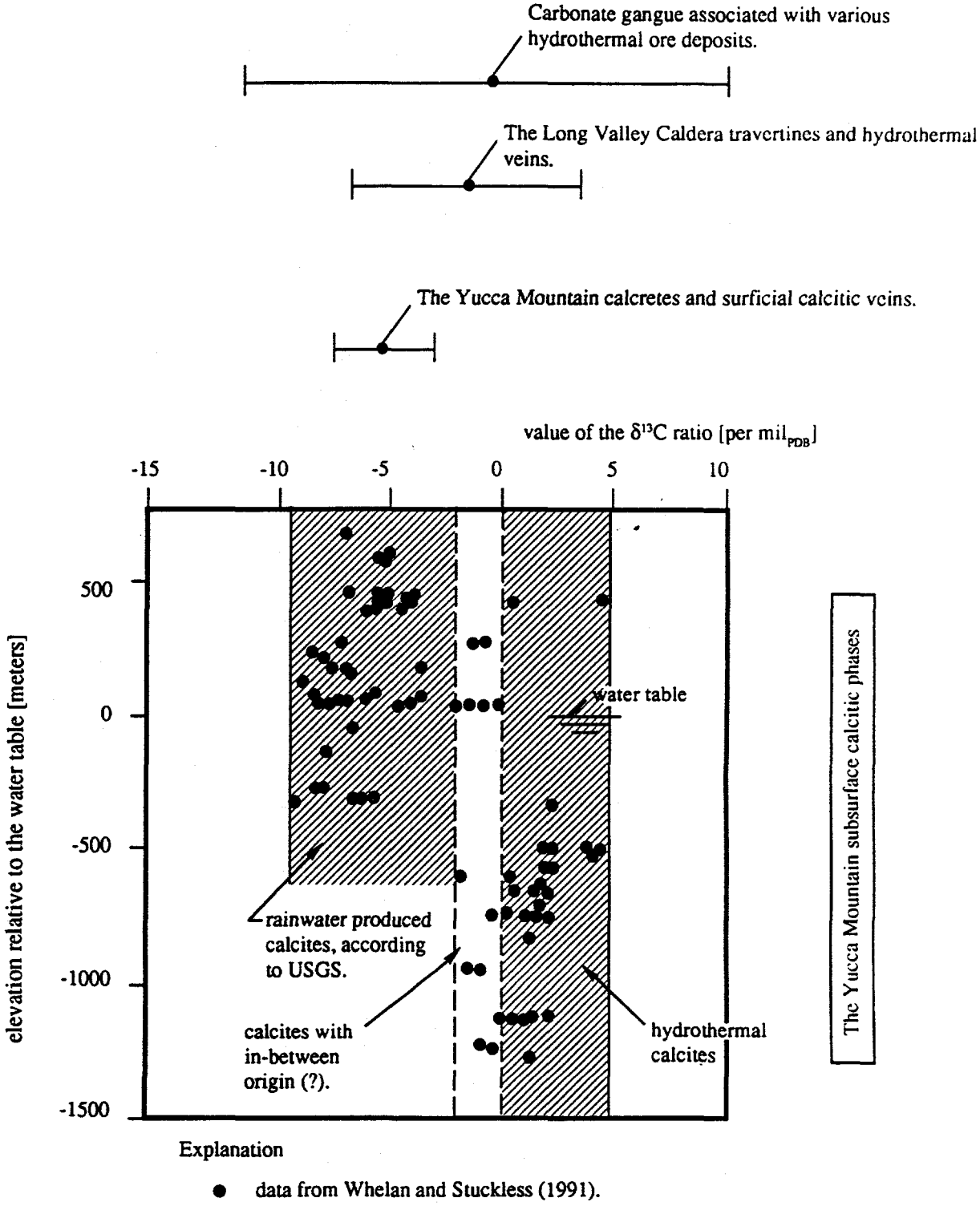

The isotopic comparative analyses, isotopic character of carbon incorporated in the Yucca Mountain calcitic phases.

Figure 8-13

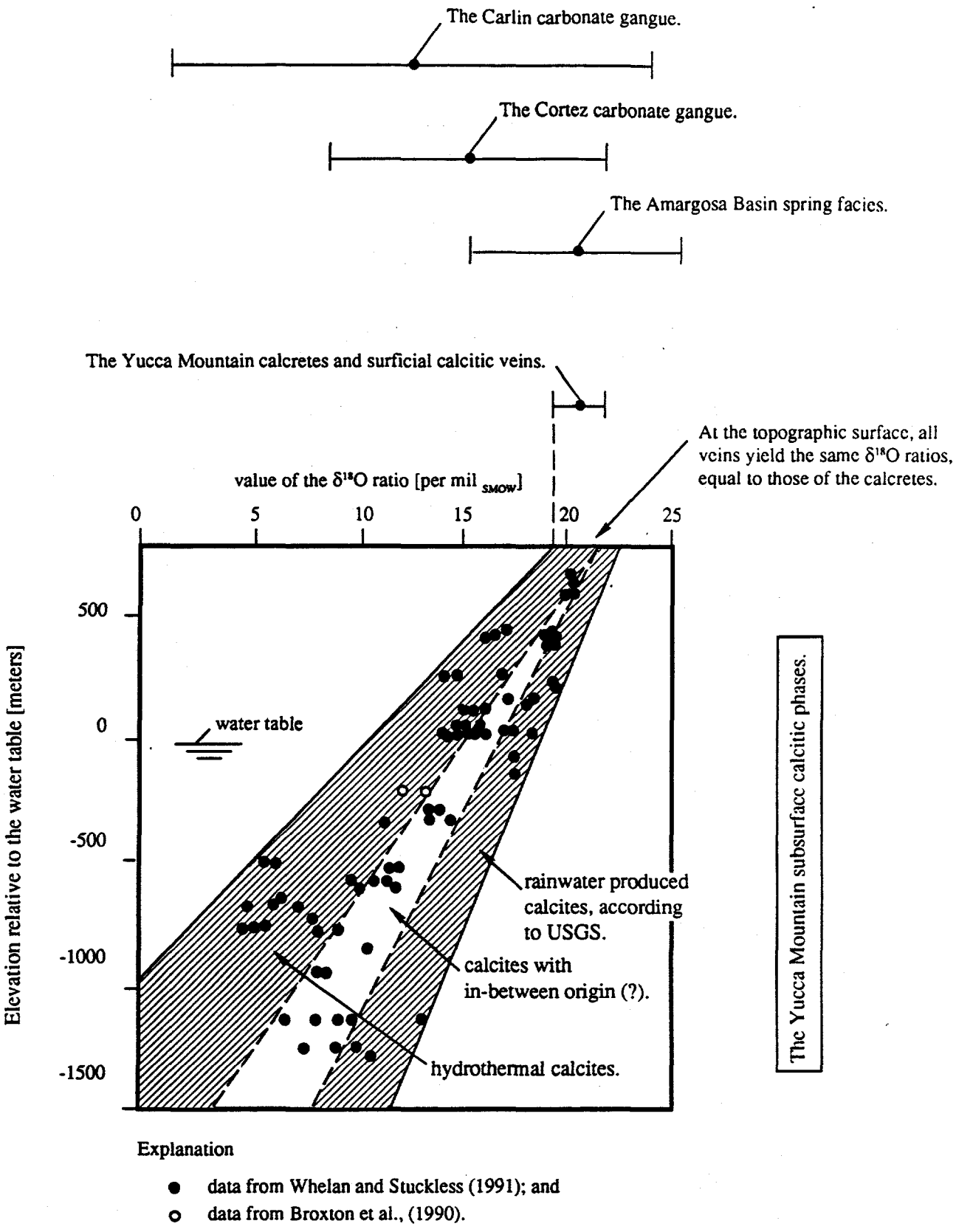

The isotopic comparative analyses, isotopic character of oxygen incorporated in the Yucca Mountain calcitic phases.

Figure 8-14

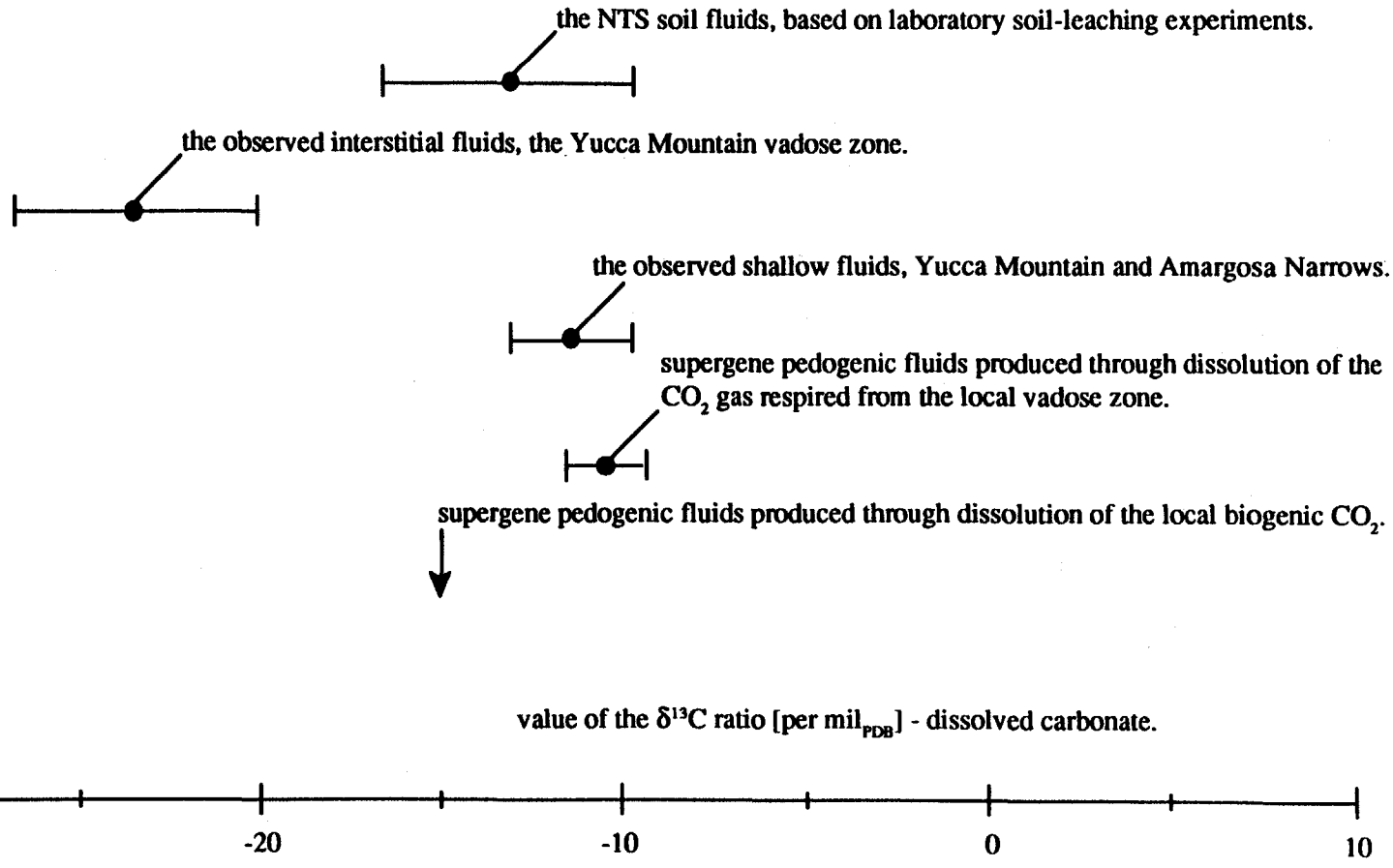

Note:

a) for the Yucca Mountain supergene fluids, the inferred isotopic character of the dissolved carbon is based on data shown in Figures 8-10a through 8-10c;

b) for the parent fluids of the subsurface veins, it has been conservatively assumed that the fractionation factor is 2 - 3 per mil_{PDB}.

A comparison of the isotopic characters of carbon dissolved in the parent fluids for the calcretes and veins with those inferred to be dissolved in the Yucca Mountain supergene fluids.

Figure 8-15

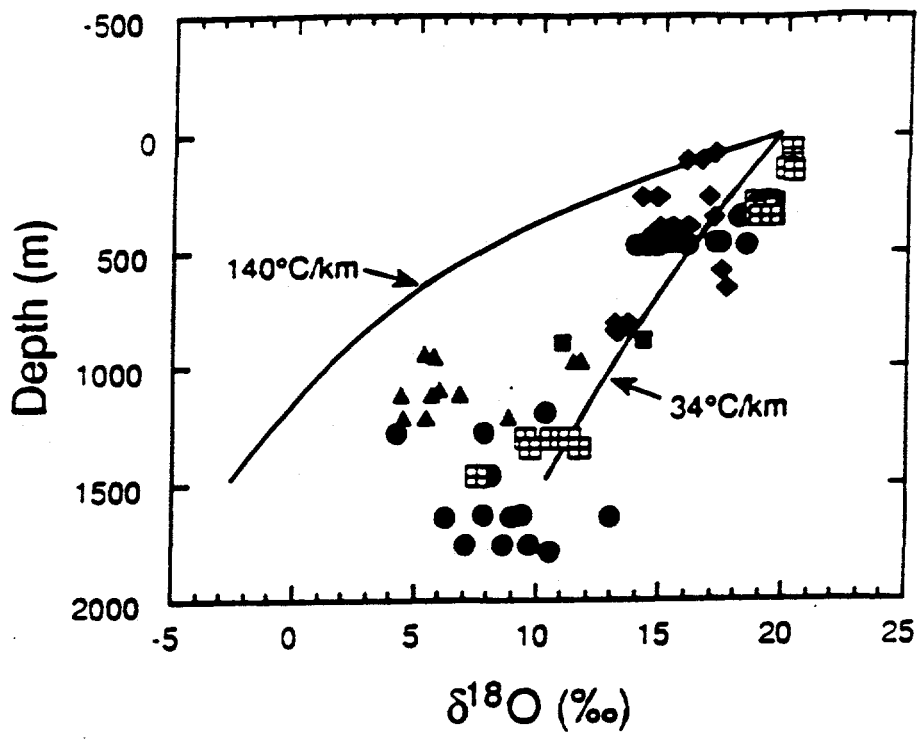

Note:

a) the paleo-geothermal reconstructions shown are based on the depth-distribution of values of the $\delta^{18}O$ ratio, as observed in boreholes USW G-1, G-2, G-3, GU-3, G-4, and UE-25b #1;

b) the actually measured values of the contemporary geothermal gradient range from 18 to no more than 24° C/km (USW G-1 - 18° C/km; G-2 - 24° C/km; G-3 - 22° C/km; G-4 - 24° C/km; and UE-25 b#1 - 20° C/km, Sass et al., 1987);

c) a factor of ≥ 1.5 discrepancy, between the observed and the reconstructed values of the geothermal gradient, indicates that the Yucca Mountain veins were formed exclusively in association with hypogene geothermal processes; and

d) similarly as with values of the $\delta^{13}C$ ratio, the observed values of the $\delta^{18}O$ ratio are strongly distinct from those that may reasonably be attributed to supergene processes.

The results of paleo-geothermal reconstructions, the Yucca Mountain calcitic veins.
From Whelan and Stuckless (1992).

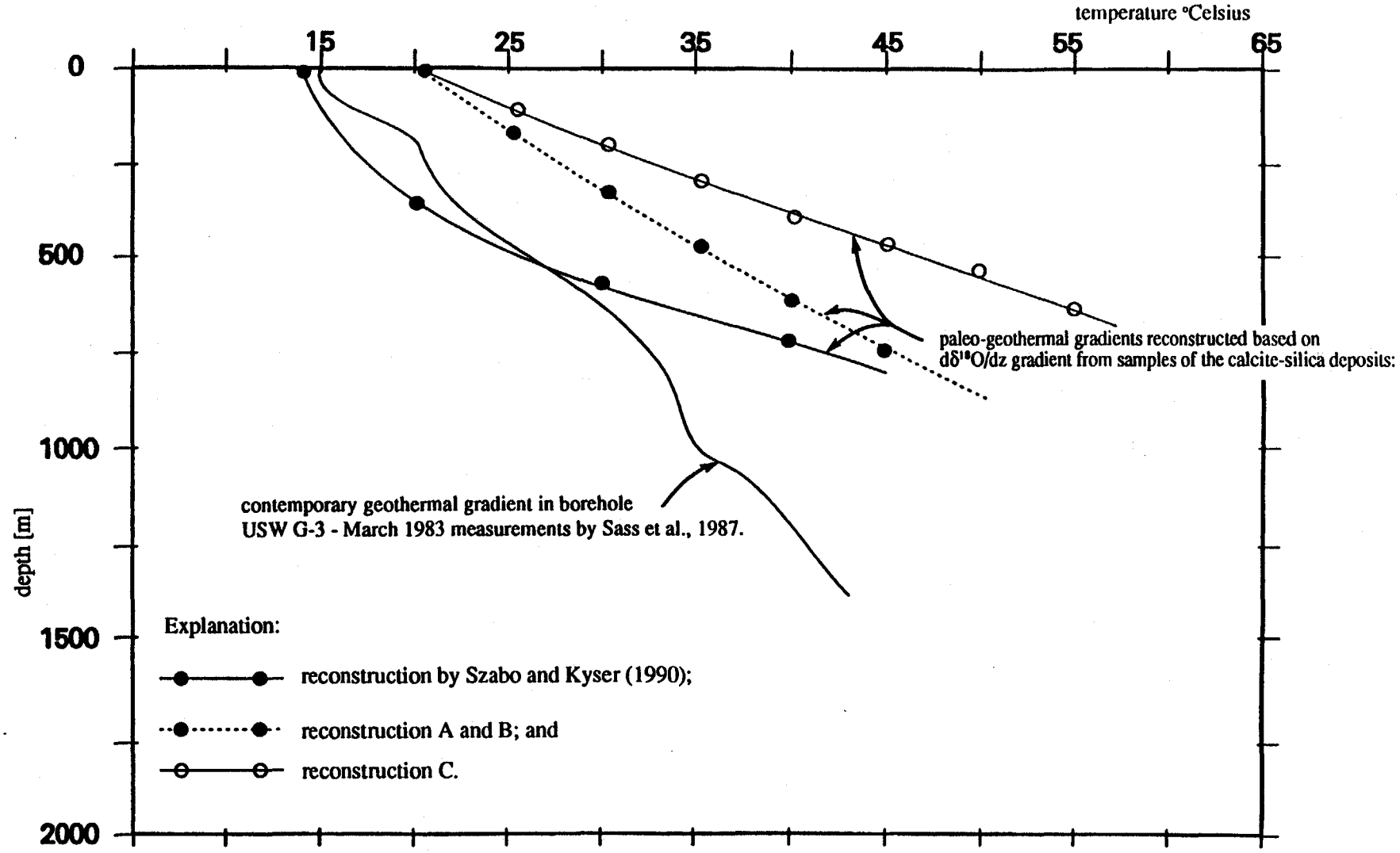

Comparison between the contemporary geothermal gradient and the paleo-geothermal gradients, as reconstructed based on the $d\delta^{18}O/dz$ gradient from samples of the calcite-silica deposits and using various assumptions.

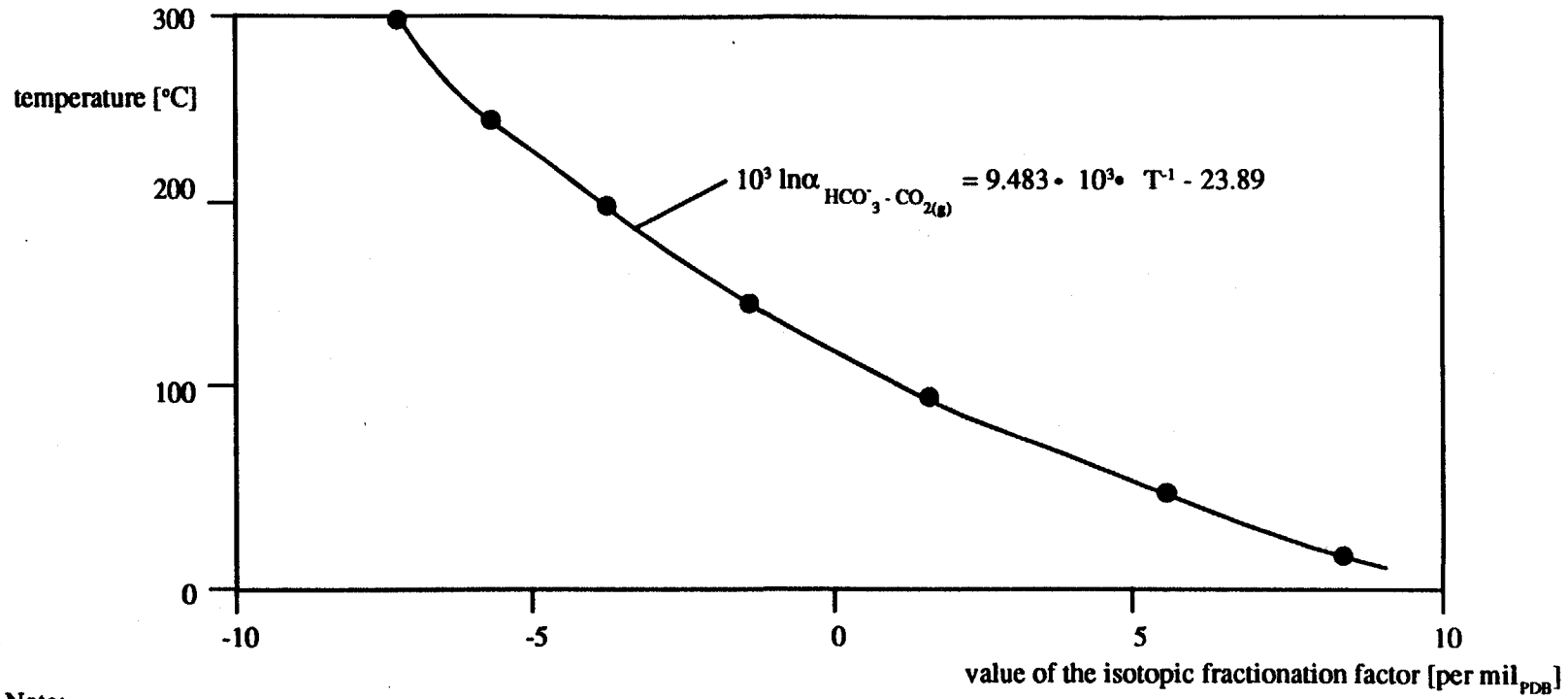

Note:

a) the fractionation equation is from Turi (1986);

b) mean value of the $\delta^{13}C$ ratio, for deep-seated igneous CO_2, may be taken as ~-6 per mil $_{PDB}$, Hoefs (1987);

c) depending upon reaction temperature, dissolution of deep-seated igneous CO_2 may be expected to produce fluids with values of the $\delta^{13}C$ ratio ranging from + 1.45 (T = 20°Celsius) to -10 per mil $_{PDB}$ (T = 200°Celsius); and

d) the expected range of the $\delta^{13}C$ ratio, for fluids produced through dissolution of deep-seated igneous CO_2, is similar to that observed for the Nevada Test Site geothermal fluids.

The HCO^-_3 - $CO_{2(gas)}$ isotopic fractionation factor as a function of temperature.

Figure 8-18

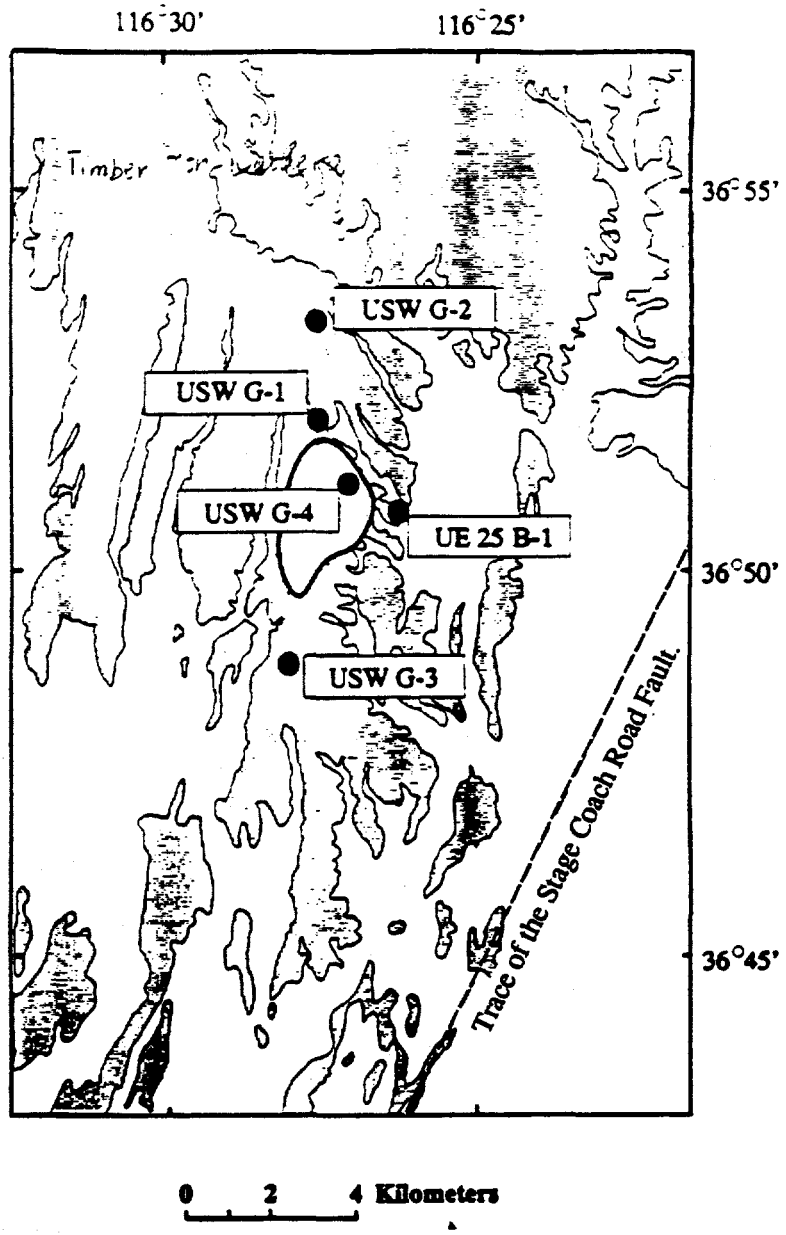

Note:

a) data from boreholes USW G-4 and UE-25 b#1 represent the south-eastern alteration center, Figures 7-14a, 7-20, and 7-27; and

b) data from boreholes USW G-1, G-2, and G-3 represent overprinting of the earlier north-western alteration center by the subsequent south-eastern alteration center, Figures 7-14b, 7-20, 7-29, and 7-30.

Location map for boreholes considered in developing the interpretation of paragenetic relationships for the Yucca Mountain calcitic phases.

Depth [m]	Homogenization temp. of fluid inclusions [°C]	Source
Borehole USW G-2		
1640	from 94 to 115	Bish, 1989
1756	147	do
1773	from 202 to 239	do
Borehole USW G-3		
1463	97	do
Borehole USW GU-3		
32	from 101 to 227	do
130	from 125 to 170	do

Note:

a) "Other authigenic minerals in the Topopah Spring unit of USW GU-3 include silica, calcite, and fluorite. Calcite and fluorite are very rare, although sparry clacite is concentrated in veins and as a cement in fault breccia at and above 525 ft depth, and it occurs with fluorite in a fracture at 1027 ft. depth. Sparry calcite in fault breccia at 482 ft. depth is coated by a later growth of fine-grained auhedral calcite, which suggests temporary saturation within the breccia during the sparry-growth cementation, followed by vadose calcite growth" Vaniman et al., 1984.

b) see Figure 8-21, for geologic association of the fluid inclusion samples, from borehole USW GU-3.

Homogenization temperatures of fluid inclusions in calcite. Yucca Mountain.

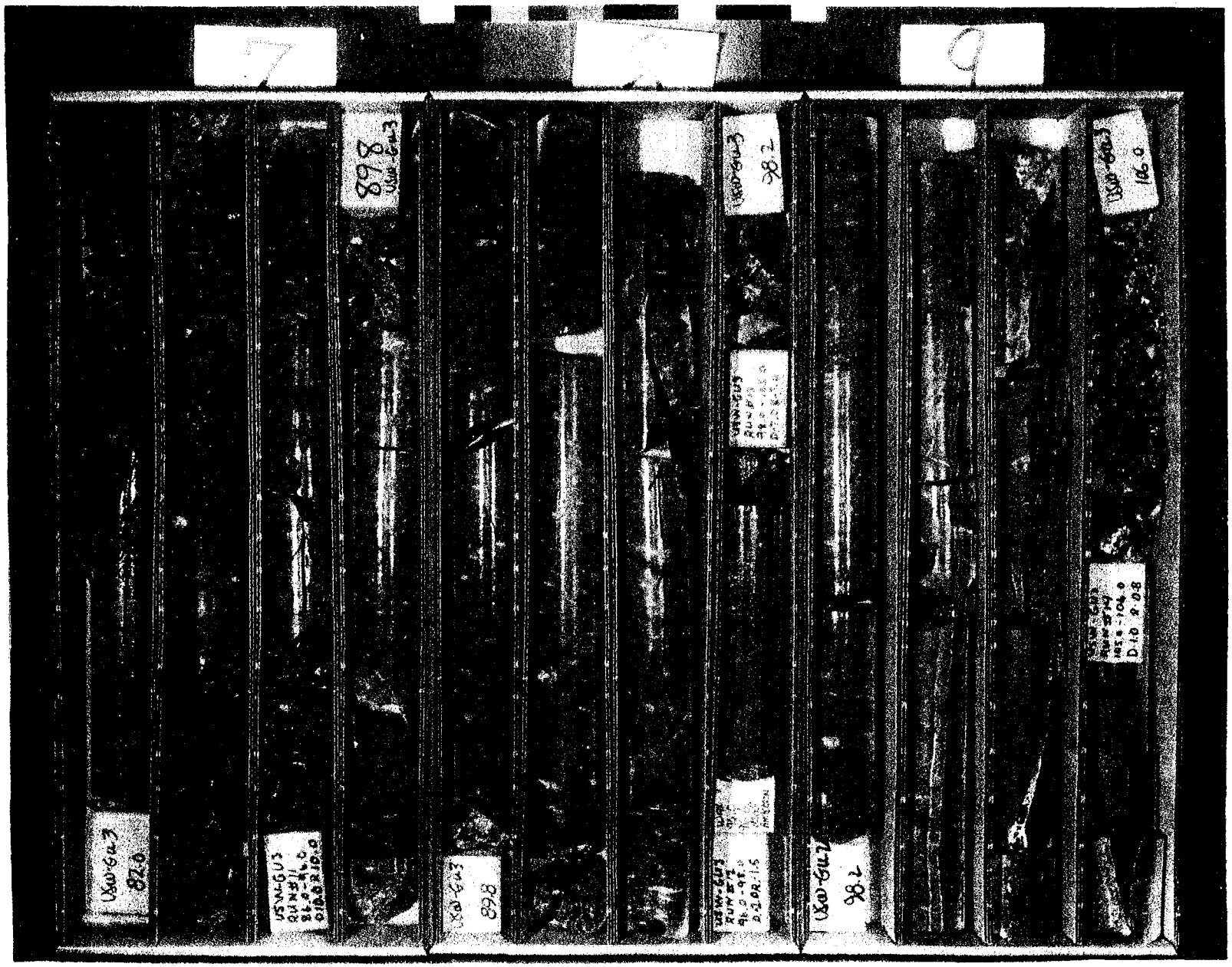

Geologic association of the fluid inclusion sample USW GU3 - 103 ft (32m).

Figure 8-21a

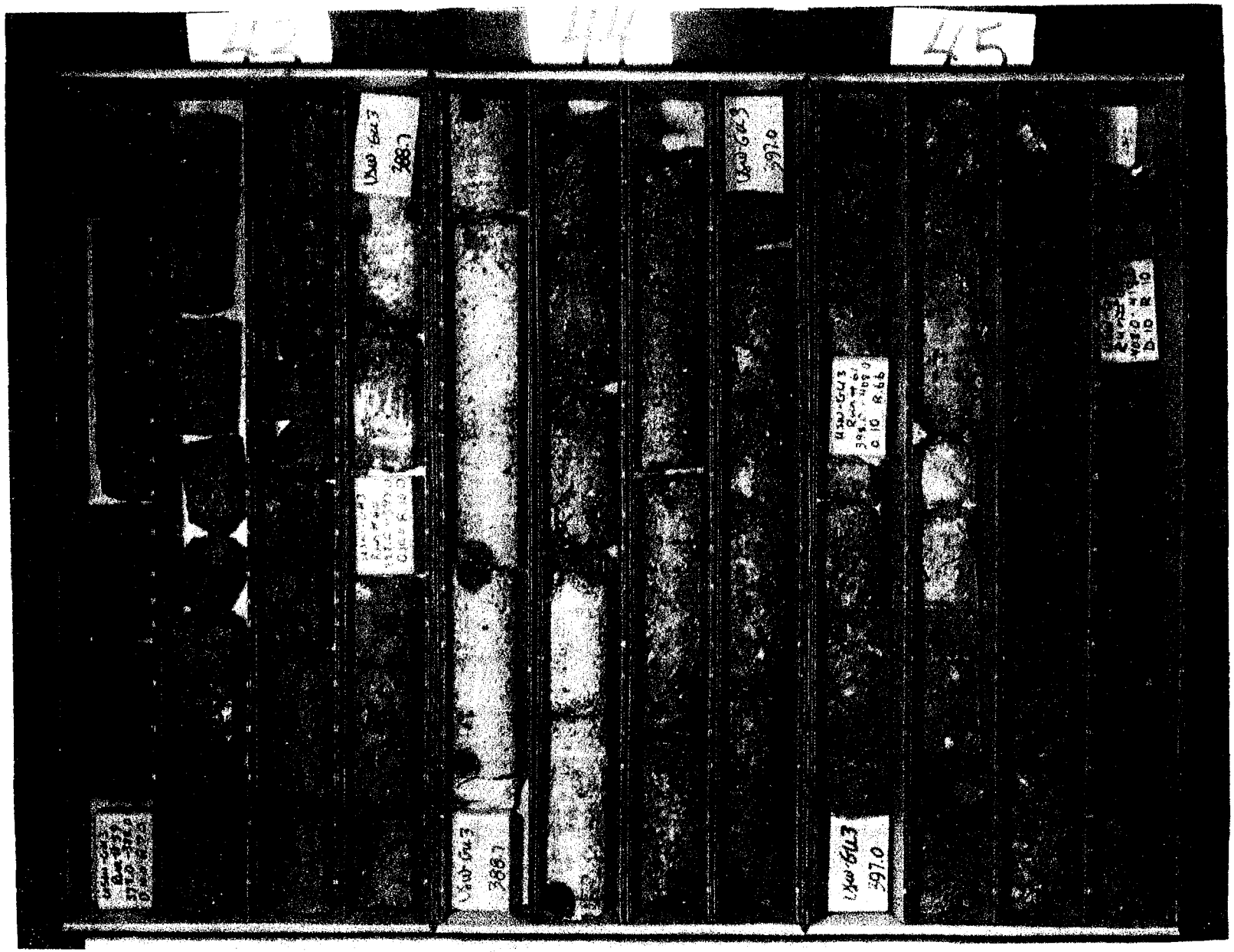

Geologic association of the fluid inclusion sample USW GU3 - 429 ft (130m) - hanging wall of the host fault zone.

Figure 8-21b

Geologic association of the fluid inclusion sample USW GU3 - 429 ft (130m) - footwall of the host fault zone.

Figure 8-21c

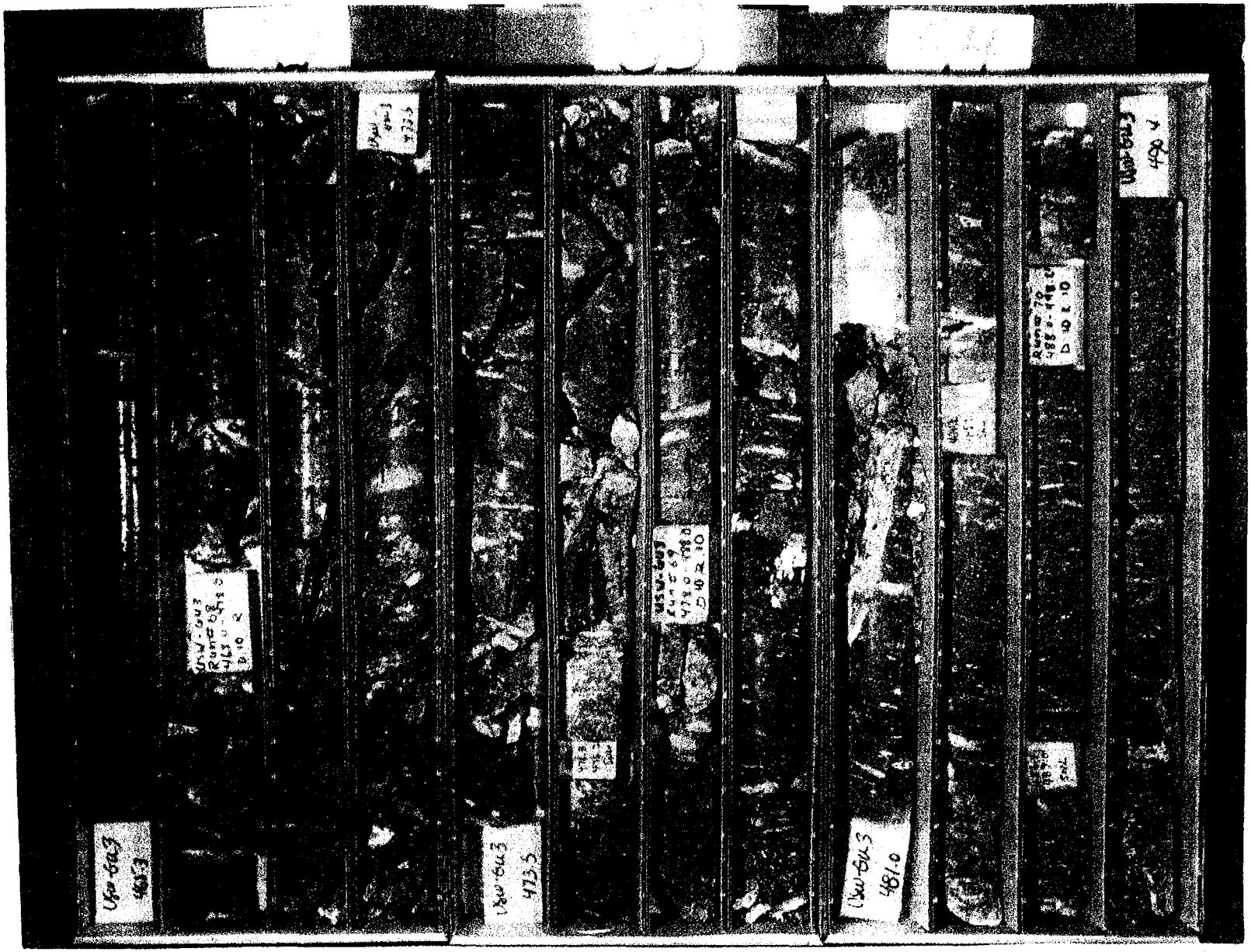

Geologic association of the fluid inclusion sample USW GU3 - 429 ft (130m) - footwall of the host fault zone.

Figure 8-21d

Note:

a) For the fluid inclusion sample USW GU3 - 103, the host rock is the Tiva Member of the Paintbrush Tuff;

b) The fluid inclusion sample USW GU3 - 429 is from a fault zone between the bedded tuff unit (equivalent of the Yucca Mountain and the Pah Canyon Members of the Paintbrush Tuff) and the Topopah Spring Member of the Paintbrush Tuff;

c) Both samples are from the Yucca Mountain vadose zone;

d) The fluid inclusion sample USW GU3 - 103 appears to represent a calcite cement from a hydraulic breccia injection dike;

e) The fluid inclusion sample USW GU3-429 is from the hydrothermally altered fault zone - footwall is bleached and hanging wall is visibly oxidized; and

f) The occurrence of the hydrothermal calcite within three different members of the Paintbrush Tuff as well as the local character of the hydrothermal alteration indicate, quite clearly, that the higher temperature inclusions, in both of the USW GU-3 samples, were not formed during deuteric mineralization episode.

Geologic association of the fluid inclusion samples USW GU3 - 103 and -429.

Figure 8-21e

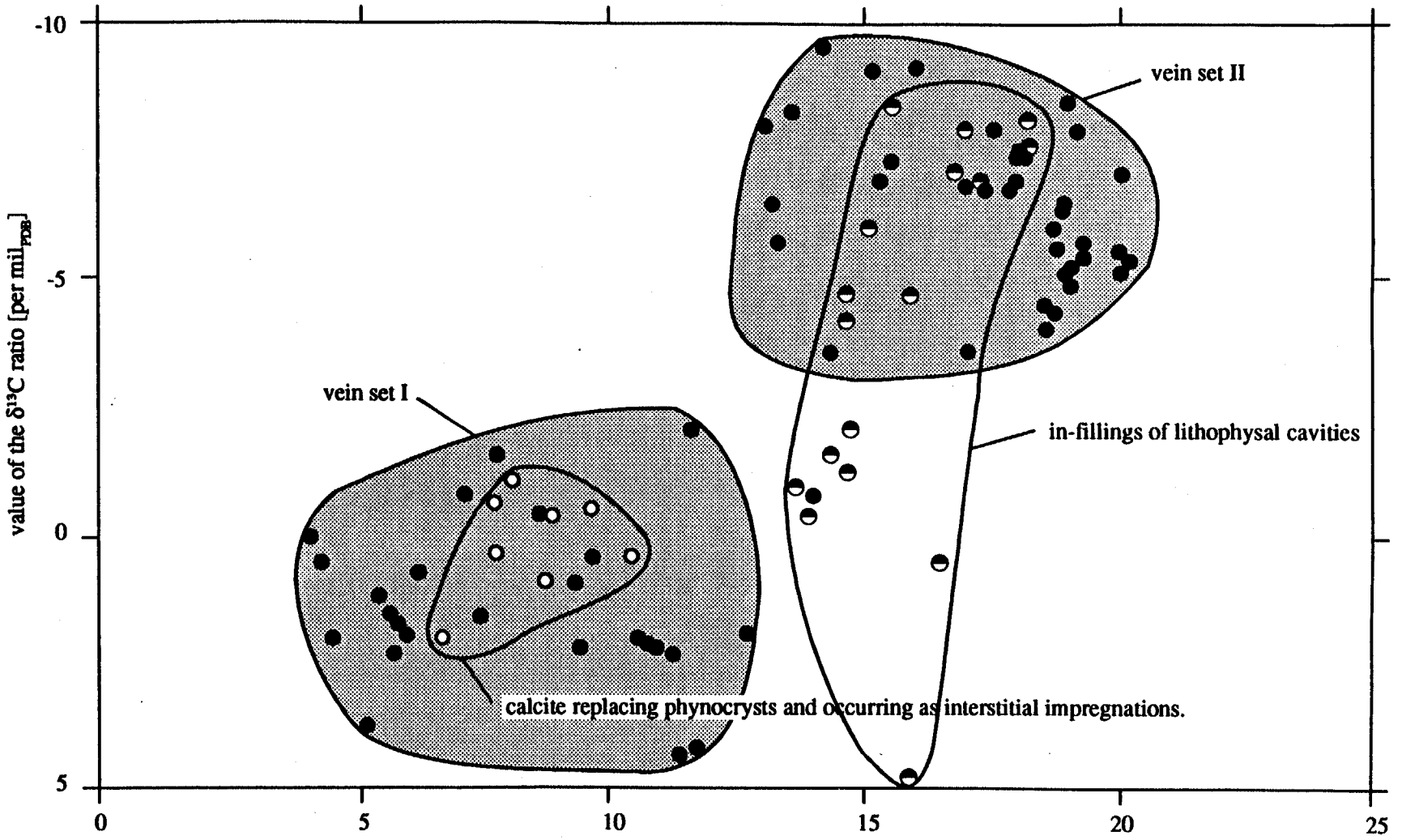

Explanation:

- ● - sample represents vein;
- ◓ - sample represents in-filling of lithophysal cavities; and
- ○ - sample represents calcite replacing phynocrysts and occurring as interstitial impregnations (cements).

Note: Isotopic data are from Whelan and Stuckless (1991).

$\delta^{13}C$ vs. $\delta^{18}O$ field, samples of calcitic phases from the Yucca Mountain ignimbrites.

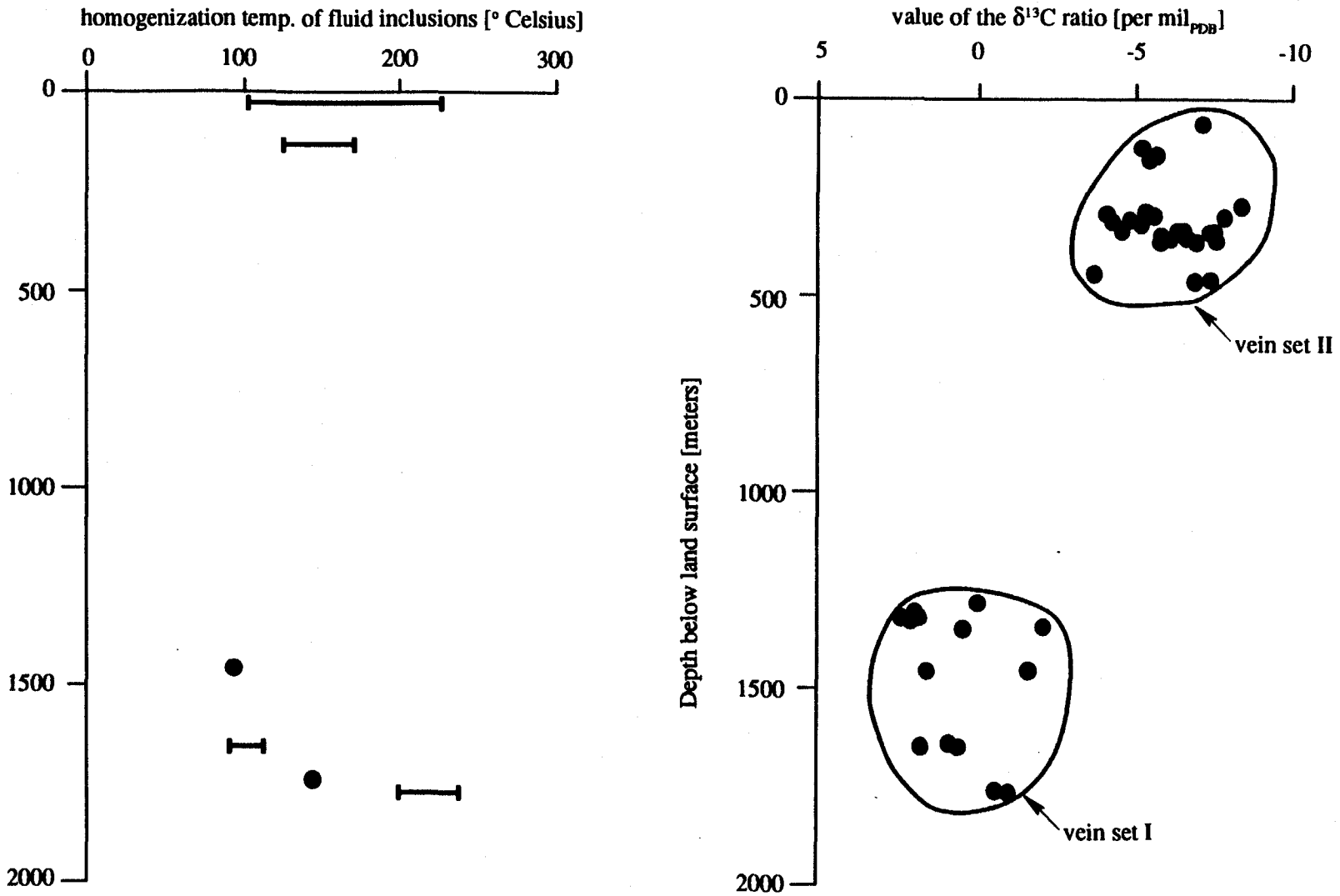

Note:

a) all data used to construct both of these depth profiles are from the northwestern sector of Yucca Mountain (boreholes USW G-2, G-3, and GU-3).

Comparison of homogenization temperatures of fluid inclusions with the $\delta^{13}C$ ratios, from samples of the corresponding calcitic veins.

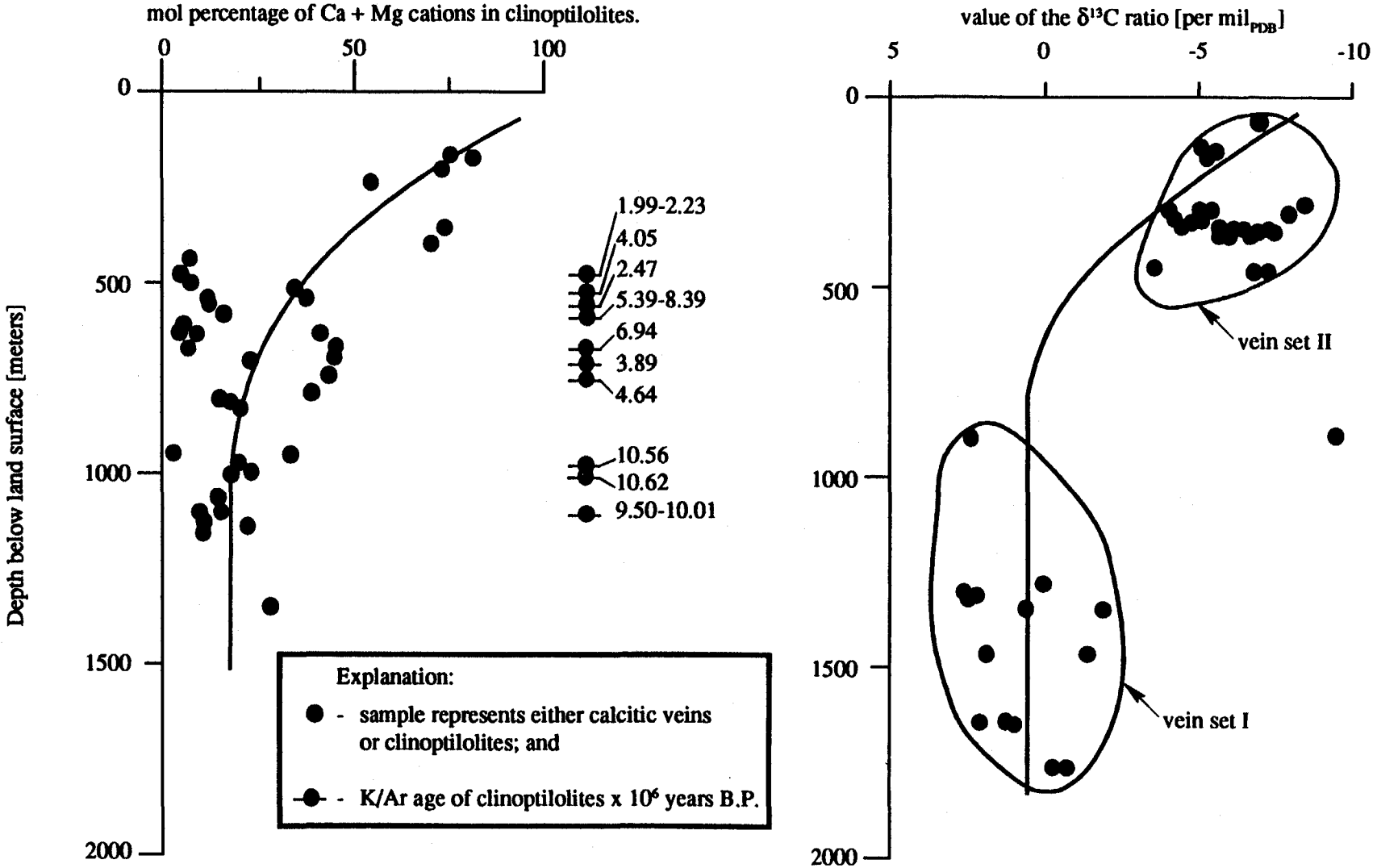

Note:

a) all data used to construct both of the depth profiles are from the northwestern segment of Yucca Mountain (boreholes USW G-1, G-2, G-3, and GU-3).

Comparison of the chemical compositions and K/Ar ages of clinoptilolites with the $\delta^{13}C$ ratios, from samples of the corresponding calcitic veins.

Figure 8-24a

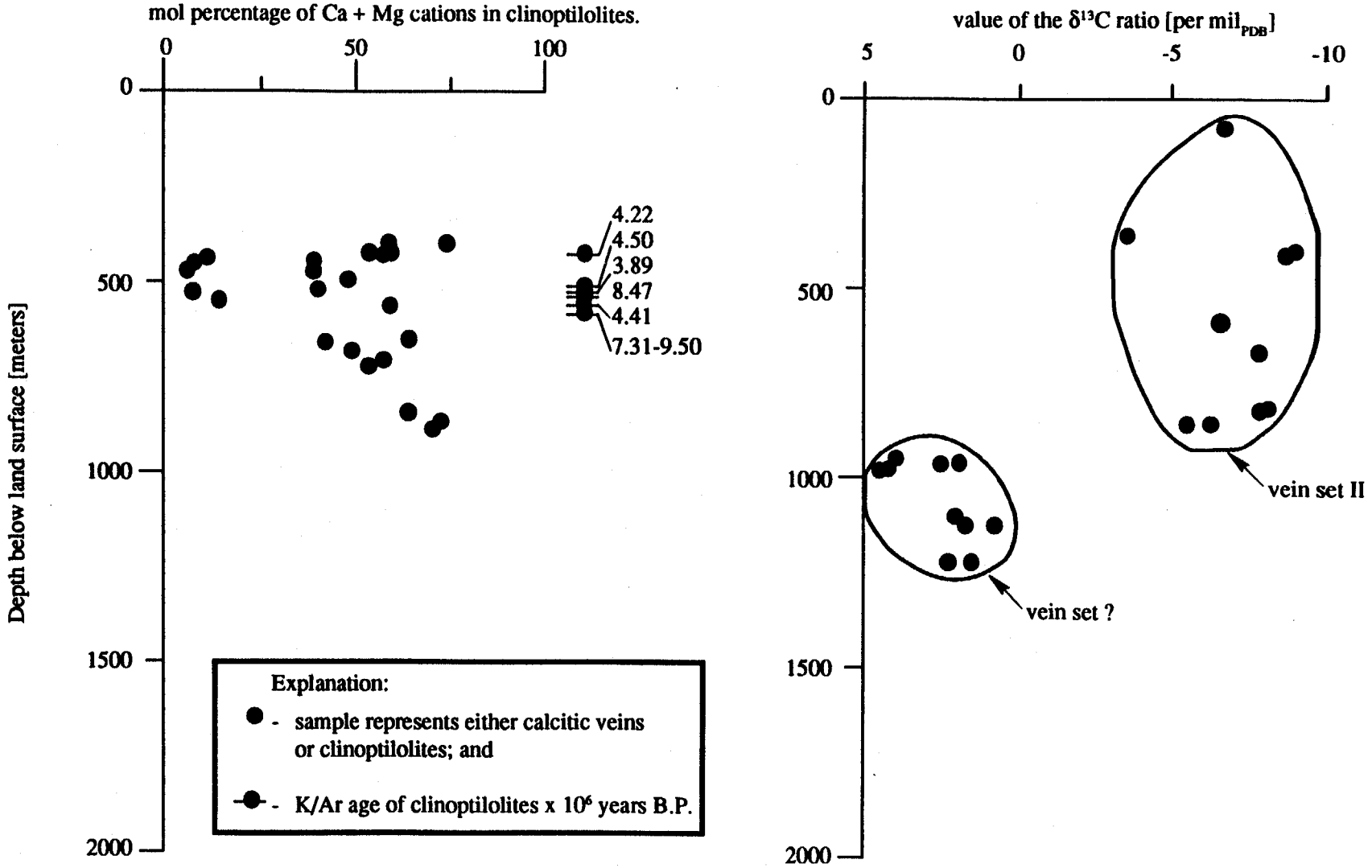

Note:

a) all data used to construct both of the depth profiles are from the southeastern segment of Yucca Mountain (boreholes USW G-4, and UE-25 a#1 and b#1).

Comparison of the chemical compositions and K/Ar ages of clinoptilolites with the $\delta^{13}C$ ratios, from samples of the corresponding calcitic veins.

Figure 8-24b

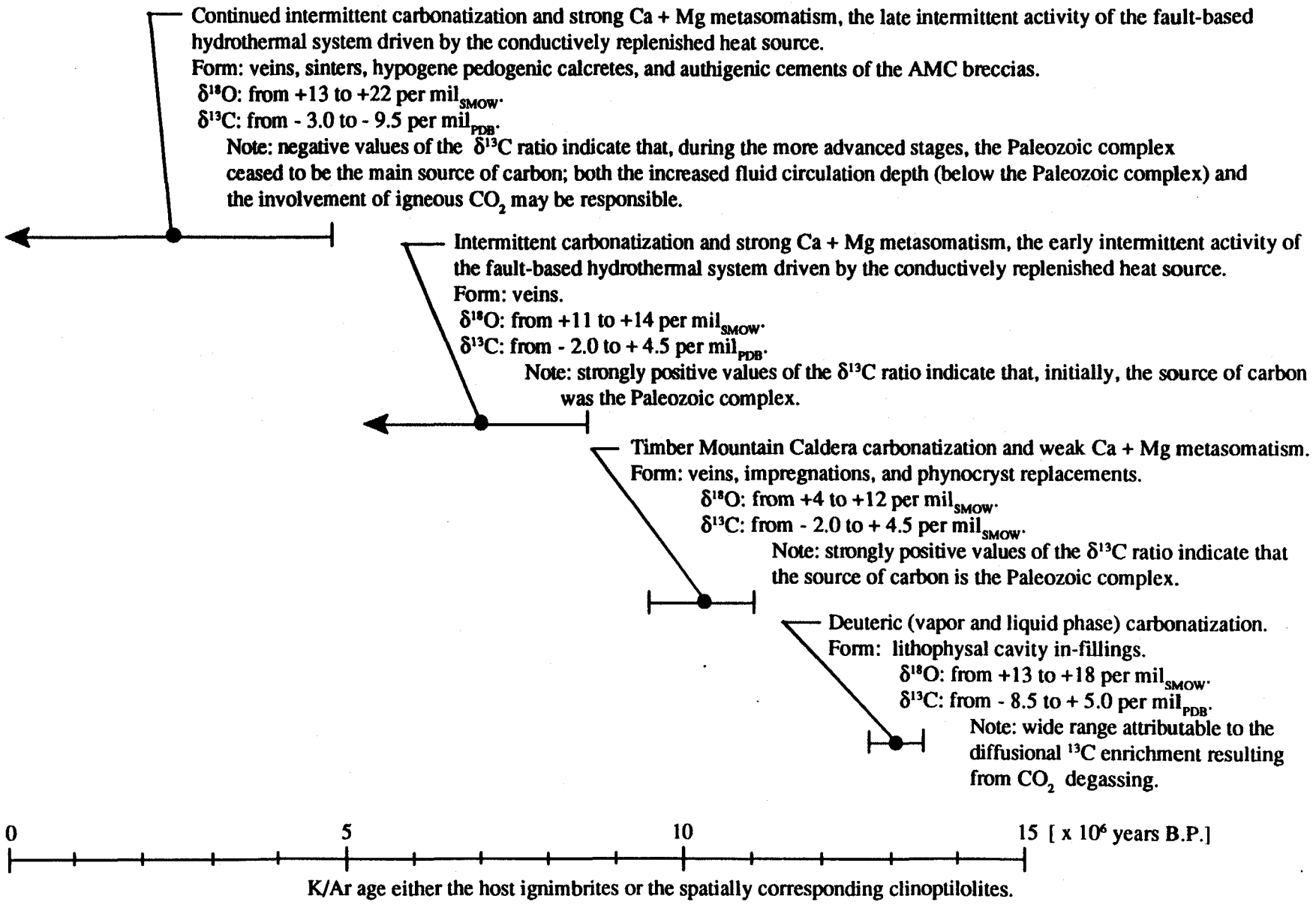

Paragenetic relationships based on: a) the form of occurrance; b) the spatial association with alteration minerals; c) the homogenization temperature of fluid inclusions; and d) the stable isotope characteristics. The calcitic phases from Yucca Mountain.

Location	Rock Type	$^{87}Sr/^{86}Sr$	Source	Note
Unaltered ignimbrites				
Long Valley Caldera	Inyo Domes Rhyolites	0.70630	Gaff et al. (1990)	mean of 3 samples
do	do	0.70606	do	mean of 7 samples
do	Mafic and intermediate	0.70630	do	mean of 3 samples
do	Moat rhyolites	0.70601	do	mean of 6 samples
do	Early rhyolites	0.70665	do	mean of 2 samples
do	do	0.70716	do	hydrothermally alt
do	do	0.70742	do	do
do	Bishop Tuff	0.7070	do	mean of 2 samples
do	do	0.70713	do	mean of 6 samples
do	do	0.70645	do	sanidine seperates
do	do	0.70745	do	hydrothermally alt
do	Pre-caldera volcanic	0.70610	do	mean of 3 samples
representative mean value: 0.70667				
Paleozoic carbonates				
Spring Mountains	limestone	0.70913	Peterman (1990)	outcrop
do	do	0.70823	do	do
do	do	0.70837	do	do
Ash Meadows	do	0.70990	do	do
Rock Valley	do	0.70934	do	do
representative mean value: 0.70899				
The Pre-Cambrian basement				
Round Vly Peak, Ca.	schist	0.71656	Goff et al(1990)	PC-derivative
do	hornfels	0.72201	do	do
do	sandstone	0.71126	do	do
Dish Hill, Ca.	granodiorite	0.7177	Peterman et al(1970)	xenolith
representative mean value: 0.71688				

Estimate of the isotopic character of strontium contained in the main local litho-stratigraphic complexes, based on the strontium isotopic analyses of the unaltered and representative samples.

	Rb	Sr	Y	Zr	Nb	Rb/Sr	Ma	87Sr/86Sr	IR(Sr)
	Parts per million								
Tiva Canyon									
UD-18	192	24	36	187	32	8.00	12.9	0.71574	0.7115
UD-29	222	10	25	64	30	22.20	12.9	0.72024	0.7084
UD-32-1	208	49	29	67	33	4.24	12.9	0.71353	0.7113
UD-34	148	44	37	326	24	3.36	12.9	0.71267	0.7109
Yucca Mt. 2AA-6	175	31	34	193	32	5.65	13.0	0.71495	0.7119
Topopah Spring(12)	176	22	26	109	22	8.07	13.4	0.71603	0.7116
2AA-5(upper)	146	57	25	320	21	2.56	13.4	0.71231	0.7109
2AA-2 (bas.vit)	192	58	22	118	25	3.31	13.4	0.71239	0.7106
2AA-1(basal)	204	63	28	104	24	3.24	13.4	0.71345	0.7117
Calico Hills(4)	159	66	24	91	19	2.41	13.4	0.71328	0.7119
2A-1-1	85	77	10	53	12	1.10	13.4	0.71239	0.7118
2A-1-2	158	92	18	99	18	1.72	13.4	0.71239	0.7114
Prow Pass(2)	155	52	30	148	27	2.99	13.5	0.71172	0.7101
3A-7	116	196	21	93	19	0.59	13.5	0.71139	0.7111
Bullfrog(16)	139	124	29	135	24	1.12	13.5	0.70953	0.7089
3A-6 (upper)	159	122	26	108	20	1.30	13.5	0.70976	0.7090
3A-4 (ba. vit.)	165	239	27	177	31	0.69	13.5	0.70879	0.7084
3A-3 (ba. vit.)	151	464	27	251	26	0.33	13.5	0.70834	0.7082
3A-2 (basal)	169	118	25	131	23	1.43	13.5	0.70944	0.7086
Air Fall 31-1	144	149	29	204	31	0.97	13.5	0.71012	0.7096
Tram(11)	131	196	20	149	19	0.67	13.6	0.70974	0.7094
4A-1	219	705	27	179	32	0.31	13.6	0.71026	0.7101
4B-4	161	178	21	108	17	0.90	13.6	0.71042	0.7099
4B-6	149	79	17	113	20	1.89	13.6	0.71105	0.7100
Flow Breccia(4)	103	729	32	331	17	0.14	13.7	0.70928	0.7092
Lithic Ridge(6)	131	240	24	165	21	0.55	13.8	0.70909	0.7088
1C-3	151	144	19	128	26	1.05	13.8	0.70947	0.7089
Unit A(6)	157	161	25	151	27	0.98	14.0	0.70955	0.7090
Unit B(1)	131	181	26	186	23	0.72	14.0	0.70921	0.7088
Unit C(7)	130	511	23	244	17	0.25	14.0	0.70892	0.7088
Yucca Flat 1C-1	108	105	32	177	32	1.03	14.0	0.71013	0.7095

Isotopic character of strontium and strontium concentrations, whole-rock samples from boreholes USW G-1 and G-2. From Peterman (1989).

Depth feet	Rb, ppm	Sr, ppm	$^{87}Rb/^{86}Sr$	$^{87}Sr/^{86}Sr$	IR(Sr)	Sm, ppm	Nd, ppm	$^{147}Sm/^{144}Nd$	$^{143}Nd/^{144}Nd$	ϵ_{Nd}
268.0	89.7	401	0.65	0.71044	0.71032					
277.8	115	169	1.97	0.70953	0.70917					
304.0	92.7	114	1.75	0.70977	0.70946					
387.7	144	52.9	7.88	0.71287	0.71145					
510.4	185.9	26.03	20.68	0.71663	0.71290	5.57	26.48	0.1271	0.51206	-11.2
609.6	185.3	28.16	19.05	0.71638	0.71294					
669.5	181.8	35.53	14.81	0.71538	0.71271					
990.0	187.4	46.44	11.68	0.71451	0.71240					
1093.0	171	64.0	7.74	0.71397	0.71257					
1170.0	200	37.2	15.57	0.71530	0.71249	6.15	29.07	0.1280	0.51205	-11.4
1274.0	178	237	2.02	0.71243	0.71207					
1274.4	76.6	582.0	0.38	0.71198	0.71191	4.30	20.98	0.1238	0.51207	-11.0
1295.0	160.4	296.3	1.57	0.71236	0.71208	6.44	30.17	0.1290	0.51207	-11.0
1324.3	102.8	568.0	0.52	0.71099	0.71090	5.03	24.72	0.1231	0.51206	-11.2

Note:

a) Rb and Sr concentrations from samples 268.0 to 387.7, 1093, 1170 and 1274 are by EDXRF.

b) all others by isotope dilution.

Isotopic character of strontium and strontium concentrations, whole-rock samples from borehole UE-25a#1. From Peterman et al. (1991).

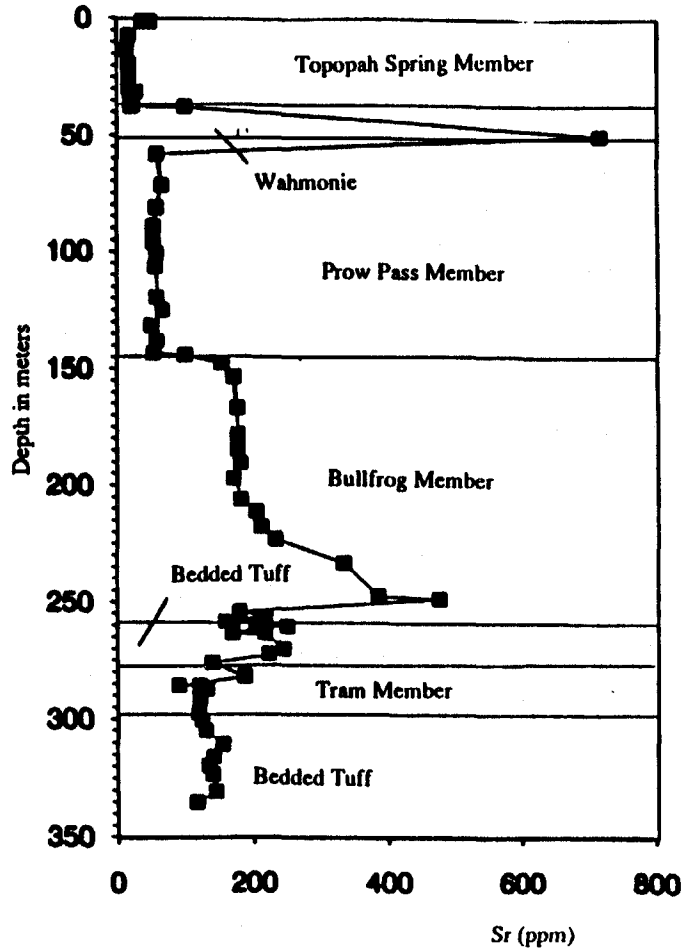

Whole-rock concentrations of strontium, southernmost end of Yucca Mountain. From Peterman et al. (1991).

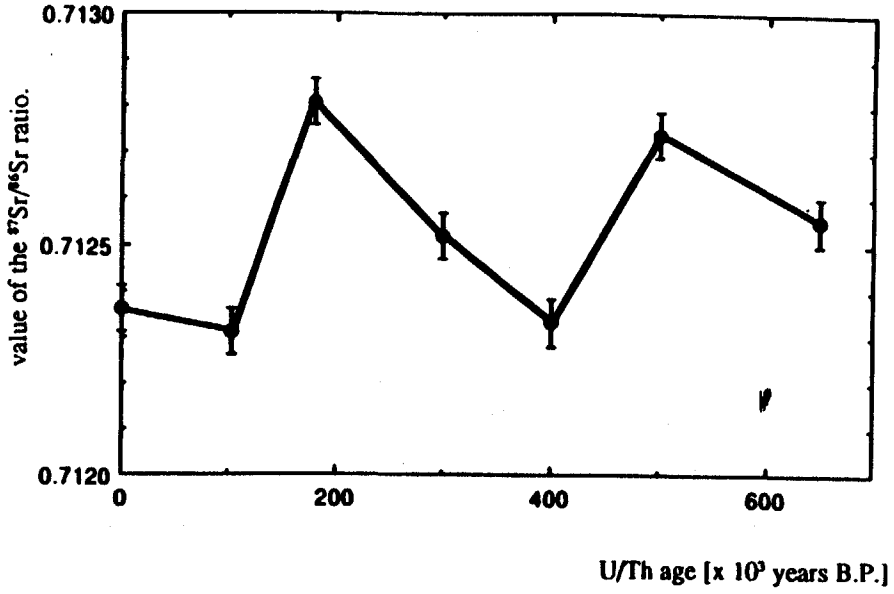

a) isotopic character of strontium contained in the Devil's Hole calcitic vein. From Marshall et al. (1990).

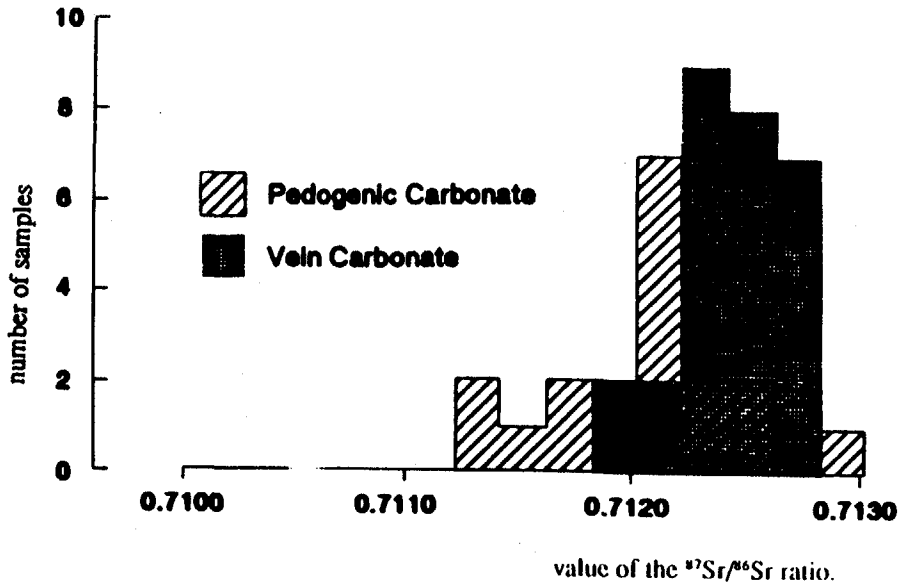

b) isotopic character of strontium contained in the Yucca Mountain calcretes and veins. From Stuckless (1990).

Note:

a) the Devil's Hole vein has been precipitated from the local thermal fluids - these calcium-magnesium fluids are known to carry abnormally high values of the $^{87}Sr/^{86}Sr$ ratio; and

b) the phrase "pedogenic carbonate" is used to denote the Yucca Mountain calcretes.

Isotopic character of strontium contained in samples of the Yucca Mountain calcretes and associated veins.

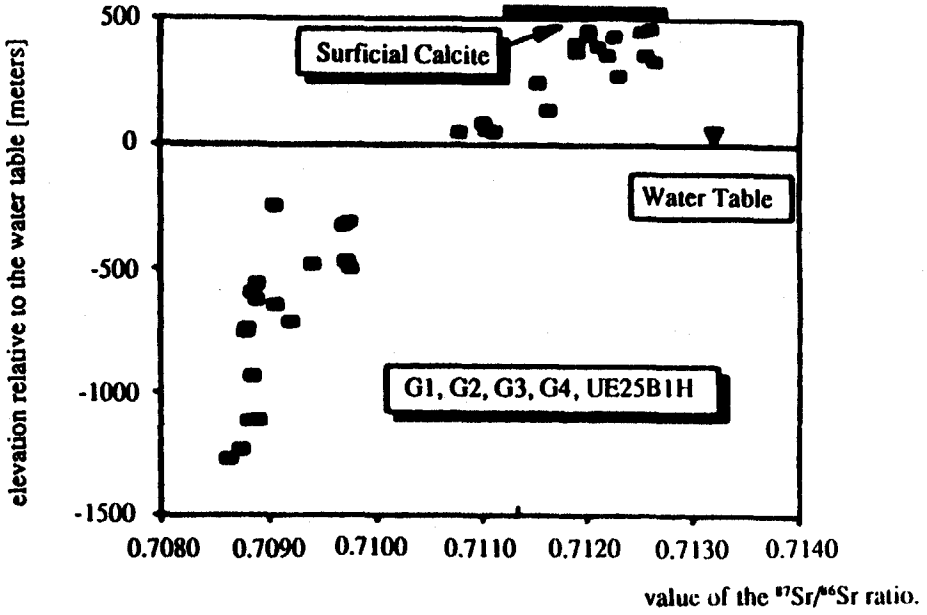

Isotopic character of strontium contained in the Yucca Mountain subsurface calcitic veins. From Peterman et al.(1991).

Location	Sampling site	$^{87}Sr/^{86}Sr$	Source
Chemically immature fluids			
Yucca Mountain	well J-13	0.7114	Peterman (1990)
do	well J-12	0.7100	do
do	well VH-2	0.7103	do
do	well UE-25p#1	0.7110	do
do	well UE-25b#1	0.7114	do
Amargosa Meadows	well	0.7105	do
do	well	0.7113	do
mean: 0.7108			
Chemically more evolved fluids			
Nuclear Engr. Co.	well #1	0.7116	Peterman (1990)
do	do	0.7109	do
do	do	0.7113	do
do	do	0.7119	do
mean: 0.7114			

Isotopic character of strontium dissolved in the sodium-potassium type of subsurface fluids, region at and around Yucca Mountain.

Location	Sampling site	$^{87}Sr/^{86}Sr$	Source
Chemically and isotopically immature fluids			
Spring Mtns	spring	0.7084	Stuckless(1990)
Spring Mtns	spring	0.7088	do
Indian Sprg Val	spring	0.7100	do
Indian Sprg Val	spring	0.7096	do
mean: 0.7092			
Chemically and isotopically mature thermal fluids			
northern NTS	UE-15d	0.7135	Stuckless(1990)
Yucca Flat	C-1	0.7149	do
Yucca Mtn	UE-25p#1	0.7118 (?)	do
south of Mercury	16S/5IE	0.7117	do
Ash Meadows	spring	0.7127	do
do	spring	0.7125	do
do	spring	0.7123	do
do	spring	0.7124	do
do	spring	0.7124	do
do	spring	0.7124	do
do	spring	0.7125	do
do	spring	0.7170	do
do	spring	0.7190	do
Greenwtr Range	well	0.7165	do
mean:0.7136			

Isotopic character of strontium dissolved in the calcium-magnesium type of subsurface fluids, region around Yucca Mountain.

Location	Sampling site	$\delta^{13}C$	Source
Chemically and isotopically immature fluids			
Yucca Mountain	well J-13	-7.3	Benson and McKinley (1985)
do	well J-12	-7.9	do
do	well VH-2	-8.5	do
do	well UE-25p#1 upper	-4.2	do
do	well UE-25b#1	-10.4	do
Amargosa Narrows	seep	-11.4	White and Chuma (1987)
do	do	-13.50	do
mean: -9.2 per mil$_{PDB}$			
Chemically and isotopically more mature fluids			
Nuclear Engr. Co.	well #60	-5.9	Claassen (1985)
Yucca Mountain	well USW H-3	-4.9	Benson and McKinley (1985)
Bullfrog Valley	spring	-4.2	White and Chuma (1987)
do	do	-6.2	do
mean: -5.3 per mil$_{PDB}$			

Isotopic character of carbon dissolved in the sodium-potassium type of subsurface fluids, region at and around Yucca Mountain.

Location	Sampling site	$\delta^{13}C$	Source
Chemically and isotopically immature fluids			
Spring Mountain	spring	-8.00	Stuckless (1990)
do	do	-9.70	do
Sheep Range	spring	-7.70	do
do	well	-7.70	do
Indian Springs Valley	spring	-7.50	do
do	well	-7.60	do
do	do	-6.90	do
mean: -7.87 per mil$_{PDB}$			
Chemically and isotopically mature fluids			
Yucca Flat	well C	-3.80	Stuckless (1990)
Yucca Mountain	well 25p#1	-2.30	Benson and Mckinley (1985)
Ash Meadows	spring	-5.20	DOE (1988)
do	do	-4.90	do
do	do	-4.60	do
do	do	-4.80	do
do	do	-4.70	do
do	do	-5.00	do
do	do	-5.00	do
do	do	-4.70	do
do	do	-4.60	do
mean: -4.50 per mil$_{PDB}$			

Isotopic character of carbon dissolved in the calcium-magnesium type of subsurface fluids, region around Yucca Mountain.

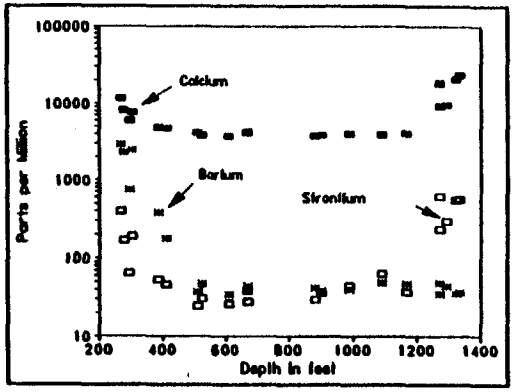

a) Ca, Ba, and Sr, in the Topopah Spring Member.

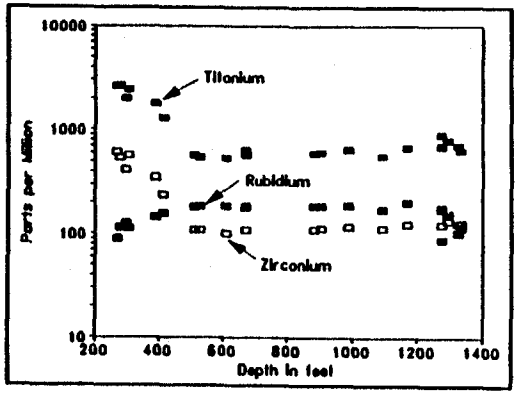

b) Ti, Rb, and Zr, in the Topopah Spring Member.

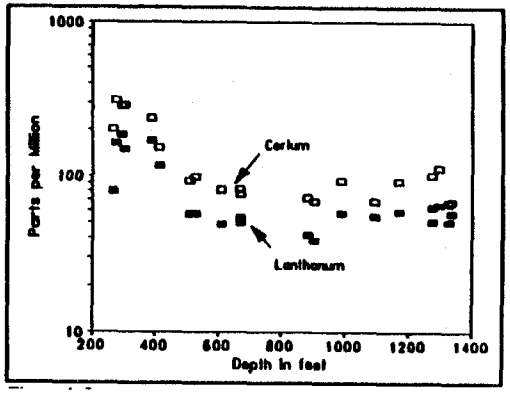

c) La and Ce, in the Topopah Spring Member.

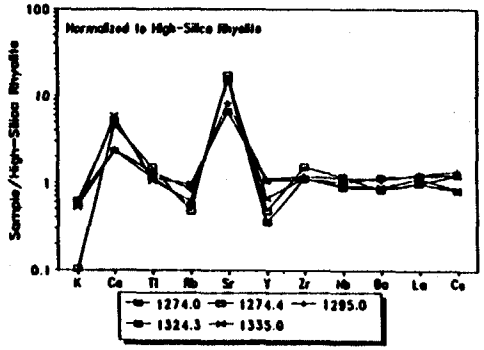

d) normalized concentrations, altered lower vitrophyre of the Topopah Spring Member.

Sample 268.0 is from the zone of nonwelded vitric, ash-flow tuff at the top of the unit and consists of approximately 90 percent pumice and sparse lithic fragments. Samples 277.8 through 413.0 are moderately to densely welded quartz latite with phenocrysts generally decreasing in abundance with depth. Samples 510.4 to 1170.0 are from the densely welded, devitrified zone composed of high-silica rhyolite. Samples 1274.0, 1274.4, and 1295.0 are from the lower vitrophyre and represent various degrees of alteration. Sample 1274.0 is a dull black vitrophyre with abundant fractures and veining. Sample 1274.4 is predominantly smectite and clinoptilolite, and sample 1295.0 is approximately half smectite and clinoptilolite. Sample 1324 is 80 ± 12 percent clinoptilolite and 6 ± 2 percent mordenite; the remainder is alkali feldspar and silica minerals [27]. Sample 1335.0 is from a non- to partially welded, slightly altered zone near the base of the unit.

Major and trace element concentrations, whole-rock ignimbrites from the vadose zone, borehole UE-25a#1. From Peterman et al. (1991)

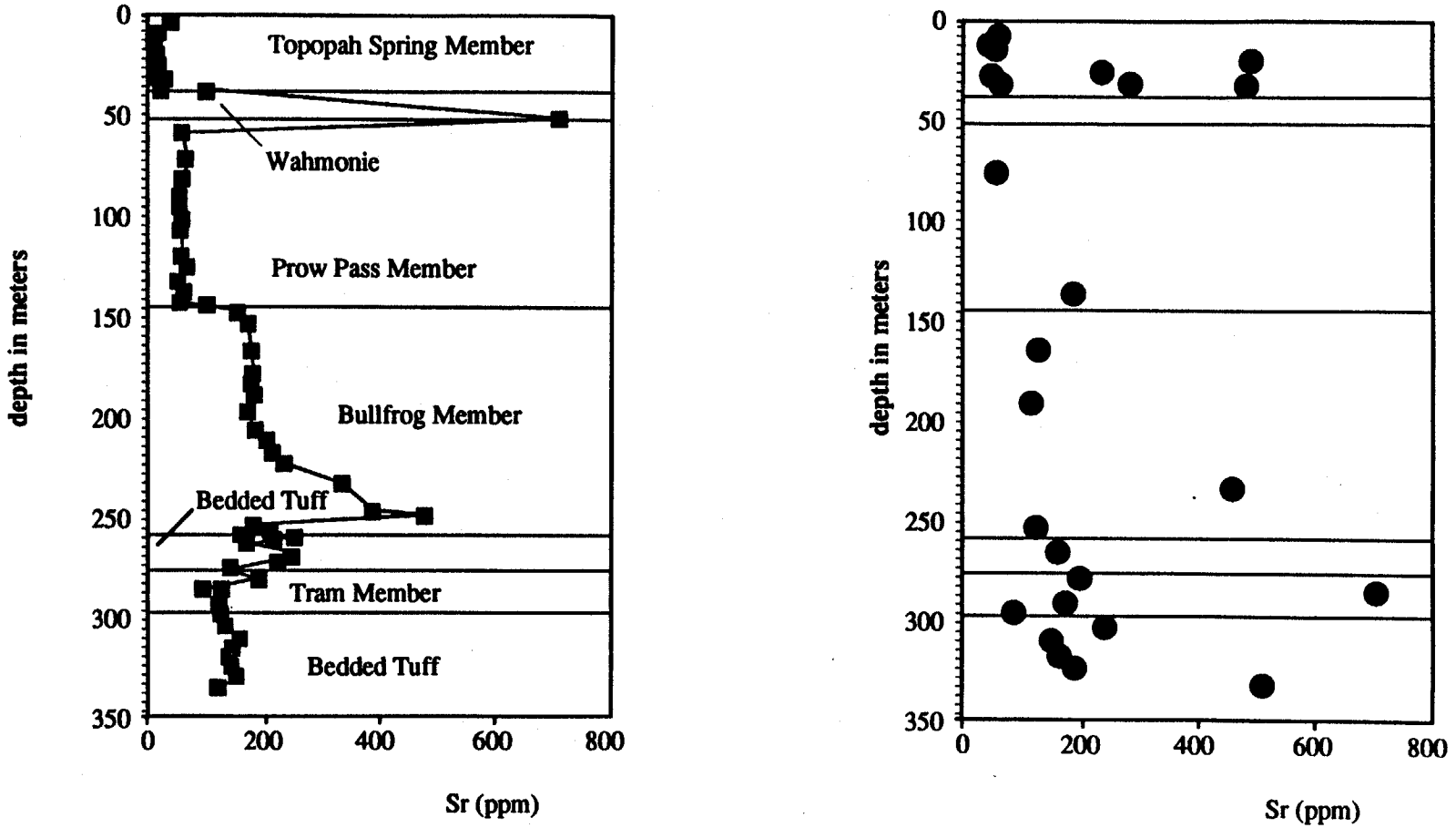

a) southernmost end of Yucca Mountain.

b) northernmost end of Yucca Mountain.

Comparisons of concentrations of strontium, whole-rock samples of the stratigraphically equivalent ignimbrites.

UE -25a#1.

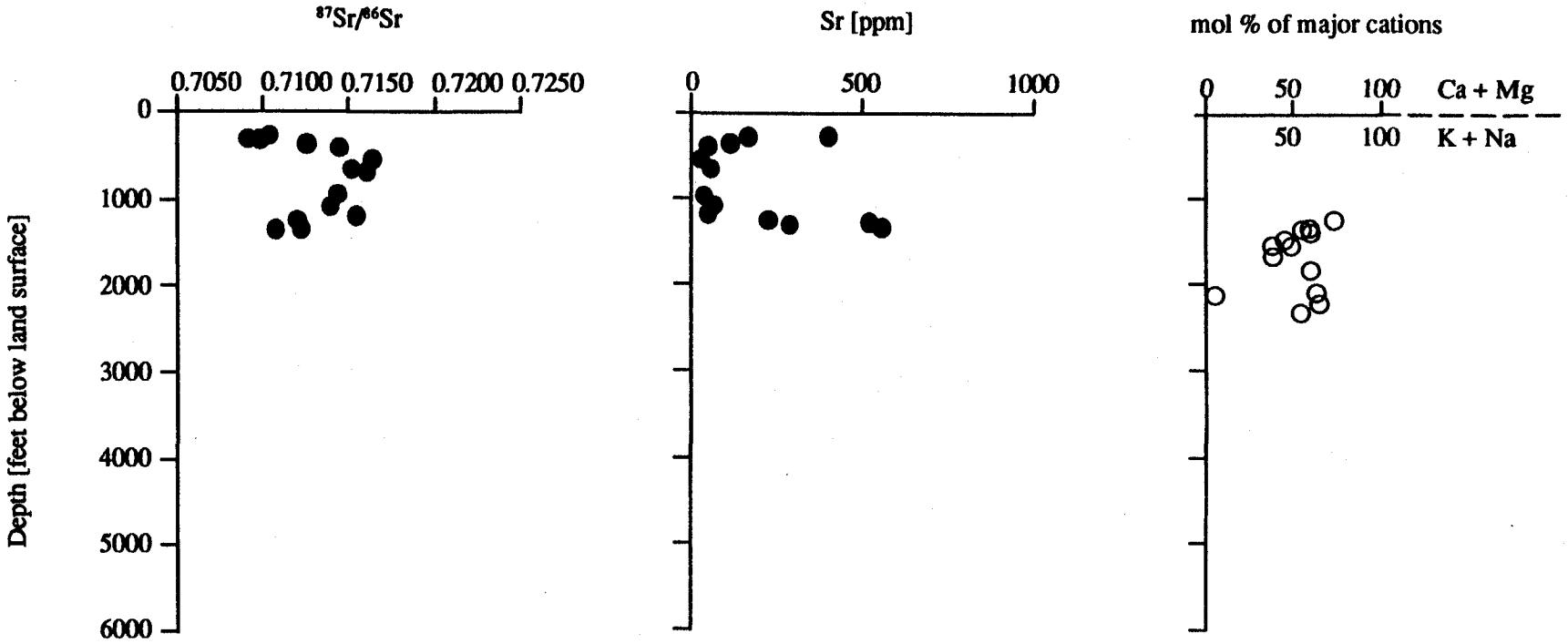

Explanation:

● - value represents either $^{87}Sr/^{86}Sr$ ratio or Sr concentration; and

○ - major cations content from samples of clinoptilolites.

Depth comparison - the $^{87}Sr/^{86}Sr$ ratios, the Sr concentrations, and the major cation concentrations in clinoptilolites.

Figure 8-33a

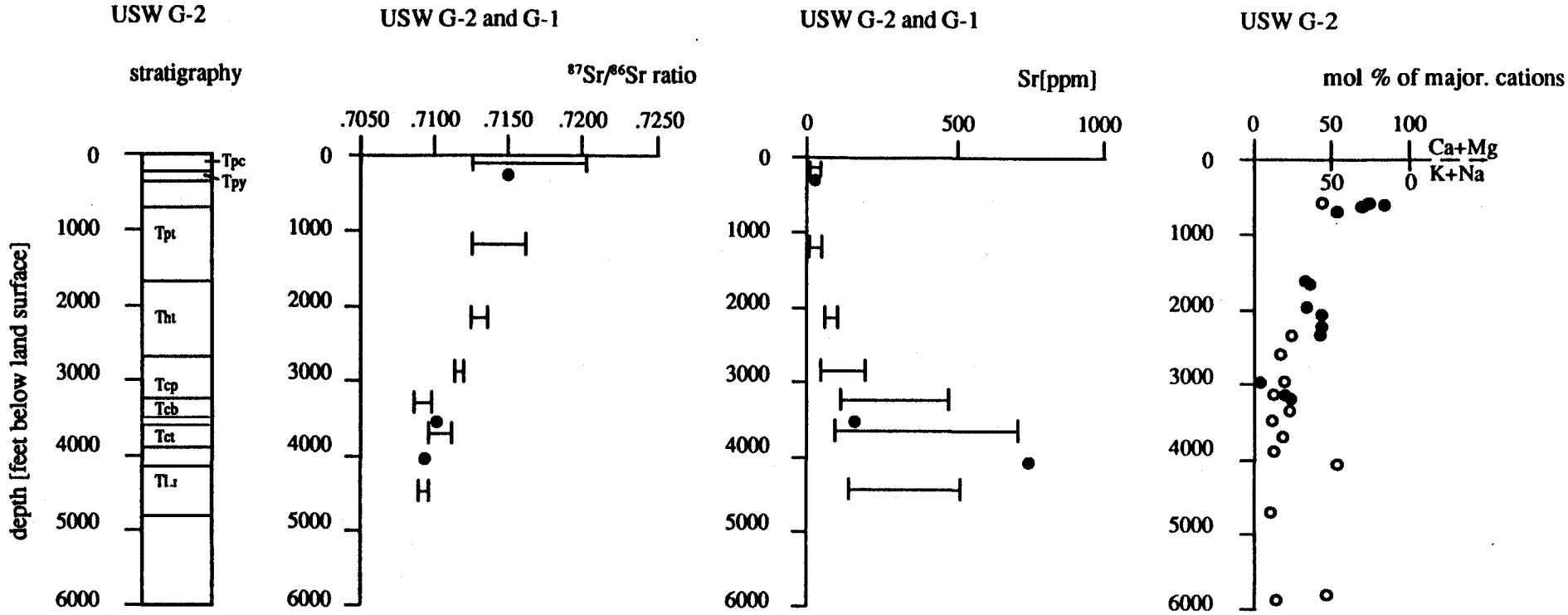

Explanation:

- ● - major cations content from samples of clinoptilolites;
- o - major cations content from whole-rock samples;

bar indicates range of values for either $^{87}Sr/^{86}Sr$ ratio or concentrations of Sr, whole-rock samples; and
Tpc - the Tiva Canyon Member, Tpy - the Yucca Mountain Member, Tpt - the Topopah Spring Member, Tht - the Tuffs of Calico Hills, Tcp - the Prow Pass Member, Tcb - the Bullfrog Member, Tct - the Tram Member, and Tlr - the Lithic Ridge Tuff.

Depth comparison - the $^{87}Sr/^{86}Sr$ ratios, the Sr concentrations, and the major cation concentrations, samples of the alteration products (whole-rock and clinoptilolites).

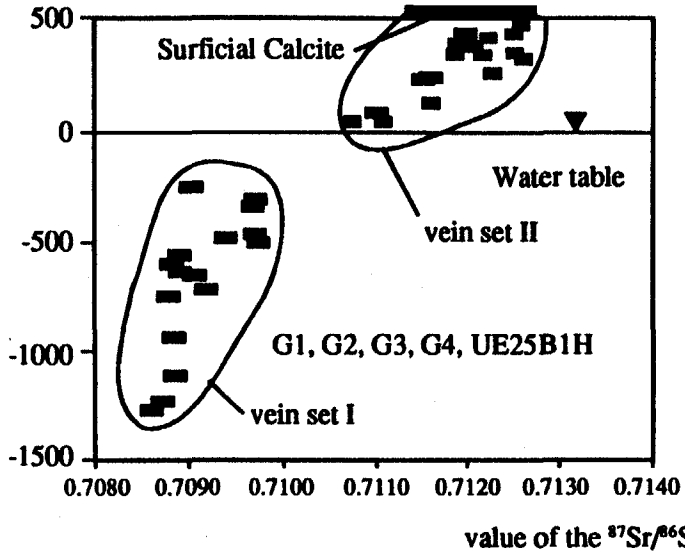

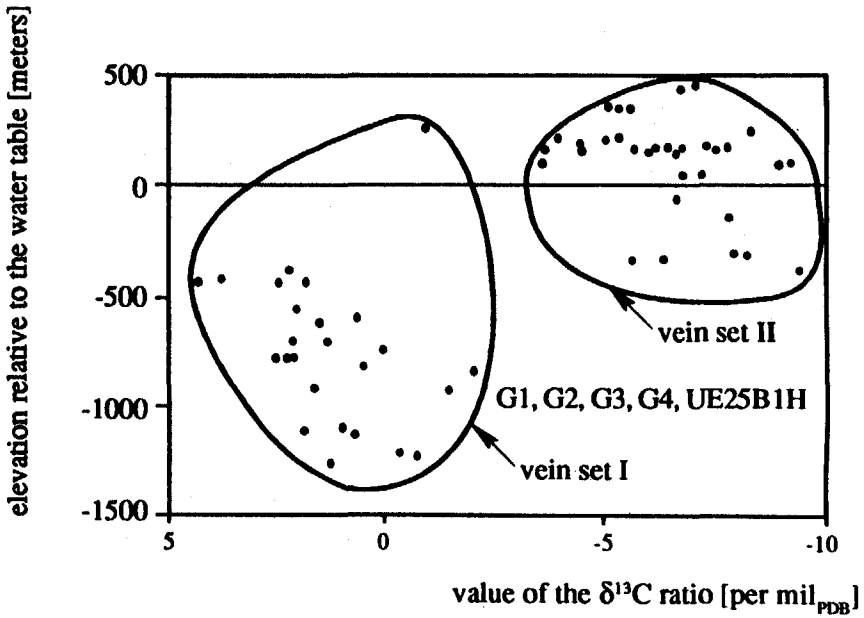

Note:

a) strontium isotopic data are from Peterman et al. 1990; and

b) carbon isotopic data are from Whelan and Stuckless (1991).

Comparison of the $^{87}Sr/^{86}Sr$ ratios with the $\delta^{13}C$ ratios, samples of the corresponding calcitic veins.

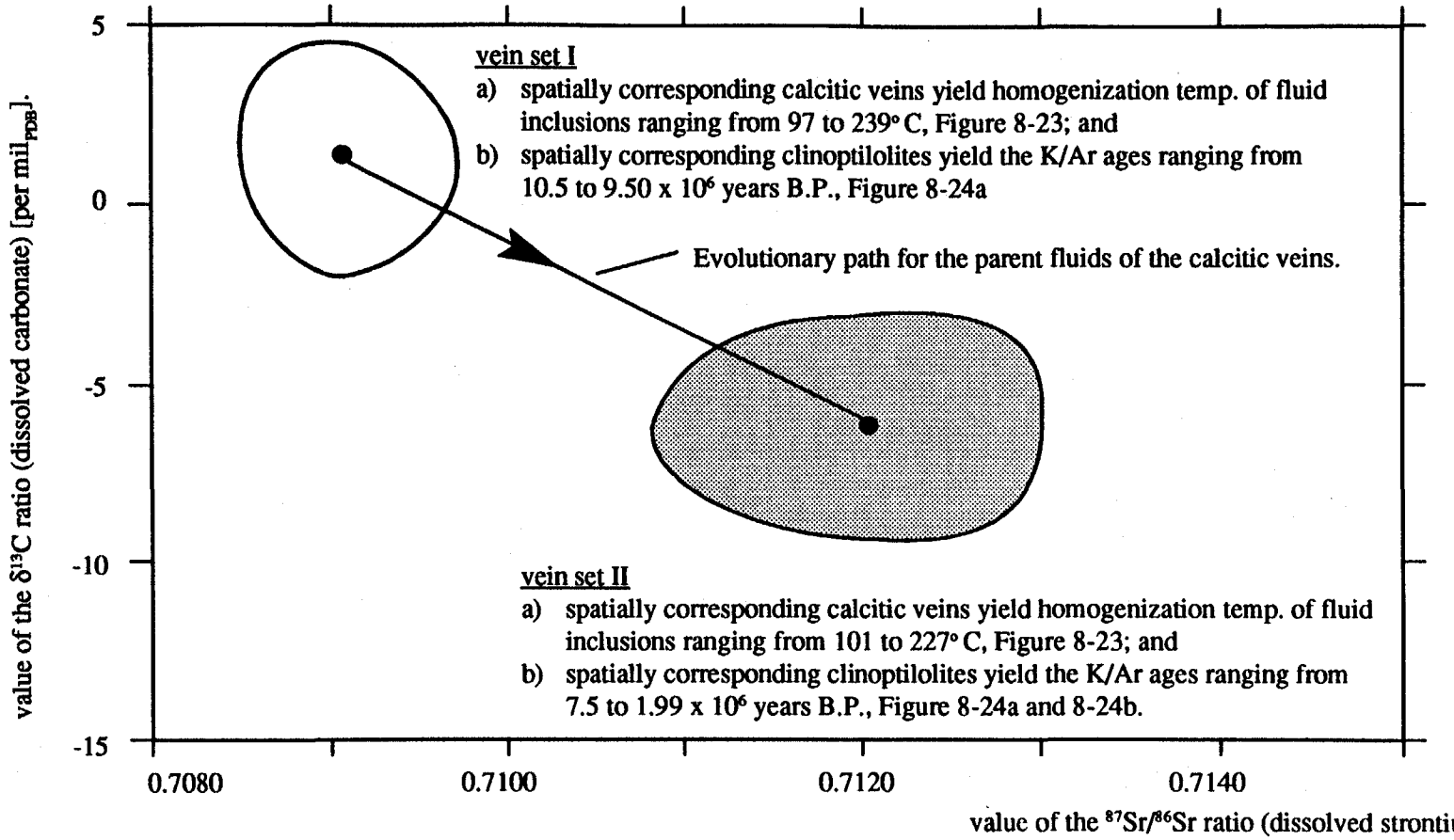

Note:

a) in constructing this plot, it has been assumed that the analyzed calcitic veins were precipitated from highly supersaturated fluids and, consequently, the rates of calcite precipitation were very large; and

b) under these conditions, the carbon isotopic fractionation factor is negligible, see for example Usdowski et al. (1979) and Turi (1986).

Comparison of the $^{87}Sr/^{86}Sr$ vs. $\delta^{13}C$ fields, the parent fluids for the two temporally distinct sets of the calcitic veins, Yucca Mountain.

Figure 8-35

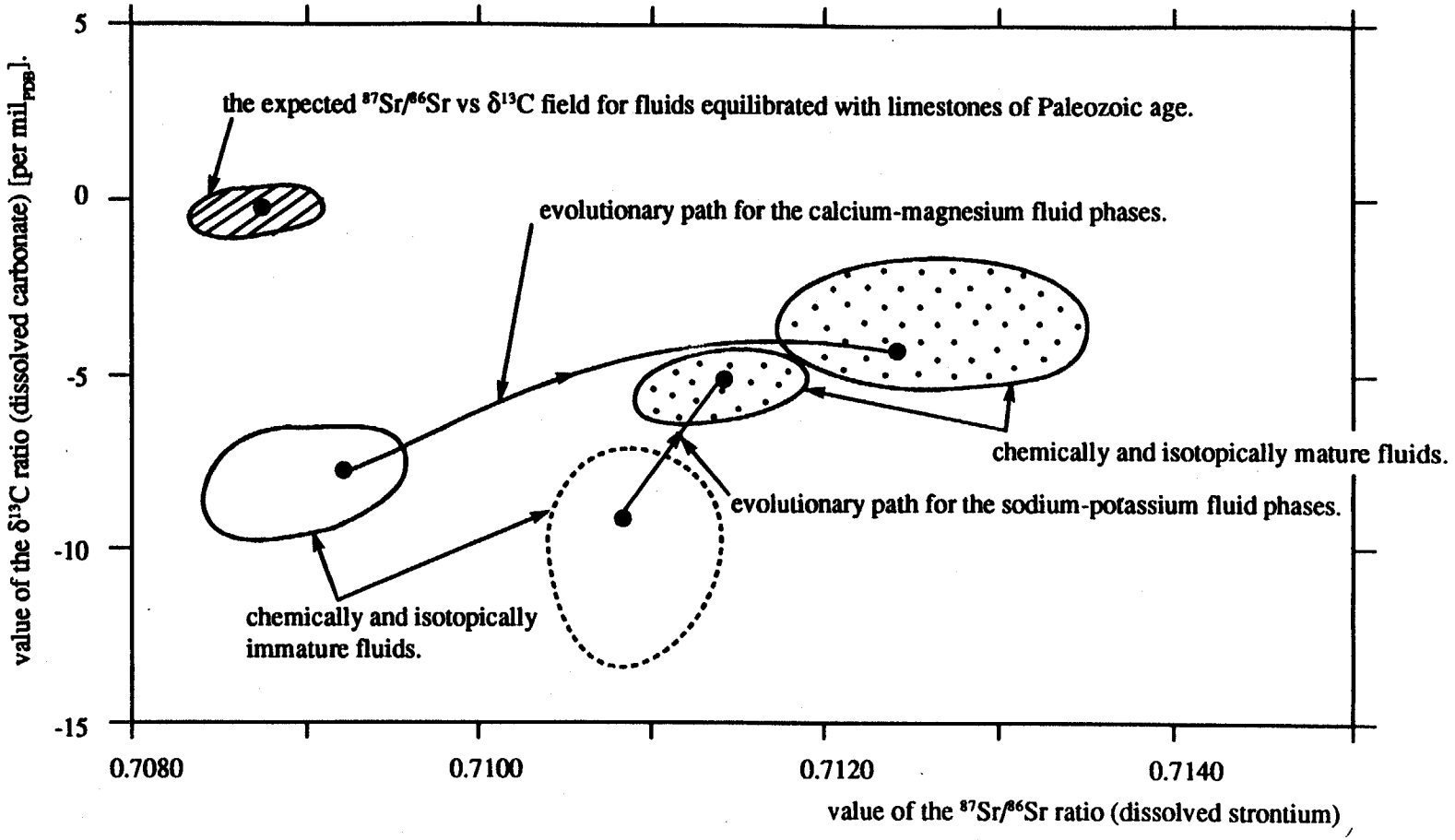

Note:

This plot has been constructed excluding the $\delta^{13}C$ data from upper parts of UE-25p#1 (mixed fluids) and the highly strontium radiogenic fluids from Ash Meadows ($^{87}Sr/^{86}Sr > 0.7150$).

Comparison of the $^{87}Sr/^{86}Sr$ vs. $\delta^{13}C$ fields, the calcium - magnesium fluid phases (Paleozoic carbonates - based) and the sodium - potassium fluid phases (ignimbrites - based), region around Yucca Mountain.

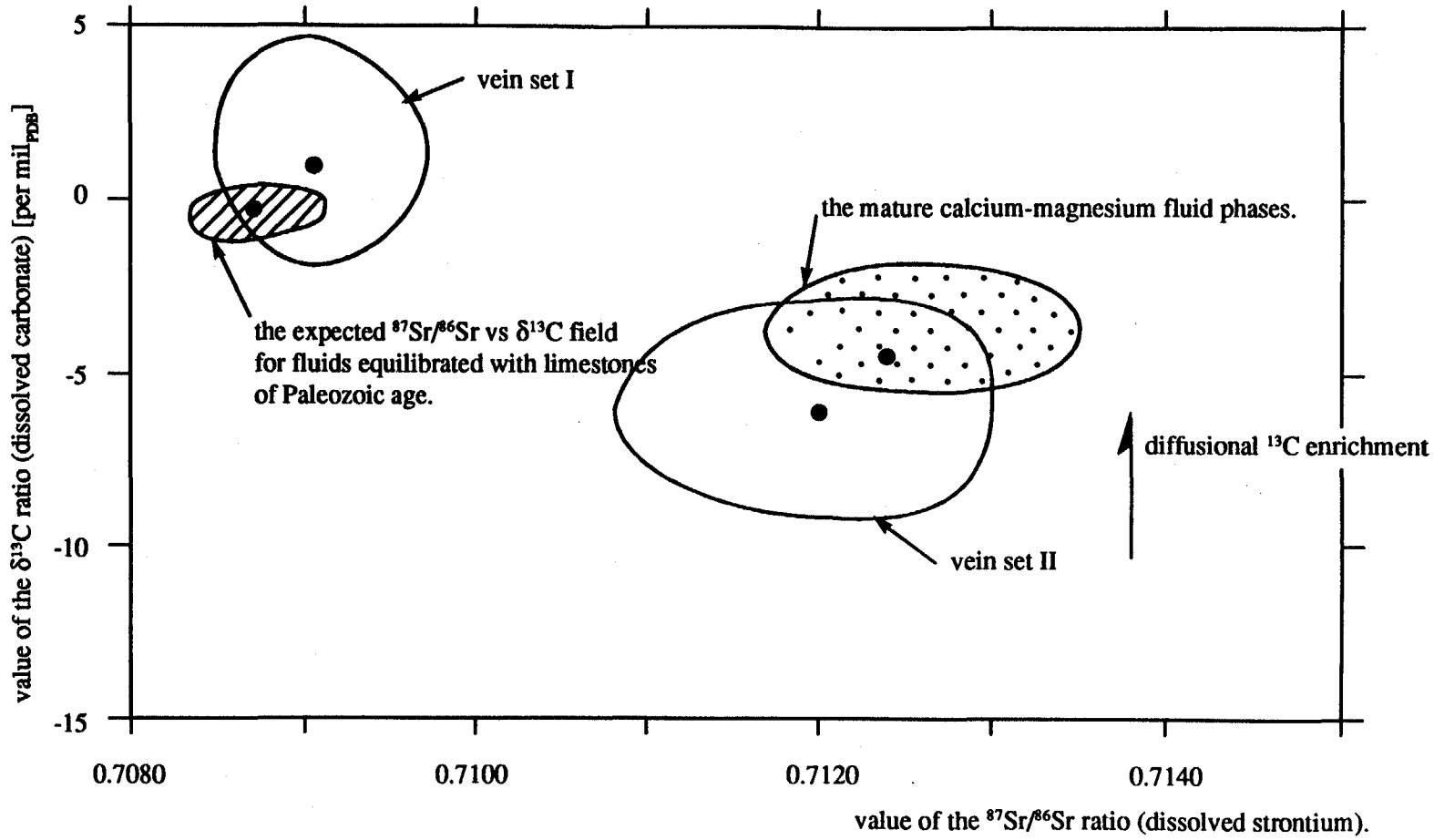

Comparison of the $^{87}Sr/^{86}Sr$ vs. $\delta^{13}C$ fields, the isotopic characters of strontium and carbon dissolved in: a) fluids equilibrated with the Paleozoic carbonates; b) the contemporary and mature fluids from the Paleozoic carbonates; and c) the parent fluids for both sets of the Yucca Mountain calcitic veins.

Sample	Material dated	U-series age [x10^3yrs B.P.]	Source
Crater Flat			
199	acid leach	30	Szabo et al. (1981)
368	do	70±5	Szabo and O'Malley (1985)
386	do	27±3	do
387	do	33±4	do
Yucca Mountain			
113	acid leach	>5	Szabo et al. (1981)
115	do	>20	do
106	do	78±5	do
395	acid leach	>32	Szabo and O'Malley (1985)
412-1	do	>400	do
412-1	opal	>350	do
412-3	do	>400	do
412-7	do	>400	do

U-series ages, samples of the Yucca Mountain calcretes and surficial calcitic veins.

Sample	Material dated	U-series age [x10^3yrs B.P.]	Source
Borehole USW G-2			
280	calcite	>400	Szabo and Kyser (1985)
346.7	do	190±20	do
348.7	do	142±30	do
348.8	do	>400	do
348.8	do	280±70	do
359-A	do	170±18	do
359-B	do	185±18	do
Borehole USW GU-3			
63	calcite	227±20	Szabo and Kyser (1985)
131	do	26±2	do
318	do	>400	do
331	do	30±4	do
Borehole UE-25a#1			
34	calcite	310^{+60}_{-50}	Szabo and Kyser (1985)
283	do	310^{+70}_{-45}	do
611	do	>400	do

U-series ages, samples of the Yucca Mountain subsurface calcitic veins.

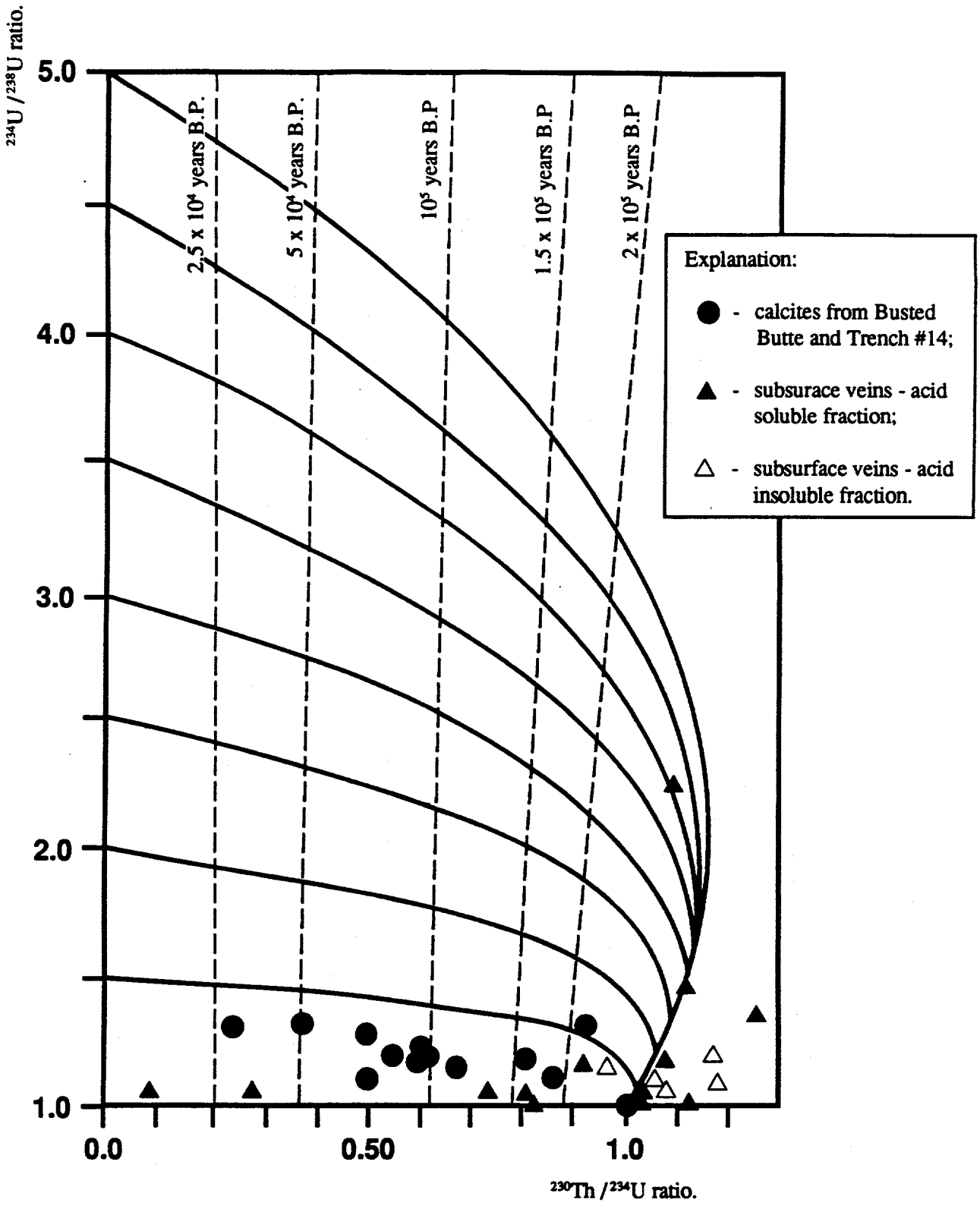

^{234}U / ^{238}U vs. ^{230}Th / ^{234}U ratios, samples of Yucca Mountains calcretes, surficial veins and subsurface veins.

Figure 8-40a

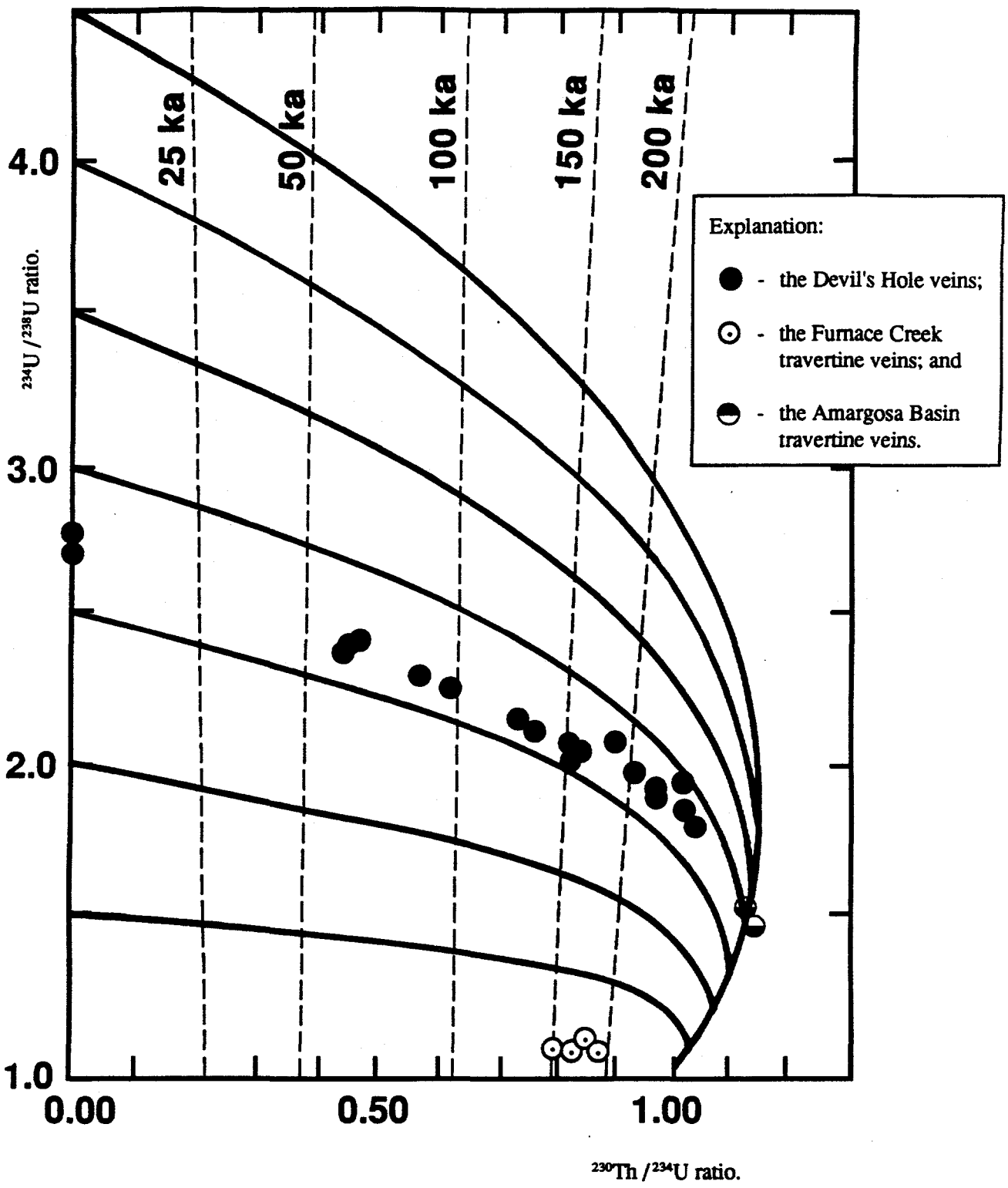

$^{234}U/^{238}U$ vs. $^{230}Th/^{234}U$ ratios, samples of the travertine veins from Devil's Hole, Amargosa Basin, and Furnace Creek Wash.

Figure 8-40b

Depth Interval (cm)	Bulk Density (g/cm^3)	$CaCO_3$ (%)	$CaCO_3$ (kg/m^2)	^{14}C Age (yr)	$\delta^{13}C_{PDB}$ (‰)	$\delta^{18}O_{SMOW}$ (‰)	$\frac{^{230}Th}{^{234}U}$ Age (yr)
0–2	0.60	0.03	0.00				
2–7	1.22	3.90	2.38		+2.9 ± 1.8	+27.8 ± 0.3	
7–50	1.69	0.07 ± 0.00	0.47				
50–57	1.76 ± 0.07	7.41 ± 1.12	9.13	13040 ± 1500	-6.3 ± 0.7	+30.0 ± 0.5	23000 ± 3000
57–90	1.53 ± 0.13	3.20 ± 0.52	16.16				
90–100	1.74	6.07 ± 1.07	10.56	19260 ± 80	-6.4 ± 0.4	+30.6 ± 1.0	28250 ± 5000
100–125	1.55	2.42	9.38				
125–135	1.70	12.44	21.15	19090 ± 90	-5.1 ± 0.8	+32.2 ± 0.8	23000 ± 2000
			69.23				
0–2	0.60	0.00	0.00				
2–8	1.56	2.11	1.97		+4.2 ± 0.5	+29.8 ± 0.2	
8–49	1.52	0.09	0.56				
49–100	1.82	0.00	0.00				
100–110	1.60 ± 0.03	4.71	7.54	20140 ± 150	-5.9 ± 0.3	+29.7 ± 0.3	31000 ± 4000
110–135	1.28	2.12	6.78				
135–155	1.86 ± 0.13	3.93 ± 0.44	14.62	19770 ± 520	-6.9 ± 1.0	+30.0 ± 0.8	32000 ± 4000
155+		2.59					
			31.47				

a) ^{14}C and U/Th ages from samples of the Eagle Mountain indurated calcic horizons.

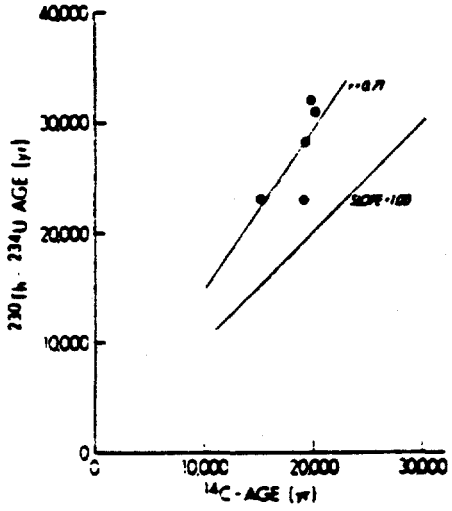

b) Correlation of the U/Th ages, from samples of pebble coatings, with the ^{14}C ages, from bulk samples from the same calcic horizon.

Note:

a) Linear regressions (y = 1.468x + 61.8) assumes that ^{14}C age is the independent variable; exact agreement would show the slope of 1.0.

A comparison of the U/Th and ^{14}C ages, coexisting samples. From Schlesinger, 1985.

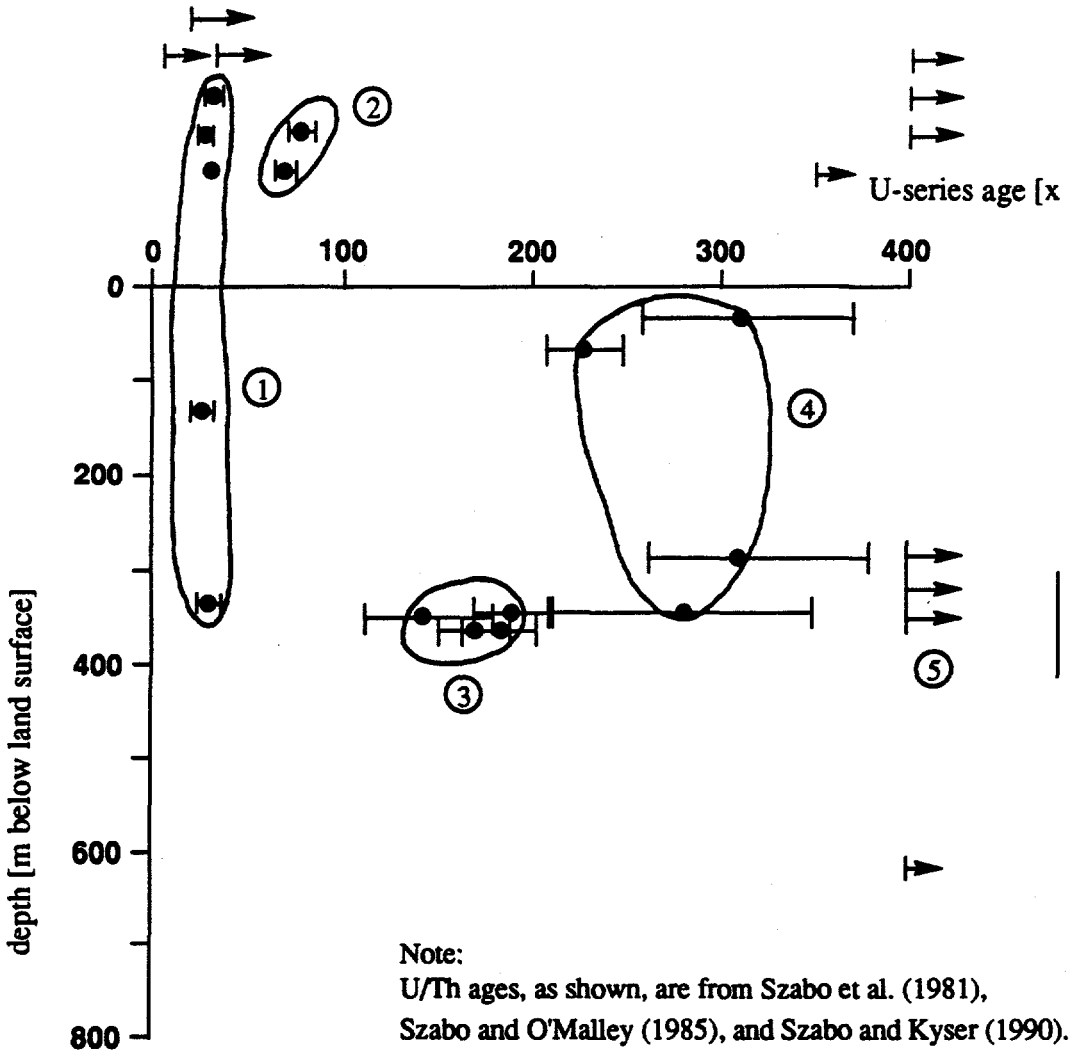

Note:
U/Th ages, as shown, are from Szabo et al. (1981), Szabo and O'Malley (1985), and Szabo and Kyser (1990).

Explanation:
- ● - the U-series age, bar indicates value of the experimental error, and
- ⊢► - actual U-series age exceeds value shown.

Note:
The U-series ages suggest that, during the last 400×10^3 years B.P. the precipitation of calcites occurred in association with, at least, four distinct hydro-tectonic episodes.

The U-series ages from sample of the Yucca Mountain calcretes, surficial calcitic veins, and subsurface calcitic veins.

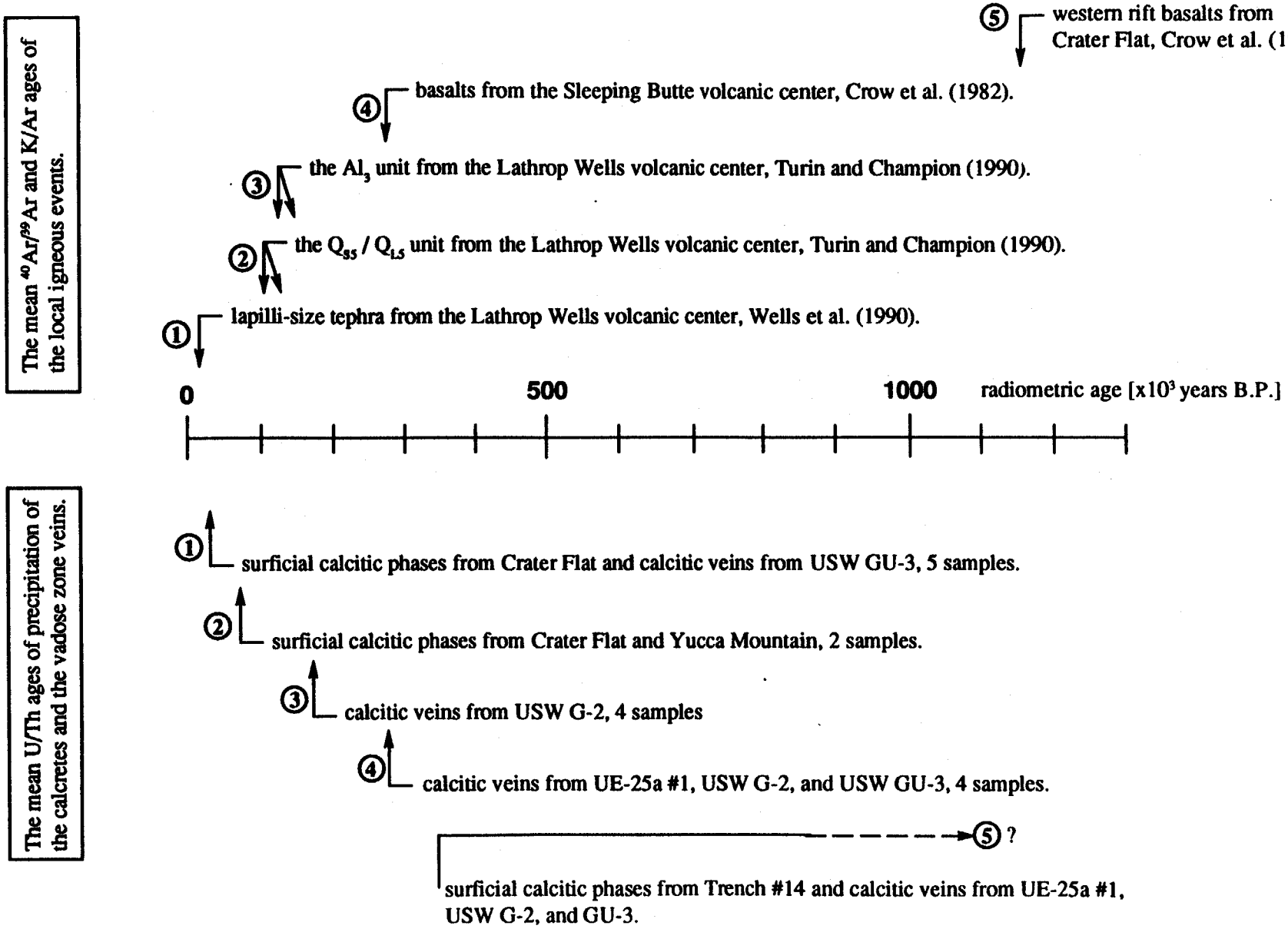

The interpreted history of formation of the Yucca Mountain calcretes and the vadose zone veins, based on radiometric ages of the local igneous events, and the corresponding carbonatization events.